



UNIVERSITÀ  
DEGLI STUDI  
DI PADOVA

Head Office: Università degli Studi di Padova

Department of Biology

---

Ph.D. COURSE IN: BIOSCIENCES

CURRICULUM: GENETICS, GENOMICS AND BIOINFORMATICS

SERIES XXX

**Pharmacological Modulation of Mitochondrial Dynamics: Identification of a Specific OPA1  
Inhibitor to Enhance Apoptotic Release of Cytochrome C**

**Coordinator:** Prof. Ildikò Szabò

**Supervisor:** Prof. Luca Scorrano

**Ph.D. student:** Anna Pellattiero



# Table of contents

<b>Table of contents</b>	<b>iii</b>
<b>List of Figures</b>	<b>v</b>
<b>Summary</b>	<b>vii</b>
<b>Chapter 1 Mitochondria</b>	<b>1</b>
1.1 Mitochondrial ultrastructure	2
1.2 Mitochondrial dynamics	5
1.2.1 Mitochondrial fission	5
1.2.2 Mitochondrial fusion	9
1.2.3 Biological functions of mitochondrial dynamics	12
<b>Chapter 2 Dynamin superfamily</b>	<b>17</b>
2.1 Common features	17
2.2 Subclasses	17
2.3 Structure and domains architecture	19
2.3.1 GTPase domain	19
2.3.2 Middle domain and GED	20
2.3.3 PH domain	20
2.4 GTPase activity	21
2.4.1 Oligomerization-stimulated GTPase activity	22
2.4.2 Mechanism of GTP hydrolysis	25
2.5 Mechanoenzyme	25
2.5.1 Conformational changes induced by GTP hydrolysis	25
2.5.2 Oligomerization and mechanochemical activity	26
<b>Chapter 3 OPA1</b>	<b>31</b>
3.1 OPA1 gene and mRNA splicing transcripts	31
3.2 OPA1 protein: structure and processing	32

3.3	Functions	34
3.3.1	Inner mitochondrial membrane fusion	34
3.3.2	Cristae maintenance	35
3.3.3	Bioenergetics	37
3.3.4	mtDNA stability	38
3.3.5	Apoptosis	38
3.3.6	Redox homeostasis	39
3.3.7	Mitochondrial quality control and aging	40
3.4	Physiopathological relevance of OPA1	41
3.4.1	Autosomal dominant optic atrophy (ADOA)	41
3.4.2	Cancer	45
<b>Chapter 4 Apoptosis</b>		<b>49</b>
4.1	The extrinsic apoptotic pathway	50
4.2	The intrinsic apoptotic pathway	52
4.2.1	Check point: the Bcl-2 family proteins	52
4.2.2	First step to die: OMM permeabilization	54
4.2.3	Second step to die: cristae remodeling and cytochrome c release	56
4.3	Apoptosis and mitochondrial dynamics	57
<b>Results</b>		<b>61</b>
1. Flaming Mitochondria: The Anti-inflammatory Drug Leflunomide Boosts Mitofusins		62
2. The cristae modulator Optic atrophy 1 requires mitochondrial ATP synthase oligomers to safeguard mitochondrial function		67
3. A high throughput screening identifies a small molecule inhibitor of the GTPase activity of OPA1 that enhances apoptotic release of cytochrome c		94
<b>Discussion</b>		<b>165</b>
<b>References</b>		<b>169</b>

# List of Figures

Figure 1. Mitochondrial ultrastructure. ....	2
Figure 2. Change in IMM cristae topology associated with the orthodox-condensed transition.....	3
Figure 3. Mitochondrial fusion and fission in mammalian cells.....	5
Figure 4. Structural domains of the mitochondrial fission proteins and their post-translational modifications.....	6
Figure 5. Structural domains of the mitochondrial fusion proteins and their post-translational modifications.....	10
Figure 6. Biological functions of mitochondrial dynamics.....	13
Figure 7. Classification and domain architecture of the human dynamin superfamily.....	18
Figure 8. Structure of nucleotide-free human dynamin 1.....	21
Figure 9. Comparison of GTPase domains from different GTPases and oligomerization model of DRPs.....	23
Figure 10. Model for dynamin GTP cycle conformational changes..	26
Figure 11. Constriction model for dynamin oligomerization and function .....	28
Figure 13. Models for mitochondrial membrane fusion.....	29
Figure 14. OPA1 isoforms generated by alternative splicing and site of proteolytic processing.....	32
Figure 15. Schematic representation of OPA1 domain.....	33
Figure 16. Mutation spectrum of OPA1..	42
Figure 17. Overview of apoptosis pathways.....	51
Figure 18. Sequence alignment of core Bcl-2 family proteins and bH3-only proteins..	54
Figure 19. Model of cristae remodelling during apoptosis.....	59



## Summary

Mitochondria are essential organelles for life and death of the cell. They are the major source of ATP and play a key role in  $\text{Ca}^{2+}$  signaling and programmed cell death. Following an apoptotic insult, mitochondria release cytochrome c and other proteins in the cytosol to activate the effector caspases and initiate the apoptotic cascade required for cell death.

Thanks to 3D electron microscopy studies, it was demonstrated that cristae are not just invagination of the inner mitochondrial membrane (IMM), as previously depicted by Palade (Palade, 1952), but rather distinct compartments separated from the inter membrane space (IMS) by tubular narrow cristae junctions. The majority of cytochrome c is restricted in this compartment. During programmed cell death mitochondrial morphological and ultrastructure changes. The “cristae remodeling” process induces the widening of the narrow cristae junctions to mobilize the cytochrome c from the cristae to the intermembrane space allowing its complete release into the cytosol (Scorrano et al., 2002).

The key regulator of this dynamic process is the IMM dynamin-related protein Optic atrophy protein (OPA)1 (Cipolat et al., 2006). OPA1 oligomers, containing both the membrane bound and the soluble forms of the protein, participate in the formation and in the maintenance of tight cristae, sequestering cytochrome c in the intra-cristae compartment (Frezza et al., 2006b). During apoptosis, OPA1 oligomers are early targets of BID, BIM-1, BNIP3 (Frezza et al., 2006b; Landes et al., 2010; Yamaguchi et al., 2008), and they are rapidly dissociated, thus causing cristae widening and leading to cytochrome c mobilization from cristae and its subsequent release into the cytosol. (Frezza et al., 2006b; Scorrano et al., 2002). Downregulation of OPA1 leads to mitochondrial network fragmentation and increases cell sensitivity towards apoptosis, while mutations that abolish OPA1 catalytic activity impair its antiapoptotic function (Frezza et al., 2006b).

Independently from the apoptotic cristae remodeling process (Frezza et al., 2006), OPA1 promotes mitochondrial fusion by cooperating with Mitofusins (MFN) 1 and 2, that reside in the OMM (Cipolat, 2004). Furthermore, through its control of cristae morphology, OPA1 regulates mitochondrial metabolism by stabilizing the respiratory chain supercomplexes (Cogliati, 2013).

In 2000 two distinct laboratories demonstrated that mutations in OPA1 gene cause dominant optic atrophy (ADOA), the leading cause of inherited blindness in human, which is characterized by selective death of retinal ganglion cell (Alexander et al.,

2000; Delettre et al., 2000). Interestingly, the hotspots for ADOA-associated mutations are localized within with the OPA1 GTPase domain and GTPase effector domain (GED). However, the physiological importance of OPA1 is also enhanced by its overexpression in different type of cancers, where it correlates with an increased chemotherapy resistance and a lower survival rate (Fang et al., 2012; Kong et al., 2014; Zhao et al., 2013).

The recent advances in high-throughput technologies allowed the genetic characterization of several tumor types and expanded the number of molecular targets. These advances rapidly increased the rush to the personalized cancer therapies. However, many challenges need to be overcome, as tumor heterogeneity and evolution, potential morbidity of biopsies, but especially the lack of effective drugs against most genomic aberrations and the absence of a specific genetic profile for each tumor type (Meric-Bernstam and Mills, 2012). Since survival of tumor cells hinges on dysregulation of their apoptotic pathway, novel drugs that selectively target mitochondrial protein are becoming of great interest.

During my PhD project I investigated the role of altered mitochondrial dynamics in human diseases, particularly in cancer, and how they could be exploited to enhance cancer cells sensitivity towards apoptosis.

Despite the enzymatic nature of the dynamin-related proteins, pharmacological small molecules that modulate mitochondrial morphology are very few. An exception is the recent work of Miret-Casals et al. (2018), where they used a phenotypic HTS for the identification of a small molecule modulator of mitochondrial dynamics. They discover a new role of leflunomide, an anti-inflammatory molecule used in the treatment of rheumatoid arthritis, as an inducer of MFN2 expression. Furthermore, they identified mitochondrial morphology changes as an adaptation mechanism to the cellular metabolic alteration caused by pyrimidine biosynthesis defects. Drug repurposing, which is the process of discovering other applications for an already approved drug, obtained growing attention (Verbaanderd et al., 2017). The work of Zorzano and colleagues is an example of how a library of FDA-approved drugs whose mechanisms of action, pharmacokinetic properties and safety profiles were already extensively described, can be investigated to open new routes in therapeutic treatment exploiting drugs already in use in the clinics.

The modification of apoptotic mechanisms allows cancer cells to escape from drug-induced death, proliferate in unfavorable conditions, acquire further genetic mutations, induce angiogenesis and perhaps metastatisation (Hanahan and Weinberg, 2011; Lopez and Tait, 2015). Among all mitochondria-shaping proteins, OPA1 plays a central antiapoptotic role. Numerous studies demonstrated that OPA1 is an antiapoptotic protein that plays a fundamental role in the control of the apoptotic cristae remodeling to achieve a complete release of cytochrome c from the mitochondria (Del Dotto et al., 2017; Frezza et al., 2006b; Griparic et al., 2004; Olichon et al., 2003b). Higher levels of OPA1 protein were reported in different tumor types, as lung adenocarcinoma, breast and endometrial cancers (Anderson et al., 2018; Fang et al., 2012; Wee et al., 2018). Overexpression of OPA1 correlates with an increased resistance to



conventional chemotherapeutics, such as cisplatin and sorafenib, and with a lower survival rate (Fang et al., 2012; Kong et al., 2014; Zhao et al., 2012). Noteworthy, the OPA1 antiapoptotic activity depends on its ability of hydrolyse GTP, since mutations that abolish OPA1 GTPase activity also impair its antiapoptotic function (Frezza et al., 2006b). Given these observations, we decided to develop an HTS to discover small molecule inhibitors of OPA1 GTPase activity, with the aim of using them in combination therapy to increase apoptosis sensitivity and overcome drug resistance of tumor cells.

Since there are no published three-dimensional crystal structures of OPA1, to identify inhibitor of OPA1 GTPase activity we decided to use a recombinant OPA1 (rOPA1) taking advantage of an established protocol. The rOPA1 was expressed in *E. coli* and purified by affinity chromatography. The protein lacks the mitochondria targeting sequence and the transmembrane domain (aa 1-167) and is fused to a C-terminal 6X His-tag (Quintana-Cabrera et al., 2018). The stability and the activity of the rOPA1 was measured by reverse phase chromatography. In the work of Quintana-Cabrera et al. 2018, the recombinant protein was used to verify if OPA1 could directly promote or stabilize the ATP synthase oligomeric forms. rOPA1 was incorporated in the lumen of proteoliposomes containing ATP synthase, but it failed to stimulate or stabilize ATP synthase oligomerization (Quintana et al., 2018).

Therefore, we designed an *in vitro* high throuput screening (HTS) of a library of 10,000 novel drug-like molecules and we tested their inhibitory activity towards the GTPase activity of the rOPA1. By means of HTS we identify the most potent and selective inhibitor of OPA1 GTPase activity, named MYLS22. Docking experiments using a molecular homology model of rOPA1, revealed that the best scoring pose of MYLS22 was, indeed, within the hydrophobic GTP-binding pocket of OPA1. Since the *in vitro* conditions do not reproduce the physiological conditions, we tested the inhibitory capacity of the selected compound in a MEF cells culture model. One recurrent problem of the small molecule drugs is their low water solubility. We first determined MYLS22 cellular bioavailability. Solid-phase extraction followed by reverse-phase HPLC allowed us to detect the inhibitor in the cell lysates and to calculate a cellular uptake of ~20%. To improve the cellular uptake of MYLS22 and its potency could be useful the conjugation with a positively charged lipophilic cation, as the triphenyl-phosphonium group (TPP<sup>+</sup>).

Another major struggle in the development of an effective dynamin inhibitor is the specificity. In fact, some published compound failed to selectively inhibit a specific dynamin. For examples the DRP1 inhibitor mdivi-1 can stimulate cell death also in DRP1 knockout cells and has off-target effects, like complex I inhibition (Bordt, 2017). The lack of specificity could be explained by considering the high homology of the GTPase catalytic domain of the dynamin superfamily proteins. In this regard, MYLS22, even if it targets the GTP-binding pocket of OPA1, appeared to retain a high grade of specificity, since it does not inhibit Dynamin-1 activity, even at concentration four times higher than its IC<sub>50</sub>. This is likely due to the ability of the drug to bind to specific residues that lie out of the GTPase domain and are OPA1 specific.

After defining a safe range of MYLS22 concentrations, which did not induce cell death *per se* or lead to mitochondrial toxicity, we could evaluate the inhibitor-specific cellular functions without unrelated cytotoxic side effects. We found that MYLS22 can recapitulate some phenotypic characteristics of OPA1<sup>-/-</sup> cells. Indeed, the inhibitor induces mitochondrial network fragmentation decreasing mitochondrial length and stimulates the release of cytochrome c in response to apoptotic stimuli in a concentration-dependent manner. Notably, in cells treated with MYLS22 without any apoptotic stimuli, mitochondria were fragmented, but still retained cytochrome c, further confirming that MYLS22 *per se* is not cytotoxic. Finally, we turned our attention to the activity of MYLS22 on cancer cells. OPA1 was significantly overexpressed in breast cancer where (Wee et al., 2018). We selected the MDA-MB-231 cells, a human metastatic breast adenocarcinoma cell line, and measured if MYLS22 could block MDA-MB-231 migration, an essential feature of cancer metastatization. The inhibitor was efficacious against metastatic MDA breast cancer cells migration, but it did not produce any additive effects over OPA1 silencing, confirming its specificity for OPA1.

Overall, MYLS22 represents the first reported OPA1 inhibitor that specifically target OPA1 GTPase activity and enhances apoptotic cytochrome c release. The significance of this work resides in the identification of a chemical candidate that can be used for further evaluations as anticancer drug leads to design more effective therapeutic treatments. For example, by using it in combination with the current therapy to increase apoptosis sensitivity and overcome drug resistance of tumor cells.

# Chapter 1 Mitochondria

Mitochondria were first described in 1857 by the anatomist Rudolf Albrecht von Koelliker, who called them “sarcosome”, but was the German microbiologist Carl Benda that gave them the name “mitochondria”. They are double-membrane organelles essential for many fundamental cellular processes. It is there that the majority of cellular ATP is generated. According to Peter Mitchell’s chemiosmotic theory, the enzymatic respiratory complexes at the inner mitochondrial membrane, pump protons across the membrane during the transfer of electrons from NADH and FADH<sub>2</sub> downhill their redox potentials to molecular O<sub>2</sub>, thus generating an electrochemical gradient. The free energy stored in this electrochemical gradient drives the F<sub>1</sub>F<sub>0</sub>-ATP-synthase to generate ATP. The whole process is named oxidative phosphorylation (OXPHOS), because oxygen is the final electron acceptor and the ultimate reaction is the phosphorylation of ADP to produce ATP (Mitchell and Moyle, 1967). Mitochondria are the only organelle that possesses its own DNA; in vertebrates mitochondrial DNA (mtDNA) consists of a double stranded circular DNA molecule. The mtDNA encodes 13 mRNAs for subunits of the oxidative phosphorylation complexes (OXPHOS) (Fernandez-Silva et al., 2003). Moreover, mitochondria participate in the synchronization of Ca<sup>2+</sup> transients inside the intracellular compartments, thus regulating multiple Ca<sup>2+</sup>-dependent signaling pathways (Jouaville et al., 1995). One of them, is the apoptotic pathway. Mitochondria are key player of apoptosis, they integrate the diverse stimuli and amplify the death signal releasing multiple pro-apoptotic factors (Wang, 2001). Taken together, these features support the Endosymbiotic Theory, developed in 1971 by Margulis (Margulis, 1971). According to this theory, mitochondria originated from the integration of an alpha-proteobacterial endosymbiont into a larger host cell, more than 1.5 billion years ago. Mutations in mtDNA are associated with a number of genetic, multisystemic diseases that highlight the importance of this organelle in physiology of multiple organs. Several pathological conditions, including cancer, neurodegenerative diseases and neuropathies, are consequences of mitochondrial dysfunctions (Schapira, 2000). This highlights the physiological importance of this organelle for the regulation of the cell and the whole organism homeostasis.

## 1.1 Mitochondrial ultrastructure

The earlier images of mitochondria were obtained by electron microscopy and allowed to identify the organelle as a double membrane system. However, it was only with the use of the electron tomography of isolated rat liver mitochondria that it was

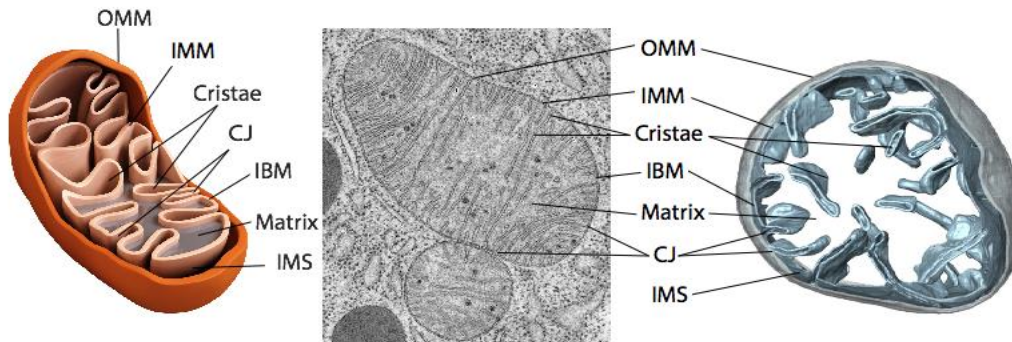


**Figure 1. Mitochondrial ultrastructure.** (a) Schematic representation of mitochondrial structural organization. (b) Electron micrograph of two mitochondria from a thin section of the pancreas from a bat. Original resource provided by Keith R Porter Archives (University of Maryland Baltimore County, Baltimore, MD). (c). Surface rendering volume of a mitochondrion from WT yeast strain. Light grey-outer membrane, sky blue-inner membrane. (Scale bar, 200 nm) From (Davies et al., 2012). Outer mitochondrial membrane (OMM); inner mitochondrial membrane (IMM); intermembrane space (IMS); inner boundary membrane (IBM); cristae junction (CJ)

described for the first time the current model of mitochondrial ultrastructure (Mannella et al., 1994).

The mitochondrion is structurally defined by two membranes: an outer mitochondrial membrane (OMM), permeable to small molecules, and an impermeable inner mitochondrial membrane (IMM), that encloses a protein-rich matrix. The compartment between the two membrane is called inter-membrane space (IMS). The IMM has a larger surface compared to the OMM and forms two morphologically distinct subdomains. (i) The inner boundary membrane (IBM) is the portion of the inner membrane that lies parallel to the OMM with which it forms “morphological contact sites.” (ii) The cristae are internal compartments formed by invaginations of the inner membrane. The tight neck-like segments that connect the IBM with the cristae are called cristae junctions (CJ) (**Fig.1**) (Vogel et al., 2006). To mediate morphological changes, as fusion or fission, the IMM must undergoes structural rearrangements. Hackenbrock defined two morphologic mitochondrial ultrastructures: condensed and orthodox. In the condensed state, mitochondria have wide cristae and a contracted matrix compartment. In the orthodox state, the matrix compartment is expanded and cristae are contracted; thus mitochondria are less dense (**Fig.2**) (Hackenbrock, 1966). Isolated mitochondria were commonly found to oscillate between the orthodox and

condensed conformations, with CJ diameter typically in the range of 20-50 nm, that likely represents a balance between membrane fusion and fission processes (Frey et al., 2002; Mannella et al., 1994).

### ***Outer mitochondrial membrane***

The OMM forms an envelope and connects the mitochondria with the cytosol and the other organelles. It is impermeable for the macromolecules, but allows the passage of solutes, with a molecular mass up to a few thousand Dalton, across its pore-forming proteins. Metabolites and cations can be easily exchanged between cytosol and IMS. The lipid composition of the OMM is more homogenous and contains fewer proteins compared to the IMM.

OMM proteins, integral or peripherally bound, are all nuclear encoded and are involved various processes. For example, there are proteins that regulate the mitochondrial import, as the translocase of the outer membrane (TOM) complex, regulate apoptosis, as the pro-apoptotic (BAK, BAX) and anti-apoptotic (Bcl-2) proteins, mediate organelles contacts, as (MFN1-2), or form pore in the membrane, as the voltage dependent anion channel (VDAC).

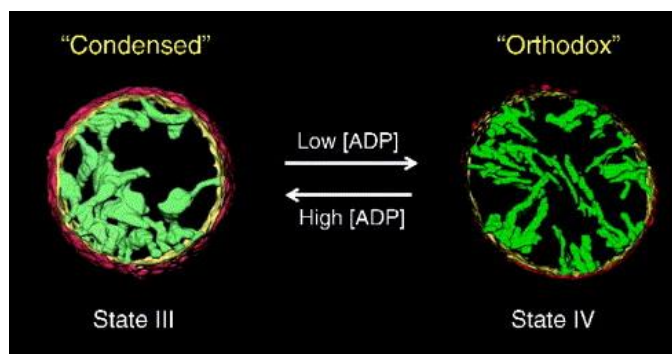


**Figure 2. Change in IMM cristae topology associated with the orthodox-condensed transition.** 3D reconstruction of isolated, condensed and orthodox rat liver mitochondria obtained by electron tomography. OMM (red), IMM periphery (yellow), IMM cristae (green). Mitochondria diameters: 1500 nm (left) and 500 nm (right). From (Mannella et al., 1994)

### ***Inner mitochondrial membrane***

Contrary to the OMM, the IMM is impermeable to small molecules, metabolic substrates and ions. This ensures energy conservation by maintaining a transmembrane potential in form of a proton gradient. It is characterized by high cardiolipin content (de Kroon et al., 1997) and an elevated protein: lipid mass ratio of ~75:25 (Ardail et al., 1990). The IMM can be further subdivided in: inner boundary membrane (IBM), cristae and cristae junctions (CJ). (Vogel et al., 2006).

**The inner boundary membrane.** The IBM is the portion of the IMM that lies parallel to the OMM without invaginations. It forms tight attachments with the OMM forming the so called membrane contact sites (Reichert and Neupert, 2002). At the contact sides reside numerous complexes that connect the two membranes. For example, the translocase of the inner membrane (TIM) closely interacts with TOM in the OMM to import protein in the mitochondria (Schwaiger et al., 1987). The IBM also

participate in the energy transfer from matrix to cytosol (Brdiczka et al., 2006), in apoptosis and in the lipid exchange between IMM and OMM (Tatsuta et al., 2014). Moreover, IMM and OMM undergo to fusion and fission processes in a coordinated manner.

**The cristae.** The cristae are deep invagination into the matrix of the IMM membrane (Perkins et al., 1997). Cristae play a key function in the mitochondria: they are involved in the assembly of respiratory chain complexes and supercomplexes (Cogliati et al., 2013b), in the protein synthesis and translocation, in the nucleoids maintenance (Vogel et al., 2006), in the iron-sulfur biogenesis (Zick et al., 2009b), and in the apoptotic signalling (Scorrano et al., 2002). The regulation of cristae morphology is a crucial process whose physiological relevance will be discussed in detail in Chapter 4.2.3.

**Cristae junctions.** CJ connects cristae with the IMM and reside at the base of the cristae. They are narrow tubular structures that were proposed to form barriers to separate the intracristal space to the IMS and to regulate the flow of metabolites. CJ diameter varies in the range of 20-50 nm (Mannella et al., 1994). The formation of the CJ is mediated by the mitochondrial contact site and cristae organizing system (MICOS) complex (Hoppins et al., 2011).

### ***Mitochondrial DNA***

Mitochondria have their genome distributed in multiple copies in the matrix. In humans, the mitochondrial DNA (mtDNA) is a circular, closed, double-stranded structure with a 16,569-bp genome that encodes 37 genes. The heavy strand (or H-strand), with a high content of guanine nucleotides, encodes 28 genes, while the light strand (or L-strand) cytosine-rich, encodes 9 genes. 13 genes encode for polypeptides (subunits of respiratory complexes; seven subunits of complex I, one of complex III, three of complex IV and two subunits of ATP-synthase), 22 are for transfer RNA and 2 are for the small and large subunits of ribosomal RNA (Fernandez-Silva et al., 2003). mtDNA is organized in structural units called nucleoids. These structures comprise multiple proteins, as the transcription factor A (TFAM), the main packaging polypeptide, scaffold proteins, transcription and translation factors (Kukat et al., 2015)

## 1.2 Mitochondrial dynamics

The development of live cell imaging radically changed the concept of mitochondria. Rather than being static and isolated, mitochondria are highly dynamic organelles that reorganize themselves into tubular or fragmented networks by modulating their morphology through coordinate cycles of fission and fusion events. The balance between fusion and fission regulates mitochondrial shape, size and distribution, and is referred to as “mitochondrial dynamics” (**Fig. 3**). Mitochondrial dynamics are involved in a number of crucial processes, as metabolic adaptations, cell cycle, immunity, apoptosis and mitochondrial quality control (Tilokani et al., 2018). The fusion and fission processes are mostly triggered by a group of “mitochondrial shaping-proteins”, large GTPases belonging to the dynamin superfamily (a detailed description in Chapter 2) (Praefcke and McMahon, 2004).

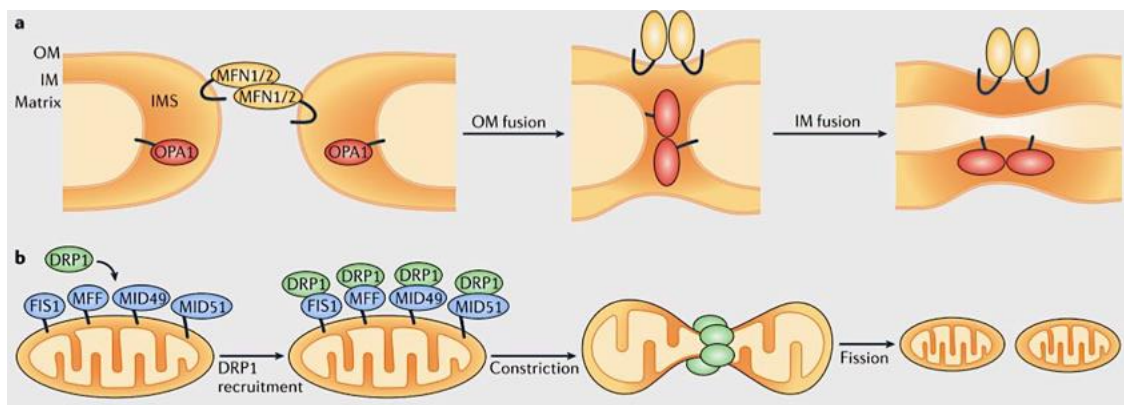


**Figure 3. Mitochondrial fusion and fission in mammalian cells.** (a) OMM fusion is mediated by the dynamin-related GTPases mitofusin 1 (MFN1) and 2 (MFN2). IMM fusion is mediated by the dynamin-related protein optic atrophy 1 (OPA1). (b). Mitochondrial fission requires the recruitment of dynamin-related protein 1 (DRP1) from the cytosol to the mitochondrial OMM. Assembly of DRP1 on the mitochondrial surface causes constriction of the mitochondria and division of the organelle into two separate entities. Four DRP1 receptors exist in mammals: mitochondrial fission 1 (FIS1), mitochondrial fission factor (MFF), mitochondrial dynamics protein of 49 kDa (MID49) and of 51 kDa (MID51). Adapted from (Mishra and Chan, 2014)

### 1.2.1 Mitochondrial fission

#### 1.2.1.1 Mitochondrial fission machinery

Two classes of molecules have been identified as essential for the fission of mitochondria. The master regulator is the dynamin-related protein 1 (DRP1), a mechanoenzyme that mediates constriction and scission of mitochondria in a GTP-dependent process. Since the majority of DRP1 resides in the cytosol, it requires a

scaffold protein is required to reach the fission sites on the OMM. FIS1, MFF, MiD49, and MiD51 belong to this group (**Fig.4**).

### ***The master regulator: DRP1***

DRP1 is a dynamin-like GTPase protein evolutionary conserved from yeast (DNM1) (Bleazard et al., 1999; Sesaki and Jensen, 1999) to mammals (DRP1) (Smirnova et al., 2001). DRP1 is mostly found in the cytosol, but it is recruited to mitochondrial and peroxisomal membranes where it oligomerizes and provokes membrane division upon GTP hydrolysis. DRP1 is essential for embryonic development (Ishihara et al., 2009; Wakabayashi et al., 2009) and its inhibition or genetic loss of DRP1 results in an elongation of both mitochondria and peroxisomes (Koch et al., 2003). DRP1 comprises three functional domains typical of dynamin superfamily (see Chapter 2.1): (i) a N-terminal GTPase domain, (ii) a middle domain and a (ii) C-terminal GED. It lacks the PH and the PRD domains, and but include an additional (iv) variable domain, or B-insert (**Fig. 4**). Structurally, DRP1 resembles the classical dynamins. it comprises the GTPase domain and the stalk domain connected by the BSE, that allows the protein oligomerization at the membrane and the transmission of the movement to the rest of the structure (Kalia et al., 2018). DRP1 self-assembles into large oligomeric structures forming spirals around the constriction sites on the OMM upon GTP hydrolysis (Lu et al., 2018). Interestingly, it was recently discovered that the ER is not only required for the initial step of mitochondrial division, but it also forms a signalling platform for metabolite exchange, and cell death. Upon dephosphorylation by calcineurin, DRP1 is specifically recruited to mitochondria-ER contact sites (Friedman et al., 2011).

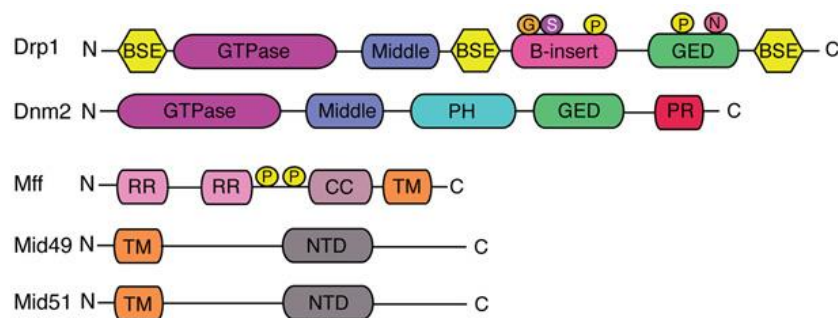


**Figure 4. Structural domains of the mitochondrial fission proteins and their post-translational modifications.** Post-translational modifications are indicated by P (Phosphorylation), N (S-nitrosylation), S (SUMOylation), G (O-GlcNAcylation). BSE, bundle signalling elements; CC, coil-coil; GED, GTPase effector domain; NTD, nucleotidyl transferase domains; PH, Pleckstrin homology; PR, Proline rich; RR, repeat regions; TM, transmembrane. Adapted from (Tilokani et al., 2018)



### ***The coplayers: FIS1, MFF, MiD49 and MiD51***

Unlike classical dynamin, DRP1 does not have a definite PH domain. Therefore it is recruited to membrane fission sites by specific adaptor proteins. In yeast, the DRP1 orthologue DNM1 is recruited to the OMM via the membrane-anchored protein FIS1 (Mozdy et al., 2000) and two receptors MDV1 (Tieu and Nunnari, 2000) and CAF4 (Griffin et al., 2005). However, orthologues for MDV1 and CAF4 has not been identified yet in higher eukaryotes.

**FIS1.** FIS1 is anchored at the C-terminal to the OMM. It was initially described as the only DRP1 adaptor protein, although conflicting evidences regarding its function were recently reported. Early studies showed that FIS1 overexpression resulted in mitochondria fragmentation, while its inhibition induced mitochondria elongation (Stojanovski et al., 2004; Yoon et al., 2003; Yu et al., 2005). Nevertheless, FIS1 inhibition does not abrogate DRP1 recruitment on OMM (Lee et al., 2004). Moreover, in a recent work, *Fis1*<sup>-/-</sup> HeLa cells does not significantly show an alteration of the mitochondrial morphology, and deletion of FIS1 gene does not disrupt mitochondrial morphology and DRP1 recruitment to OMM (Otera et al., 2010). An hypothesis, which was recently proposed, concerns the main role of FIS1 in mitochondrial fission as possibly cell-specific (Chan, 2012).

**MFF.** The tail-anchored mitochondrial fission factor (MFF) protein is a well-established receptor for DRP1. Overexpression of MFF produces mitochondrial fragmentation (Otera et al., 2010), while MFF knockdown causes mitochondrial and peroxisome elongation and a reduction in DRP1 recruitment on the OMM (Gandre-Babbe and van der Blik, 2008; Otera et al., 2010). Immunoprecipitation experiments showed a direct association between MFF and DRP1 (Lee et al., 2004; Otera et al., 2010).

**MiD49 and MiD51.** The mitochondrial dynamics protein of 49 kDa (MiD49) and the mitochondrial dynamics protein of 51 kDa/mitochondrial elongation factor 1 (MiD51/MIEF1) are similar proteins with a transmembrane domain at the N-terminus. They have a nucleotidyltransferase domain and MiD51 requires ADP as a cofactor to stimulate DRP1 oligomerization and GTPase activity (Loson et al., 2014; Richter et al., 2014). Two-hybrid and coimmunoprecipitation experiments demonstrated a direct interaction of the MiD proteins with DRP1 (Palmer et al., 2013). Overexpression of either protein in mammalian cells causes an elongation or a collapse of the mitochondrial network with an increased recruitment of DRP1 on OMM (Gomes et al., 2011; Palmer et al., 2013). It was hypothesized that the increased DRP1 recruitment, caused an inactivation of the protein, thus producing a fission defect. Interestingly, knockdown of either MiD49 or MiD51/MIEF1 had no effect on mitochondrial morphology, but double knockdown of both phenocopies MFF knockout. However, another study found that MiD51 KO results in mitochondrial fragmentation, leading to

the conclusion that MiD51 recruits DRP1 and acts as an inhibitor of its fission activity (Osellame et al., 2016). Furthermore, Palmer and colleagues discovered that MFF and MiDs act independently on Drp1 recruitment and activity (Palmer et al., 2013). Thus, it was hypothesized that MFF and MiDs have distinct but complementary roles. In particular, MiDs recruit DRP1 GTP-bound state to facilitate its oligomerization, whereas MFF recruits oligomeric and active forms of DRP1. Intriguingly, MiD49/MiD51-dependent recruitment of DRP1 to mediate mitochondrial fission has been linked with cristae remodelling during intrinsic apoptosis. Otera and colleagues found that MiD49/MiD51 KO and DRP1 KO cells counteract cristae remodeling and cytochrome c release during apoptosis, but disassemble OPA1 complexes (Otera et al., 2016). These evidences indicate that the MiD proteins are important regulators of DRP1 activity, but more studies are necessary to understand the exact regulatory mechanisms.

### 1.2.1.2 Regulation of mitochondrial fission

Multiple post-translational modifications are involved in the regulation of DRP1 activity (**Fig. 4**). The most studied are the phosphorylation at serine 616 (S616), pro-fission form, and serine 637 (S637), pro-fusion form (the numbers correspond to the aminoacids of the human DRP1 isoform 1). During mitosis, cdk1/cyclin B kinase phosphorylates DRP1 S616, inducing its oligomerization and mitochondrial fission (Taguchi et al., 2007). Protein kinase C (PKC) (Qi et al., 2011) and the Ca<sup>2+</sup>-calmodulin-dependent kinase II (CaMKII) phosphorylate S616 during cell death (Kim et al., 2016; Xu et al., 2016b), while ERK-1/2 phosphorylates it during cancer cell invasion (Kashatus et al., 2015; Serasinghe et al., 2015) and cell reprogramming (Prieto et al., 2016). Instead, during starvation, protein kinase A phosphorylates DRP1 on S637 inhibiting fission and protecting mitochondria from autophagy (Gomes et al., 2011) and cell death (Chang and Blackstone, 2007; Cribbs and Strack, 2007). S637 is located in the GTPase effector domain, and phosphorylation impairs the interaction of the GED with the middle domain and reduces the GTP hydrolysis activity (Chang and Blackstone, 2007). Dephosphorylation of S637 is performed by the calcium-dependent phosphatase calcineurin during cell death (Cereghetti et al., 2008; Cribbs and Strack, 2007; Slupe et al., 2013) and PGAM5 during necrosis (Wang et al., 2012b). Other kinases that phosphorylated DRP1 are Rho-associated coiled coil-containing protein kinase 1 (ROCK1) (Wang et al., 2012a) and glycogen synthase kinase 3 $\beta$  (GSK3B) (Yan et al., 2015). The effect of S637 phosphorylation on DRP1 function seems to be dependent on the cellular context.

DRP1 activity can be also modulated through the sumoylation of residues in the B domain controlling the protein association with the membrane, fission activity and cell death (Braschi et al., 2009; Prudent et al., 2015; Wasiak et al., 2007). In addition, DRP1 variable domain can be ubiquitinated, for example by Parkin (Wang et al.,

2011), S-nitrosylated (Haun et al., 2013) and be subject to O-GluNAcylation (Chang and Blackstone, 2010; Gawlowski et al., 2012)

Notably, DRP1 receptors can be similarly controlled by post-translational modifications. For example, MFF phosphorylation enhances DRP1 recruitment to OMM, fission and degradation of damaged mitochondria (Toyama et al., 2016). Whereas, MiD49 ubiquitination by MARCH5/MITOL leads to its degradation (Xu et al., 2016a).

### **1.2.1.3 In search for an IMM fission machinery**

IMM fission occur in coordination with OMM fission to ensure the correct division of the organelle. In contrast to OMM fission, the molecular events that induce IMM division are poorly understood and, until now, no machinery has been discovered. However, some model for IMM fission were recently proposed:

- a. Cho and colleagues discovered that the IMM constriction occurs at mitochondria-ER contact sites through a  $\text{Ca}^{2+}$ -dependent process. It was shown that independently of OMM fission,  $\text{Ca}^{2+}$  influx in mitochondria leads to IMM constriction, while the loss of the mitochondrial calcium uniporter (MCU) induces mitochondrial elongation (Chakrabarti et al., 2018; Cho et al., 2017; Hom et al., 2007).
- b. Instead, in neurons,  $\text{Ca}^{2+}$  influx in mitochondria induces a decrease of the membrane potential that lead to OMA1 activation and OPA1 processing. With the accumulation of s-OPA1, the MICOS complex can no longer stabilize OMM-IMM tethering. This might lead to the IMM constriction (Cho et al., 2017). This proposed mode of action confirms the role previously described for S-OPA1 in fission.

## **1.2.2 Mitochondrial fusion**

### **1.2.2.1 Mitochondrial fusion machinery**

During mitochondrial fusion, two events take place: OMM and IMM fusion. Live images indicate that the two fusion events are coordinate and normally occur simultaneously. They result in mixing of the membranes, the IMS and the matrix of the mitochondria. However, outer and inner membrane fusion can be temporally separated under specific experimental conditions. In mammals, the key players of mitochondrial fusion are three dynamin superfamily large GTPases: the mitofusins MFN1 and MFN2 for the OMM, and OPA1 for the IMM (**Fig. 5**).

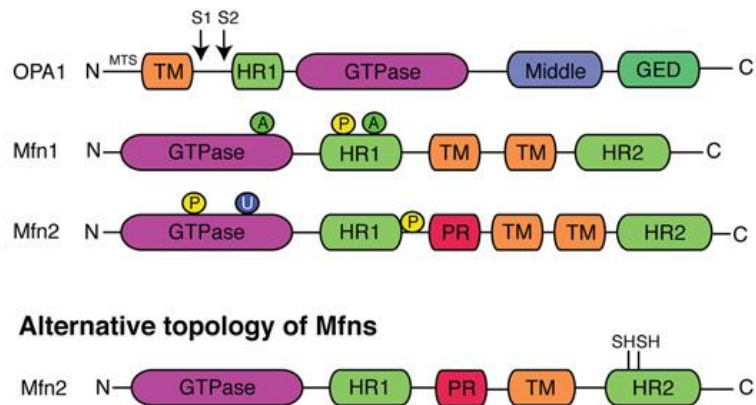


**Figure 5. Structural domains of the mitochondrial fusion proteins and their post-translational modifications.** The classical model proposes that MFNs contain two transmembrane (TM) domains in between HR1 and HR2 domains. Alternatively, MFNs have been recently demonstrated to have only one TM that lies between the two HR domains. Cysteine residues, sensitive to oxidative stress are located in the C-terminal located in the IMS (only MFN2 structural domains are represented but this new topology is also applicable to MFN1). Post-translational modifications are indicated by P (Phosphorylation), A (Acetylation) or U (Ubiquitination). GED, GTPase effector domain; HR, heptad repeat; MTS, mitochondrial targeting sequence; PR, Proline rich; TM, transmembrane. Adapted from (Tilokani et al., 2018)

### ***The architects of the OMM: MFN1 and MFN2***

Mitofusins are conserved from yeast to humans and the first mitofusin orthologue, fuzzy onion (FZO1), was characterized in *Drosophila melanogaster*. Mammals have two mitofusins, MFN1 resides in the OMM and promotes membrane fusion, while MFN2 localizes to both mitochondria and ER and is also able to tether the two organelles in trans. They have two transmembrane domains separated by a short loop and expose in the cytosol the GTPase domain at the N-terminal region, a coil-coil heptad repeat 1 (HR1) domain and the HR2 domain at the C-terminal (**Fig. 5**) (Chen et al., 2003; Rojo et al., 2002; Santel and Fuller, 2001). Mitofusins overexpression lead to aggregation of the mitochondrial network near the nucleus (Eura et al., 2003). MFN1 KO induces mitochondrial fragmentation, while MFN2 KO produces swollen spherical mitochondria with a less marked defects, both are required for embryonic development (Chen et al., 2003). This phenotype can be explained by the fact that MFN1 has a greater GTPase activity (Ishihara et al., 2004) and is also necessary for OPA1-mediated IMM fusion (Cipolat et al., 2004), whereas MFN2, in addition to its role in mitochondrial fusion, is implicated in the regulation of the mitochondria-ER contact sites tethering (de Brito and Scorrano, 2008; Dorn and Maack, 2013; Filadi et al., 2015). In fact, MFN1 is able to fully rescue the phenotype of MFN1<sup>-/-</sup> or MFN2<sup>-/-</sup> cells, while MFN2 can only partially correct the mitochondrial defects of MFN1<sup>-/-</sup> cells. (Chen et al., 2005).

### ***The architect of the IMM: OPA1***

The IMM fusion is mediated by the large GTPase dynamin OPA1 and specific membrane lipid components, as cardiolipin. OPA1 knockout leads to mitochondrial fragmentation, while OPA1 overexpression produces mitochondrial elongation (Griparic et al., 2004). OPA1 is evolutionary conserved and was initially described in the yeast model (Mgm1p) (Sesaki et al., 2003). Mammalian OPA1 exists in eight splice-variants and its structural organization resembles that of the classical dynamins, but with some variation. OPA1 is inserted in the IMM with its transmembrane domain at the N-terminal, while the majority of the protein is exposed to the IMS (**Fig. 5**) (Olichon et al., 2002). OPA1 retain at least two proteolytic cleavage sites, which allow the generation of a shorter and soluble fragments (s-OPA1). Reduction of OPA1 results in mitochondrial fragmentation (Chen et al., 2005; Cipolat et al., 2004; Griparic et al., 2007), cristae disorganization (Frezza et al., 2006b; Griparic et al., 2004; Olichon et al., 2003b), impaired respiratory capacity (Cogliati et al., 2013b), and higher sensitivity to apoptosis (Frezza et al., 2006b; Griparic et al., 2004). Also OPA1 has also a role in the control of the cristae junctions diameter during apoptosis (Frezza et al., 2006b). OPA1 architecture, functions and the proposed IMM fusion mechanism will be extensively discussed in Chapter 3.

#### **1.2.2.2 Regulation of mitochondrial fusion**

OPA1 is regulated through several mechanisms. The OPA1 gene encodes eight mRNA splice variants, regulated by differential splicing (Delettre et al., 2001). In each mRNA splice the transmembrane is followed by a protease cleavage site (S1). Four variants have an additional protease cleavage site (S2). Consequently, each mRNA splice variant can potentially produce two or more protein isoforms. Upon import, the mitochondrial targeting signal is cleaved by the mitochondrial processing peptidase to produce a long isoform (l-OPA1) anchored to the IMM. The protein can also be cleaved at either S1 or S2 to produce a short isoform (s-OPA1) without the transmembrane segment (**Fig.13**). Since mitochondrial fusion depends on a balance ratio of long to short OPA1 isoforms, the proteolytic processing of OPA1 at S1 and S2 is the major source of regulation (Song et al., 2007). OPA1 proteolytic cleavage is enhanced in different situations:

- Mitochondrial dysfunction, as loss of membrane potential, apoptosis, high number of mtDNA mutations. In these situation s-OPA1 represent the major isoform and fusion activity decrease (Duvezin-Caubet et al., 2007; Ishihara et al., 2006).
- The mitochondrial protease OMA1 cleaves OPA1 at S1 under stress conditions and mitochondrial membrane depolarization.
- The mitochondrial protease Yme1L cleaves OPA1 at S2 site and is activated after stimulation of OXPHOS.

- The prohibitins also play a role in the regulation of OPA1 processing, in fact, PHB2 knockout cells selectively loss I-OPA1 and exhibit defects in mitochondrial fusion (Merkwirth et al., 2008).

Only few modifications were associated with MFN1-2 (**Fig. 5**). The activity of MFN1 is regulated by:

- ubiquitination and acetylation promote MFN1 degradation during mitochondrial stress (Park et al., 2014).
- deacetylation of MFN1 enhances fusion during starvation (Lee et al., 2014).
- phosphorylation of MFN1 HR1 domain by the extracellular-signal-regulated kinase (ERK) inhibits mitochondrial fusion and promotes apoptosis (Pyakurel et al., 2015).

The activity of MFN2 is also regulated by:

- ubiquitination by Huwe1 (Leboucher et al., 2012), Parkin (Chen and Dorn, 2013), and MARCH5 (Nagashima et al., 2014; Sugiura et al., 2013) to control its activity and stability.
- Phosphorylation by PINK1 Parkin lead to mitophagy (Chen and Dorn, 2013).
- Phosphorylation by JNK and ubiquitination by Huwe1 induce MFN2 degradation and leads to mitochondrial fragmentation and apoptosis (Leboucher et al., 2012).

### **1.2.3 Biological functions of mitochondrial dynamics**

The regulation of mitochondrial dynamics through fusion and fission allows the fast adaptation of mitochondria to the cell requirements. Both fused and fragmented networks are fundamental during different physiological process and conditions.

#### ***Mitochondrial inheritance***

Mitochondrial network fragmentation during mitosis allows an equal partitioning of mitochondria to the daughter cells, in a stochastic manner. DRP1 regulates this process upon activation by Cdk1/cyclin B (Kashatus et al., 2011; Taguchi et al., 2007)(Kashatus et al., 2011; Taguchi et al., 2007).

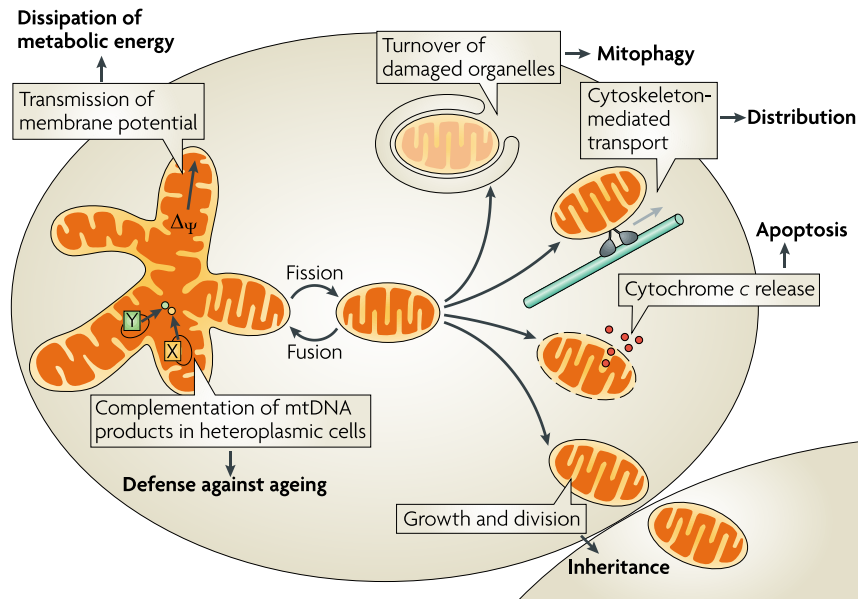


**Figure 6. Biological functions of mitochondrial dynamics.** Division is required for inheritance and partitioning of organelles during cell division, for the release of pro-apoptotic factors from the intermembrane space, for intracellular distribution by cytoskeleton-mediated transport and for turnover of damaged organelles by mitophagy. Fused mitochondrial networks are important for the dissipation of metabolic energy through transmission of membrane potential along mitochondrial filaments and for the complementation of mitochondrial DNA (mtDNA) gene products in heteroplasmic cells to counteract decline of respiratory functions. Adapted from (Westermann, 2010)

### ***Mitochondrial distribution***

Proper mitochondrial distribution within the cell depends on balanced fission/fusion processes that allow to split the mitochondrial network into transportable units. Defects in mitochondrial fission, as DRP1 or deficiency, result in highly interconnected networks that accumulate in restricted areas, leaving the major part of the cell devoid of mitochondria. This defective phenotype is particularly severe in neurons, where the mitochondria accumulate in the cell body leaving only few clumped mitochondria in the neurites (Ishihara et al., 2009). On the contrary, defects in mitochondrial fusion produce highly fragmented networks that fail to distribute across the long and branched neurite processes. Indeed, *Mfn2*<sup>-/-</sup> conditional knockout mice show specific degeneration of Purkinje neurons, which are among the largest brain neurons, located in the cerebellum, characterized by a single long axon and a large number of branched dendritic spines (Chen et al., 2007).

### ***mtDNA stability***

Cell with impaired mitochondrial fusion show a severe reduction (up to two thirds) of the mtDNA level (Chen et al., 2010). Furthermore, they also display a defect in the distribution of mtDNA nucleoids with a mitochondrial subpopulation devoid of them (Chen et al., 2007). Since mtDNA encode 13 essential subunits of respiratory chain, reduction of mtDNA levels generates serious respiratory deficiencies. This is

particularly true for the muscle cells that undergo to a high increase of mtDNA levels, relative to nuclear DNA, during the first two months of life (Chen et al., 2010). A study by Chen and colleagues show that transgenic mice lacking MFN1 and MFN2 in skeletal muscle display 90% loss of mtDNA levels, compared to WT, and increased accumulation of point mutations and mtDNA deletions, followed by loss of respiratory complex activity and muscle atrophy (Chen et al., 2010).

### ***Respiratory functions***

Beyond the negative effects caused by a decline in mtDNA levels, the mitochondrial respiratory capacity is also directly reduced by defects in mitochondrial fusion, as in MFN1-2 DKO or OPA1 KO cells (Chen et al., 2005). In particular, *OPA1*<sup>-/-</sup> cells display a severe defect in cristae structure that seems to further enhance the respiratory deficiency (Cogliati et al., 2013b). In case of Purkinje and skeletal muscle cells, there is a compensatory but futile increase in mitochondrial content (Chen et al., 2007; Chen et al., 2010).

### ***Mitochondrial quality control***

The content mixing between mitochondria occurs in two occasions: the mitochondrial fusion, and the “kiss-and-run” events, where two mitochondria touch each other, mix their content, but do not merge neither change their morphology (Liu et al., 2009). Content exchange has multiple fundamental roles. (i) In healthy cells, during mitochondrial biogenesis, it is necessary that nuclear- and mitochondrial-encoded sets of proteins are coordinately regulated. Content mixing guarantees that mitochondria within the cell act as a coherent population, while maintaining genetic and biochemical uniformity, and preventing the mitochondria to act autonomously, and their biochemical and functional profiles to diverge. (ii) Mitochondrial fusion plays also a protective role in certain pathological conditions. Cells can tolerate a high number of mtDNA mutations without a reduction in respiratory activity thanks to the high copy number of mtDNA and the inter-mitochondrial complementation of mtDNA mutation (DiMauro and Schon, 2003; Nakada et al., 2001). As an example, if two isolated mitochondria carry mutations in two different genes, both will have defects in respiration. However, if these mitochondria fuse, each of them will contribute with a functional allele and produce a functional protein, thus restoring the respiratory activity. The coexistence of WT and mutant mtDNA in the same cells is called heteroplasmy. OPA1 KO and MFN1-2 DKO display an increased heterogeneity in the mitochondrial population (Chen et al., 2007).



### ***Dissipation of metabolic energy***

In muscle cells, the mitochondrial fusion is required for the dissipation of metabolic energy. In these cells, a large continuous mitochondrial network connects the high amount of mitochondria of the oxygen-rich periphery with the mitochondria of the oxygen-poor cell core. This network acts as an electrical system to dissipate the membrane potential generated in the periphery over the entire cell body, in order to allow to generate ATP also in the remote parts of the cell (Amchenkova et al., 1988; Skulachev, 2001).

### ***Adaptation to cellular stress***

The stress-induced mitochondrial hyperfusion (SIMH) is a mitochondrial pro-survival response to different cellular stresses, as UV irradiation, nutrient starvation, inhibition of RNA transcription or protein translation, which results in an increased fusion prompted by MFN1, OPA1 and stomatin-like protein 2 120. Other studies highlighted the role of mitochondrial fission inhibition in the escape from autophagy. During starvation, autophagy is activated but mitochondria with inhibited fission elongate and escape. Mutant cells that are unable to elongate show an increased mitophagy (Gomes et al., 2011; Rambold et al., 2011). Indeed, upon autophagy activation, MFN1-2 and MIRO1-2, which are involved in the mitochondrial trafficking, are rapidly degraded, while DRP1 is recruited to the OMM (Chan et al., 2011; Gegg et al., 2010; Poole et al., 2010; Tanaka et al., 2010). Probably fission is needed to reduce the size of the mitochondria providing substrates more suitable for the engulfment process. Moreover, mitochondrial fusion is increased under stress conditions that involve mitochondrial ATP production (Tondera et al., 2009) and during the G1 to S transition, when mitochondrial ATP synthesis is enhanced (Mitra et al., 2009).

### ***Regulation of apoptosis***

Both mitochondrial fusion and fission play an important role in the regulation of apoptosis. DRP1 mediates mitochondrial fragmentation prior to OMM permeabilization. Furthermore, it was shown that DRP1 and mitofusins interact with the pro-apoptotic proteins BAX and BAK, emphasising the link between the mitochondrial shaping proteins and apoptotic proteins (Brooks et al., 2007; Karbowski et al., 2002; Wasiak et al., 2007). Despite several controversial persist on the exact role of DRP1 in apoptosis, there are more evidences on the anti-apoptotic function of OPA1. OPA1 is the key regulator of apoptotic cristae remodelling process and cytochrome c release (see Chapter 4.3) (Cipolat et al., 2006; Cogliati et al., 2013b; Frezza et al., 2006b; Glytsou et al., 2016; Scorrano et al., 2002).



# Chapter 2 Dynamin superfamily

## 2.1 Common features

Dynamin superfamily proteins comprise multidomain mechano-chemical GTPases, which are generally involved in nucleotide-dependent membrane remodeling events (Praefcke and McMahon, 2004). Dynamins differ from small Ras-like and regulatory GTPases, because they show five main features that are not conserved in the latter ones: (i) a large GTPase domain (~ 300 aminoacids); (ii) a low nucleotide binding affinity that do not require GTPase-activating proteins (GAPs) and guanine nucleotide exchange factors (GEFs); (iii) a nucleotide-dependent dimerization; (iv) a high basal rate of GTP hydrolysis that cooperatively increase with protein oligomerization; (v) an ability to assemble into regular oligomers on appropriate templates (Daumke and Praefcke, 2016; Heymann and Hinshaw, 2009; Praefcke and McMahon, 2004).

Based on their domain architecture, dynamin superfamily proteins are classified into two subclasses. (i) The “classical dynamins” show sequence homology with the founder member of the dynamin family, the mammalian dynamin, discovered as a microtubule-associated protein in 1989 (Shpetner and Vallee, 1989). They include five identifiable domains: a GTPase domain, a middle domain, a pleckstrin homology (PH) domain, a GTPase effector domain (GED) and proline-rich domain (PRD). (ii) The dynamin-related proteins (DRPs) have homology to dynamin in the GTPase domain, but they lack one or more domains or have more additional regions not present in the classical dynamins (Praefcke and McMahon, 2004). Unlike classical dynamins, they comprise a wider group of different dynamins subclasses.

## 2.2 Subclasses

Despite common biochemical and structural features, dynamin superfamily members have distinct subcellular localizations and domain architectures related to their specific functions in the cell (Heymann and Hinshaw, 2009). Thus, they commonly fall into the following subclasses (**Fig.7**):

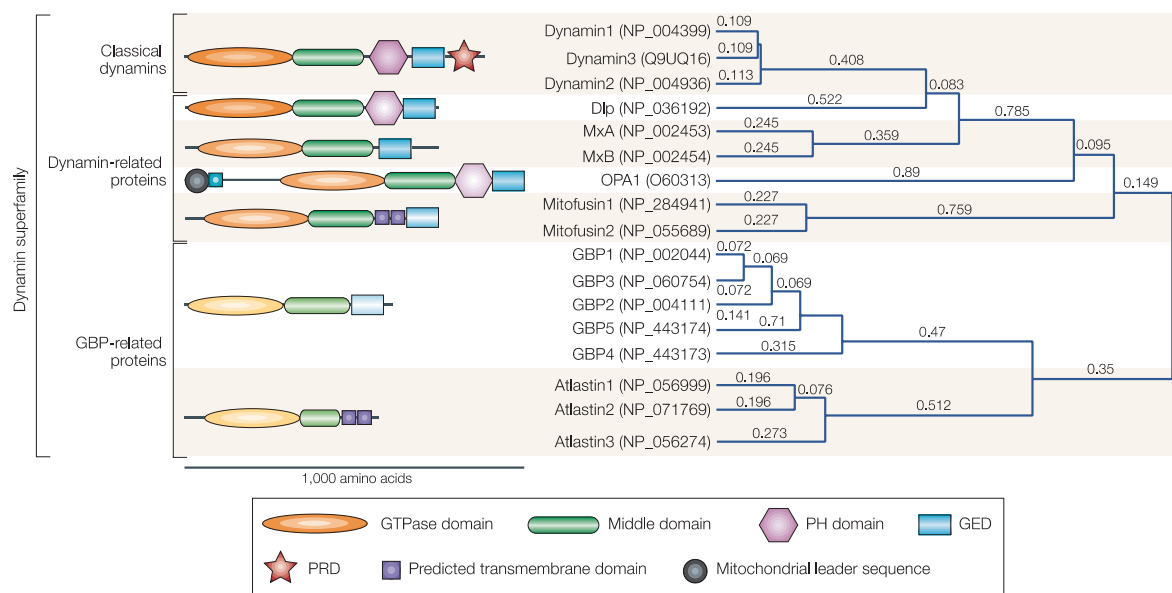


**Figure 7. Classification and domain architecture of the human dynamin superfamily.** Dynamin-superfamily members have been grouped according to their domain structure and their accession numbers are shown. The decreasing intensities of the colours of the domain correspond to decreasing sequence homology. All dynamins contain a GTPase domain that binds and hydrolyses GTP, a middle domain and a GTPase effector domain (GED) involved in oligomerization and stimulation of GTPase activity. Most dynamins contain a domain for interactions with lipid membranes: the pleckstrin-homology (PH) domain, a transmembrane domain or a particular sequence. Classical dynamins contain a proline-rich domain (PRD) at the C-terminus that interacts with Src-homology-3 (SH3) domains. DLP, dynamin-like protein; GBP1-4, guanylate-binding protein 1-4; OPA1, optic atrophy 1. From (Praefcke and McMahon, 2004)

**Classical dynamins.** This family owns the five aforementioned domains: GTPase domain, middle domain, PH domain, GED and PRD, and comprises mammalian dynamins 1, 2 and 3. Dynamin 1 (DNM1) is enriched in the presynapse of neurons, dynamin 2 (DNM2) is ubiquitously expressed and dynamin 3 (DNM3) is prevalently found in the brain and in the testis. Each of the three mammalian dynamins has multiple splice variants, while *D. melanogaster* and *C. elegans* retain only one isoform (Cao et al., 1998). They have a role in scission of clathrin-coated vesicles leading to endocytosis, but also in non clathrin-mediated budding events at caveolae and phagosomes. They function in synaptic vesicle recycling, in Golgi trafficking, in the formation of podosomes, in actin rearrangement and cytokinesis (Hinshaw, 2000).

**Dynamamin-like proteins (Dlps).** These proteins are missing the PRD and comprise a PH-like domain between the middle domain and the GED. There is a single Dlp homologue per organism, conserved from yeast to human, involved in division of organelles, as mitochondria or peroxisomes (Gammie et al., 1995; Labrousse et al., 1999; Shin et al., 1997).

**Mx-like proteins.** Proteins of this family are missing the PRD and the PH domain. The expression of human MxA and MxB is induced by type I interferons and MxA displays antiviral activity (Staeheli et al., 1986).

***OPA1/Mgm1 proteins.*** This family presents the same domain architecture of Dlps, but it also contains additional regions: a mitochondrial import sequence at the N-terminal followed by a transmembrane domain and a coiled-coil domain. These proteins are conserved from yeast to human, are localized in the inner mitochondrial membrane and are involved in mitochondrial fusion (Alexander et al., 2000; Delettre et al., 2000; Olichon et al., 2002).

***Mitofusin/Fzo1 proteins.*** Proteins within this family have a transmembrane domain in place of the PH domain and their C-terminal has weak homology with GED of dynamin. They are present from yeast to humans, are localized in the cytoplasmic side of the outer mitochondrial membrane and are involved in mitochondrial fusion (Hales and Fuller, 1997; Santel and Fuller, 2001).

***Guanylate-binding proteins (GBPs)/atlastins.*** They are two groups of similar proteins that are not comprised in the DRPs, but were probably arisen from a common ancestor. They only display homology with GTPase domain of dynamin. GBP are involved in interferon II-induced photogenic resistance and are not found in *D. melanogaster* and *C. elegans* (Anderson et al., 1999). Unlike dynamins, they can hydrolyze GTP to GDP and also to GMP (Schwemmle and Staeheli, 1994). Atlastin plays a role in the vesicle trafficking at the cis-Golgi (Zhu et al., 2003).

## 2.3 Structure and domains architecture

The minimal architectural structures shared by all dynamins are the large GTPase domain, the middle domain and the GED, involved in the oligomerization and the regulation of the GTPase activity.

### 2.3.1 GTPase domain

The defining feature of dynamin superfamily is the amino-terminal GTPase domain of approximately 300 aminoacids. This is the most highly conserved region and its length allows distinguishing it from those of the other GTPase proteins.

As many regulatory GTP-binding proteins, GTPase domain of dynamin superfamily members contains five conserved GTP-binding motifs (G1-G5). The G1 motif, with the consensus GXXXXGKS/T, forms the P-loop region, also present in ATPases. It coordinates the  $\beta$ -phosphate, while the terminal serine/threonine participates in  $Mg^{2+}$  binding (Saraste et al., 1990). The conserved threonine of the G2 motif and the DxxG residues of G3 motif mediate respectively a direct or water-mediated contact with  $Mg^{2+}$ . The regions encompassing these two motifs directly interact with  $\gamma$ -phosphate and undergo a conformational change during GTP hydrolysis. Therefore, they are called switch I (G1) and switch II (G3) regions. The switch region is flexible in the GDP-bound state but are stabilized in GTP-bound form

(Vetter and Wittinghofer, 2001). A hydrophobic residue following the G3 motif stabilizes the conformation of switch II. The highly conserved aspartate in the N/TKxD motif of G4 mediates the specific binding to GTP (Niemann et al., 2001). The G5 motif is not well conserved among dynamin superfamily and is involved in binding the ribose moiety.

### 2.3.2 Middle domain and GED

The middle domain is the most divergent region among dynamin superfamily and lacks sequence homology to any known structural motif. Cryo-electron microscopic studies of assembled dynamins in GDP-bound and nucleotide-free states suggested the presence of a stalk region, composed of the middle domain and the GED, that mediate inter-molecular interaction (Zhang and Hinshaw, 2001). Based on a structural visualization of the protein, the middle domain and the GED arrange themselves into two distinct domains: the stalk and the bundle signaling element (BSE). The stalk comprises the C-terminal sequence of the middle domain and the N-terminal of the GED (**Fig. 8**). Mutagenesis experiments of dynamin, demonstrated the critical role of the middle domain in intermolecular interactions (Ramachandran et al., 2007). In 2011, two independent groups resolved the crystal structure of human dynamin 1, providing insight into the mechanism of dynamin assembly and mechanochemical coupling during GTP hydrolysis. The stalk forms an antiparallel four-helix bundle that was shown to mediate the assembly of dynamin 1 by providing three different assembly interfaces (Ford et al., 2011b). It was found to mediate dynamin 1 oligomerization and the formation of high-order structures, as rings or spirals. The stalk interacts also with the PH domain and the BSE. In the majority of dynamin superfamily members, the C-terminal helix of the helical bundles folds back to the GTPase domain, allowing a tight coupling of GTP binding/hydrolysis and oligomerization. (Faelber et al., 2011; Ford et al., 2011b) .

### 2.3.3 PH domain

The PH domain derives its name from pleckstrin, the major substrate of protein kinase C in platelets, where it was first identified. This domain is a membrane binding motif located at the tip of the stalk, at the opposite end relative to the GTPase domain. In dynamin this region mediates the binding to lipid membranes containing phosphatidyl-inositol phosphates, whereas the other members of the dynamin superfamily do not contain such a specialized domain. At the same position to interact with membranes Mx and DNML1 contain a large loop region, while EHD2 retains a polybasic helix. Instead, atlastin, mitofusin and BDLP have a transmembrane domain (Daumke and Praefcke, 2016). OPA1/Mgm1p is a special case, because it holds a N-terminal transmembrane domain, which is, however, not necessary for *in vitro* tubulation and not required for efficient liposome binding (DeVay et al., 2009). Thus,

has been suggested the existence of a membrane-binding region at the tip of the stalk that can specifically interact with negatively charged phospholipids of mitochondrial membranes (Meglei and McQuibban, 2009).

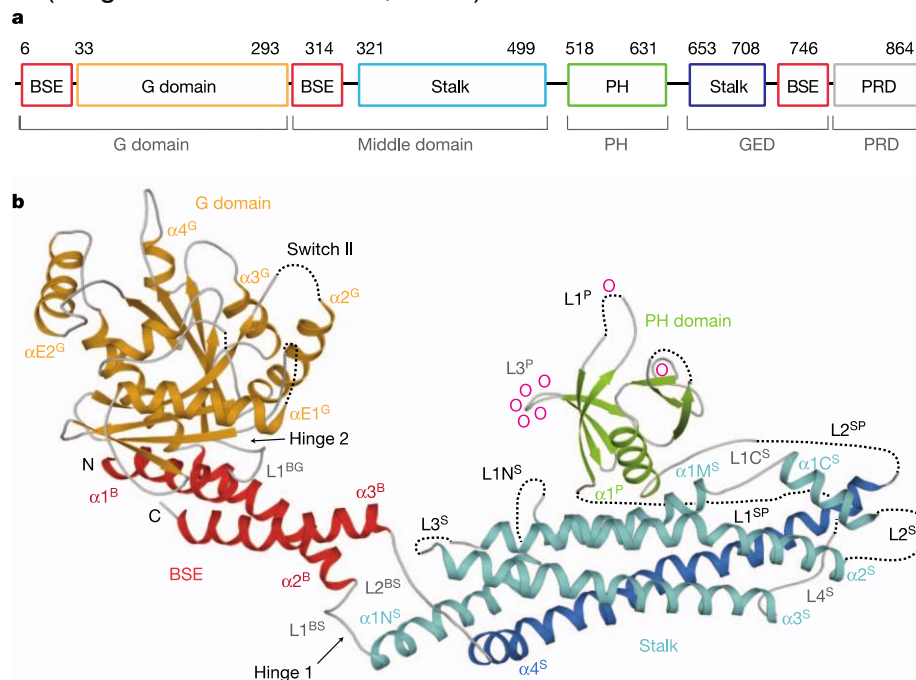


**Figure 8. Structure of nucleotide-free human dynamin 1.** (a) Structure-based domain architecture of human dynamin 1. The correspondent classical domains are indicated below. (b) Crystal structure (ribbon-type) of human dynamin 1. Not resolved regions are indicated with dotted lines. Domains and secondary structure elements are labelled and represented with the colour assigned in (a). Lipid-binding residues are indicated as o. From (Faelber et al., 2011)

## 2.4 GTPase activity

All dynamin proteins share a highly conserved GTPase core domain of about 300 aminoacids residues, comprising four motifs (G1-G4) that participate in specific interactions with the nucleotide. The structure of the GTP-binding domain consists of eight-stranded  $\beta$ -sheets, with six parallel and two antiparallel strands, surrounded by nine  $\alpha$ -helices (Niemann et al., 2001). DRP comprise the core G domain of Ras-related GTPases, six-stranded  $\beta$ -sheets, with one antiparallel strand, surrounded by five  $\alpha$ -helices (**Fig. 9a**). However, the specific insertions that extend the GTPase domain of dynamin proteins confer them unique biochemical and biophysical properties in respect of Ras GTPases.

Given the low affinity of dynamins for GTP, they do not require guanine nucleotide exchange factors (GEFs) or GTPase-activating factors (GAFs) for catalyzing nucleotide release. Furthermore, unlike Ras GTPases, they display a relatively high basal GTP hydrolysis rate and are predicted to be constitutively loaded

with GTP (Krishnan et al., 2001). These unique properties make DRP extremely sensitive to the changes of the cell energy status.

### 2.4.1 Oligomerization-stimulated GTPase activity

How is the GTPase domain dimerization, and thus the related GTPase activity, controlled to prevent futile cycles of GTP hydrolysis? A unique property of DRPs, unlike Ras regulatory GTPases, is their ability to self-assemble into oligomers on specific membrane templates. This characteristic behavior was found to modulate their GTPase activity. In fact, while Ras GTPase activity is controlled by GAPs, DRPs activity is controlled by self-oligomerization. Dynamin's basal rate of GTP hydrolysis cooperatively increases with protein concentration. Upon self-assembly or reconstruction in target membrane templates, GTP activity is further enhanced by more than 200-fold.

Despite the great advances in high-resolution structural biology, the molecular mechanisms triggering the basal GTPase activity of DRPs and its functional significance have remained mostly unresolved. An interesting recent work of Lu and colleagues (Lu et al., 2018) showed that the basal and the assembly-stimulated GTPase activities of Drp1 both play critical and distinctive roles in endocytic vesicle scission. Based on their findings with Drp1, they speculated that the basal GTPase activity of dynamin and Drp1 play a role in the generation of membrane-active dimers from tetramers or higher-order oligomers in solution, respectively. Their data suggested that the Drp1 basal GTPase activity shifts the oligomerization equilibria of Drp1 in solution toward a more favorable assembly-competent dimers that can bind membranes and induce the nucleation of higher-order helical self-assembly (**Fig.9b**).

To date, dynamin remains the most extensively characterized DRP and has become the archetype to study the structures and the dynamics of DRPs. In cytosol dynamin predominantly forms tetramers, consisting of two dimers dimerized via interface 2, the central region of the stalk. The two dimers are then associated to form tetramers via interface 1, at the tips of the interacting stalks adjacent to the GTPase domain and the BSE, and interface 3, at the distal end of the stalks (**Fig.9c**) (Faelber et al., 2011; Ford et al., 2011b). Further assembly of DRPs in solution is auto-



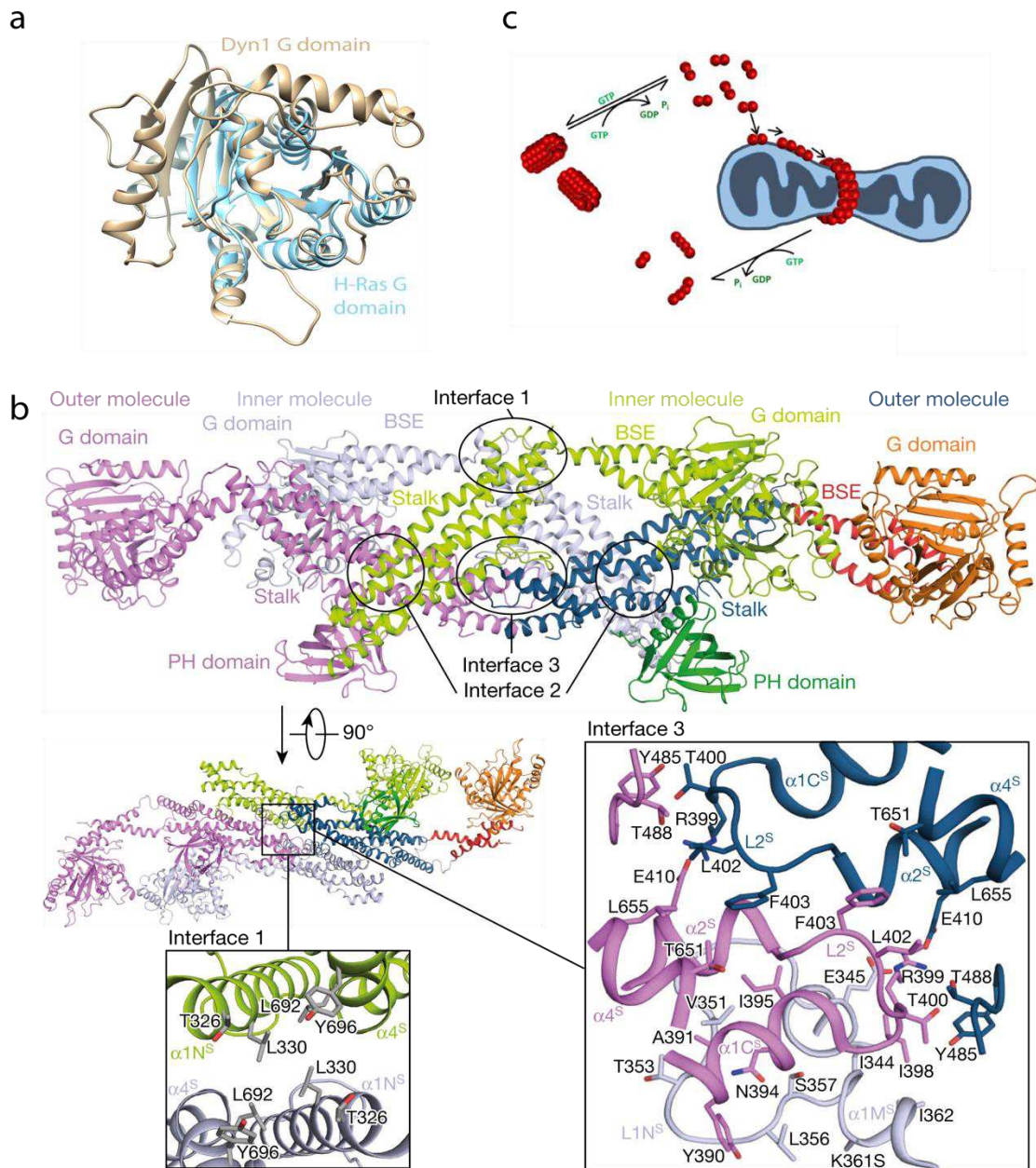


**Figure 9. Comparison of GTPase domains from different GTPases and oligomerization model of DRPs.** (a) Superposition of Dyn1 (tan, PDB ID: 1JX2) and H-Ras (sky blue, PDB ID: 121P) GTPase domains showing the extended  $\beta$ -sheet in Dyn1 (eight-stranded versus six-stranded in HRas) along with additional  $\alpha$ -helices and loops. (b) Model of Drp1 dimer nucleation and oligomerization-stimulated GTPase activity of Drp1 on OMM. Upon membrane binding, Drp1 optimizes the nucleotide-dependent G-domains dimerization to achieve a robust cooperative GTPase activity. Specific CL interactions locates the variable domain (VD) and relieves the strong VD-dependent steric interference of helical inter-rung G-domain dimerization result in an enhancement of the cooperative GTPase activity necessary for the membrane constriction and fission. Adapted from (Lu et al., 2018). (c) Structure of Dyn3 tetramer. The four molecules in the tetramer are coloured with different colours; in the molecule on the right each domain is individually coloured with the same colour-domain association as in Fig.8. The tetramer consists of two dimers, each formed via the central interface 2. The two dimers are connected via interfaces 1 (left box) and 3 (right box) to build the tetramer. One inner molecule is omitted from the detailed view for clarity. Adapted from (Reubold et al., 2015a)

inhibited by the interaction between PH and stalk domains (**Fig. 10a**). Instead, at the neck of clathrin-coated vesicles, dynamins oligomerize to mediate constriction and scission of the membrane. In a recent work, Reubold and colleagues (Reubold et al., 2015b) crystallized the dynamin tetramer suggesting a mechanism by which dynamins oligomerization at the membrane sites is linked to the release of intramolecular autoinhibitory interactions. In solution, the PH domain preferentially interacts with stalk domain in an autoinhibitory “closed” conformation. However, upon membrane recruitment, the PH domain is shifted along the stalk and toward the lipid surface releasing the autoinhibitory contacts (“open” conformation) (**Fig.10b**).

It follows that the PH domain of classical dynamins plays key functions in both membrane binding and oligomerization. It should be noted that the affinity of a single PH domain for lipid headgroup is low, so the strong interaction between dynamins and lipids relies on high avidity caused by protein oligomers. However, as previously described (Chapter 2.2), the DRPs do not possess a definite PH domain, unlike classical dynamins of the dynamin superfamily. Nevertheless, Dlps contain a PH-like domain, between the middle domain and the GED, that is involved in mitochondrial membrane binding (Adachi et al., 2016) and similarly MxA protein localizes in the endoplasmic reticulum (ER) (Accola et al., 2002). OPA1/Mgm1 has a mitochondrial targeting sequence followed by a transmembrane domain that allow the insertion of the protein in the IMM. OPA1 also contains a PH-like domain at the tip of the stalk involved in cardiolipin interactions (Ban et al., 2017; Ban et al., 2018; DeVay et al., 2009). Mitofusins/Fzo1 likewise contain a transmembrane domain that ensures the insertion of the protein in the external surface of the OMM (Rapaport et al., 1998; Rojo et al., 2002).

Dynamins self-assembly into high order helical polymers around membranes containing phosphatidylinositol-4,5-bisphosphate, by interacting with -SH and curvature-generating BAR-domain containing proteins. *In vivo*, dynamin helices are built by incorporation of dimer or tetramer elements rather than larger assemblies of dynamin (**Fig.9b**) (Cocucci et al., 2014; Grassart et al., 2014). From a thermodynamic point of view, this assembly mode involves many low-affinities contact sites, so that the formation of new interactions during helices assembly is compensated by the release of autoinhibitory contacts in the dynamin tetramer. The low-affinity interaction mode retains an important biological significance, because it facilitates reversibility and allows regulation of the dynamins assembly, for example through nucleotide binding, hydrolysis or phosphorylation (Reubold et al., 2015b). In conclusion, the strictly regulated oligomerization-stimulated GTPase activity on membrane binding ensures a thight control of GTPase activation and prevents futile cycles of GTP hydrolysis. Although DRPs exhibit different structural reorganizations and oligomeric states, this regulatory mechanism could be extended to all the dynamin superfamily members.

## 2.4.2 Mechanism of GTP hydrolysis

Upon self-assembly, conformational changes within G domain in the active site of dynamin superfamily proteins, prime them for GTP hydrolysis. Efficient GTP hydrolysis requires three conditions: (i) the presence of a water molecule for a nucleophilic binding with the  $\gamma$ -phosphate, (ii) the neutralization of the negative charge arising between the  $\beta$ - and  $\gamma$ -phosphates during the transition state, and (iii) the stabilization of the flexible switch regions within the catalytic core (Chappie et al., 2010). As mentioned before, dimerization of the nucleotide-binding pocket of G domains results in cooperative GTP hydrolysis, however, the catalytic mechanism differs among dynamins superfamily members.

GPBs and atlastins possess an internal arginine finger in the P-loop that rearranges upon G domain dimerization to stabilize the negative charge arose during the transition state of GTP hydrolysis (Ghosh et al., 2006; Praefcke et al., 2004). By contrast, the other DRPs and classical dynamins contain a monovalent cation (sodium or potassium) in place of the catalytic arginine, which interact with a conserved serine in the P-loop and two glycines on switch I to stabilize the transition state. Crystal structures of dynamin revealed also the presence of a network of hydrogen bonding, salt-bridge and chain interactions that contribute in the cooperative GTP hydrolysis and in the stabilization of the G domains dimerization (as described in Chapter 2.3.1) These features allow the *in cis* and *in trans* coordination of guanine base by the G4 loop. In particular, three key residues were found to be well retained among all dynamin superfamily members: Q40, S41 in the P-loop and D180 in the trans stabilizing loop. D180 forms in trans interactions across the dimer interface with Q40 and S41 of the partner domain stabilizing and position the P-loop and switch I for an efficient catalysis. Mutations of Q40, S41 and D180 impair assembly-stimulated GTP hydrolysis without significantly modifying basal GTPase activity, attesting the importance of these residues in the stabilization of G domain interactions (Chappie et al., 2010).

## 2.5 Mechanoenzyme

Dynamin superfamily proteins are described as mechanochemical enzyme, as they use the energy derive from GTP hydrolysis to perform a mechanical work that involves mainly the lipid membrane remodeling.

### 2.5.1 Conformational changes induced by GTP hydrolysis

What conformational changes occur upon GTP hydrolysis and how these are translated into a mechanical force? Structural analysis of few dynamins in various

nucleotide-loading states showed quite different structural changes between the different dynamin superfamily proteins.

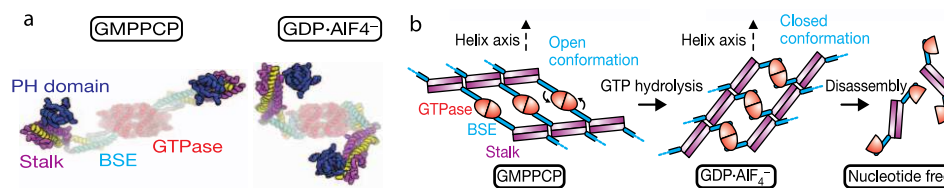


**Figure 10. Model for dynamin GTP cycle conformational changes.** (a) Nucleotide-dependent dynamin conformations. Left, GTP-bound state with open BSE conformation as fitted into the GMPPCP-bound dimer. Right, transition state of dynamin obtained from the GDP·AlF<sub>4</sub><sup>-</sup>-bound dimer. Transition from open to closed BSE conformation results in movement of stalk domains. The interactions between PH and stalk domains inhibits further assemblies of dynamin in solution. (b) Model explaining how the GTP hydrolysis-triggered BSE conformational change is transmitted to oligomerized stalk domains. Adapted from (Ford et al., 2011b).

The BSE domain of dynamin adopts two distinct conformation relative to the GTPase domain, according to the nucleotide state. In the GDP-bound state, the BSE tightly folds against the backside of the G domain in a “closed” conformation. GTP binding and self-assembly promotes the dimerization of G domains via an opening of the BSE relative to the GTPase domain (“open” conformation). Relaxation of the switch regions following GTP hydrolysis, may stimulate the dissociation of the G domain dimer. MxA dimerizes and change conformation upon GTP hydrolysis with a similar mechanism. Indeed, the dimeric DNML1 shows a “closed” BSE domain conformation in the presence of GTP and an “open” conformation for the nucleotide-free state. The movement of atlastin between the two nucleotide-loading state is completely different compared to dynamin. In the “open” GDP-bound conformation the two helical domains protrude in opposite directions with respect to the GTPase domain dimer in the center. The GTP binding leads to the tightening of the GTPase domain interface in a “closed” conformation, where the helical domains cross over and extend in parallel directions directly contacting each other. BDLP dimerizes in the GDP-bound form. The membrane-binding “paddle” regions at the tips of the two helical domains assemble in a “closed” conformation. In the presence of GTP, the “paddle” inserts into membrane and the two helical domains open and protrude in parallel orientation.

## 2.5.2 Oligomerization and mechanochemical activity

The G domains dimerization of fission DRPs occurs between adjacent rungs of the helical polymer formed around membrane tubules (**Fig.11**); whereas for fusion DRPs it occurs between flat lattices in opposing membrane bilayers (**Fig.12**). Instead, for Drp1 and Mx the nucleotide-dependent G domain dimerization may also occur upon self-assembly in solution. An interesting structure difference between fission and fusion DRPs is that the interfaces of G domain dimerization are smaller in fusion DSPs

(as MFN1-2) than in fission DSPs (as Dyn1). It has been speculated that this difference implies a reduced affinity for GTP and a lower rate of cooperative GTP hydrolysis of fusion compared to fission DRPs. This means that fusion DRPs would survive longer in a GTP-bound state, more favorable for protein polymerization at membrane sites, leaving more time to connect and fuse opposing membranes.

### ***Constriction model***

The energy of GTP hydrolysis is exploited by dynamin superfamily to perform a mechanochemical work on the membrane. Classical dynamins are involved in many vesicle scission reactions. The stalk domain mediates the assembly of a right-handed helical filament in a relax conformation, that allows the polymer to adopt different diameters (**Fig.11c**, state I). When the filament completes the oligomerization around the template, the GTP-bound G domains of adjacent turn dimerize and disrupt the inhibitory interaction between the BSE and the stalk. The GTP-induced powerstroke constricts the filament, if the membrane template is flexible (“constrictase” model in **Fig.11c-d** state IV), or compact it, if the template is rigid (“poppase” model in **Fig.11c** state II). The constriction of the dynamin helix induces a sliding of the adjacent filaments, that is observed as a rotary movement of the helix upon addition of GTP (“twistase” model in **Fig.11c**, state III), and eventually a cleavage of the membrane. To reach the constriction of the entire dynamin filament are necessary several cycles of local binding and release of adjacent dynamins, that may be triggered by GTP-dependent G domains dimerization and dissociation after GTP hydrolysis (Faelber et al., 2011).

### ***Homotypic and heterotypic fusion models***

The GTPase domains of atlastin dimerize in an open conformation across ER tubules. The GTP hydrolysis induce the cross-over conformation, pulling the opposing membranes toward each other and leading to membrane fusion (Faust et al., 2015; Liu et al., 2012). The GTP-bound form of BDLP oligomerizes in an open conformation membrane surface and induce a high curvature of the membrane, more likely due to the insertion of the “paddle” region. After GTP hydrolysis, BDLP is converted in its closed conformation and is released from the membrane. The fusion is then made easier thanks to the highly tight membrane (Low et al., 2009). The mechanism of OMM membrane fusion, triggered by mitofusins, was derives from structural data of BDLP and atlastins. The *cis* dimers of GTP-bound mitofusin1 interact *in trans* to generate a planar lattice of G domains dimers tethering membrane surface. GTP loading induce a conformational change from the “closed” tethering-constrained state to the “open” tethering-permissive state. In the open state, strained mitofusins allow a more efficient

tethering of two OMMs (at about 30 nm distance). The powerstroke generated by GTP hydrolysis, induce the return to the “closed” state, thus leading the opposing membranes to approach (**Fig.12a**). This process may be reversible and controlled by the local GTP and mitofusins concentration to avoid excessive tethering (Cao et al., 2017). Since a full-length OPA1 crystal structure is not yet available and the mechanism of IMM fusion is experimentally difficult to study, it is less well understood than OMM fusion process. It was proposed that OPA1 long isoform mediates tethering of outer and inner mitochondrial membranes, while the short isoform mediates

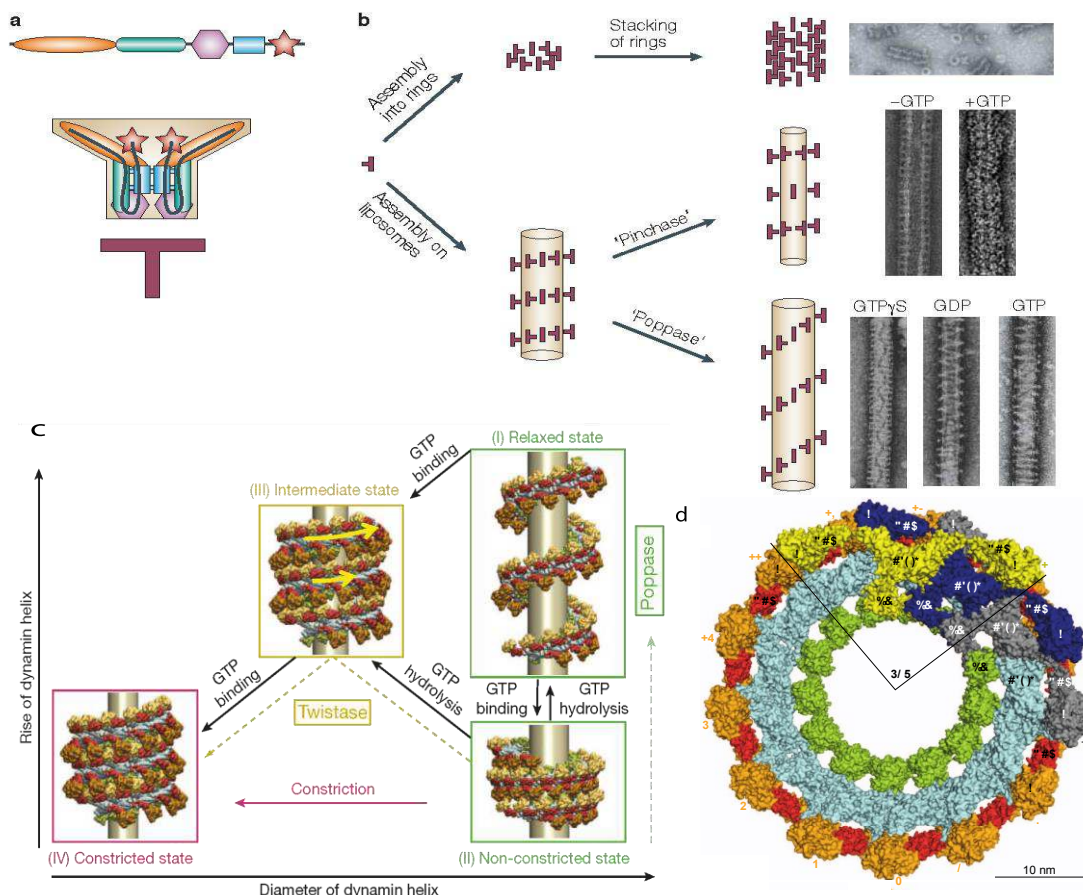


**Figure 11. Constriction model for dynamin oligomerization and function** (a) Classical dynamins, Dlps and Mx proteins assemble into stable dimers/tetramers involving inter- and intra-molecular interactions of GED, middle and GTPase domains. The dimeric building blocks for oligomeric Dyn1 resemble T-bar structures in which the PH domains are at the base of the T-bar. (b) Models of different assemblies in low ionic conditions or in the presence of GDP or GTP-analogues into rings and stacks of rings. These proteins induce *in vitro* tubulation of liposomes that are seen to be decorated with helical oligomers. Nucleotide hydrolysis by Dyn1 can lead to an increase in the pitch of the helix (“poppase” activity) or to a decrease in the tubule diameter (“pinchase” activity). (c) Proposed constriction mechanism of dynamin oligomers. Variations in the assembly of consecutive dynamin molecules lead to dynamin helices of different rise and diameter. For further explanations, see the main text. (d) Model of the oligomerized dynamin helix in the constricted state, view from top. Three dimers (1–3) are uniformly coloured. 13 stalk dimers complete one turn, the G domain of dimer (*i*) associates with the G domain of dimer (*i* + 10). (a,b). adapted from (Praefcke and McMahon, 2004), (c,d) from (Faelber et al., 2011)

membranes fusion in a GTP-dependent manner (DeVay et al., 2009; Zick et al., 2009a) All the described mechanisms concerning the intracellular membrane fusion require *trans* protein complexes for membrane tethering. However, Ban and colleagues (Ban et al., 2017) recently proposed a novel heterotypic IMM fusion model where L-OPA1 on one side of the membrane and CL in the other side are sufficient to promote fusion. In contrast, the CL-independent homotypic *trans*-OPA1 interaction mediates membrane tethering, supporting the cristae structure (**Fig.12b**). The authors discovered that the GTP-independent L-OPA1-CL binding mediates the tethering of the opposite membranes, while GTP hydrolysis is required membrane fusion. They succeeded in the reconstitution of the minimal *in vitro* IMM fusion machinery using proteoliposomes, consisting of PC and L-OPA1 expressed in silkworm, and liposomes, consisting of phosphatidylcholine (PC) and CL. However, the role of S-OPA1 has still not been clarified since S-OPA1 can promote homotypic CL-containing membrane fusion, but it is not sufficient to mediate alone a heterotypic membrane fusion (Ban et al., 2018)

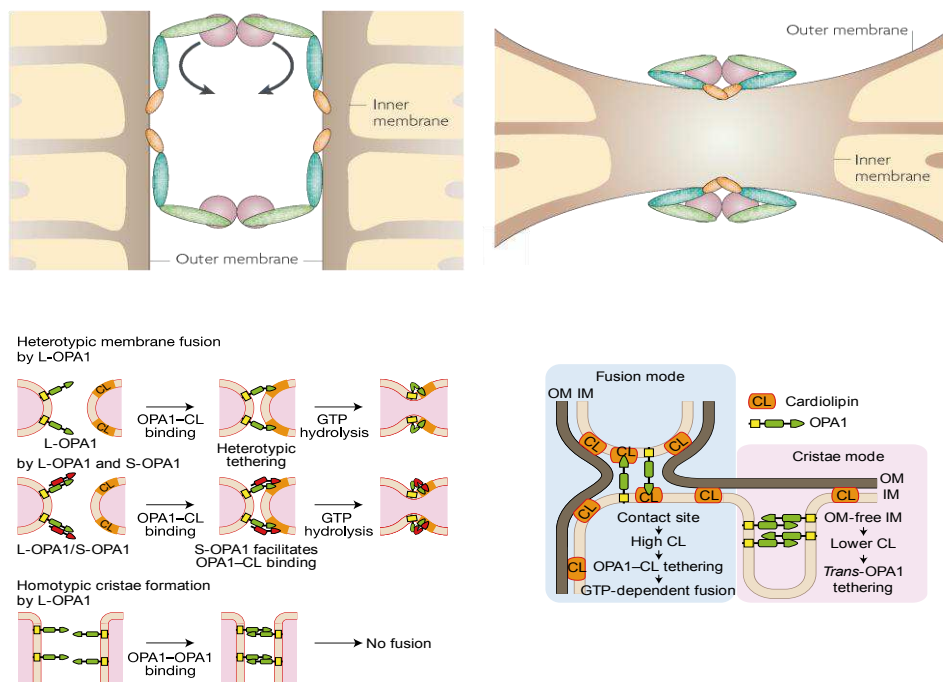


**Figure 12. Models for mitochondrial membrane fusion.** (a) Proposed model for MFN2-mediated OMM fusion. The MFN2 dimer binds OMMs with its hydrophobic paddle domain and fuses them through a conformational change induced by GTP hydrolysis in its trunk and paddle region. (b) Models for membrane fusion and tethering by OPA1 variants. Top left, l-OPA1 binds directly to CL for tethering of the opposite membrane, and then GTPase hydrolysis mediates membrane fusion. Middle left, s-OPA1 supports a bridge between L-OPA1 and CL. Bottom left, homotypic *trans*-OPA1 association mediates CL- and GTP-independent cristae membrane tethering. At right, model depicting the two modes of OPA1 function. In ‘fusion mode’ (left), CL-to- OPA1 pairing facilitates IM fusion. In ‘cristae mode’ (right), the homotypic interactions of OPA1 result in tethering IMs and formation of cristae. (a) adapted from (Knott et al., 2008), (b) from (Ban et al., 2017)





## Chapter 3 OPA1

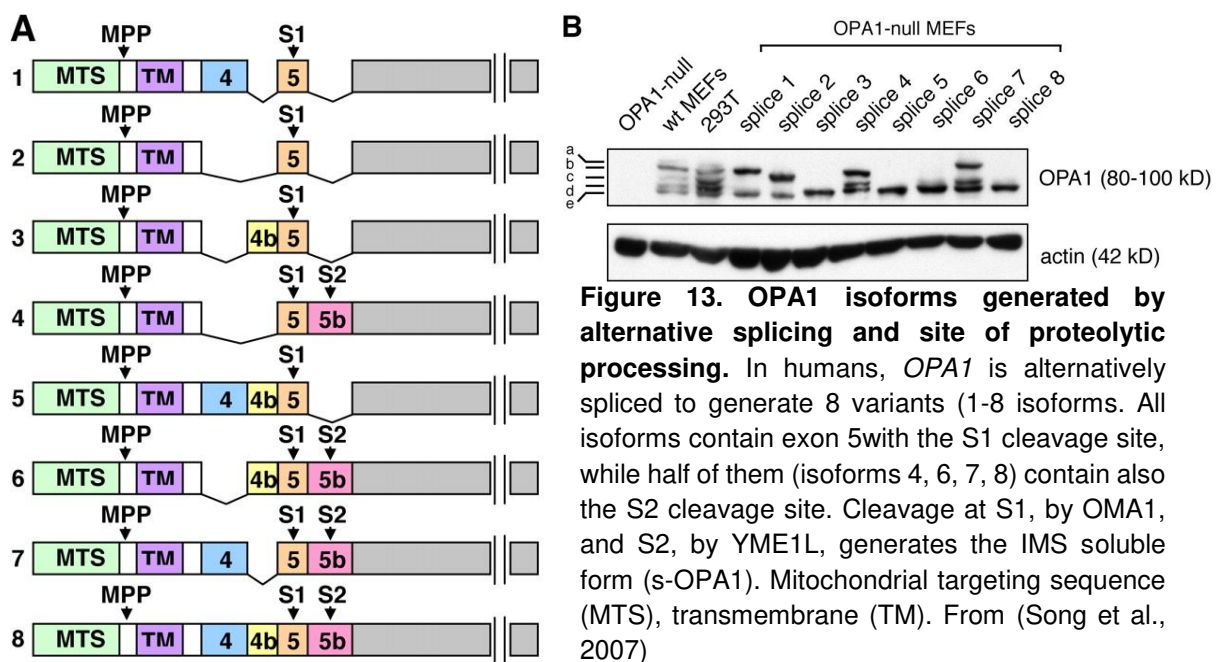
In 1992 a genetic screening in the budding yeast *S. cerevisiae* led to the discovery of a dynamin-like GTPase protein required for the maintenance of mitochondrial DNA (mtDNA), referred to as Mgm1p (Jones and Fangman, 1992). Later, Pelloquin and colleagues demonstrated that the conditional loss of function of Msp1, the *S. pombe* homolog of *Mgm1*, similarly affects the maintenance of mtDNA and results in growth arrest associated with respiratory deficiency (Pelloquin et al., 1998). In 2000 two groups independently identified the human orthologue *OPA1* gene, localized on chromosome 3q28-q29 and mutated in Autosomal Dominant Optic Atrophy (ADOA) disease (Alexander et al., 2000; Delettre et al., 2000). Further analysis showed that OPA1 is a component of the mitochondrial network and localizes in the IMS, tightly associated with the IMM (Delettre et al., 2000; Olichon et al., 2002). The functional relevance of OPA1 is emphasized by the ubiquitous expression of its transcripts in all tissues and its requirement during embryonic development (Davies et al., 2007). Furthermore, despite OPA1 shares only 34% and 30% identity to Mgm1p and Msp1, respectively, they exhibit evolutionary conserved function and secondary structure.

### 3.1 OPA1 gene and mRNA splicing transcripts

Delettre et colleagues mapped *OPA1* by fluorescence *in situ* hybridization (FISH) on 3q28-q29, within the locus of Optic atrophy type 1 (Delettre et al., 2000). The *OPA1* gene spans more than 100 kb and includes 30 coding exons and a last non-coding exon. The alternative splicing of 3 exons (4, 4b and 5b) generates 8 mRNA coding 8 different protein isoforms (Delettre et al., 2001). Remarkably, only exon 4 is evolutionary conserved, while exons 4b and 5b are both specific of vertebrates (Olichon et al., 2007a).

According to its mitochondrial localization, OPA1 transcripts are ubiquitously expressed, nevertheless significant distribution variability is found among the organs. Splicing variants containing exon 4 are consistently more abundant. For instance,  $\Delta 4/4b$  and  $\Delta 4b/5b$  isoforms predominate in fetal brain, retina, heart, lung, ovary and skeletal muscle,  $\Delta 4b$  showed the highest expression in kidney, liver and colon.  $\Delta 4/5b$

and  $\Delta 4/4b/5b$  isoforms are weakly expressed in all tissues, while the combination of no $\Delta$ OPA1,  $\Delta 4b$  and  $\Delta 5b$  is expressed in all tissues (**Fig.13**) (Delettre et al., 2001). These differential expressions might suggest distinct biochemical properties of the isoforms and their fine regulation by selective alternative splicing. All 8 OPA1 transcripts shared four conserved regions: a N-terminal mitochondrial targeting sequence (MTS), a transmembrane domain (TM) and, following the alternate spliced domains, a coiled coil domain (CC1) and the conserved dynamin region. Exon 4 domain does not exhibit any remarkable feature, while exons 4b and 5b provide two additional hydrophobic domains, TM2a and TM2b. 5b exon encodes also a coiled-coil domain (CC0) (**Fig.14**).



### 3.2 OPA1 protein: structure and processing

OPA1 protein exists in 8 isoforms of 924-1014 aminoacids, derived from the alternative splicing of exons 4, 4b and 5b. OPA1 belongs to the dynamin superfamily, with which it shares the minimal highly conserved architectural features: a large GTPase domain, a middle domain and a GTPase effector domain (GED). However, OPA1 differs from the “classical dynamins” (see Chapter 2.2) because of the absence of the PRD, thus it is referred to as a “dynamin-related protein”. Another specificity of OPA1 is a N-terminal basic mitochondrial targeting sequence (MTS) followed by a transmembrane domain (TM1), which anchors the protein to the IMM, and the three alternate spliced domains corresponding to exons 4, 4b and 5b. Exon 4 does not exhibit any particular feature, while exons 4b and 5b provide two additional hydrophobic domains, TM2a and TM2b. Exon 5b includes also a coiled-coil domain

(CC0). The next part of the protein comprises a coiled coil domain (CC1), and the conserved dynamin regions: the GTPase domain, the middle domain and the GED, containing an additional coiled coil domain (CC2) (Belenguer and Pellegrini, 2013). Moreover, a predicted PH-like domain is located between middle and GED domains (Fig.14).

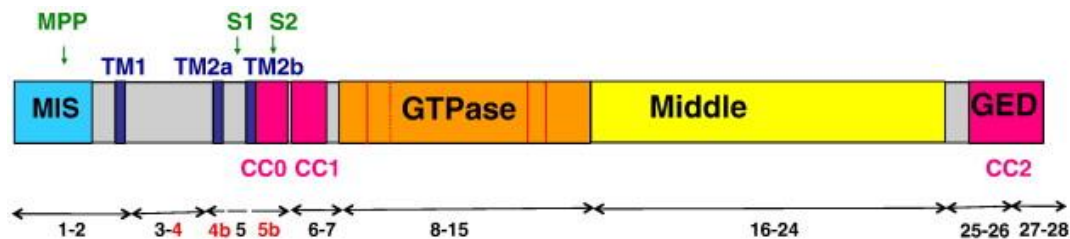


**Figure 14. Schematic representation of OPA1 domain.** OPA1 shares several structural features with dynamins: a GTPase domain containing the four consensus GTP binding sequences (red bars), a middle domain and a GTPase effector domain (GED) containing a coiled-coil region (CCII). Before the GTPase domain, OPA1 displays a mitochondrial targeting sequence (MTS) followed by a transmembrane region (TM1), two hydrophobic segments (TM2a and TM2b), and coiled-coil regions (CC). TM2a, TM2b, and CC-0 are only present in spliced exons 4b and 5b. The numbers below the structure correspond to OPA1 exons. Intra-mitochondrial proteolytic cleavage sites for mitochondrial processing peptidase (MPP), OMA1 (S1) and YME1L (S2) are indicated. (Belenguer and Pellegrini, 2013)From

OPA1 precursor proteins are targeted to mitochondria via the MTS, which is removed by the mitochondrial processing peptidase (MPP) upon protein import through the IMM. The MTS cleavage generates the membrane-anchored long isoforms (l-OPA1) (Olichon et al., 2002). Each l-OPA1 isoforms could be further proteolytically processed distinctly at S1 and S2 cleavage sites, on exons 5 and 5b respectively, to produce the short isoforms (s-OPA1) (Song et al., 2007). s-OPA1, lacking the TM1 domain, can be peripherally attached to the IMM or diffuse in the IMS and associate to the OMM (Ishihara et al., 2006; Olichon et al., 2002; Satoh et al., 2003).

Several issues concerning OPA1 processing remain to be clarify. All OPA1 isoforms contain an S1 cleavage site at exon 5 and four of them include also the S2 site in exon 5b (Ishihara et al., 2006) (Fig.13), the constitutive proteolytic processing of OPA1 keeps the balance between l- and s-isoforms during steady state conditions. Some evidences proposed the involvement of the presenilins-associated rhomboid-like protease (PARL) and the m-AAA protease paraplegin in the processing of OPA1 (Cipolat et al., 2006; Ishihara et al., 2006). However, it was demonstrated (Duvezin-Caubet et al., 2007) that OPA1 is normally processed in murine cells lacking paraplegin or PARL. Then, two IMM proteases were found to be involved in the proteolytic cleavage of OPA1: the metalloendopeptidase OMA1 at S1 (Ehses et al., 2009) and the ATP-dependent zinc metalloprotease YME1L at S2 (Ehses et al., 2009; Griparic et al., 2007; Song et al., 2007). Although regulatory mechanisms of YME1L

activity are poorly understood, it appears to be constitutively active during state conditions. Instead, *ex vivo* and *in vivo* experiments revealed an enhancement of OMA1 activity under stress conditions and mitochondrial membrane depolarization (Griparic et al., 2007; Guillery et al., 2008).

### **3.3 Functions**

OPA1 is a multifunctional protein that controls several fundamental cellular functions. In the last years, several cellular pathways or mechanisms, involving OPA1 activity, were described. OPA1 major functions will be described in the following sections, taking into account mitochondrial-confined processes (e.g. fusion, cristae maintenance, bioenergetics and mtDNA stability), and broader cellular processes (e.g. apoptosis, redox homeostasis, mitochondrial quality control and aging).

#### **3.3.1 Inner mitochondrial membrane fusion**

OPA1 is one of the few known actors that participate in the inner mitochondrial membrane dynamics. Along with mitofusins 1 and 2 is involved in mitochondrial fusion process. OPA1-depleted or OPA1<sup>-/-</sup> cells display mitochondrial fusion impairment (Chen et al., 2005; Song et al., 2007) and loss of function of OPA1 or Mgm1p by RNAi or gene knockout causes mitochondrial network fragmentation (Griparic et al., 2007; Guillou et al., 2005; Olichon et al., 2003a; Wong et al., 2000). Unexpectedly, OPA1 overexpression in mouse embryonic fibroblasts induced mitochondrial fragmentation (Griparic et al., 2004; Misaka et al., 2002), while elongation occurred in cells with already fragmented mitochondria (Cipolat et al., 2004; Olichon et al., 2002). This appears to be, however, a level-dependent effect since, high OPA1 overexpression is associated with fragmentation, while a mild overexpression slightly increases mitochondrial length (Cipolat et al., 2004). Furthermore, experiments in mitofusins knockout cells showed that OPA1 requires MFN1 for its profusion activity, while MFN2 is dispensable (Cipolat et al., 2004; Song et al., 2009). By visualizing real-time mitochondrial fusion, Liu et colleagues (Liu et al., 2009), identified two types of fusion events: the “complete fusion” and the “transient fusion”, in which mitochondria rapidly exchange soluble IMS and matrix components and then they separate again without affecting the morphology of mitochondria. Interesting, they found that the levels of OPA1 differentially influence the two types of fusion. The percent of complete fusion was maximal at moderate OPA1 overexpression and decreased or disappeared when OPA1 is lowered or highly increased. However, the transient fusion showed a complementary pattern, increasing at low or very high OPA1 levels, and decreasing at moderate levels.

Several works suggested that I-OPA1 may be sufficient to mediate mitochondrial fusion. The Oma1/Yme1l double knockout, where the formation of s-OPA1 is blocked, (Anand et al., 2014) and the expression of an un-cleavable isoform 1 in OPA<sup>-/-</sup> MEFs allow for normal mitochondrial fusion (Del Dotto et al., 2017; Lee et al., 2017). Moreover, a recent *in vitro* membrane fusion assay using purified human L-OPA1, expressed in silkworm, showed that I-OPA1 on one side of the membrane and CL on the other side are sufficient for fusion (Ban et al., 2017). However, this hypothesis remains controversial since a balance of s- and I-isoforms are required for a fully recovery of the normal mitochondrial network in Opa1<sup>-/-</sup> cells (Song et al., 2007). The involvement of s-OPA1 in fusion is less clear. s-OPA1 can tubulate membranes *in vitro*, but is unable to induce membrane fusion (Ban et al., 2010). *In vitro* liposome fusion experiments demonstrate that s-OPA1 alone is not sufficient to promote fusion, but it accelerates I-OPA1-dependent fusion and liposome binding (Ban et al., 2017). It was demonstrated that GTP hydrolysis is needed for OPA1-mediated fusion, however, it is still important to fully understand how GTP hydrolysis leads to fusion and what is the role of CL in the process. Regarding the two OPA1 forms, it was then proposed that the s- and I-OPA1 are both involved in mitochondrial fusion, although with different roles. Further investigations are however needed to better understand the whole process.

Moreover, it is becoming clearer that not only s- and I-OPA1 form, but also the presence of the eight OPA1 isoforms contribute to the development of a normal mitochondrial network morphology. In fact, the expression of at least two OPA1 isoforms and a balance of s- and I-form levels, are required for a full recovery of mitochondrial network in Opa1<sup>-/-</sup> MEFs (Del Dotto et al., 2017).

Finally, it is interesting to note how yeast and mammals retain some important differences regarding mechanisms of mitochondrial fusion. As an example, OPA1<sup>-/-</sup> cells produce an accumulation of multi-matrix structures resulting from fusion of OMM without IMM fusion (Song et al., 2009), while knockdown of Mgm1p show no OMM fusion (Sesaki et al., 2003). This suggest that fusion of OMM and IMM is not as tightly coupled in mammals as in yeast. Moreover, unlike mitofusins, OPA1 is sufficient only on one mitochondrion to promote fusion between two adjacent mitochondria *ex vivo*, while *in vitro* Mgm1p is required on both mitochondria (Meeusen et al., 2006; Song et al., 2009).

### **3.3.2 Cristae maintenance**

OPA1 is referred as a “mitochondrial shaping” protein for its role in cristae structure maintenance. During apoptosis, mitochondrial cristae undergo a remodeling process to allow the mobilization of cytochrome c and its release in the cytosol. OPA1 controls this process, as the disruption of OPA1 high molecular weight complexes is

a necessary condition for cristae junction widening and cytochrome c release (Frezza et al., 2006b). OPA1-deficient cells show drastic defects in cristae width and organization (Griparic et al., 2004; Olichon et al., 2003b), while OPA1 overexpression maintained tight cristae junctions and protected cells from apoptotic cell death (Frezza et al., 2006b). Furthermore, mild OPA1 overexpression corrects models of primary mitochondrial dysfunction with altered cristae shape (Civiletto et al., 2015, Varanita et al., 2015). As for mitochondrial fusion, a functional GTPase domain is needed for cristae maintenance (Del Dotto et al., 2017). OPA1 oligomers appear to participate in the formation and the maintenance of the cristae junction. It was proposed that transmembrane l-OPA1 forms oligomers with the soluble OPA1 form to “staple” the membranes of the cristae. Moreover, the disruption of OPA1 oligomers is a necessary condition for cristae junction opening and cytochrome c release during apoptosis. Nevertheless, the cristae modulatory activity of OPA1 during apoptosis is independent from mitochondrial fusion, as mitofusins are not required to exert this function. (Frezza et al., 2006b).

It is still a matter of debate the roles of s- and l-OPA1 forms in cristae organization. The manipulation of the proteases involved in OPA1 processing, lead to the idea that s-OPA1 is incompetent for cristae maintenance. *Oma1*<sup>-/-</sup> cells, where l-OPA1 is stabilized and the formation of s-OPA1 is prevented, display normal cristae morphology. *Yme1l*<sup>-/-</sup> cells, where the constitutive processing of OPA1 at S2 is prevented and s-OPA1 accumulates due to *Oma1* activation, exhibit a perturbation in cristae structure. Furthermore, the deletion of both *Oma1* and *Yme1l* restores cristae morphogenesis. (Anand et al., 2014). In addition, prohibitin 2 (*Phb2*) deletion, that induces OPA1 cleavage, results in mitochondrial fragmentation and cristae disruption, while reintroduction of l-OPA1 can restore the defects (Merkwirth et al., 2008). However, it is possible that the observed phenotypes may be caused by effects not directly related to OPA1 processing. Indeed, cells exclusively expressing s-OPA1 maintain normal cristae structure (Del Dotto et al., 2017; Lee et al., 2017), showing that the short form of OPA1 is competent for mitochondrial cristae maintenance, despite lacking fusion activity. Besides OPA1, other proteins were found to play a role in the shaping of mitochondrial cristae. Remarkably, MICOS subunits *Mic60/mitofilin* and *Mic25/CHCHD6* were found to directly interact with OPA1 (Ding et al., 2015), in particular, OPA1 is epistatic with *Mic60/mitofilin* in the biogenesis and remodeling of cristae junctions (Glytsou et al., 2016). OPA1 is at the center of a complex array of protein interaction comprising MICOS subunits and OMM components, like *Sam50* (Ding et al., 2015), operating in close functional association with phospholipids, as phosphatidylethanolamine and cardiolipin, to influence the properties of the IMM (Ban et al., 2018). Overall these results highlighted the role of OPA1 as the main actor in the biogenesis and maintaining of cristae junctions and in the control of apoptotic cristae remodeling.

### 3.3.3 Bioenergetics

Respiratory chain complexes (RCCs) localize inside the cristae at the IMM (Vogel et al., 2006), here they assemble into dynamic supercomplexes (RCSs), comprising different ratio of RCCs (Acin-Perez et al., 2008), for an efficient ATP production (Lapuente-Brun et al., 2013). Cristae shape regulates RCS stability and assembly, thus influencing respiratory and mitochondrial energetic efficiency (Cogliati et al., 2013b). In line with its role in fusion and mitochondrial ultrastructure, OPA1 was found to have a role in RCS organization and in the control of respiratory efficiency. Indeed, tighter cristae, resulting from elevated levels of OPA1, facilitate RCS assembly. In contrast, lower levels of OPA1 lead to an inefficient assembly of RCS thus resulting in less efficient ATP synthesis driven by complex I substrates, as observed in fibroblast from ADOA patients (Zanna et al., 2008).

OPA1 reduction produces a significant decrease of respiration, with no stimulation upon addition of uncoupler, a decrease of ATP levels and oxygen consumption rate driven by complexes I, II, IV, loss of RCS organization and incomplete assembly of complex V (Chen et al., 2005; Lee et al., 2017; Patten et al., 2014). In the mouse model of OPA1 mild overexpression, increasing levels of OPA1 induces cristae tightening, RCS assembly and mitochondrial energetic efficiency (Cogliati et al., 2013b). Also, OPA1-dependent cristae stabilization increases mitochondrial respiratory efficiency and diminishes mitochondrial dysfunction, cytochrome c release, and reactive oxygen species production (Varanita et al., 2015).

The analysis of fibroblast from ADOA patients, also highlighted the connection between OPA1 mutations and energetic defects. In particular, it was found defective oxidative phosphorylation with a decrease of ATP production (Lodi et al., 2004). Zanna and colleagues examined the effect of five pathogenic OPA1 mutations on the energetic efficiency and mitochondrial dynamics of fibroblasts from ADOA patients. They linked the OPA1 mutations to a mitochondrial respiratory chain dysfunction, mainly mediated by a reduction of complex I-driven ATP synthesis, caused by a direct interaction of OPA1 with the respiratory complexes and other proteins, such as the apoptosis inducing factor (AIF), subsequently confirmed by immunoprecipitation experiments (Agier et al., 2012; Takahashi et al., 2017; Zanna et al., 2008).

As a consequence of energetic disfunctions, OPA1 depleted cells show an impairing of the  $\text{Ca}^{2+}$  homeostasis, caused by a reduction of mitochondrial  $\text{Ca}^{2+}$  uptake and retention capacity (Kushnareva et al., 2013). Finally, OPA1 was also found to be required for transient matrix alkalization, or “mitopHlashes”. Possibly OPA1 has a role in the stabilization of RCS during mitopHlash biogenesis, allowing proton pumping to compensate drops in membrane potential thus preserving the ability of mitochondria to convert energy (Rosselin et al., 2017; Santo-Domingo et al., 2013).

### 3.3.4 mtDNA stability

Due to the role of OPA1 in mtDNA maintenance, Mgm1p, the OPA1 yeast homologue, was first identified (Jones and Fangman, 1992). Regarding OPA1, it was first hypothesized that its role in mtDNA maintenance may be linked to its mitochondrial cristae remodelling activity. A direct role of OPA1 in mtDNA maintenance was proposed by Elachouri et al. By demonstrating that OPA1 N-terminus containing exon 4b directly interacts with TFAM, POL $\gamma$  and mtDNA, the authors proposed that OPA1 contributes to nucleoid attachment to the IMM thus regulating mtDNA replication and distribution. (Elachouri et al., 2011). Since Mgm1p lacks the correspondence sequence encoded by OPA1 exon 4b, it follows that the mechanisms involved in mtDNA maintenance through OPA1 could be different in human and yeast.

Therefore, it seems then reasonable to suppose a connection between mtDNA maintenance and mitochondrial bioenergetics. Alteration of cristae morphologies, through OPA1 depletion, could lead to defective oxidative phosphorylation, which, in turn, could also originate from loss of mtDNA. To clarify this, Cogliati and colleagues produced an OPA1 conditional ablation mouse model that allows to dissociate cristae biogenesis from mtDNA maintenance. Contrary to chronic OPA1 depletion, that reduces mtDNA copy number and translation, acute OPA1 ablation alters cristae organization, affecting RCS assembly, respiratory function and growth, despite normal levels of mtDNA. Thus, mtDNA reduction appears to be a consequence of chronic fusion inhibition, rather than a direct effect of OPA1 ablation (Cogliati et al., 2013b). Supporting this theory, MFN1<sup>-/-</sup> and MFN2<sup>-/-</sup> cells similarly display higher levels of mtDNA mutation and mitochondrial genome instability (Chen et al., 2010).

Interestingly, mtDNA integrity appears to be specifically affected in ADOA “plus” patients carrying OPA1 gene missense mutations, in which the accumulation of mtDNA multiple deletions in postmitotic tissues contributes to the pathogenic mechanism (Amati-Bonneau et al., 2008). While ADOA patients showed slightly reduction or no change in mtDNA copy number (Zanna et al., 2008).

### 3.3.5 Apoptosis

Following a specific apoptotic stimulus, Bcl-2 family proteins permeabilize OMM and mitochondria undergo an ultrastructure remodeling. (Scorrano et al., 2002; Scorrano and Korsmeyer, 2003). OPA1 high molecular weight complexes, containing both s- and l-forms, resides at cristae junctions and maintain the cristae tightened sequestering cytochrome c in the intra-cristae compartment. Upon apoptosis induction, OPA1 complexes are the early targets of BID, BIM-1, BNIP3 and intrinsic cell death stimuli that rapidly dissociate the oligomers leading to cristae widening.



Cytochrome c is then mobilized from the intra-cristae compartment to the IMS and released across the OMM into the cytosol (Frezza et al., 2006b).

Whether OPA1 s-form, l-form or both confer resistance to apoptosis is still under debate. The selective loss of l-OPA1 was found to increase cells apoptotic sensitivity (Merkwirth et al., 2008). *Yme1l<sup>-/-</sup>* cells, where s-OPA1 accumulates due to the activation of OMA1, are more susceptible to apoptosis, whereas loss of OMA1, or both OMA1 and YME1L, protect cells against apoptosis. These experiments suggested that the l-form is responsible for the antiapoptotic effect of OPA1 (Anand et al., 2014). However, another explanation could rely on YME1L activity that, by maintaining the steady state balance of s- and l-forms of OPA1, may be necessary for the antiapoptotic activity, while OMA1 stress-induced processing of OPA1 abolishes its protective function.

Downregulation of OPA1 or pathogenic OPA1 mutations increase apoptosis sensitivity of cells. As an example, cells isolated from ADOA patients were found to be more sensitive to apoptosis (Olichon et al., 2007b). Conversely, OPA1 overexpression stabilizes OPA1 oligomers and inhibits tBID-induced cytochrome c mobilization, conferring resistance to apoptosis (Frezza et al., 2006b). Furthermore, expression of a disassembly-resistant mutant of OPA1 (Q297A) blocked the full release of cytochrome c and apoptosis (Yamaguchi et al., 2008). Recent *in vivo* works sustain the close connection between the role of OPA1 cristae remodeling regulation and cell sensitivity to apoptosis. Mild increase of OPA1 level protects mice from apoptosis-inducing tissue damage (Varanita et al., 2015) and improves the conditions of two mouse models of mitochondrial diseases, with profound neurological and muscular defects (Civiletto et al., 2015).

Finally, it must be said that, despite the beneficial effect of a mild overexpression of OPA1, high protein levels become toxic (Cipolat et al., 2004). Moreover, a strain-specific lifespan reduction was described, which followed an increase in the incidence of spontaneous cancer in OPA1 overexpressing mice (Varanita et al., 2015). Even in humans, higher levels of OPA1 were correlated with lung adenocarcinoma (Fang et al., 2012). Thus, the beneficial effect of OPA1 appears to be strictly regulated by the protein level.

### **3.3.6 Redox homeostasis**

Via oxidative phosphorylation, mitochondria are the main producers of the reactive oxygen species (ROS) within the cell. OPA1 controls RCS organization and cristae sharpening. Therefore, it could have an indirect role in the regulation of ROS production. Indeed, a mutual relationship between OPA1 and ROS was highlighted. Increased ROS levels were reported in lymphoblastoid cells with OPA1 mutations (Zhang et al., 2017), while an alteration in the levels of antioxidant enzymes was

discovered in fibroblasts from ADOA patients (Millet et al., 2016). Instead, OPA1 overexpression reduces mitochondrial ROS by stabilizing RCS (Varanita et al., 2015). On the other hand, overexpression of long-chain acyl-CoA synthetase 1 (ACSL1), which causes an increase of ROS, induces an alteration in the proteolytic processing of OPA1 (Tsushima et al., 2018).

Nevertheless, it should be recalled that mitochondria have their own ROS defense system and that ROS are not only harmful species, they are also important signaling molecules. Multiple aspects remain to be elucidated. In particular, the specific variations in ROS levels in the different cell compartments and how these correlates with normal and pathological conditions. Sometimes ROS production is not the direct cause of a disease, but it can contribute to an increased risk of developing other disorders (Holzerova and Prokisch, 2015). Understanding the mechanism of ROS scavenging, identify specific ROS targets and their function, investigate ROS evolutionary origin, might help to clarify specific pathological problems and potential therapies.

### **3.3.7 Mitochondrial quality control and aging**

Mitochondrial quality control (MQC) allows mitochondria to adapt to energetic and metabolic cellular demands, reduces mitochondrial damages, recycles or selectively degrades dysfunctional mitochondria via different pathways. MQC is regulated through mitochondrial network dynamics and thus also OPA1 takes part to this process. The maintenance of mitochondrial dynamics is particularly important in post-mitotic cells that do not divide, as neurons and cardiac and skeletal muscles. Therefore, MQC results fundamental to neurodegenerative diseases (Cho et al., 2010), but also to other pathological conditions, as cancer (Grandemange et al., 2009). Kane and colleagues recently identified a correlation between some pathological OPA1 mutations in ADOA and increasing autophagy, in case of missense mutations, or reduced mitochondrial turnover autophagy, in haploinsufficiency (Kane et al., 2017).

An interesting protein that couples mitochondrial dynamics with mitochondrial stress response and MQC is the OMM protein FUNDC1, which normally interacts with OPA1. However, under stress conditions, it undergoes dephosphorylation, while the FUNDC1-OPA1 complex is disrupted and FUNDC1 recruits DRP1 at the OMM (Chen et al., 2016). Other proteins that link OPA1 to MQC are the mitochondrial sirtuins SIRT3 (Samant et al., 2014), SIRT4 (Lang et al., 2017), SIRT5 (Polletta et al., 2015), involved in metabolic homeostasis. All the three sirtuins promote mitochondrial fusion through OPA1, in order to attenuate clearance of dysfunctional mitochondria, leading to their accumulation. This process is characteristic of senescence cells and became important during aging. As mentioned before, cells that do not divide are the most vulnerable to mitochondrial dynamics dysfunctions leading to MQC failures. For

example, old *Opa1*<sup>+/-</sup> mice display a selective loss of glutamatergic synaptic sites, that induces dendritic degeneration (Williams et al., 2012). Whereas, adult mice muscle-specific *Opa1* KO undergo to precocious senescence and premature death. In particular, the deletion of *OPA1* leads to ER stress, which via the unfolded protein response (UPR) and FoxOs, induces a catabolic program of muscle loss and systemic aging (Tezze et al., 2017). Furthermore, the enhancement of mitochondrial fusion by increasing the levels of *OPA1* and *MFN1* in old fibroblasts, induces a metabolic reprogramming from glycolysis to oxidative metabolism (Son et al., 2017).

## 3.4 Physiopathological relevance of *OPA1*

### 3.4.1 Autosomal dominant optic atrophy (ADOA)

#### ***OPA1 mutations and clinical features***

Autosomal dominant optic atrophy (ADOA) (OMIM 165500) is the most common inherited optic neuropathy, characterized by progressive visual impairment, starting during the first decade of life. It is associated with different severity grades of vision acuity loss, pallor of the optic disc, central scotoma (blind spot) and deficits in colour vision. The disease involves the primary selective loss of retinal ganglion cells (RGCs), located in the inner retina and projecting their axons via the optic nerve to the brain. This is accompanied by the bilateral degeneration of the optic nerve, that transmits the visual information from the photoreceptors to the lateral geniculus of the brain (Lenaers et al., 2012).

The two groups of Alexander and Delettre (Alexander et al., 2000) (Delettre et al., 2000) independently identified mutations in *OPA1* gene associated with ADOA. Until now, more than 350 *OPA1* variants were annotated in a dedicate locus-specific database (<https://databases.lovd.nl/shared/genes/OPA1>) (Ferre et al., 2015). Beside *OPA1*, other three genetic loci have been associated with ADOA: *OPA3*, *OPA4* and *OPA5*. Nevertheless, between 60% and 80% of ADOA patients exhibit *OPA1* mutations spread throughout the coding region of the gene, which are but mainly localized in the GTPase and in the middle domain of the protein, thus highlighting the importance of these domains for *OPA1* function. Most *OPA1* mutations are substitutions (65%) or deletions (26%), while few duplications (4.5%), indels (1%) and insertions (1%) were reported (**Fig.16**) (Ferre et al., 2015). Overall, there is a significant prevalence of nonsense and frameshift mutations that introduce premature stop codons. The truncated protein transcripts are then degraded via mRNA decay leading to a depletion of *OPA1* protein levels. However, were reported cases of asymptomatic patients were reported, albeit bearing the mutations.

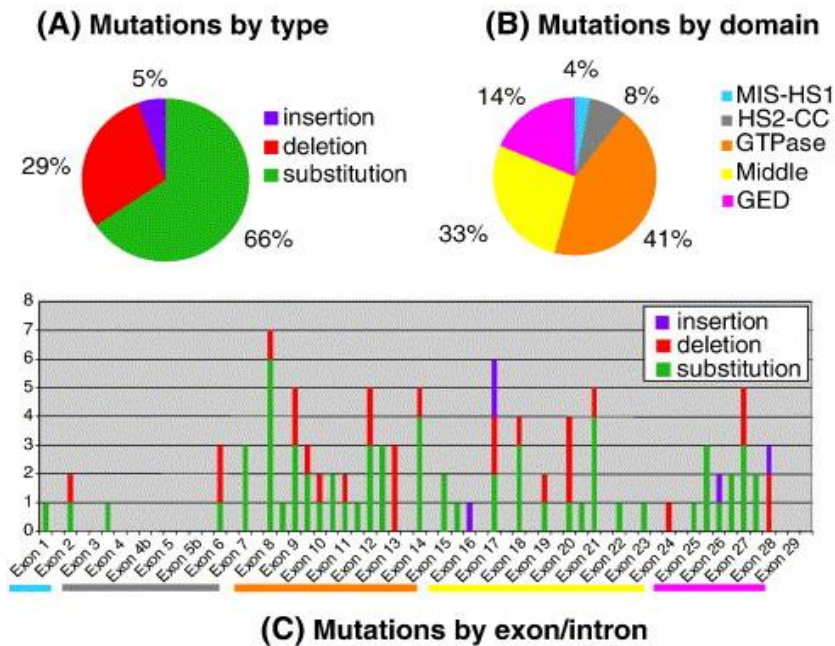


**Figure 15. Mutation spectrum of OPA1.** Distribution of the 96 mutations of OPA1 according to their type (a), domain (b) and location (c). In B, only mutations affecting exons are considered. In (c), spaces between two consecutive exons correspond to introns and coloured bars under exons indicate their belonging to OPA1 domains.

Furthermore, about 20% of patient with OPA1 mutations also develop additional extra-ocular signs that typically occur during the second or third decade of life (ADOA plus syndrome). These include sensorineural hearing loss, chronic progressive external ophthalmoplegia, proximal myopathy, ataxia and axonal sensory motor polyneuropathy (Amati-Bonneau et al., 2009).

### Physiopathology

Recently, many *in vivo* animal models of ADOA were developed to better clarify genotype-phenotype relationship and understand the physiopathological processes that lead to the disease. Some years ago, two mouse models of ADOA were generated, which were carrying a premature stop codon at the beginning of the GTPase domain (*OPA1*<sup>Q285STOP</sup>) (Davies et al., 2007) or a in frame deletion of 27 aminoacids (*OPA1*<sup>Q329-355del/+</sup>) (Alavi et al., 2007). Both *Opa1* models recapitulate the key features of the human disease. The homozygous mice mutants showed early embryonic lethality, while heterozygous mice expressed an age-dependent disease with progressive visual disfunctions, alongside loss of RGC, degeneration of ganglion cells and fiber layer, swelling or abnormal shape and myelinization of axons.

In both models full-length OPA1 levels were reduced by 50%, compared to wt animals, while truncated mutant proteins were undetectable. Furthermore, mutations leading to *OPA1* transcripts with premature terminations were found unstable and were assumed to be degraded by nonsense-mediated decay (Alavi et al., 2007). These findings supported haploinsufficiency as a crucial disease mechanism in ADOA. However, missense or in-frame mutations did not lead to reduction of the mutant transcript (Schimpf et al., 2008). Furthermore, no changes in OPA1 levels were observed in fibroblast from patients carrying missense in the GTPase domain, suggesting a dominant negative effect, rather than haploinsufficiency (Olichon et al.,

2007b). Noteworthy, negative dominance was also been proposed for multi-systemic forms of ADOA caused by OPA1 missense mutations in the GTPase domain (Amati-Bonneau et al., 2009).

In most cases ADOA is clinically presents as non-syndromic bilateral optic neuropathy. The principal genetic mechanism is haploinsufficiency caused by heterozygous OPA1 mutations resulting in a frameshift or by insertion of a stop codon (Cohn et al., 2007). By contrast, syndromic ADOA plus (about 20% of all ADOA cases) shows a complicated phenotype with extra-ocular signs, peripheral neuropathy, deafness, cerebellar ataxia, spastic paraparesis and myopathy. Dominant negative effect was proposed for syndromic form, triggered by heterozygous missense mutations of OPA1. (Yu-Wai-Man et al., 2010a).

It is still unclear the mechanism through which the impairment of OPA1 functions contribute to the ADOA pathogenesis. OPA1 is a multifunctional protein implicated in numerous cellular pathways. In mitochondria OPA1 mediates the IMM fusion, maintains cristae tightness, mtDNA stability and bioenergetics. Moreover, OPA1 dysfunction were been linked to dysregulation of cellular redox homeostasis, increased apoptosis sensitivity and aging. Thus, to identify the link between genotype and phenotype of the disease, ADOA models and patients' samples were assessed for the effect of OPA1 mutations.

Adult heterozygous *OPA1*<sup>Q285STOP</sup> mice revealed an increased mitochondrial fragmentation in fibroblasts (Davies et al., 2007) and elevated levels of autophagy in RGCs (White et al., 2009). Mitochondrial fragmentation correlates with an impaired fusion. Moreover, it was demonstrated that mitochondria undergoing autophagy showed reduced OPA1 levels and mitochondrial membrane potential, and mitochondrial fragmentation facilitated this process (Twig et al., 2008). Similarly, skin fibroblasts from ADOA patients also revealed mitochondrial network fragmentation, decreased mitochondrial membrane potential and defects in oxidative phosphorylation (Amati-Bonneau et al., 2005).

Using phosphorus magnetic resonance spectroscopy, Lodi and colleagues demonstrated aberrant ultrastructure and impaired bioenergetics, with reduced rate of mitochondrial ATP production, in fibroblasts of patients carrying a 4 bp deletion in exon 27 of *OPA1* (Lodi et al., 2004). They concluded that defective oxidative phosphorylation in skeletal muscle is a hallmark of OPA1-related ADOA (Lodi et al., 2011), in agreement with the role of OPA1 in stabilizing respiratory chain supercomplexes (Cogliati et al., 2013b). These deficiencies were explained by a reduced activity of Complex IV (COX), as lower levels of the mitochondrial-encoded subunits COX I and COX II (but not nuclear-encoded COX Va subunit) were found in OPA1 mutated fibroblast (Kushnareva et al., 2016).

Since OPA1 is implicated in the maintenance of mtDNA (Elachouri et al., 2011), one could speculate that reduction in oxidative phosphorylation and Complex IV subunits proteins are linked to mtDNA instability. 2- to 4-fold increase in mtDNA copy number, but low levels of WT mtDNA, was observed in COX-negative fibers of ADOA and ADOA+, the latter with greater mtDNA proliferation. The authors of the study proposed a “maintenance of wild-type” hypothesis, where secondary mtDNA deletions induced by OPA1 mutations stimulate a compensatory mitochondrial proliferation to maintain adequate levels of WT mtDNA. However, when deletion reach a critical level, mitochondrial proliferation leads to replication of the mutant species at the expense of WT mtDNA, resulting in the loss of COX activity (Yu-Wai-Man et al., 2010b). Subsequent analysis in ADOA mice models and skin fibroblast from ADOA patients with decreased COX activity did not display any change in the mtDNA copy number (Agier et al., 2012; Kushnareva et al., 2016). Whether OPA1 dysfunction leads to a reduction in mtDNA is still debated. Moreover, RCS assembly is facilitated by increased OPA1 levels and tighter cristae. It was demonstrated that chronic OPA1 depletion reduces mtDNA copy number and translation. Whereas OPA1 acute ablation preserves normal levels of mtDNA and translation of mitochondrially encoded subunits, but leads to disorganized cristae morphology, defects in RCS assembly, respiratory function and cell growth (Cogliati et al., 2013b). Further studies will be needed to determine whether OPA1 haploinsufficiency in ADOA could directly affect RCS assembly.

Silencing of OPA1 increase cell sensitivity toward different apoptotic stimuli (ref). Indeed, was reported an increased susceptibility to cell death of fibroblast from ADOA patients (Olichon et al., 2007b; Zanna et al., 2008), and improved sensitivity to staurosporine of *OPA1*<sup>Q285STOP</sup> MEFs (Kushnareva et al., 2016). Surprisingly, ADOA fibroblasts are more resistant to ER stress-inducers tunicamycin and thapsigargin (Kushnareva et al., 2016). Since ER stress leads to a rapid Ca<sup>2+</sup> release from the ER and an increase of Ca<sup>2+</sup> in mitochondria, this could be explained by a compromised Ca<sup>2+</sup> uptake from OPA1-depleted RGCs (Fulop et al., 2015; Kushnareva et al., 2013).

### ***Is ADOA tissue specific?***

Since OPA1 is ubiquitously expressed in tissues, what makes the optic nerve so vulnerable to mitochondrial dysfunction? To date no conclusive answers were provided. Neurons have a high energy demand required for the conduction of electrical impulses through the anterior unmyelinated portion of the axons and the long course of the axons. These regions reside at a considerable distance from the cell body, where the biogenesis of the mitochondria occurs. Thus, bioenergetic defects, following OPA1 inactivation, may impair the conduction of action potentials and the mitochondrial transport. Then, why are RGCs predominantly affected by ADOA disease? Photoreceptors are the most oxygen-consuming cells in the retina, nevertheless light perception and signal processing is not impaired, but signal

transmission from the eye to the brain is altered (Heiduschka et al., 2010). It was suggested that the particular vulnerability to OPA1 inactivation of RGC cells may result from two aspects: (i) a particular sensitivity to mitochondrial membrane disorders inducing mitochondrial dysfunction (Amati-Bonneau et al., 2005; Chen et al., 2005; Lodi et al., 2004), or (ii) mitochondrial mislocalization. In fact, mitochondria accumulate in the cell body of RGCs and in the varicosities of intraretinal unmyelinated axons, while relatively few mitochondria reside in the myelinated parts of axons (Andrews et al., 1999; Bristow et al., 2002; Wang et al., 2003).

### ***A heterogeneous clinical representation***

The clinical representation of ADOA is heterogeneous. Not all the family members that carry pathogenic mutations develop visual impairments. Although most of the OPA1 mutations are associated with a non-syndromic, slowly progressive form of optic neuropathy, there are mutations linked to a broad range of extra-ocular symptoms. An intriguing example that discards the hypothesis of a tissue specificity of ADOA, is the R445H OPA1 mutation associated with a syndromic form of sensorineural hearing loss, ptosis, and ophthalmoplegia (Amati-Bonneau et al., 2003; Payne et al., 2004). The whole spectrum of the disease, from unaffected, to non-syndromic, to syndromic patients was observed within the members of one family carrying the same OPA1 mutation (Li et al., 2005). It is not clear why the R445H mutation, located within the GTPase domain of OPA1, cause a wider spectrum of the disease, whereas other mutations are associated with only optic atrophy. Auditory performances examination of ADOA patients, screening for OPA1 mutations in patients suffering sensorineural hearing loss and investigation for muscular, cardiac and neuronal deficits that could indicate a more generalized mitochondrial dysfunction, will be particularly helpful to understand the molecular basis of the ADOA plus syndrome.

In conclusion, this scenario depicts a “continuous” clinical disease, rather than a “discrete” one, which may suggest the implication of secondary modulatory factors on the phenotypic expression of the shared OPA1 mutation. Identifying the underlying molecular pathways and the principle mechanism that are affected in ADOA, will shed light to the complex processes that lead to specific dysfunctions in classic and syndromic forms of ADOA

### **3.4.2 Cancer**

Higher OPA1 protein levels were first reported in lung adenocarcinoma cells (Fang et al., 2012; Garber et al., 2001). Strikingly, high OPA1 levels correlate with an increase in resistance to conventional chemotherapeutics, such as cisplatin, and a lower survival rate (Fang et al., 2012; Kong et al., 2014; Zhao et al., 2012). Indeed, knockdown of OPA1 in hepatocellular carcinoma cells sensitized them to cytotoxic

treatment (Zhao et al., 2012) and indirect Akt-dependent downregulation of OPA1 facilitated cytochrome c release and apoptosis in lung cancer cells (Cho, 2011).

Mitochondrial dynamics ensure organelle plasticity and are also associated with several human disorders and tumors (Wallace, 2005). Mitochondrial-shaping proteins were first related to cancer because of their role in apoptosis, which is altered in cancer cells. However, recent studies revealed that changes in mitochondrial fission-fusion balance confer cancer cells the ability to adapt their metabolism to environmental modifications, as hypoxia, starvation, stress signals and drug treatments. Among all shaping-proteins, OPA1 activity exerts a central role in apoptosis resistance. It controls, in a fusion-independent manner, the mitochondrial cristae remodelling process, to achieve the complete release of cytochrome c from mitochondria, which is essential to activate the caspases and the apoptotic cascade (Frezza et al., 2006b; Scorrano et al., 2002). Downregulation of OPA1 leads to mitochondrial network fragmentation and increase cell sensitivity towards apoptosis, while mutations that abolish OPA1 catalytic activity impair its antiapoptotic function. Interestingly, it was discovered that OPA1 is overexpressed in different type of cancers and it correlates with a poor prognosis and an increased chemotherapy resistance (Fang et al., 2012). Moreover, knockdown of OPA1 in hepatocellular carcinoma cells sensitized them to cytotoxic treatment (Zhao et al., 2013) and Akt-dependent downregulation of OPA1 facilitated cytochrome c release and apoptosis in lung cancer cells (Hwang et al., 2012).

A pioneer study of Fang and colleagues discovered a significant overexpression of OPA1 in lung adenocarcinoma (LADC) patients. In particular, OPA1 expression correlates with expression levels of other mitochondrial-associated proteins MFN1, DRP1, and ATAD3A. Statistical analysis showed that OPA1 overexpression correlates with cell differentiation, histopathological tumor subtypes, stage, and lymphovascular invasion. Furthermore, OPA1 increases cisplatin resistance via inactivation of caspase-dependent apoptosis and is associated with poor prognosis and metastasis. Remarkable, higher OPA1 expression is also found in early stage tumors (Fang et al., 2012). Lung cancer is one of the leading cause of cancer-related death worldwide. The 5-year survival rate is approximal 18%. Poor prognosis mostly correlates with the small number of lung cancer cases diagnosed at a localized stage, for which the 5-year survival rate is 56% (Siegel et al., 2018). This claims for the need of novel targets for therapeutic interventions in early stages of the disease. Recently, Anderson and colleagues discovered that genes controlling mitochondrial dynamics are recurrently amplified in multiple tumor types. Moreover, altered expression of DRP1 and OPA1 lead to different sensitivities toward specific anticancer drugs (Anderson et al., 2018).

A rising number of studies examined the possibility of pharmacologically target mitochondrial proteins as a powerful method to reactivated cell death program and



sensitize chemoresistant cell to therapies. There are many advantages in using mitochondrial dynamics-targeted drugs: (i) they can escape from the resistance mechanisms of the conventional therapies. Pro-apoptotic drugs act on signalling pathways that converge on mitochondria. Since mitochondrial apoptosis pathways are frequently dysregulated in cancer (overexpression of Bcl-2 proteins or caspase inhibitors), cells fail to properly respond and become resistant. (ii) In contrast to chemotherapeutic treatments that target all proliferating cells (of either normal or cancerous tissue) small-molecule inhibitors of mitochondrial proteins are more specific and with less toxic side-effects.



## Chapter 4 Apoptosis

The term “apoptosis” was coined by Kerr, Wyllie and Currie in 1972 to describe a “mechanism of controlled cell deletion, which is complementary to mitosis in the regulation of animal cell population” (Kerr et al., 1972). “Apoptosis” derives from the Greek word “απόπτωση”, that means “falling off” of leaves from trees, to suggest the detachment of apoptotic cells from their natural surroundings, following programmed cell death.

In multicellular organisms, apoptosis occurs normally during development (Brill et al., 1999) and in adulthood, as a homeostatic mechanism to maintain cell populations in tissues (Henson and Hume, 2006). Apoptosis also play an important role as a mechanism of defence. In the regulation of immunity (Cohen et al., 1992) apoptosis performs two main tasks: (i) the negative selection of non-reactive leukocyte precursors and (ii) the negative selection of thymocytes that show reactivity against antigens of the own body (Pinkoski et al., 2006). Apoptosis is involved in tissues repair, as regulation of wound healing (Greenhalgh 1998). Furthermore, through apoptosis cells that represent a potential risk for the organism are eliminated, such as virally infected cells, misplaced or damaged cells (Norbury and Hickson, 2001). Thus, a precisely tuned apoptosis regulation appears of vital importance for the organism. Consequently, dysregulation of apoptosis is associated with a wide number of diseases: excessive apoptosis results in degenerative disease, while apoptosis deficiencies can lead to autoimmunity or cancer (Danial and Korsmeyer, 2004).

It is important to note that not all cells respond in the same way to a death stimulus. In some cases, the type and the degree of stimuli determines whether to commit or not cell death, and, if the cell die, the type of death response. For example, at low doses, hypoxia, irradiation, cytotoxic chemotherapeutic drugs can induce apoptosis, but the same stimuli at higher doses can result in necrosis. Furthermore, some hormones, as glucocorticoids, could lead specific cells (thymocytes) to apoptotic death, although other cells are unaffected (Gruver-Yates and Cidlowski, 2013).

Considering the relevance of apoptosis for the organism, many novel therapeutic and diagnostic interventions are now attempting to target genes and proteins involved in the regulation and execution of apoptosis, both to restore defective apoptosis or to suppress excessive apoptosis. Although there are a wide variety of

stimuli and conditions, both physiological and pathological, which can trigger apoptosis, not all cells will necessarily die in response to the same stimulus. Irradiation or drugs used for cancer chemotherapy results in DNA damage in some cells, which can lead to apoptotic death through a p53-dependent pathway. Some hormones, such as corticosteroids, may lead to apoptotic death in some cells (e.g., thymocytes), although other cells are unaffected, nor stimulated.

The objective of this thesis work will be focus on the key mechanisms of intrinsic apoptosis pathway. Thus, after providing an overview of the main apoptotic pathways, we will further investigate the role of mitochondria and mitochondrial-shaping proteins, in particular OPA1, in the regulation of apoptosis. How is the deregulation of mitochondrial-shaping proteins leading to the onset of diseases, and how could these proteins be exploited to find a cure?

Depending on the cell type, the death stimulus and the relative role of mitochondria, apoptosis can be induced via two different pathways, illustrated in **Fig.16** that converge in the caspases activation. (i) The extrinsic pathway, triggered by an external signal, activate death receptors on the cell surface, leading directly to caspase 8 activation. (ii) The intrinsic pathway is originated by an internal cell damage signals, as DNA or organelle damage, hypoxia or lack of nutrients, and is regulated by mitochondria. The extrinsic and intrinsic pathways ultimately converge on the execution pathway of caspases activation. The cleavage of caspase-3 and activation of the executioner caspases results in DNA fragmentation, degradation of nuclear and cytoskeletal proteins, as laminin and DNA repairing enzymes, culminating with the characteristic apoptotic morphological changes: nuclear membrane breakdown, externalization of phosphatidylserine and formation of apoptotic bodies expression of phagocytic cell receptors ligands and lastly uptake by phagocytic cells (Hengartner, 2000).

## 4.1 The extrinsic apoptotic pathway

The extrinsic signalling pathway is triggered by the interaction between a pro-apoptotic ligand and a death receptor on the plasma membrane. Death receptors belongs to the tumor necrosis factor (TNF) receptor superfamily. The TNF receptor family includes more than 20 proteins, that regulates many signal transduction pathways, including apoptosis and survival, proliferation, differentiation and inflammation. They share cysteine-rich extracellular domains and a conserved cytoplasmic domain of about 80 aminoacids, the “death domain”, which plays transmit the death signal from the surface of the cell to intracellular signalling pathways (Ashkenazi and Dixit, 1998). The sequence of events that define the extrinsic apoptotic pathway are best described for the FasL/FasR and TNF- $\alpha$ /TNFR1 models. Ligand

binding to the TNF receptors results in the recruitment of adaptor proteins to form the death inducing signalling complex (DISC). This complex recruits procaspase-8 molecules, resulting in the activation of caspase-8 via the proximity induced autoproteolytic processing. Caspase-8 in turn activates the downstream cascade of effector caspases. including caspase-3, 6 and 7 (Walczak and Krammer, 2000).

The two apoptotic pathways are not, however, completely independent from each other. In fact, in certain cell types, it was proven a cross-talk provided by

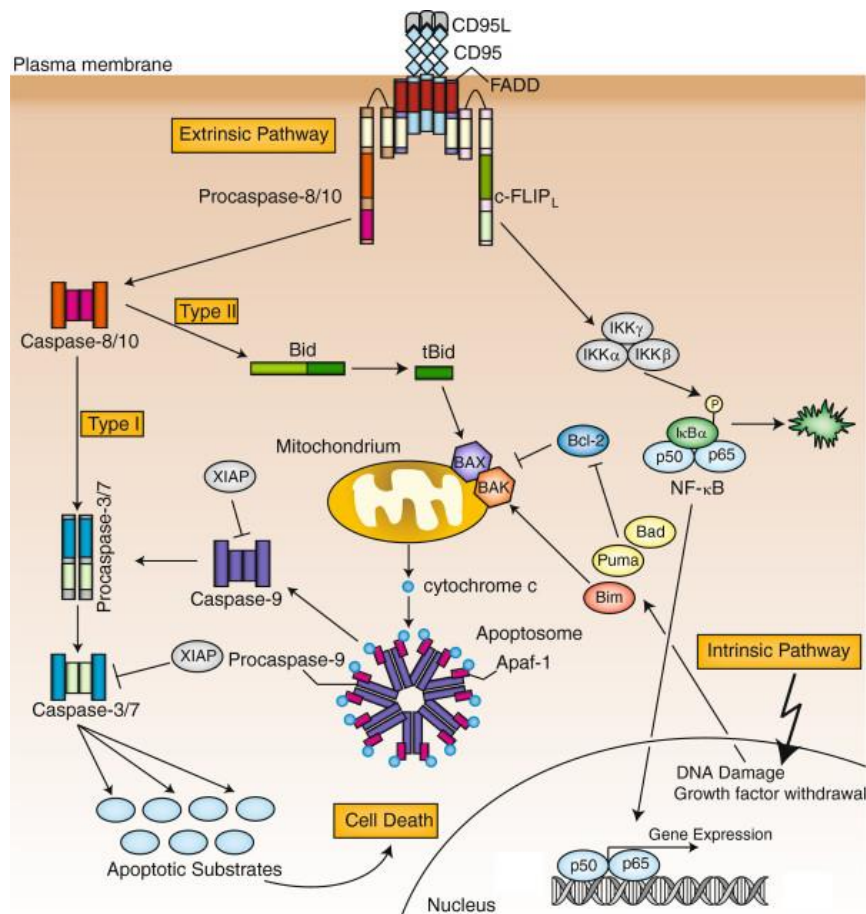


**Figure 16. Overview of apoptosis pathways.** Apoptosis can be induced by extracellular (extrinsic) or intracellular (intrinsic) stimuli. The extrinsic pathway is initiated via stimulation of DRs, e.g. CD95 or TRAIL-R, on the cell surface. Stimulation of CD95 results in the recruitment of different proteins including FADD, procaspase-8, procaspase-10 and c-FLIP proteins, which form the death-inducing signaling complex (DISC). Procaspase-8 is activated at the DISC which is regulated by c-FLIP proteins. Active caspase-8 cleaves and activates effector caspase-3 and -7 and/or the Bcl-2 protein Bid. The truncated Bid (tBid) translocates to the mitochondria, triggering OMM permeabilization and the release of cytochrome c and other pro-apoptotic proteins into the cytosol. Cytochrome c form with procaspase-9 the apoptosome. Procaspase-9 activates procaspase-3 and -7 resulting in cell death. Type I cells efficiently activate caspase-8 and subsequently effector caspases without amplification through tBid-mediated OMM permeabilization. Type II cells form less DISC and therefore rely on Bid cleavage and the intrinsic amplification loop. Additionally, CD95 can initiate non-apoptotic pathways, such as NF- $\kappa$ B or MAPK and cell survival. The intrinsic pathway is activated by various intracellular stimuli, such as DNA damage or growth factor withdrawal. From (Schleich and Lavrik, 2013)

caspase-8. In “type I” cells, there are sufficient amounts of activated caspase 8 to trigger the activation of effector caspases and to induce apoptosis in the absence of the mitochondrial outer membrane permeabilization (MOMP). Instead, the “type II” cells, as hepatocytes, produce insufficient amounts of active caspase 8 to activate downstream caspases, thus requiring the activation of the mitochondrial amplification loop and the MOMP to induce apoptosis. Therefore, caspase-8 can cleave other caspases (“type I” cells) or BID protein (“type II” cells), generating the active 15kDa truncated BID (tBID). tBID translocate to mitochondria to activate the mitochondrial amplification loop and promoting the cytochrome c release (**Fig.16**) (Li et al., 1998; Luo et al., 1998).

## 4.2 The intrinsic apoptotic pathway

The intrinsic apoptotic pathway originated from non-receptor-mediated stimuli that generate intracellular signals. Examples of these signals are radiations, hypoxia, hyperthermia, viral infections, toxins, but also the absence of specific growth factors, hormones or cytokines, which cause the loss of apoptosis suppression. These signals converge to mitochondria, where cytochrome c and other proapoptotic proteins are released, following the MOMP. In the cytosol, cytochrome c binds the apoptotic protease-activating factor 1 (APAF1), inducing its oligomerization originating the apoptosome. It recruits and activates the initiator caspase-9, which cleaves and activates the effector caspase-3 and 7. Furthermore, the mitochondrial released proteins Smac/Diablo and Omi/HtrA2 neutralize the cytosolic X-linked inhibitor of apoptosis proteins (XIAP), thus contributing to promote apoptosis (**Fig.16**) (Danial and Korsmeyer, 2004).

The upstream apoptotic signals converge at the mitochondria through the activity of the B cell lymphoma 2 (Bcl-2) family proteins. The functional balance between pro- and anti-apoptotic members of Bcl-2 family play a critical role in the regulation of cell survival or in apoptotic commitment.

### 4.2.1 Check point: the Bcl-2 family proteins

The Bcl-2 family proteins are divided in three groups based on their function and Bcl-2 homology (BH) domain organization (**Fig. 18**).

- Anti-apoptotic Bcl-2 proteins contain four BH1-4 domains. They are typically integrated in the OMM and also reside in the cytosol or in the ER membrane. They include: Bcl-2-related gene A1 (A1), Bcl-2, Bcl-2-related gene, long isoform (Bcl-XL), Bcl-w and myeloid cell leukemia 1 (Mcl-1). They directly inhibit apoptosis by binding and sequestering the BH3-only proteins. By doing so, activation of the proapoptotic BAX and BAK proteins and MOMP are prevented.

- The pro-apoptotic Bcl-2, or “effector”, proteins. They contain three BH1-3 domains, even if structure-based alignment revealed the presence of a conserved BH4 (Kvansakul et al., 2008). They include: Bcl-2 antagonist killer 1 (BAK) and Bcl-2-associated X protein (BAX). BAK and BAX play a fundamental role in the induction of intrinsic apoptosis. In healthy cells, BAK interact with the anti-apoptotic Mcl-1 and Bcl-XL proteins to keep them in an inactive state. In response to an apoptotic stimulus, this complex is disrupted through the action of the BH3-only proteins. A similar step is thought to contribute to BAX activation. The activation of BAX/BAK leads to their oligomerization and insertion into the OMM to promote MOMP.
- The BH3-only proteins have anti-apoptotic activity, but they share a conservation only in the amphipathic  $\alpha$ -helical BH3 region (Scorrano and Korsmeyer, 2003). They can be described as upstream sentinel of the status of the cell and are activated by series of cellular stresses. Once activated, they initiate apoptosis by binding the Bcl-2 anti-apoptotic proteins via the BH3 domain, inhibiting their anti-apoptotic action. To avoid unwanted cell death, BH3-only proteins are regulated by multiple mechanisms, such as transcriptional control (BIM, Puma and Noxa) and posttranscriptional modifications (PTMs). Since BH-3 only proteins promote apoptosis commitment by interacting with (i) the anti-apoptotic or (ii) both the anti-apoptotic and the pro-apoptotic Bcl-2 proteins. For this reason, they are further subdivided in two groups:
  - (i) The “sensitizer” and/or “derepressor” interact only with anti-apoptotic proteins: BAD (Bcl-2 antagonist of cell death) and Noxa;
  - (ii) The “direct activators” bind to anti-apoptotic and pro-apoptotic Bcl-2 “effector” proteins: BID (Bcl-2- interacting domain death agonist), BIM (Bcl-2-interacting mediator of cell death) and Puma. Thus, these group of proteins can directly activate BAK and BAX oligomerization and MOMP (Cheng et al., 2001; Ren et al., 2010).

The interaction between pro-apoptotic and anti-apoptotic proteins depends on the BH domains. The anti-apoptotic proteins homo- or heterodimerize within the other family members through a hydrophobic groove formed by BH1, 2 and 3. The pro-apoptotic BAX interacts with the anti-apoptotic protein BCL-XL by inserting its BH3 domain into the hydrophobic groove of BCL-XL (Nouraini et al., 2000). BAX and BAK can also form oligomers in the OMM interacting with the BH3-only domain members, as the “direct activator” BID (Desagher et al., 1999; Eskes et al., 2000).

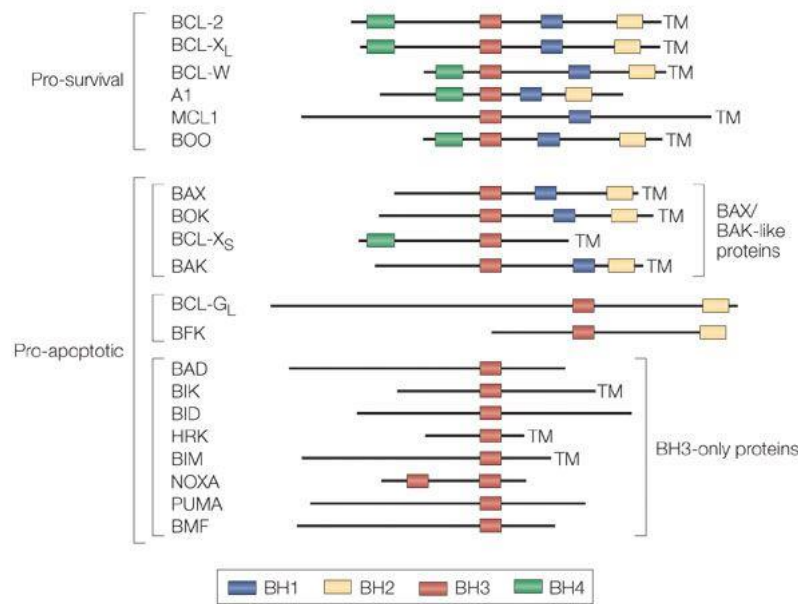


**Figure 17. Sequence alignment of core Bcl-2 family proteins and BH3-only proteins.** Sequence homologies of the BH1 (blue), BH2 (yellow), BH3 (red) and BH4 (green) regions are shown. The BH1, BH2 and BH3 domains fold to line a hydrophobic pocket that can bind BH3-only peptides. The BH3 domain, particularly among the BH3-only proteins, mediates interaction between the BH3-only proteins and core BCL-2 family proteins and thereby promotes apoptosis. BCL-2, BCL-XL, BCL-W, A1 and MCL1 are generally anti-apoptotic. The lower 14 proteins are considered pro-apoptotic. BID has a unique role as both a BCL-2 homologue and a BH3-only protein and links the intrinsic and extrinsic apoptosis pathways. BIM, BAD and BMF are unstructured proteins.

#### 4.2.2 First step to die: OMM permeabilization

It was originally believed that cytochrome c release takes place rapidly and completely, in an all-or-nothing manner (Goldstein et al., 2000). However, it was later demonstrated that mitochondria undergo an ultrastructure remodelling, after different death stimuli, including the BH3-only proteins BID (Scorrano et al., 2002) and BIK (Germain et al., 2005) or the activation of the Fas pathway (Mootha et al., 2001), thus changing the original view. The cristae remodelling process allows the mobilization of intra-cristae cytochrome c to achieve its complete release through the OMM. Therefore, the cytochrome c release is better described as a biphasic kinetic process, in which two distinct pathways are involved: (i) the release of cytochrome c across the OMM, and (ii) the mobilization and redistribution of cytochrome c stored in the cristae. These two pathways will be further described in the following chapters, and it will be shown how mitochondrial fusion and fission machinery intersect them.

The first necessary step for the cytochrome c release is the permeabilization of the OMM, triggered by the oligomerization of the Bcl-2 pro-apoptotic BAX/BAK proteins (Wei et al., 2001). As mentioned before, the caspase-8 cleaved tBID



translocate to cardiolipin-rich region of OMM, where it interacts with the anti-apoptotic Bcl-2 proteins, as Bcl-2 or Bcl-XL, to inhibit their activity (Li et al., 1998; Luo et al., 1998).

Since few years ago, it was believed that the pro-apoptotic BAX protein of non-apoptotic cells could be predominantly found in the cytosol and it could be translocated to mitochondria following an apoptotic stimulus. However, in 2013 was demonstrated that BAX was, instead, constitutively targeted to mitochondria, and that, in non-apoptotic cells, it was constantly translocated to the cytosol by anti-apoptotic Bcl-2 proteins to prevent unwanted cell death (Schellenberg et al., 2013; Todt et al., 2013). Schellenberg showed that BAX is in a dynamic equilibrium between cytosol and mitochondria, so that apoptotic sensitivity can be finely regulated by variations of the survival signals. In fact, the inhibition of survival signals increases the mitochondrial concentration of BAX, thereby sensitizing cells to apoptosis (Schellenberg et al., 2013). Conversely, the pro-apoptotic BAK is constitutively anchored to the OMM, through its hydrophobic C-terminal  $\alpha$  helix, and interacting with the voltage dependent anion channel 2 (VDAC2) (Cheng et al., 2003). However, it was recently reported that BAK retro-translocation from the OMM to the cytosol is also occurring to a certain extent (Todt et al., 2015).

Interestingly, active BAX and BAK are also involved in ER membrane permeabilization, leading to the release of luminal ER chaperones, and in the ER leaking of  $\text{Ca}^{2+}$  with a consequently increasing  $\text{Ca}^{2+}$  uptake by mitochondria (Oakes et al., 2005; Scorrano et al., 2003b). However, the specific relevance of ER permeabilization for intrinsic apoptosis remains to be clarified. Thus, the retro-translocation of BAX and BAK may be necessary to integrate the different roles of the proteins in the diverse cellular compartments.

Under physiological conditions, the two pro-apoptotic Bcl-2 proteins are found in inactive monomers or dimers. When activated by BH-3 only proteins, BAK and BAX arrange in homodimers, or heterodimers in specific conditions (Gavathiotis et al., 2010; Iyer et al., 2015). A subsequent dimer-by-dimer oligomerization finally generates a toroidal lipidic pore (Grosse et al., 2016; Oh et al., 2010; Salvador-Gallego et al., 2016). This pore alters the mitochondrial membrane permeability and induce a profound remodelling of mitochondrial ultrastructure.

The BAK/BAX triggered OMM permeabilization is a necessary condition for triggering apoptosis, still it is not sufficient. To ensure a complete release of cytochrome c, is also necessary a remodelling of the mitochondrial cristae, characterized by fusion of the individual cristae and opening of the cristae junctions (Scorrano et al., 2002).

### 4.2.3 Second step to die: cristae remodeling and cytochrome c release

The earlier kinetics studies on cytochrome c release during apoptosis, stated that cytochrome c is released from mitochondria in a single step, rapidly and completely, without mitochondria swelling (Goldstein et al., 2005; Goldstein et al., 2000). However, it was demonstrated that only 15%-20% of total cytochrome c resides in the IMS, while the majority is confined within the cristae fold (Bernardi and Azzone, 1981; Scorrano et al., 2002; Vogel et al., 2006). Thus BAX/BAK OMM permeabilization can release only a small subset of the entire amount of mitochondrial cytochrome c. Nevertheless, depending on the cell type, the level of cytoplasmic released cytochrome c is critical for the activation of the downstream caspases (Khodjakov et al., 2004; Zhivotovsky et al., 1998) and to overcome the inhibitor of apoptosis protein (IAP) (Fong et al., 2000). How can cytochrome c be completely released without mitochondria swelling?

Successive studies demonstrated that, following diverse apoptotic stimuli, as tBID, BIK or Fas receptor activation, mitochondria remodel their internal structure to allow a complete release of cytochrome c, in a process independent from OMM permeabilization (Germain et al., 2005; Mootha et al., 2001; Scorrano et al., 2002; Yamaguchi et al., 2008). 3D reconstruction of morphometry and electron microscopic tomography measurements allowed to define the steps of the so-called cristae remodelling process: it involves the widening of the narrow cristae junctions and fusion of independent cristae. tBID induces a complete release of cytochrome c in a time- and concentration-dependent manner in isolated mitochondria or intact cells. This process requires BAX, but it is independent of BAX/BAK-mediated OMM permeabilization, thus suggesting that tBID has two molecular targets: (i) BAX and BAK proteins to induce OMM permeabilization and the cytochrome c release across the OMM, and (ii) an unidentified target to allow cristae remodelling and cytochrome c mobilization from cristae. Nonetheless, the requirement of the BH3 domain of BID to mediate cristae remodelling is still controversial as opposing results have been published (Scorrano et al., 2002; Yamaguchi et al., 2008). Cytochrome c is a basic hydrophilic protein that is present in the IMM bound to anionic phospholipids, as cardiolipin. Depending on the strength of the binding, cytochrome c is present as two pools: (i) a loosely bound and (ii) a tightly bound, where the hydrophobic interactions induce a change of conformation of the protein tertiary structure and a partial embedding into the membrane. To achieve a complete release of cytochrome c is thus also necessary that it detaches from its high affinity cardiolipin binding sites on the IMM to generate a soluble pool (Ott et al., 2002). In fact, only cells “primed” for apoptosis by Fas activation can release all the mitochondrial cytochrome c upon selective permeabilization of the OMM by digitonin (Hajek et al., 2001). Furthermore, it was shown that, before the release of cytochrome c across the OMM, there is an

increase of the soluble pool of cytochrome c triggered by the mobilization process (Scorrano et al., 2002). Nevertheless, the exact molecular mechanism that triggers cristae remodelling is still not clear and will need further investigations.

### 4.3 Apoptosis and mitochondrial dynamics

Numerous works show that proteins involved in mitochondrial fusion and fission also participate in the apoptosis process. Mitochondrial cristae remodelling and mitochondrial fragmentation during apoptosis seem to intersect the mitochondrial dynamics pathway that maintain mitochondrial shape and regulate their fusion and division under healthy conditions. In fact, mitochondria elongation via genetic or pharmacological inhibition of DRP1, downregulation of FIS1, and overexpression of MFN1 decreases susceptibility to apoptotic stimuli (Cassidy-Stone et al., 2008; Head et al., 2009; Lee et al., 2004; Li et al., 2010). In contrast, mitochondria fragmentation via MFN2 degradation (Leboucher et al., 2012), OPA1 knockdown, or overexpression of FIS1 and DRP1 increases sensitivity to apoptotic stimuli (Lee et al., 2004).

#### ***DRP1: the traveller***

Mitochondrial fission is an early event in apoptosis, but mitochondrial fragmentation can occur independently of apoptosis, for example by incubating cells with an uncoupling agent, as FCCP, that disrupts the IMM potential. Nevertheless, DRP1, whose role in mitochondrial fission is well known, is also implicated in the apoptotic process. DRP1 is a cytosolic protein that is recruited to the OMM during mitochondrial fission, but also after an apoptotic stimulation (Arnoult et al., 2005b; Frank et al., 2001; Wasiak et al., 2007). In the OMM, DRP1 colocalizes with BAX and MFN2 at fission sites (Karbowski et al., 2002). It was demonstrated that after apoptotic activation, BAX/BAK oligomerize and form rings on the OMM. Interestingly, in DRP1 knockdown cells, the formation of these rings is not followed by cytochrome c release (Grosse et al., 2016). Similarly, DRP1 knockdown MEFs exhibit a delay in cytochrome c release, caspase activation and nuclear DNA fragmentation (Ishihara et al., 2009).

Scorrano and colleagues hypothesised that the DRP1 binding to OMM induces a membrane constriction altering its topology to facilitate BAX insertion. Accordingly, binding of a DRP1 mutant for GTP hydrolysis to the OMM is sufficient to stimulate BAX oligomerization (Montessuit et al., 2010). Interestingly, the hyper-fragmented mitochondria in *Mfn1*<sup>-/-</sup> MEFs are too small to allow the BAX insertion into the OMM (Renault et al., 2015), a strategy utilized by hepatitis C virus to attenuate apoptosis (Kim et al., 2014). *Mfn1*<sup>-/-</sup> and *Mfn2*<sup>-/-</sup> MEFs are also less susceptible to OMM permeabilization due to a heterogeneous distribution of OMM proteins caused by a lack of fusion (Weaver et al., 2014).

These experiments suggest that DRP1 facilitates the progression of apoptosis, in fact inhibition of mitochondrial fragmentation by activation of pro-fusion proteins inhibits apoptosis progression. Indeed, recently Otera and colleagues stated that DRP1-dependent mitochondrial fission through MiD49/MiD51 regulates cristae remodelling during intrinsic apoptosis. They demonstrated that DRP1 knockout cells do not undergo cristae remodelling and cytochrome c release during apoptosis, even if OPA1 oligomers are disassembled (Otera et al., 2016). Scorrano and colleagues stated that fusion and fission mitochondrial proteins regulate cristae to effect release of IMS proteins that may be selectively retained by tight membrane junctions within cristae (Scorrano et al., 2002). Consistently with this view, it was discovered a novel role for DRP1 in the regulation of cristae remodelling, after ER BIK stimulation, and the enhancement of cytochrome c release from mitochondria through Ca<sup>2+</sup>-mediated ER signal operating through this pathway enhances. DRP1 was shown to regulate cristae remodelling (Germain et al., 2005). However, it remains unclear the exact role of DRP in apoptosis. Instead, a large number of studies confirm the key role of OPA1 in the apoptotic process.

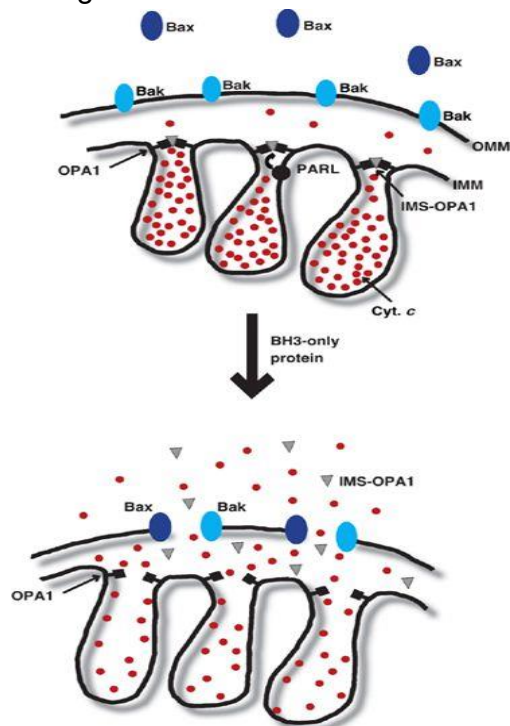
### ***OPA1: the glue of the cristae***

Downregulation of OPA1 leads to mitochondrial fragmentation, changing in mitochondrial ultrastructure and cytochrome c release. An early work revealed that Bcl-2 overexpression inhibits cell death caused by OPA1 RNAi, indicating that OPA1 acts upstream of OMM permeabilization (Olichon et al., 2003b). These results made OPA1 a potential candidate in the regulation of the apoptotic cristae remodelling process.

As demonstrated by Frezza and colleagues (Frezza et al., 2006b), OPA1 oligomeric complexes reside in the IMM at the cristae junctions and regulate cristae shape and width. Following death stimuli, as the BH3-only proteins BID, OPA1 complexes are early targeted and rapidly disrupted. This provokes the opening of the cristae junctions and the redistribution in the IMS of the cytochrome c trapped inside the cristae. Accordingly, overexpression of OPA1 stabilizes the protein complexes at the cristae junctions and protects cell from apoptosis by preventing cytochrome c mobilization. Furthermore, it also restores apoptosis sensitivity in a Huntington's disease model (Costa et al., 2010) and during FAS-induced liver apoptotic damage in vivo (Varanita et al., 2015). Conversely, OPA1 downregulation disrupts normal cristae structure, but it also increases cristae junction diameter and sensitize cells to apoptosis (Arnoult et al., 2005a; Frezza et al., 2006b; Olichon et al., 2003b; Yamaguchi et al., 2008). Yamaguchi and colleagues, through pharmacological and genetic approaches, uncoupled OPA1 complex disassembly and crista remodelling from OMM permeabilization. The expression of a disassembly-resistant mutant OPA1<sup>Q297V</sup> that does not exhibit GTPase activity (Griparic et al., 2004; Misaka et al., 2002) blocked both the complete release of cytochrome c, Omi/Htra2 and

Smac/DIABLO, and apoptosis (Yamaguchi et al., 2008). This experiment corroborates the previous hypothesis: the expression of OPA1 mutant, favouring constitutive self-assembly, blocks apoptosis by inhibiting the release of mitochondrial proteins, despite BAX activation. It can also be concluded that OPA1 controls the passage of cytochrome c through crista junctions. Furthermore, the anti-apoptotic and the fusion activities of OPA1 remain independent from each other, as OPA1 overexpression can also protect from apoptosis *Mfn* double knockout cells, where mitochondrial fusion is impaired (Frezza et al., 2006b). One might ask if the GTPase activity is critical for the anti-apoptotic function of OPA1, as for the fusion process. To address this question, Frezza and colleagues overexpressed the GTPase mutant OPA1<sup>K301A</sup>, that impairs the fusion activity, and observed the same effects as for OPA1 downregulation. Taken together, these results suggest that GTPase activity is important for the oligomerization of OPA1 and to keep the cristae junctions tight (Frezza et al., 2006b).

The high molecular weight OPA1 complexes targeted during apoptosis consist of both the l- and s-OPA1. Interestingly, PARL, involved in the post-transcriptional processing of OPA1, was found to participate in the regulation of cytochrome c release from mitochondria during apoptosis. PARL is positioned upstream of OPA1, because it is involved in the regulation of OPA1 oligomerization, by generating a balance amount of soluble OPA1. In *Parl*<sup>-/-</sup> mitochondria, s-OPA1 levels in IMS and OPA1 oligomers are reduced. Consequently, upon apoptosis induction, they are disrupted faster, and cells exhibit an early cytochrome c mobilization and an increased sensitivity to intrinsic apoptotic stimuli (Cipolat et al., 2006). Cogliati and colleagues succeeded in the genetical dissociation of OMM permeabilization from cristae remodelling using



two BID mutants. (i) BID<sup>G94E</sup> carries a mutation in the BH3 domain and is unable to induce OMM permeabilization. (ii) BID<sup>G94E</sup> is able to induce OMM permeabilization but is unable to induce cristae remodelling. **Figure 18. Model of cristae remodelling during apoptosis.** In healthy cells (top), OPA1 oligomers regulate the openings of the cristae junctions and restrict the passage of cytochrome c, as well as other proteins, into the mitochondrial intermembrane space (IMS). The inner membrane rhomboid protease, PARL, is required for correct assembly of OPA1 oligomers. In response to proapoptotic stimuli that activate BH3-only proteins and induce BAX/BAK-dependent OMM permeabilization (bottom), OPA1 oligomers become destabilized resulting in remodelling of the IMM and release of the fraction of cytochrome c contained within the cristae (~85%). OPA1 may also be released from the intermembrane space during this process. OMM, mitochondrial outer membrane; IMM, mitochondrial inner membrane. From (Delivani and Martin, 2006)

OMM permeabilization (Wei et al.,

2000). (ii) BID<sup>KKAA</sup> carries two mutations in the highly conserved 157 and 158 Lys of its  $\alpha 6$  helix. This sequence shares high homology with the transmembrane domains of Bnip3, BimS and mastoparan, all known to perturb the mitochondrial inner membrane (Cogliati et al., 2013b; Landes et al., 2010; Pfeiffer et al., 1995; Yamaguchi et al., 2008). As expected, BID<sup>G94E</sup> is not able to induce cytochrome c release, while BID<sup>KKAA</sup> is able to induce OMM permeabilization and release 20%-30% more cytochrome c than the baseline, which corresponds to the free IMS cytochrome c. Furthermore, BID<sup>KKAA</sup> and BID<sup>G94E</sup> are both incompetent in disrupting OPA1 high molecular weight complexes and in inducing apoptosis. Therefore, BID seems to exert two distinct functions in mitochondria via two different protein domains (Cogliati et al., 2013b).

How does tBID disassemble OPA1 oligomers during apoptosis? It was suggested that tBID acts as a bifunctional molecule: (i) it binds to cardiolipin in the mitochondrial membrane via its helix  $\alpha H6$  to destabilize mitochondrial structure and function, and then (ii) it promotes through its BH3 domain the activation of BAX/BAK oligomerization. Interaction of tBID with cardiolipin may lead to the reorganization of the mitochondrial phospholipids into microdomains, thus affecting the activity of the enzymes involved in mitochondrial functions; this results in ROS production and mitochondrial lipid peroxidation. According to this hypothesis, cardiolipin and its oxidation is essential for BID induced apoptosis (Gonzalez et al., 2010; Lutter et al., 2000; Ott et al., 2002).

In line with this model, an intriguing discovery was made by Jiang and colleagues. They proposed that, upon apoptotic stimulation, OPA1 is cleaved by the zinc metallopeptidase OMA1 activated after a decrease of mitochondrial membrane potential. The authors suggest that BAX/BAK oligomerization causes both OMM permeabilization and OMA1 activation (Jiang et al., 2014). This discovery leads to the rise of a model that link apoptosis, mitochondrial ultrastructure remodelling and mitochondrial bioenergetics.

Finally, it must be kept in mind that multiple OPA1 containing complexes do exist. (Cogliati et al., 2013b; Glytsou et al., 2016). This suggest that other proteins could participate in OPA1 complexes assembly and disruption. More studies will be needed to understand the molecular mechanism that link BAK/BAX activation, cristae remodelling and the complete cytochrome c release, as well as the protein machinery that regulate these processes.

## Results

# **1. Flaming Mitochondria: The Anti-inflammatory Drug Leflunomide Boosts Mitofusins**

Anna Pellattiero<sup>1,2</sup> and Luca Scorrano<sup>1,2\*</sup>



## Flaming Mitochondria: The Anti-inflammatory Drug Leflunomide Boosts Mitofusins

Anna Pellattiero<sup>1,2</sup> and Luca Scorrano<sup>1,2,\*</sup>

<sup>1</sup>Department of Biology, University of Padua, Padua, Italy

<sup>2</sup>Venetian Institute of Molecular Medicine, Padua, Italy

\*Correspondence: [luca.scorrano@unipd.it](mailto:luca.scorrano@unipd.it)

<https://doi.org/10.1016/j.chembiol.2018.02.014>

Despite the significance of mitochondrial dynamics in many diseases, drugs that modulate it are lacking. In this issue of *Cell Chemical Biology*, Miret-Casals et al. (2018) use a phenotypic high-throughput screen to discover a pro-fusion role for the anti-inflammatory drug Leflunomide, paving the way to screen for mitochondrial pro-fusion drug candidates.

Mitochondria are highly dynamic organelles that modify their shape in response to energetic and metabolic demands. This adaptation is achieved by tilting the balance between mitochondrial fusion and fission events, whose master regulators also participate in the control of cell metabolism. Fission is controlled by the dynamin-related protein 1 (DRP1), while fusion depends on three GTPases: mitofusins 1 and 2 (MFN1 and MFN2), located in the outer mitochondrial membrane (OMM), and optic atrophy 1 (OPA1), anchored to the inner mitochondrial membrane (IMM) (Pernas and Scorrano, 2016). Despite the enzymatic nature of these proteins, pharmacological modulators of mitochondrial morphology are very few: peptides that powerfully inhibit or stimulate Mfn or Drp1 are available (Cereghetti et al., 2010; Franco et al., 2016; Guo et al., 2013), but small molecule inhibitors or activators of mitochondrial dynamics are conversely lacking, especially since the mitochondrial division inhibitor 1 (Mdivi-1) molecule, a chemical inhibitor of DRP1 self-assembly in yeast, works via a completely different mechanism in mammalian cells, promoting metabolic-stress-induced mitochondrial fusion (Bordt et al., 2017).

In this issue of *Cell Chemical Biology*, Miret-Casals et al. (2018) address the challenge of identifying new small molecule modulators of mitochondrial dynamics by taking advantage of a phenotypic high-throughput screen (HTS). Instead of generally looking for mitochondrial shape changes, they decided to search for activators of MFN2 transcription. This approach led to the discovery of a novel role for leflunomide, an established anti-

inflammatory molecule widely used in the treatment of rheumatoid arthritis. Their exploration of how leflunomide promotes MFN2 expression identifies mitochondrial morphology changes as an adaptation mechanism to the cellular metabolic alteration caused by pyrimidine biosynthesis defects (Figure 1).

The phenotypic cell-based HTS used by Zorzano and colleagues (Miret-Casals et al., 2018) is simple and elegant in its design: it relies on the use of HeLa cells expressing a luminescence reporter gene under the control of MFN2 promoter. From a library of FDA-approved compounds, the authors successfully identify leflunomide as the most potent positive modulator of MFN2 expression. Leflunomide increases both MFN2 and MFN1 transcripts and proteins levels in HeLa and C2C12 muscle cells, resulting in mitochondrial elongation, without changes in respiration. Using genetics, Miret-Casals et al. (2018) show that the activity of leflunomide on mitochondrial elongation depends on MFNs. Furthermore, leflunomide preferentially acts on the promoter of MFN2 relative to MFN1.

Next, the authors examine the mechanism of action of leflunomide, known to inhibit the inner mitochondrial membrane enzyme dihydroorotate dehydrogenase (DHODH), which catalyzes the rate-limiting step of the *de novo* synthesis of pyrimidine (Löffler et al., 1997). Consequently, leflunomide exhausts intracellular pyrimidine pools, inhibiting cell proliferation. Exogenous uridine, which restores the pyrimidine levels through the salvage pathway, fully blocked the pro-elongation effect of leflunomide, placing pyrimidine reduction upstream

of MFN2 induction. Interestingly, DHODH interacts with complex III, whose inhibition similarly results in MFN2-mediated elongation, indicating that the pyrimidine pool unbalance unveiled here by the chemical biology approach used by Zorzano and colleagues might also occur in other conditions where complex III is dysfunctional. Overall, the discovery of a link between DHODH inhibition, complex III, pyrimidine pool, and mitochondrial elongation opens several avenues for further research.

First, pyrimidine requirement varies among cell types and developmental stages. Fully differentiated or resting cells mainly utilize the salvage pathway to synthesize pyrimidine. Conversely, rapidly proliferating cells, such as cancer cells and T lymphocytes, use both the *de novo* and salvage pathways to meet their high demand for nucleic acid precursors. Thus, do distinct tissues respond differently to leflunomide treatment and at large to complex III inhibition? What is the molecular link between the changes in pyrimidine pools and the transcription of MFN2? Can this link, once identified, be explored therapeutically to induce mitochondrial elongation, e.g., in differentiated cells to boost mitochondrial dynamics and intervene on mitochondrial dysfunction? Miret-Casals et al. (2018) do not find any change in known MFN transcriptional regulators. They suggest the involvement of some yet unidentified transcriptional regulators. Are these cell specific? Are the transcriptional regulators the same for both MFNs? By which intracellular signal or mechanism are they activated?



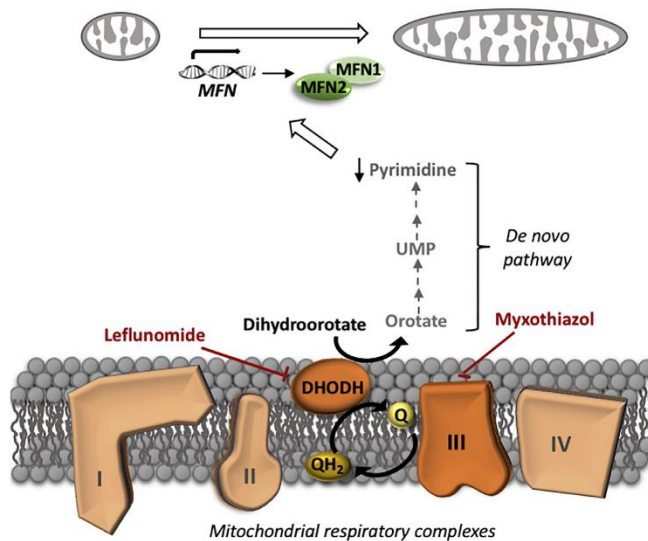


**Figure 1. Leflunomide, an Anti-inflammatory Drug Used against Rheumatoid Arthritis, Increases Mitochondrial Elongation by Depleting the Pyrimidine Pool**  
The cartoon depicts the central role of pyrimidine pool depletion by DHODH inhibition at the inner mitochondrial membrane in triggering MFN-mediated mitochondrial elongation, as discovered by Miret-Casals et al. (2018). The complex III inhibitor myxothiazol similarly increases mitochondrial elongation by indirect inhibition of DHODH.

Leflunomide is an anti-inflammatory drug effective in modulating T cell responses in autoimmune conditions like rheumatoid arthritis. Traditionally, this function is ascribed to its ability to induce pyrimidine pool exhaustion. However, the study of Miret-Casals et al. (2018) points to the potential involvement of mitochondria and of mitochondria-ER tethering, controlled by MFN2 (de Brito and Scorrano, 2008), in anti-inflammatory responses. In the bone marrow, high levels of MFN2 are required to maintain hematopoietic stem cells with potential to differentiate into the lymphoid lineage, including T cells. MFN2 operates by lowering activity of the nuclear factor of activated T cells, essential for T cell activation (Luchsinger et al., 2016) and also targeted by the widely used corticosteroid anti-inflammatory drugs.

Second, the addition of exogenous uridine reverses the mitochondrial elongation downstream of DHODH inhibition, but it fails to recover DHODH inhibition. Therefore, leflunomide leads to an accumulation of DHO irrespective

of mitochondrial shape changes. The role of DHO on cellular metabolism and intracellular signaling is, however, poorly understood. In principle, it might be responsible for some of the reported actions of leflunomide, including its anti-cancer effects. Further studies are required to map the connection between DHODH inhibition, DHO accumulation, and metabolic changes.

Finally, Zorzano and colleagues reported that other key modulators of mitochondrial morphology like OPA1 and DRP1 are affected by DHODH inhibition but in a cell-type-specific manner. This tissue specificity might be the key to understanding how mitochondrial dynamics is linked to changes in the pyrimidine pool. Indeed, by identifying where and how other mitochondrial dynamics regulators are affected by DHODH inhibition, we could learn about the downstream molecular links between the pyrimidine pool and transcription of mitochondrial genes.

Drug repurposing, the process of discovering other applications for an

already approved drug, has obtained growing attention (Verbaanderd et al., 2017). The work of Zorzano and colleagues is an example of how a library of FDA-approved drugs whose mechanisms of action, pharmacokinetic properties, and safety profiles have already been extensively described can be used to open new therapeutic potential for drugs already in the clinics. In the case of leflunomide, it would be interesting to test it in preclinical trials against diseases where mitochondrial fission is aberrant and also in models of Charcot-Marie-Tooth IIa, a peripheral polyneuropathy caused by MFN2 mutations (Züchner et al., 2004).

In conclusion, while more work is needed to clarify how mitochondrial dynamics is influenced by cellular pyrimidine metabolism, the identification of this connection between inhibition of the *de novo* pyrimidine biosynthesis pathway and enhancement of mitochondrial fusion provides an excellent starting point to rationally modulate mitochondrial shape and function.

#### ACKNOWLEDGMENTS

Work in the L.S. lab is supported by Telethon GGP15192, AIRC IG19991, and Fondation Leducq TNE004015.

#### REFERENCES

- Bordt, E.A., Clerc, P., Roelofs, B.A., Saladino, A.J., Tretter, L., Adam-Vizi, V., Cherok, E., Khalil, A., Yadava, N., Ge, S.X., et al. (2017). The putative Drp1 inhibitor mdv1-1 is a reversible mitochondrial complex I inhibitor that modulates reactive oxygen species. *Dev. Cell* 40, 583–594.e6.
- Cereghetti, G.M., Costa, V., and Scorrano, L. (2010). Inhibition of Drp1-dependent mitochondrial fragmentation and apoptosis by a polypeptide antagonist of calcineurin. *Cell Death Differ.* 17, 1785–1794.
- de Brito, O.M., and Scorrano, L. (2008). Mitofusin 2 tethers endoplasmic reticulum to mitochondria. *Nature* 456, 605–610.
- Franco, A., Kitsis, R.N., Fleischer, J.A., Gavathiotis, E., Kornfeld, O.S., Gong, G., Biris, N., Benz, A., Qvit, N., Donnelly, S.K., et al. (2016). Correcting mitochondrial fusion by manipulating mitofusin conformations. *Nature* 540, 74–79.
- Guo, X., Disatnik, M.H., Monbureau, M., Shamloo, M., Mochly-Rosen, D., and Qi, X. (2013). Inhibition of mitochondrial fragmentation diminishes Huntington's disease-associated neurodegeneration. *J. Clin. Invest.* 123, 5371–5388.
- Löffler, M., Jöckel, J., Schuster, G., and Becker, C. (1997). Dihydroorotat-ubiquinone oxidoreductase

links mitochondria in the biosynthesis of pyrimidine nucleotides. *Mol. Cell. Biochem.* 174, 125–129.

Luchsinger, L.L., de Almeida, M.J., Corrigan, D.J., Mumau, M., and Snoeck, H.W. (2016). Mitofusin 2 maintains haematopoietic stem cells with extensive lymphoid potential. *Nature* 529, 528–531.

Miret-Casals, L., Sebastián, D., Brea, J., Rico-Leo, E.M., Palacin, M., Fernández-Salguero, P.M.,

Loza, M.I., Albericio, F., and Zorzano, A. (2018). Identification of new activators of mitochondrial fusion reveals a link between mitochondrial morphology and pyrimidine metabolism. *Cell Chem. Biol.* 25, this issue, 268–278.

Pernas, L., and Scorrano, L. (2016). Mito-morphosis: mitochondrial fusion, fission, and cristae remodeling as key mediators of cellular function. *Annu. Rev. Physiol.* 78, 505–531.

Verbaanderd, C., Meheus, L., Huys, I., and Pantziarka, P. (2017). Repurposing drugs in oncology: next steps. *Trends Cancer* 3, 543–546.

Züchner, S., Mersyanova, I.V., Muglia, M., Bissar-Tadmouri, N., Rochelle, J., Dadali, E.L., Zappia, M., Nelis, E., Patitucci, A., Senderek, J., et al. (2004). Mutations in the mitochondrial GTPase mitofusin 2 cause Charcot-Marie-Tooth neuropathy type 2A. *Nat. Genet.* 36, 449–451.

## Fungal Secretion: The Next-Gen Target of Antifungal Agents?

Julianne Teresa Djordjevic<sup>1,2,3,\*</sup> and Sophie Lev<sup>1,2,3</sup>

<sup>1</sup>Centre for Infectious Diseases and Microbiology, The Westmead Institute for Medical Research, 176 Hawkesbury Road, Westmead, NSW 2145, Australia

<sup>2</sup>Sydney Medical School – Westmead, University of Sydney, Westmead, NSW 2145, Australia

<sup>3</sup>Marie Bashir Institute for Infectious Diseases and Biosecurity, University of Sydney, NSW, Australia

\*Correspondence: julianne.djordjevic@sydney.edu.au

<https://doi.org/10.1016/j.chembiol.2018.02.015>

Invasive fungal diseases pose a serious threat, and new drugs are urgently needed. In this issue of *Cell Chemical Biology*, Pries et al. (2018) identified benzamide- and picolinamide-based small-molecule inhibitors with antifungal properties, including some active against pathogenic *Candida* species. These compounds target an essential component of the fungal secretion machinery, suggesting a new approach to antifungal development.

Invasive fungal diseases (IFDs) cause significant morbidity and mortality, affecting both human and animal health and compromising food security. Annually, they affect 300 million people and cause 1.6 million deaths, equaling or exceeding tuberculosis and malaria, respectively (Fungal Infection Trust, 2017). Individuals with a compromised immune system are the primary group affected by IFDs and include those with HIV/AIDS or hematological malignancies, as well as stem cell and solid organ transplant recipients. The most common cause of IFDs in humans is *Candida* and *Aspergillus* species (commonly acquired in hospitalized patients), as well as *Pneumocystis* and *Cryptococcus* species. Azoles and polyenes (targeting plasma membrane ergosterol or its synthesis) and echinocandins (targeting the cell wall) are the three main classes of drugs used in IFD therapy. However, these drugs have limitations. For example, the polyene, Amphotericin B, is toxic despite its “gold standard” status for treating IFDs (Falci

et al., 2015), and resistance to azoles and echinocandins is emerging (Fungal Infection Trust, 2017). Novel therapies that are selective for fungal targets, and that preferentially have a different mechanism of action from currently available antifungals, are therefore needed urgently to overcome drug limitations and hence reduce the high global morbidity, mortality, and cost associated with treating these infections.

By screening a small-molecule inhibitor library of >3,000 compounds, Pries et al. (2018) identified a picolinamide-containing molecule (compound 1) that inhibited the growth of the model non-pathogenic yeast, *Saccharomyces cerevisiae*, but exhibited low cytotoxicity against mammalian cells. They then performed chemogenomic profiling on barcoded, hetero- and homozygous *S. cerevisiae* deletion collections and confirmed that the essential yeast phosphatidylinositol (PI) transfer protein (PITP), Sec14p, is the specific target of inhibition. The screen involving the homozygous *S. cerevisiae* deletion

mutants also identified non-essential genes that were previously shown to genetically interact with Sec14p, further supporting the discovery of Sec14p as the primary target of compound 1.

Sec14p is the PITP with the most significant functional impact on yeast cellular function (Bankaitis et al., 1990). Although Sec14p is not strictly an enzyme, Sec14p-mediated ATP-independent exchange of PI and phosphatidylcholine (PC) between membranes can be measured *in vitro*. Historically, it has been inferred that Sec14p transfers PI and PC between the endoplasmic reticulum and Golgi to establish Golgi lipid homeostasis and facilitate protein transport from the *trans*-Golgi network (TGN). However, more recent evidence argues against this model, in favor of one in which Sec14p serves primarily as a lipid sensor, instructing specific enzymes when and where to execute their activity (for review see Grabon et al., 2015). The current model for Sec14p is that it coordinates PC and PI 4-phosphate (PI4P)





## **2. The cristae modulator Optic atrophy 1 requires mitochondrial ATP synthase oligomers to safeguard mitochondrial function**

Rubén Quintana-Cabrera<sup>1,2,9,10,11</sup>, Charlotte Quirin<sup>1,2</sup>, Christina Glytsou<sup>1,2,12</sup>, Mauro Corrado<sup>1,2,13</sup>, Andrea Urbani<sup>3</sup>, Anna Pellattiero<sup>1,2</sup>, Enrique Calvo<sup>4</sup>, Jesús Vázquez<sup>4</sup>, José Antonio Enríquez<sup>4,5</sup>, Christoph Gerle<sup>6,7</sup>, María Eugenia Soriano<sup>8</sup>, Paolo Bernardi<sup>3,8</sup> & Luca Scorrano<sup>1,2</sup>

ARTICLE

DOI: 10.1038/s41467-018-05655-x

OPEN

# The cristae modulator Optic atrophy 1 requires mitochondrial ATP synthase oligomers to safeguard mitochondrial function

Rubén Quintana-Cabrera<sup>1,2,9,10,11</sup>, Charlotte Quirin<sup>1,2</sup>, Christina Glytsou<sup>1,2,12</sup>, Mauro Corrado<sup>1,2,13</sup>, Andrea Urbani<sup>3</sup>, Anna Pellattiero<sup>1,2</sup>, Enrique Calvo<sup>4</sup>, Jesús Vázquez<sup>4</sup>, José Antonio Enríquez<sup>4,5</sup>, Christoph Gerle<sup>6,7</sup>, María Eugenia Soriano<sup>8</sup>, Paolo Bernardi<sup>3,8</sup> & Luca Scorrano<sup>1,2</sup>

It is unclear how the mitochondrial fusion protein Optic atrophy 1 (OPA1), which inhibits cristae remodeling, protects from mitochondrial dysfunction. Here we identify the mitochondrial  $F_1F_0$ -ATP synthase as the effector of OPA1 in mitochondrial protection. In OPA1 overexpressing cells, the loss of proton electrochemical gradient caused by respiratory chain complex III inhibition is blunted and this protection is abolished by the ATP synthase inhibitor oligomycin. Mechanistically, OPA1 and ATP synthase can interact, but recombinant OPA1 fails to promote oligomerization of purified ATP synthase reconstituted in liposomes, suggesting that OPA1 favors ATP synthase oligomerization and reversal activity by modulating cristae shape. When ATP synthase oligomers are genetically destabilized by silencing the key dimerization subunit e, OPA1 is no longer able to preserve mitochondrial function and cell viability upon complex III inhibition. Thus, OPA1 protects mitochondria from respiratory chain inhibition by stabilizing cristae shape and favoring ATP synthase oligomerization.

<sup>1</sup>Venetian Institute of Molecular Medicine, 35129 Padua, Italy. <sup>2</sup>Department of Biology, University of Padua, 35121 Padua, Italy. <sup>3</sup>Department of Biomedical Sciences, University of Padua, Padua 35121, Italy. <sup>4</sup>Centro Nacional de Investigaciones Cardiovasculares Carlos III, 28029 Madrid, Spain. <sup>5</sup>CIBERFES, Institute of Health Carlos III, Madrid, Spain. <sup>6</sup>Institute for Protein Research, Osaka University, Suita, Osaka, Japan. <sup>7</sup>Core Research for Evolutional Science and Technology, Japan Science and Technology Agency, Kawaguchi, Japan. <sup>8</sup>Institute of Neuroscience, Consiglio Nazionale delle Ricerche, Padua, Italy. <sup>9</sup>Present address: University of Salamanca, Consejo Superior de Investigaciones Científicas CSIC, Institute of Functional Biology and Genomics, Salamanca 37007, Spain. <sup>10</sup>Present address: Institute of Biomedical Research of Salamanca, University Hospital of Salamanca, University of Salamanca, CSIC, 37007 Salamanca, Spain. <sup>11</sup>Present address: CIBERFES, Institute of Health Carlos III, Madrid, Spain. <sup>12</sup>Present address: Department of Pathology, NYU School of Medicine, 10016 New York, NY, USA. <sup>13</sup>Present address: Max Planck Institute of Immunology and Epigenetics, 79108 Freiburg im Breisgau, Germany. Correspondence and requests for materials should be addressed to L.S. (email: luca.scorrano@unipd.it)

Cristae are a pleomorphic subcompartment of the inner mitochondrial membrane (IMM) essential for biological energy conversion and for regulation of mitochondrial apoptosis<sup>1</sup>. Cristae shape and mitochondrial function are intimately connected<sup>2</sup>; changes in cristae morphology affect stability of respiratory supercomplexes (RCS)<sup>3,4</sup>, functional quaternary assemblies of respiratory chain complexes (RCC)<sup>1,5–8</sup>. In a reductionist view, cristae shape can be defined by the curvature of two regions: the cristae junctions (CJs), narrow tubular structures connecting cristae to the inner boundary membrane<sup>9</sup>; and the cristae lumen proper. CJs limit the diffusion of cytochrome c from the cristae<sup>10,11</sup> and their enlargement (i.e., the transition from the negative curvature of a shape resembling a solid hyperboloid to the null curvature of a cylinder or to the positive curvature of a spheroid) triggered by proapoptotic BH3-only BCL-2 family members BID, BIM-S, or BNIP3 allows cytochrome c redistribution<sup>10,12–14</sup>. During this process of cristae remodeling, cristae lumen width is also altered: the transition to a more positive CJ curvature results in overall cristae widening. Functionally, cristae widening destabilizes RCS and reduces mitochondrial oxidative phosphorylation efficiency<sup>3</sup>. In sum, cristae shape is a key morphological parameter that influences mitochondrial apoptosis and respiration.

A central modulator of cristae curvature is the IMM dynamin-related protein Optic atrophy 1 (OPA1): OPA1 oligomers maintain a negative CJ curvature, controlling cytochrome c redistribution and release<sup>11,13</sup> and stabilizing RCS to increase respiratory efficiency<sup>3,4,15</sup>. Because of these pleiotropic effects on mitochondrial function, controlled OPA1 overexpression is beneficial against a variety of pathological conditions, ranging from ischemia-reperfusion to massive hepatocellular apoptosis to muscular atrophy<sup>4</sup>, and even to deletion of genes essential for assembly of RCC<sup>15</sup>. This remarkable protective effect suggests that OPA1 does not work alone in the regulation of mitochondrial structure and hence function.

Other key players in cristae morphology include the MICOS complex, a multiprotein structure conserved from yeast to mammals<sup>16</sup> and the mitochondrial F<sub>1</sub>F<sub>0</sub>-ATP synthase, whose oligomers are retrieved on the edges of the cristae and contribute to define cristae curvature<sup>17–25</sup>. In mammals, OPA1 and the core MICOS component Mic60 physically interact and cooperate to stabilize the negative CJs curvature; however, CJ and cristae diameter, the key parameters defining mitochondrial apoptosis and respiration, are solely controlled by OPA1<sup>26</sup>, ruling out a role for MICOS in the mitochondrial protection afforded by OPA1. Another potential candidate is the mitochondrial ATP synthase that also can physically interact with OPA1<sup>27,28</sup>. The ATP synthase utilizes the mitochondrial proton electrochemical gradient ( $\Delta\mu_{H^+}$ ) generated by the RCC<sup>1,29,30</sup> to recycle ATP from ADP and Pi<sup>31,32</sup>. This enzyme also forms the permeability transition pore (PTP)<sup>33</sup>, a large conductance channel whose prolonged openings collapse  $\Delta\mu_{H^+}$  and cause cell death. Finally, the ATP synthase can also sustain the  $\Delta\mu_{H^+}$  when RCC are inhibited, by running in its reverse mode, hydrolyzing ATP to pump protons across the IMM<sup>32</sup>.

However, the interplay between ATP synthase and OPA1 in mitochondrial ultrastructure and function is unclear. Here, we provide evidence that OPA1 requires ATP synthase oligomers to protect mitochondria from respiratory chain inhibition.

## Results

**OPA1 counteracts mitochondrial dysfunction by antimycin A.** OPA1 overexpression is beneficial in vivo against primary and secondary mitochondrial dysfunction<sup>4,15</sup> because of its ability to blunt mitochondrial apoptosis<sup>11</sup> and to promote RCS stability<sup>3</sup>.

However, the extent and mechanism of this mitochondrial protection are unclear. We therefore capitalized on models of *Opa1* mild overexpression and conditional ablation to investigate in real time how OPA1 levels influenced the mitochondrial electrochemical gradient in response to complex III blockage by the inhibitor antimycin A (AA)<sup>34,35</sup>.

In mouse adult fibroblasts (MAFs) from *Opa1* transgenic (*Opa1*<sup>tg</sup>) mice, OPA1 levels and oligomers were 1.5-fold higher (Supplementary Fig. 1a, b) and cristae accordingly ~30% narrower (Supplementary Fig. 1c, d), as previously reported<sup>3</sup>. Real-time measurements of the fluorescence of the potentiometric dye tetramethylrhodamine methylester (TMRM) indicated that *Opa1*<sup>tg</sup> MAFs were surprisingly protected by AA-induced mitochondrial depolarization (Fig. 1a, b). We further tested whether OPA1 was able to prevent matrix acidification in the same experimental conditions, by measuring matrix pH with mtSypHer, a ratiometric genetically encoded pH sensor targeted to the mitochondrial matrix<sup>34</sup>. Matrix pH was superimposable in WT and *Opa1*<sup>tg</sup> MAFs, irrespective of whether the cells were cultured in media containing glucose or galactose (to force mitochondrial ATP production, Supplementary Fig. 1e). Real-time mtSypHer imaging indicated that OPA1 overexpression blunted also the matrix acidification caused by AA (Fig. 1c, d). We next turned to *Opa1*<sup>flx/flx</sup> MAFs where 48 h after transfection with CRE recombinase OPA1 was almost completely absent (Supplementary Fig. 2). In this same timeframe, *Opa1* deletion does not modify mitochondrial DNA (mtDNA) content or translation<sup>1,3,36</sup>. Real-time mtSypHer imaging revealed that matrix acidification induced by AA was more severe upon *Opa1* deletion (Fig. 1e, f). Thus, OPA1 protects from electrochemical gradient loss upon CIII blockage.

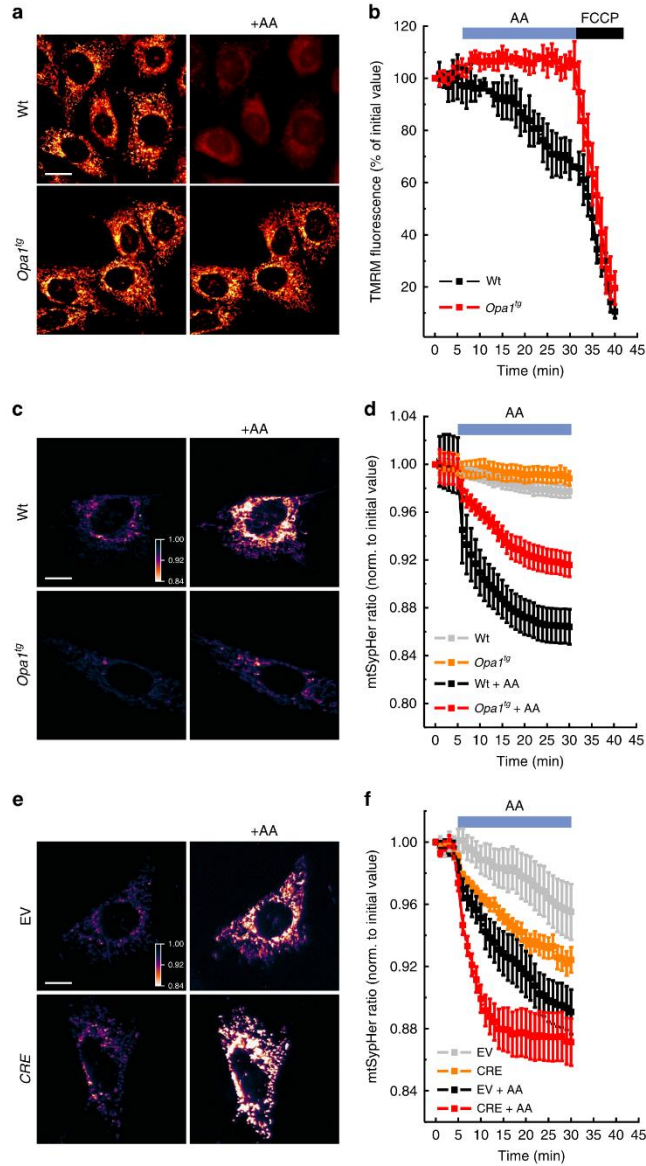
**OPA1 sustains mitochondrial function via ATP synthase activity.** We wondered how a dynamin-related protein involved in cristae morphogenesis and membrane fusion could regulate mitochondrial electrochemical gradient. Because reversal of ATP synthase activity can sustain mitochondrial membrane potential upon RCC inhibition<sup>37</sup>, we tested if OPA1 facilitated reversal ATP synthase activity to extrude protons from the matrix and maintain  $\Delta\mu_{H^+}$ . The protective effect of OPA1 overexpression on AA-induced matrix acidification and depolarization was fully abolished by the ATP synthase inhibitor oligomycin (Fig. 2a–d). Oligomycin also equalized AA-induced pH changes in empty vector (EV) and CRE-transfected *Opa1*<sup>flx/flx</sup> cells (Fig. 2e, f). The effects of OPA1 on pH could be a consequence of decreased proton leak, or of increased proton pumping by the reversal mode of the ATP synthase. If proton leak were reduced in *Opa1*<sup>tg</sup> MAFs, ATP synthase inhibition would result in a higher  $\Delta\mu_{H^+}$  compared to WT cells. However, membrane potential and matrix pH changes were superimposable in WT and *Opa1*<sup>tg</sup> MAFs treated with oligomycin (Supplementary Fig. 3a–c), indicating a similar proton leak in these two cell lines. Thus, the differences in  $\Delta\mu_{H^+}$  upon CIII inhibition recorded in WT and *Opa1*<sup>tg</sup> MAFs could be due to different stimulation of the reversal ATP synthase activity.

To directly measure if OPA1 affected ATP synthase activity in situ, we monitored ATP synthase-dependent hydrolysis of mitochondrial ATP upon complex III inhibition in real time in living cells. The FRET probe ATeam1.03<sup>38</sup> was correctly targeted to the mitochondrial matrix and revealed that basal mitochondrial ATP content was similar in WT and *Opa1*<sup>tg</sup> MAFs (Supplementary Fig. 3d). Following complex III inhibition, ATeam1.03 fluorescence decayed 3-fold faster in *Opa1*<sup>tg</sup> MAFs, suggesting faster ATP hydrolysis. These fluorescence changes were indeed due to ATP synthase activity, because they were

abolished by the ATP synthase inhibitor oligomycin (Fig. 2g–i and Supplementary Movie 1). Notably, oligomycin did not affect OPA1 oligomerization in WT or *Opa1*<sup>flg</sup> MAFs (Supplementary Fig. 4). Thus, OPA1 overexpression stimulates reversal ATP synthase activity.

**OPA1 stabilizes ATP synthase oligomers.** How does OPA1 overexpression impinge on ATP synthase to protect mitochondria from AA? Because OPA1 overexpression favors

mitochondrial RCS assembly by impinging on cristae shape<sup>3</sup>, we verified if the same was also true for ATP synthase oligomerization. Blue Native Gel Electrophoresis (BNGE) indicated that oligomeric ATP synthase was stabilized in mitochondria from *Opa1*<sup>flg</sup> cells (Fig. 3a, b). When we acutely deleted *Opa1* by expressing Cre recombinase in *Opa1*<sup>flx/flx</sup> MAFs, ATP synthase dimers and monomers were less abundant, with an increase in free F<sub>1</sub> subunit and a reduction in ATP synthase activity and total protein levels (Fig. 3c–e). Thus, OPA1 levels correlate with ATP synthase oligomerization and stability.





We next verified if OPA1 could stabilize ATP synthase oligomers also during apoptotic cristae shape changes induced by the caspase-8 cleaved, active form of the proapoptotic Bcl-2 family member BID. To this end, we compared the effects on ATP synthase levels and oligomerization of WT BID, of a BID mutant (BID<sup>KKAA</sup>) that permeabilizes the mitochondrial outer membrane (OMM) but does not remodel cristae<sup>3</sup> and of an OMM-permeabilization deficient BID mutant (BID<sup>G94E</sup>) that causes cristae remodeling but not cytochrome c release<sup>3,39</sup>. While total levels of ATP synthase were not affected by treatment of WT or *Opal*<sup>fl/fl</sup> mitochondria with the different BID mutants (Fig. 3f, g), BID and BID<sup>G94E</sup> destabilized ATP synthase oligomers only in WT mitochondria. As expected, treatment with the cristae remodeling deficient BID<sup>KKAA</sup> mutant did not affect the ATP synthase oligomerization pattern (Fig. 3f, h).

To further corroborate these biochemical experiments, we turned to an approach of proteomic profiling of high molecular weight (HMW) complexes (complexomic) that allowed us to identify dynamic changes of MICOS during cristae remodeling<sup>26</sup>. We therefore performed a similar analysis focused on ATP synthase complexes. First, we confirmed by immunoblotting and complexomic analysis of native protein complexes separated by BNGE from purified heart mitochondria that treatment with WT BID, but not BID<sup>KKAA</sup>, caused the disassembly of OPA1-containing HMW complexes<sup>26</sup> (Fig. 4a–c). We next focused our attention on the oligomeric ATP synthase assemblies. We found that in the BNGE regions corresponding to ATP synthase dimers and oligomers, the spectral counts corresponding to the F<sub>1</sub> core subunits ATP5A (α), ATP5B (β), ATP5C1 (γ), ATP5D (δ) and ATP5O (OSCP; see details on the analyzed subunits in supplementary Data 1) were reduced in mitochondria treated with WT BID but not with BID<sup>KKAA</sup> (Fig. 4d). The accuracy of this complexomic profiling was further supported by the analysis of the ATP5K (ε) subunit essential for ATP synthase dimerization<sup>40–43</sup>: ATP5K was retrieved only in the BNGE region corresponding to dimers and its spectral counts dropped to ~40% of control mitochondria upon BID-treatment; the drop was caused by cristae remodeling, because the spectral counts remained ~72% of the untreated in mitochondria challenged with BID<sup>KKAA</sup> (Fig. 4e), as further confirmed by immunoblotting (Fig. 4f). Overall, the analysis of the median of ATP synthase subunits spectral counts confirmed that ATP synthase dimers and oligomers were reduced in BID- but not in BID<sup>KKAA</sup>-treated mitochondria (Fig. 4g). In conclusion, independent biochemical approaches indicate that ATP synthase oligomers are stabilized upon OPA1 overexpression and destabilized when *Opal* is deleted, or cristae remodeled with concomitant OPA1 HMW oligomers disassembly.

**OPA1 does not directly stimulate ATP synthase oligomerization.** Because OPA1 levels are proportional to ATP synthase

oligomerization, we wished to understand how OPA1 sustained ATP synthase oligomerization. Levels of the ATP synthase inhibitory factor (IF<sub>1</sub>), whose oligomerization is influenced by matrix pH<sup>44</sup> and that in its oligomeric form can stabilize ATP synthase dimers<sup>45</sup>, were similar in WT and *Opal*<sup>fl/fl</sup> MAFs (Supplementary Fig. 5), suggesting that other mechanisms were in place.

We first asked whether OPA1 could directly interact with ATP synthase. Chemical crosslinking using 1-Ethyl-3-(3-dimethylaminopropyl)carbodiimide hydrochloride (EDC) resulted in the appearance of a ~130 KDa band immunoreactive for both ATP5B (β-subunit) and OPA1 (Fig. 5a). Moreover, ATP5B and OPA1 reciprocally co-immunoprecipitated (Fig. 5b, c), confirming and extending previous results that identified several ATP synthase subunits as OPA1 interactors<sup>28</sup>. To verify if OPA1 could also directly promote or stabilize the oligomeric forms of ATP synthase, we turned to an in vitro system of purified proteins and liposomes. We prepared proteoliposomes containing highly pure ATP synthase stabilized in the high affinity lipid like detergent Lauryl Maltose Neopentyl Glycol, as confirmed by EM (Fig. 5d). We also established a protocol to produce and purify a recombinant form of soluble OPA1 (lacking the import sequence and the transmembrane domain, supplementary Figure 6a) by adding a 6-His-Tag to its C-terminus. Following induction of expression in competent bacteria we purified recombinant soluble OPA1 (rOPA1) by affinity chromatography on Ni-NTA beads. Since a contaminant protein with ATPase activity bound to rOPA1, we removed it by extensive washes with ATP, before we eluted by increasing imidazole concentrations obtaining moderate yields of rOPA1 devoid of the contaminating ATPase activity (Supplementary Fig. 6b). Enzymatic activity of the dialyzed rOPA1 determined by reverse phase chromatography was in the range of other dynamin-related GTPases, confirming that rOPA1 was active and stable. We therefore incorporated rOPA1 into the proteoliposome lumen, mimicking the relative topology of OPA1 and ATP synthase in mitochondria (Supplementary Fig. 6c). When we analyzed these proteoliposomes by BNGE, we did not observe any effect of rOPA1 on ATP synthase oligomerization (Fig. 5e, f). In a further in vitro experiment, we added increasing concentrations of rOPA1 to native purified ATP synthase in a digitonin based buffer. However, also in these conditions rOPA1 failed to stimulate ATP synthase dimerization; if anything, in the presence of rOPA1, ATP synthase was mostly monomeric (Fig. 5g, h). Thus, despite its interaction with ATP synthase subunits, OPA1 does not directly stimulate or stabilize ATP synthase oligomerization.

**OPA1 sustains mitochondrial function via ATPase oligomers.** In *Opal*<sup>fl/fl</sup> mitochondria ATP synthase oligomers are more abundant and matrix pH is maintained upon complex III inhibition. We therefore turned to a genetic approach to test whether OPA1 required ATP synthase oligomers to protect from

**Fig. 1** OPA1 prevents mitochondrial electrochemical gradient loss caused by CIII inhibition. **a** Representative color-coded frames from real time imaging of TMRM fluorescence in MAFs of the indicated genotype. Where indicated, cells were treated for 30 min with 10 μM antimycin A (AA). Scale bar, 20 μm. **b** Quantitative analysis of TMRM fluorescence over mitochondrial regions in real time imaging experiments as in **a**. Where indicated, cells were treated with AA (10 μM) and with FCCP (2 μM). Data are average ± SEM. (n = 5 for each group). **c** Representative color-coded frames from real time imaging of mtSypHer fluorescence ratio in MAFs of the indicated genotype. Where indicated, cells were treated for 30 min with 10 μM AA. Rainbow color bar: pseudocolor scale of mtSypHer fluorescence ratio. Scale bar, 20 μm. **d** Quantitative analysis of mitochondrial mtSypHer fluorescence ratio in real time imaging experiments as in **c**. Where indicated, cells were treated with AA (10 μM). Data are mean ± SEM of at least four independent experiments. **e** Representative color-coded images of mitochondrial mtSypHer fluorescence in *Opal*<sup>fl/fl</sup> cells transfected with empty (EV) or CRE-encoding vectors and treated where indicated for 30 min with AA (10 μM). Rainbow color bar: pseudocolor scale of SypHer fluorescence ratio. Scale bar, 20 μm. **f** Quantitative analysis of mitochondrial mtSypHer fluorescence ratio in real time imaging experiments as in **a**. Data are mean ± SEM of at least four different experiments

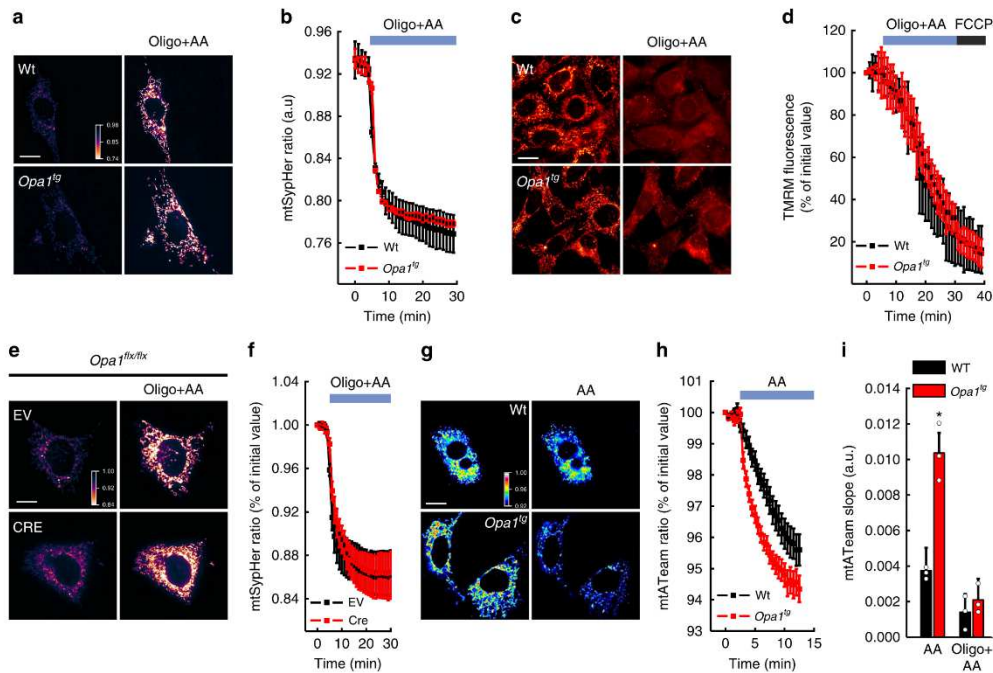


**Fig. 2** OPA1 requires ATP synthase activity to prevent mitochondrial  $\Delta$ pH loss caused by CIII inhibition. **a** Representative color-coded frames from real time imaging of mtSypHer ratio fluorescence in MAFs of the indicated genotype. Where indicated, cells were incubated with oligomycin (oligo, 1  $\mu$ M for 30 min) and antimycin A (AA) (10  $\mu$ M added 5 min after oligo, for 25 min). Rainbow color bar; pseudocolor scale of SypHer fluorescence ratio. Scale bar, 20  $\mu$ m. **b** Quantitative analysis of mitochondrial mtSypHer fluorescence ratio in real time imaging experiments as in **a**. Data are mean  $\pm$  SEM of at least four independent experiments. **c** Representative pseudocolor-coded frames from real time imaging of TMRM fluorescence in MAFs of the indicated genotype. Where indicated, cells were incubated with oligomycin (1  $\mu$ M for 5 min, before AA additions) and AA (2  $\mu$ M for 25 min). Scale bar, 20  $\mu$ m. **d** Quantitative analysis of mitochondrial TMRM fluorescence ratio in real time imaging experiments as in **c**. Where indicated, cells were treated with 2  $\mu$ M carbonyl cyanide 4-(trifluoromethoxy)phenylhydrazone (FCCP). Data are mean  $\pm$  SEM of at least four independent experiments. **e** Representative color-coded images of mitochondrial mtSypHer fluorescence in *Opa1<sup>flx/flx</sup>* cells transfected with empty (EV) or Cre-encoding vectors and treated for 30 min with AA (10  $\mu$ M) and oligomycin (1  $\mu$ M, added 5 min before AA) where indicated. Rainbow color bar; pseudocolor scale of mtSypHer fluorescence ratio. Scale bar, 20  $\mu$ m. **f** Quantitative analysis of mitochondrial mtSypHer fluorescence ratio in real time imaging experiments as in **e**. Data are mean  $\pm$  SEM of at least 4 independent experiments. **g** Pseudocolor-coded frames of mtATeam FRET fluorescence ratio in cells of the indicated genotype. Where indicated, cells were treated for 10 min with AA (10  $\mu$ M). Rainbow color bar; pseudocolor scale of ATeam fluorescence ratio. Scale bar, 20  $\mu$ m. **h** Quantitative analysis of mitochondrial mtATeam fluorescence ratio in real time imaging experiments as in **g**. Data are mean  $\pm$  SEM of at least three independent experiments. **i** Mean  $\pm$  SEM of mtATeam fluorescence ratio slopes, calculated from experiments as in **g**. Where indicated, oligomycin (1  $\mu$ M) was added 5 min before AA. \* $p$  < 0.05 in an unpaired two-sample Student's  $t$  test

mitochondrial CIII blockage. ATP synthase subunit *e* (ATP5k) is required for ATP synthase dimerization<sup>40–43</sup>, but its ablation does not compromise monomer function<sup>40,46,47</sup>. Efficient ATP5k silencing in WT and *Opa1<sup>tg</sup>* MAFs (Fig. 6a) yielded a superimposable reduction in ATP synthase dimers/total ATP synthase ratio (Fig. 6b, c)<sup>41</sup>. Because subunit *e* downregulation causes mitochondrial ultrastructural defects<sup>19,24,48</sup>, we inspected cristae shape in ATP5k silenced mitochondria. We morphometrically evaluated three parameters: cristae width, cristae number, and the ratio between CJ and cristae number, an indicator of the presence of arched or septate cristae, i.e., cristae connecting the IMM at two or more CJ. While ATP5k downregulation did not affect cristae width (Fig. 6d, e), it reduced cristae number and it increased the CJ/cristae number ratio (Fig. 6d, f, g), indicating the formation of arched and septate cristae with less tips<sup>41</sup>. In *Opa1<sup>tg</sup>*

MAFs the formation of these arched/septate cristae was blunted (Fig. 6g). Interestingly, ATP5k silencing reduced OPA1 oligomers in WT but not in *Opa1<sup>tg</sup>* MAFs (Supplementary Fig. 7a, b), suggesting that the formation of arched cristae caused by ATP5k silencing in WT cells depends on disassembly of OPA1 oligomers that are more stable upon OPA1 overexpression<sup>41</sup>. Our results indicate that OPA1 can compensate for the ultrastructural defects caused by reduced ATP synthase dimerization. A diametrically different scenario emerged when we delved into the mechanism of *Opa1<sup>tg</sup>* cells protection from AA-induced mitochondrial depolarization. ATP5k downregulation did not reduce resting ATP content in WT or *Opa1<sup>tg</sup>* cells (Supplementary Fig. 8a)<sup>40,47</sup>. Conversely, it completely abolished the effect of OPA1 on protection from AA-induced depolarization (Fig. 7a–c and Supplementary Movie 2), as well as on stimulation of ATPase reversal

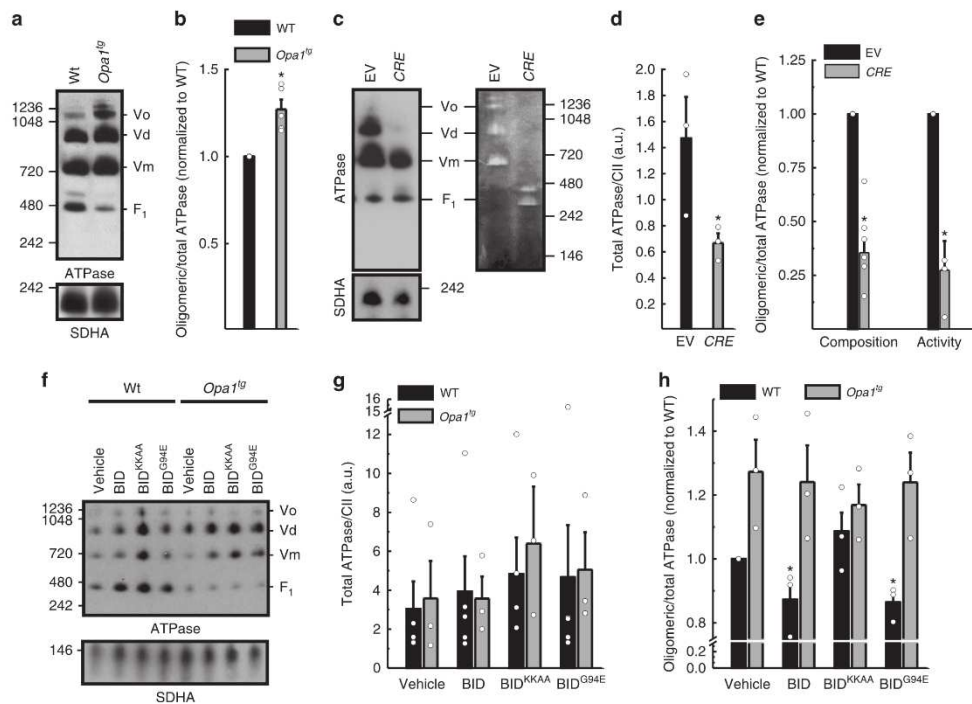


**Fig. 3** OPA1 promotes stabilization of ATP synthase oligomers. **a** Equal amounts (40  $\mu$ g) of digitonin-solubilized mitochondrial extracts from MAFs of the indicated genotype were separated by BNGE and immunoblotted with anti-ATP synthase subunit  $\alpha$  (ATPase) and Succinate Dehydrogenase (SDHA) antibodies. ATPase oligomers (Vo), dimers (Vd), monomers (Vm) and  $F_1$  are indicated. **b** Densitometric analysis of experiments performed as in **a**. Data represent mean  $\pm$  SEM of Vo + Vd (oligomeric)/total ATP synthase (Vo + Vd + Vm +  $F_1$ ) from five different experiments. \* $p < 0.05$  in a two-way ANOVA vs. control. **c** Equal amounts (40  $\mu$ g) of digitonin-solubilized mitochondrial extracts from MAFs of the indicated genotype were separated by BNGE and immunoblotted with the indicated antibodies (left) or processed for ATPase activity (right). ATPase oligomers (Vo), dimers (Vd), monomers (Vm) and  $F_1$  are indicated. **d, e** Quantitative densitometric analysis of total ATP synthase/CII (SDHA) (**d**) and of oligomeric/total ATP synthase conformations (**e**) in experiments as in **c**. Data show mean  $\pm$  SEM of at least three independent experiments. \* $p < 0.05$  in a two-way ANOVA versus EV. **f** Mitochondria from MAFs of the indicated genotypes were treated with recombinant BID as indicated for 30 min, lysed and equal amounts (40  $\mu$ g) of digitonin-solubilized extracts were separated by BNGE and immunoblotted with the indicated antibodies. **g, h** Quantitative densitometric analysis of total/CII (SDHA) (**g**) and of oligomeric/total ATP synthase conformations (**h**) in experiments as in **f**. Data are normalized to untreated cells and represent mean  $\pm$  SEM of at least three independent experiments. \* $p < 0.05$  in an unpaired two-sample Student's  $t$  test versus untreated

function, measured by following matrix ATP hydrolysis in real time (Fig. 7d, e; Supplementary Fig. 8b). Thus, OPA1 requires ATP5k and hence efficient ATP synthase dimerization to protect from mitochondrial dysfunction. If this model was correct, OPA1 should inhibit cell death induced by complex III inhibition and ATP5k should be essential for this cytoprotective effect. Indeed, WT MAFs grown in galactose-containing media rapidly died when challenged with AA, whereas *Opa1<sup>tg</sup>* MAFs were protected; downregulation of *ATP5k* equalized death levels between *Opa1<sup>tg</sup>* and WT cells (Fig. 7f). Our results indicate that the protection provided by OPA1 overexpression requires ATP5K and efficient ATP synthase oligomerization to sustain mitochondrial  $\Delta$ pH and curtail cell death following complex III inhibition.

## Discussion

How the IMM fusion and cristae biogenesis protein OPA1 preserve mitochondrial function from a plethora of tissue-damaging

insults and from respiratory chain inhibition is unclear. Here, multiple lines of evidence point to a key role for ATP synthase oligomerization status and reversal (i.e., ATP hydrolase) activity.

OPA1 overexpression counteracts multiple insults including ischemia, atrophy and death-receptor mediated apoptosis that converge on mitochondria<sup>4,49</sup>, and most remarkably it corrects electron transport chain defects in vivo<sup>15</sup>. Part of its protective action can be attributed to the inhibition of the apoptotic cristae remodeling pathway, resulting in reduced cytochrome c release and apoptosis<sup>10,12–14</sup>, but how OPA1 improves mitochondrial function when RCC are genetically impaired is less clear. Negative cristae, i.e., concave curvature at cristae junctions, correlate with increased RCS stability and increased residual RCC function<sup>15</sup>. While this could explain the correction of mitochondrial function in mitochondria lacking the complex IV assembly factor *Cox15*, it does not explain the improvement observed in mice where the essential complex I subunit *Ndufs4* is deleted<sup>15</sup>. Our results indicate that cristae shaping by OPA1 fosters ATP synthase oligomers and reversal activity, providing a unifying mechanism for

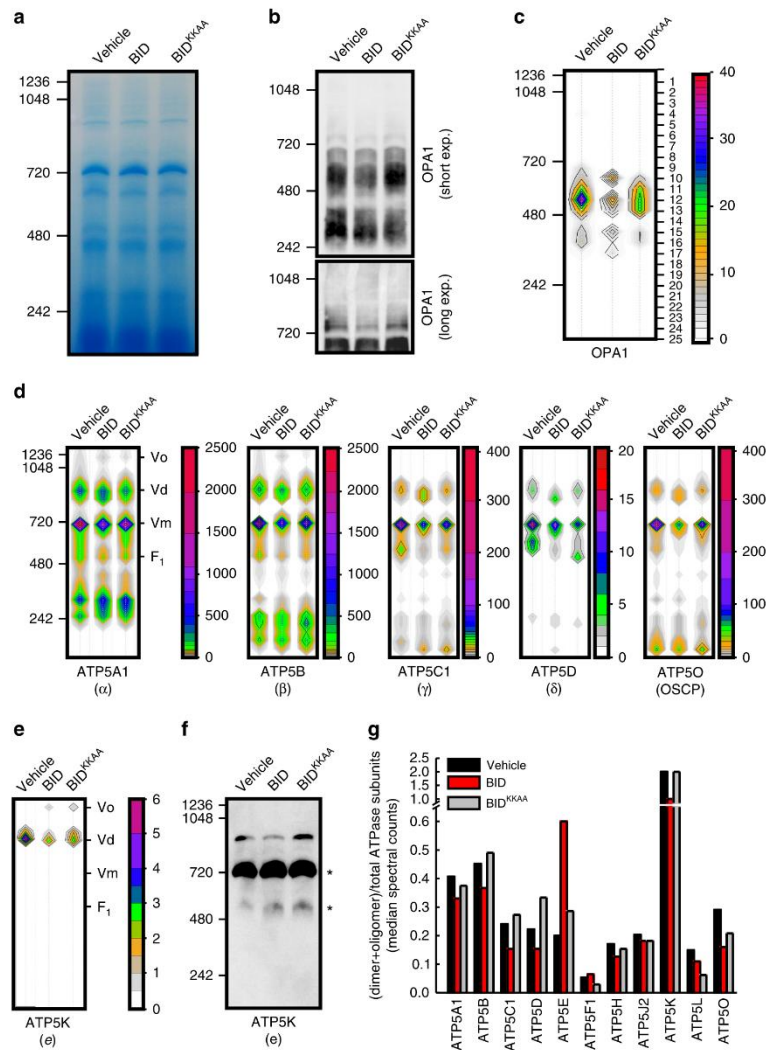


**Fig. 4** ATP synthase oligomers are reduced by cristae remodeling. **a, b** Mouse heart mitochondria were incubated as indicated and after 30 min protein lysates (30  $\mu$ g) were separated by BNGE and Coomassie stained (**a**) or immunoblotted with the indicated antibody (**b**). **c** Representative color-contour plots of spectral counts of OPA1 peptides from quantitative DiS-MS analysis of extracted mitochondrial complexes. Experiments were as in **a**. Numbers indicate the bands excised for MS analysis. The rainbow color scale indicates the number of spectral counts. **d, e** Color-contour plot of spectral counts of F<sub>1</sub> core components ( $\alpha$ ,  $\beta$ ,  $\gamma$ ,  $\delta$ , OSCP, panel **d**) and of the F<sub>0</sub> ATPase dimerization subunit e (ATP5k) from experiments as in **c**. **f** Experiments were as in **b**, except that membranes were decorated with the anti-ATPase subunit e antibody. Asterisks: cross-reactive unspecific bands. **g** Quantification of experiments as in **d, e**. The median values of the spectral counts of the indicated ATP synthase subunits were calculated in mitochondria pooled from three experiments performed as in **a**. The ratio of the median values in the dimer+oligomer region over the total forms is plotted

the ability of OPA1 to sustain mitochondrial electrochemical gradient and function when respiratory chain is inhibited.

Dynamic complexomic analysis of mitochondria undergoing cristae remodeling and OMM permeabilization is a powerful tool to inspect HMW complexes reorganization during cristae shape changes. This method can also identify unexpected OPA1 partners

in cristae morphogenesis, such as the MICOS components Mic60 and Mic19<sup>26</sup> and the SLC25A solute carriers family members that relay respiratory substrates availability to OPA1 to trigger the orthodox to condensed cristae transition<sup>28</sup>. By comparative complexomics we discovered that ATP synthase oligomers are very dynamic and that are affected by cristae shape changes.

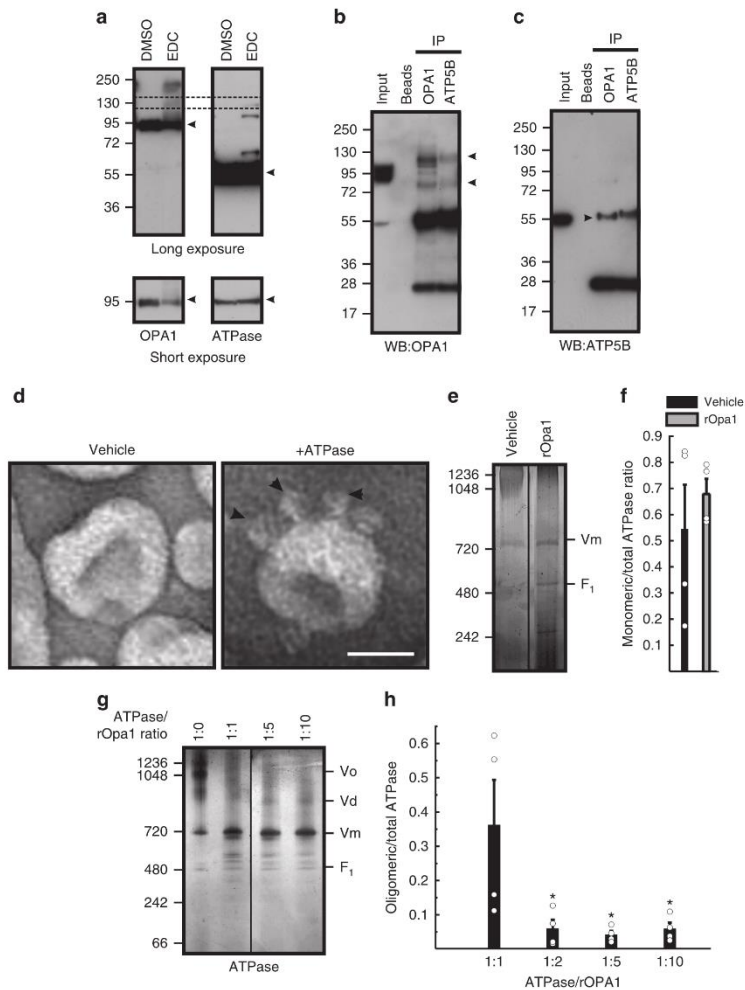


**Fig. 5** OPA1 does not directly stimulate ATP synthase oligomerization. **a** Purified mitochondria were treated where indicated with 10 mM EDC. After 30 min the reaction was quenched, mitochondria lysed and equal amounts (40  $\mu$ g) of proteins were separated by SDS-PAGE and immunoblotted using the indicated antibodies. Dashed box: OPA1 and ATPase cross-reactive adduct. Arrowheads: non-crosslinked OPA1 and ATPase. Bottom panels: short exposure blots of non-crosslinked OPA1 and ATPase. **b, c** Mitochondrial lysates (200  $\mu$ g) were immunoprecipitated with the indicated antibodies coupled to Protein A agarose beads; bound proteins were separated by SDS-PAGE and immunoblotted using the indicated antibodies. Input was diluted 1:10. **d** Representative EM image of a negatively stained proteoliposome containing rOpa1 in the lumen either in the absence (left panel) or presence (right panel) of recombinant ATP synthase in the membrane. Arrowheads: F<sub>1</sub> oriented towards the outside of the liposome. Scale bar, 50 nm. **e** Proteoliposomes harboring ATPase and either empty or containing rOpa1 were solubilized and proteins separated by BN-PAGE. **f** Densitometric quantification of ATPase composition in experiments as in **e**. Data are mean  $\pm$  SEM of four independent experiments. **g, h** Representative BN-PAGE (**g**) and densitometric quantification (**h**) of ATPase oligomeric forms upon incubation of the indicated ratios of rOpa1 with ATP synthase (3  $\mu$ g). Data are mean  $\pm$  SEM of four independent experiments. Vo: ATPase oligomers, Vd: dimers, Vm: monomers

A proteomic profiling of OPA1 interactors identified different subunits of ATP synthase<sup>28</sup>, suggesting a possible mechanism for the stabilization of the latter. Indeed, OPA1 co-immunoprecipitates with ATP synthase and both are retrieved in high-order crosslinked complexes, where OPA1 could directly stabilize ATP synthase. However, a reductionist approach of

purified recombinant OPA1 and ATP synthase containing proteoliposomes failed to prove that OPA1 directly stimulates or stabilizes ATP synthase oligomerization. These experiments suggest that the cristae curvature, promoted by OPA1, might itself stabilize ATP synthase oligomers. This effect would complement that of ATP synthase dimers on membrane curvature, in

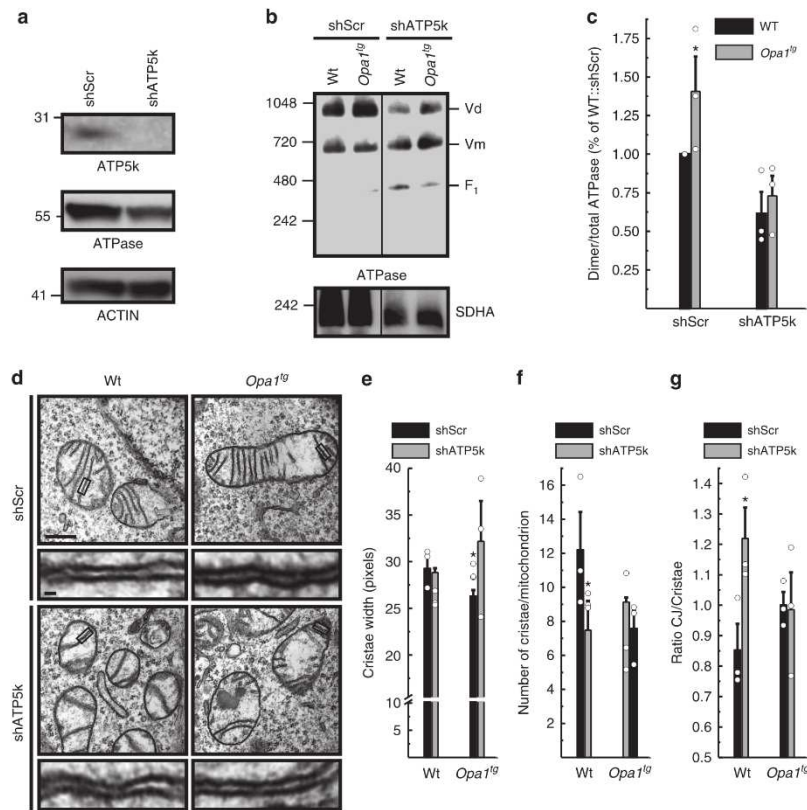


**Fig. 6** OPA1 requires ATP5k to stabilize ATP synthase oligomers. **a** Equal amounts (30 µg) of lysates from MAFs of the indicated genotype transfected for 48 h with the indicated shRNA were separated by SDS-PAGE and immunoblotted with the indicated antibodies (ATPase is ATP5A). **b** Equal amounts (40 µg) of digitonin-solubilized mitochondrial extracts from MAFs of the indicated genotype transfected with the indicated shRNAs were separated by BNGE and immunoblotted with the indicated antibodies. **c** Quantitative densitometric analysis of ATPase dimer vs. total ATPase. Data are mean ± SEM of three independent experiments performed as in **b**. **d** Representative EM micrographs of cells of the indicated genotype transfected with the indicated shRNA and GFP and after 48 h sorted for GFP<sup>+</sup> and processed for EM. Boxed areas are magnified 12× in the bottom images. Scale bars: 500 nm; 20 nm in bottom magnifications. **e–g** Morphometric analysis of cristae maximal width (**e**), number of cristae per mitochondrion (**f**) and cristae junctions per cristae (**g**) in experiments as in **d**. At least 30 mitochondria per experimental condition were analyzed. Mean values ± SEM of three independent experiments are shown. \**p* < 0.05 in a two-way ANOVA versus control (**e**) or paired two-sample Student's *t* test versus scramble shRNA (shScr) (**f**, **g**)

a feed forward loop that ultimately leads to stabilization of cristae shape by its multiple molecular determinants.

Traditionally, ATP synthase dimerization has been regarded as a cornerstone in cristae morphogenesis: rows of ATP synthase dimers at the edge of the cristae maintain the orthodox structure of the latter<sup>48,50</sup>. In yeast, genetic dimerization disruption results in aberrant mitochondrial ultrastructure<sup>19,23,48</sup>. This organization has also functional consequences: the ATP synthase dimers on the cristae edge contribute to create a proton gradient surrounding the enzyme<sup>24,51</sup>, ultimately favoring ATP synthesis<sup>50</sup>. By using apoptotic and genetic manipulations, we demonstrate that ATP synthase oligomerization is also affected by cristae curvature: ATP synthase dimers, like supercomplexes, are destabilized during cristae remodeling and when *Opa1* is ablated, and stabilized by OPA1 overexpression<sup>3</sup>.

ATP synthase dimers stabilization improves mitochondrial ultrastructure<sup>48,52</sup>, raising the question of whether the effects of OPA1 on cristae shape are secondary to the stabilization of ATP synthase dimers. Ablation of *ATP5k* (subunit *e*), a supernumerary ATP synthase subunit required to bend the IMM and enable dimer formation, but not essential for cell growth, results in loss of cristae tips, formation of cross-sectional septa and occasional onion-like cristae<sup>19,24,40,41,46,53</sup>. OPA1 overexpression reverted these shape changes, indicating that OPA1 can modulate cristae shape independently of ATP synthase dimers that shape cristae edges and tips<sup>23,48,50</sup>. Our genetic analysis places OPA1 upstream also of the ATP synthase in the pathway that controls cristae width, junctions and number<sup>26</sup>. The combination of in vivo and in vitro experiments presented here suggest that ATP synthase dimerization can also be stabilized by cristae shape, possibly by

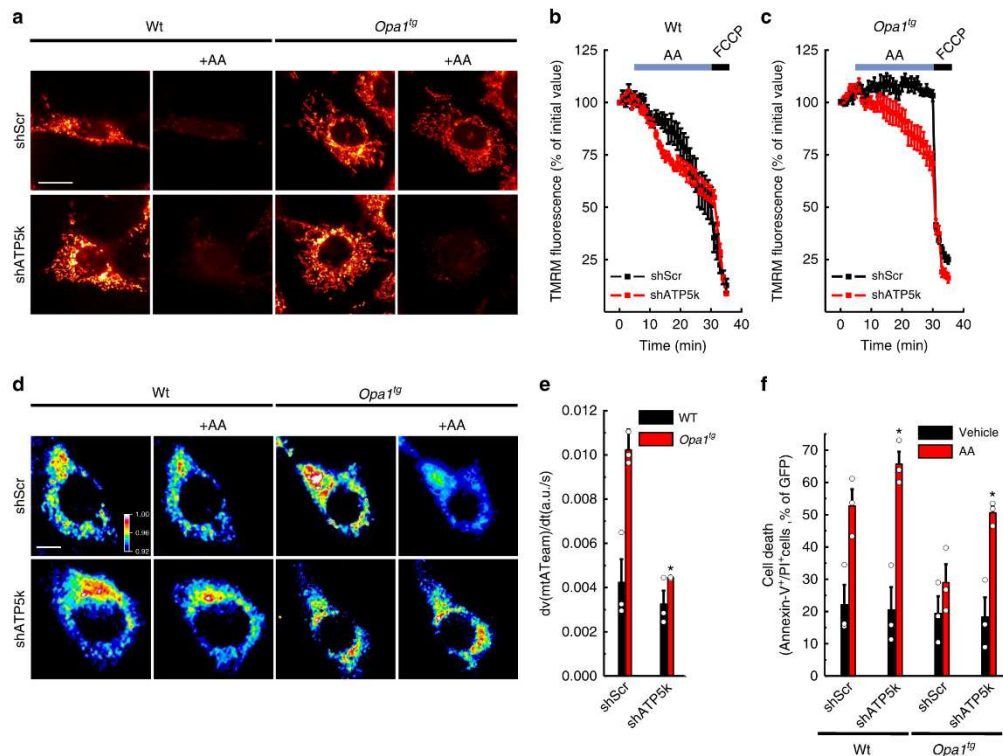


**Fig. 7** OPA1 requires ATP5k to protect from mitochondrial dysfunction. **a** Representative pseudocolor-coded frames from real time imaging of TMRM fluorescence in MAFs of the indicated genotype transfected with the indicated shRNA. Where indicated, cells were incubated with antimycin A (AA) (2  $\mu$ M for 25 min). Scale bar, 20  $\mu$ m. **b, c** Quantitative analysis of mitochondrial TMRM fluorescence ratio in experiments as in **a**. Where indicated, cells were treated with 2  $\mu$ M FCCP. Data are mean  $\pm$  SEM of at least four independent experiments. **d** Pseudocolor-coded frames of mtATeam FRET fluorescence ratio in cells of the indicated genotype. Where indicated, cells were treated for 20 min with AA (10  $\mu$ M). The rainbow indicates the pseudocolor scale. Scale bar, 20  $\mu$ m. **e** Mean  $\pm$  SEM of maximal mtATeam fluorescence ratio slopes in at least three independent experiments as in **(d)**. \* $p$  < 0.05 in an unpaired two-sample Student's  $t$  test, versus scramble shRNA (shScr). **f** MAFs of the indicated genotype were cotransfected with GFP and the indicated shRNA and after 72 h were treated with AA (5  $\mu$ M, 6 h). Data are mean  $\pm$  SEM of three independent experiments. \* $p$  < 0.05 in a two-way ANOVA test versus shScr

favoring superassembly in regions of negative curvature generated by OPA1. Conversely, when ATP synthase dimerization was genetically hampered, OPA1 failed to preserve mitochondrial function, indicating a reciprocal functional and structural crosstalk.

*Opa1<sup>tg</sup>* cells are protected from CIII inhibition in galactose-supplemented media, where the contribution of glycolysis to membrane potential maintenance is marginal<sup>7,54,55</sup>. Mechanistically, OPA1 sustains mitochondrial function by stimulating ATPase reverse activity, which is increased in *Opa1<sup>tg</sup>* mitochondria: pharmacological inhibition of ATPase activity abolishes the protective function of OPA1. Similarly, genetic inhibition of ATP synthase dimerization abolishes the ATPase activity stimulation and the maintenance of mitochondrial function by OPA1. In this context, it is conceivable that the reduced matrix acidification observed in *Opa1<sup>tg</sup>* MAFs upon complex III inhibition prevents the binding of the ATPase inhibitor IF<sub>1</sub> to the enzyme, which optimally occurs at pH 6.5<sup>44</sup>, thereby delaying a IF<sub>1</sub>-mediated ATPase inhibition and cristae shape stabilization<sup>52,56</sup>.

Our work unravels a bioenergetic mechanism accounting for OPA1 protection against mitochondrial failure and suggests that its overexpression might be beneficial to sustain bioenergetics in mitochondrialopathies<sup>57–61</sup>, germline defects<sup>62</sup> and neurodegeneration<sup>63</sup>, whereas OPA1 might be a target to correct oxidative phosphorylation changes in cancer<sup>64–66</sup>.

## Methods

**Cell culture and transfection.** WT, *Opa1<sup>tg/tg</sup>*, *Opa1<sup>tg</sup>* MAFs were generated in the Scorrano lab and grown in DMEM supplemented with 10% FBS<sup>3</sup>. Unless otherwise stated, glucose in the medium was substituted with 0.9 mg/ml galactose to force ATP production by the respiratory chain<sup>7</sup>.

Transient transfection with scramble or ATP5k (F<sub>1</sub>F<sub>0</sub>-ATP synthase sub. *c*; NM\_007507.2) shRNA encoding SureSilencing<sup>®</sup> plasmids (Qiagen, KM31364H, plasmid #3) were performed using Transfectin (Biorad). Following overnight transduction, the rate of GFP expression was typically around 60–70%, as determined by flow cytometry. Co-transfections of SureSilencing<sup>®</sup> shRNA plasmids or pcDNA3.1 vectors harboring WT or mutant tBID cDNAs were performed at a 3:1 ratio to empty pRES2-eGFP plasmid (Clontech) or vectors encoding for pSypHer-dMito<sup>44</sup> or wt (AT1.03)<sup>R122K/R126K</sup> ATeam<sup>38</sup>. Acute *Opa1* ablation in *Opa1<sup>tg/tg</sup>* MAFs was performed by co-transfections with the

Cre-recombinase under the control of a PGK promoter (pPGK-Puro, Addgene) and subjected to analysis after 48 h incubations.

**Real time imaging.** For live imaging, cells ( $5 \times 10^4$ ) seeded onto 24-mm round glass coverslips and incubated in  $\text{Ca}^{2+}/\text{Mg}^{2+}$  supplemented HEPES buffer (HBSS, Invitrogen) were transferred onto the stage of an Olympus IX81 inverted microscope (Melville, NY) equipped with a CellR imaging system and a beam-splitter optical device (Multispec Microimager; Optical Insights). Images were acquired using a 40 $\times$ , 1.4 NA objective (Olympus) and the CellR software. Analysis of fluorescence was performed following background subtraction over mitochondrial regions of interests (ROIs), using the multi-measure plug-in of Image J (NIH). Representative still frames are pseudocolor coded.

For real time imaging of mitochondrial  $\Delta\text{pH}$ , cells ( $5 \times 10^4$ ) seeded onto 24-mm round glass coverslips were transfected with pSypHer-dMito<sup>34</sup> and analyzed after 24 or 48 h after transfection to express Cre recombinase. Ratiometric images of the 535-emission fluorescence were acquired every 10 s by alternate excitation of cells at 430 and 500 nm for 100 ms. Mean fluorescence ratios of selected ROIs matching mitochondria were measured and expressed as mtSypHer (430/500 nm) ratios.

Mitochondrial ATP content was determined by FRET image analysis of cells transfected with pcDNA-ATeam1.03<sup>38</sup>. Sequential images of the 525 and 475 nm fluorescence emission after alternate excitation at 435 nm for 100 ms were acquired every 30 s.

For TMRM fluorescence analysis, sequential images were acquired every 30 s<sup>11</sup>.

**Transmission electron microscopy.** Electron microscopy (EM) imaging of cells was performed as described<sup>26</sup> on a Tecnai G2 (FEI) transmission electron microscope operating at 100 kV. Images were captured using a Veleta (Olympus Imaging System) digital camera (pixel size 13  $\times$  13  $\mu\text{m}$ ; pixel size at a 46,000 $\times$  magnification with screen magnification of 3  $\times$  0.1  $\times$  0.1 nm). For morphometric analysis of mitochondrial cristae, performed in a blind fashion on at least five mitochondria/cell from six randomly selected cells ( $n = 3$  independent experiments), maximal cristae width was measured using the ImageJ Multimeasure plug-in<sup>3</sup>; the number of horizontal cristae and cristae junctions were quantified manually.

**Immunoblotting.** For SDS-PAGE experiments, proteins (30–40  $\mu\text{g}$ ) were separated on Any-KD (BioRad) polyacrylamide precasted gels, transferred onto PVDF membranes (BioRad) and probed using the indicated antibodies and isotype matched HRP-conjugated secondary antibodies. The following primary antibodies were employed at 1:1000 dilution: OPA1 (BD, #612607), ATP5A (ab14748), ATP5B (ab14705), IF1 (ab110277), SDHA (ab14715), ATP5 subunit *e* (ab54879) from Abcam; ACTIN (Chemicon) was used at a 1:30000 dilution (MAB1501 Millipore). Densitometry was performed using ImageJ gel measure tool and analyzing the optical density of selected ROIs containing ATP synthase dimers, monomers and  $\text{F}_1$ . Uncropped scans of relevant blots are included in Supplementary Figure 9.

**Isolated mitochondria assays.** Mitochondria were extracted from cells grown in 500  $\text{cm}^2$  dishes<sup>67</sup>. After isolation, mitochondrial protein concentration was determined by Bradford assay (BioRad) and 0.5 mg/ml protein were incubated in Experimental Buffer (EB: 150 mM KCl, 10 mM Tris MOPS, 10  $\mu\text{M}$  EGTA-Tris, 1 mM  $\text{KH}_2\text{PO}_4$ , 5 mM glutamate, 2.5 mM malate) and further incubated where indicated with 10 pmol/mg cBID for 30 min at room temperature.

**Blue-native polyacrylamide gel electrophoresis.** Isolated mitochondria were resuspended (0.5 mg/ml) in NativePAGE Sample buffer (Invitrogen) containing 1.1% (w/v) digitonin (Sigma) and protease-inhibitor cocktail (Sigma). After 5 min on ice, the lysate was spun at 20,000 $\times$ g for 30 min at 4  $^\circ\text{C}$ . G250 (5%, 1  $\mu\text{l}/100 \mu\text{g}$  protein, Invitrogen) was added to the supernatant 30–40  $\mu\text{g}$  of protein were loaded onto a 3–12% native precast gel (Invitrogen).

**Protein crosslinking.** Where indicated, mitochondrial extracts were crosslinked in the presence of the zero-length crosslinker EDC<sup>11</sup>. Proteins (50  $\mu\text{g}$ ) were incubated for 30 min at 37  $^\circ\text{C}$  in PBS supplemented with 10 mM EDC. The reaction was quenched by adding 15 mM dithiothreitol (DTT) and proteins were separated by SDS-PAGE after 15 min.

**Immunoprecipitation.** Isolated mitochondria were lysed in 150 mM NaCl, 25 mM Tris-Cl pH 7.4, 1 mM EDTA, 5% glycerol, 0.1% Triton X-100 in the presence of Protease Inhibitory Cocktail (PIC) (Sigma). Lysates (250  $\mu\text{g}$ ) were precleared on 20  $\mu\text{l}$  of Protein-A agarose beads (Roche) for 30 min at 4  $^\circ\text{C}$  and subsequently immunoprecipitated with protein-A agarose beads coupled with the indicated antibodies in lysis buffer overnight at 4  $^\circ\text{C}$ <sup>26</sup>. The immunoprecipitated material was separated by SDS-PAGE.

**Liposomes preparation.** Liposomes were prepared from purified soybean alectin (L- $\alpha$ -phosphatidylcholine, Sigma). Lipids were dissolved in chloroform (5 mg/ml) until a homogeneous mixture was obtained; the solvent was then evaporated on a

nitrogen stream to yield a thin lipids layer on a glass tube bottom. The lipid film was thoroughly dried by placing the tube on a vacuum pump overnight to remove residual chloroform. To obtain large multilamellar vesicles (LMV) the lipid film was hydrated with 1 mL buffered solution (150 mM KCl, 10 mM Hepes, pH 7.4), containing where indicated 20  $\mu\text{g}$  of purified recombinant OPA1 (rOPA1), and gently agitated at room temperature. When rOPA1 was added, liposomes were then centrifuged at 30,000 $\times$ g for 5 min and resuspended in fresh buffer devoid of rOPA1. LMV were then downsized to liposomes (large unilamellar vesicles, LUV) by extrusion through a polycarbonate filter with a pore size of 100 nm (Avanti Polar Lipids).

Intact mammalian  $\text{F}_1\text{F}_0$ -ATP synthase was purified from beef heart mitochondria as described<sup>68</sup> and inserted into freshly made liposomes by direct incubation of the protein (20  $\mu\text{g}$ ) with the liposomes solution for 30 min at 4  $^\circ\text{C}$ . To remove non-inserted  $\text{F}_1\text{F}_0$ -ATP synthase complexes proteoliposomes were pelleted by centrifugation at 30,000 $\times$ g for 5 min and resuspended in buffer.

**Negative staining EM.** Twenty-five  $\mu\text{l}$  of containing freshly prepared proteoliposomes suspension were placed on a 400-mesh holey film grid, stained with 1%  $\text{UO}_2(\text{CH}_3\text{COO})_2$  and observed with a Tecnai G2 (FEI) transmission electron microscope operating at 100 kV. Images were captured using a Veleta (Olympus Imaging System) digital camera.

**Blue native PAGE and silver staining of recombinant proteins.** Purified ATP synthase was supplemented with Coomassie Blue G-250 (Serva) and applied to 1D 3–12% polyacrylamide gradient BNE (Invitrogen). After electrophoresis, proteins were eluted from BNE gels overnight as follows. Bands corresponding to monomers of F-ATP synthase were excised and diluted with 25 mM Tris, 7.5 mM Bis-Tris, and 1% (w/v) n-heptyl  $\beta$ -D-thioglycolpyranoside, pH 7.0 supplemented with 8 mM ATP-Tris, and 10 mM  $\text{MgSO}_4$ . Samples were incubated at 4  $^\circ\text{C}$ , centrifuged at 20,000  $\times$ g for 20 min at 4  $^\circ\text{C}$ , and supernatants were inserted into liposomes as described above.

Liposomes were then solubilized with 4% (wt/vol) freshly prepared digitonin, supplemented with Coomassie Blue G-250 (Serva), and loaded in 2D-BNE followed by silver staining. Gels were fixed overnight with formaldehyde, rinsed with ethanol, and pretreated with a solution of 0.8 mM  $\text{Na}_2\text{S}_2\text{O}_5$ ; gels were then stained with 11.2 mM  $\text{AgNO}_3$  for 20 min, and then with 0.6 M  $\text{Na}_2\text{CO}_3$  for the time required for the bands to be revealed.

**Production and purification of recombinant OPA1.** OPA1 mouse transcript variant 2 (NM\_133752) was amplified from position 502 to the stop codon to produce recombinant OPA1 (rOPA1) lacking the N-terminal transmembrane domain. The PCR product was cloned into pET21+ (Novagen) which adds a His-tag to the C-terminus of the encoded protein and expressed in *E. coli*. Protein production was induced with 0.5  $\mu\text{M}$  IPTG for 20 h at 18  $^\circ\text{C}$ . *E. coli* were collected by centrifugation and the pellet was resuspended in lysis buffer (40 mM Hepes/KOH, 500 mM NaCl, 10% glycerol, 5 mM  $\text{MgCl}_2$ , 5 mM  $\beta$ -mercaptoethanol, 0.5% Triton-X-100, 2% Tween-20, 1 mM PMSF, 20 mM Imidazole, Roche protease-inhibitor cocktail, pH 8.0). Cells were lysed by sonication and cell debris was removed by centrifugation at 14,000 $\times$ g for 45 min, 4  $^\circ\text{C}$ . rOPA1 was purified by Ni-NTA batch chromatography. Prior to elution, beads were washed with 1 mM ATP and 10 mM  $\text{MgCl}_2$  in lysis buffer for 30 min at room temperature followed by an intermediate washing step in wash buffer (40 mM Hepes/KOH, 300 mM NaCl, 0.05% Triton-X-100, 5 mM  $\text{MgCl}_2$ , 5 mM  $\beta$ -mercaptoethanol, 10% glycerol, 20 mM Imidazole, pH 8.0). rOPA1 was eluted with increasing concentrations of imidazole in elution buffer (40 mM Hepes/KOH, 0.05% Triton-X-100, 5 mM  $\beta$ -mercaptoethanol, 10% glycerol, pH 7.4). Imidazole was removed by dialysis and the protein was concentrated in storage buffer (40 mM Hepes/KOH, 0.05% Triton-X-100, 0.3 mM TCEP, 10% glycerol) and stored at -80  $^\circ\text{C}$  until use.

**In-gel ATPase activity assay.** ATPase in-gel activity was measured directly in the gel by incubating it for 2 h in a solution containing 35 mM Tris, 270 mM glycine, 14 mM  $\text{MgSO}_4$ , 0.2%  $\text{Pb}(\text{NO}_3)_2$ , and 8 mM ATP, pH 7.8<sup>69,70</sup>.

**BNGE based semi-quantitative proteomic analysis.** Mass spectrometry analysis of mitochondrial complexes from mouse CD1 hearts was performed as indicated<sup>26</sup>. False discovery rate (FDR) of identification was controlled as described by the algorithm Dxttractor. Median values of all identified ATP synthase subunits and representative color-contour plots of spectral counts of OPA1 peptides, core  $\text{F}_1$  ATP synthase subunits and  $\text{F}_0$  complex subunit *e* required for dimerization were considered for analysis.

**Cell death assays.** For cell death analysis,  $3.5 \times 10^3$  cells/ $\text{cm}^2$  of the indicated genotype were co-transfected with SureSilencing<sup>®</sup> shRNA and pIRES2-eGFP plasmids (3:1 ratio). After 48 h, the medium was replaced with galactose-supplemented DMEM and after 24 h cells were treated with 5  $\mu\text{M}$  antimycin A for 6 h. Cell death was assessed by flow cytometry detection (FACSCalibur) of double Annexin-V-APC/PI positive events from the transfected GFP<sup>+</sup> cell population<sup>3</sup>.



**Statistical analysis.** Results are expressed as the mean  $\pm$  SEM values of the indicated number ( $n$ ) of independent experiments. Individual data points are overlaid on the bar graphs. Statistical significance was determined by Student's  $t$  test or ANOVA between the indicated samples.  $P$  values are indicated in the legends and  $P < 0.05$  was considered significant.

**Data availability.** The data that support the findings of this study are available from the corresponding author upon reasonable request. The uncropped blots can be found in Supplementary Figure 9.

Received: 23 May 2017 Accepted: 18 July 2018

Published online: 24 August 2018

## References

- Cogliati, S., Enriquez, J. A. & Scorrano, L. Mitochondrial cristae: where beauty meets functionality. *Trends Biochem. Sci.* **41**, 261–273 (2016).
- Hackenbrock, C. R. Ultrastructural bases for metabolically linked mechanical activity in mitochondria. I. Reversible ultrastructural changes with change in metabolic steady state in isolated liver mitochondria. *J. Cell. Biol.* **30**, 269–297 (1966).
- Cogliati, S. et al. Mitochondrial cristae shape determines respiratory chain supercomplexes assembly and respiratory efficiency. *Cell* **155**, 160–171 (2013).
- Varanita, T. et al. The OPA1-dependent mitochondrial cristae remodeling pathway controls atrophic, apoptotic, and ischemic tissue damage. *Cell. Metab.* **21**, 834–844 (2015).
- Dudkina, N. V., Eubel, H., Keegstra, W., Boekema, E. J. & Braun, H. P. Structure of a mitochondrial supercomplex formed by respiratory-chain complexes I and III. *Proc. Natl Acad. Sci. USA* **102**, 3225–3229 (2005).
- Lapiente-Brun, E. et al. Supercomplex assembly determines electron flux in the mitochondrial electron transport chain. *Science* **340**, 1567–1570 (2013).
- Acin-Perez, R. et al. Respiratory complex III is required to maintain complex I in mammalian mitochondria. *Mol. Cell* **13**, 805–815 (2004).
- Enriquez, J. A. Supramolecular organization of respiratory complexes. *Annu. Rev. Physiol.* **78**, 533–561 (2016).
- Frey, T. G. & Mannella, C. A. The internal structure of mitochondria. *Trends Biochem. Sci.* **25**, 319–324 (2000).
- Scorrano, L. et al. A distinct pathway remodels mitochondrial cristae and mobilizes cytochrome *c* during apoptosis. *Dev. Cell* **2**, 55–67 (2002).
- Frezza, C. et al. OPA1 controls apoptotic cristae remodeling independently from mitochondrial fusion. *Cell* **126**, 177–189 (2006).
- Yamaguchi, R. et al. Opa1-mediated cristae opening is Bax/Bak and BH3 dependent, required for apoptosis, and independent of Bak oligomerization. *Mol. Cell* **31**, 557–569 (2008).
- Cipolat, S. et al. Mitochondrial rhomboid PARL regulates cytochrome *c* release during apoptosis via OPA1-dependent cristae remodeling. *Cell* **126**, 163–175 (2006).
- Olichon, A. et al. Loss of OPA1 perturbs the mitochondrial inner membrane structure and integrity, leading to cytochrome *c* release and apoptosis. *J. Biol. Chem.* **278**, 7743–7746 (2003).
- Civiletto, G. et al. Opa1 overexpression ameliorates the phenotype of two mitochondrial disease mouse models. *Cell. Metab.* **21**, 845–854 (2015).
- Munoz-Gomez, S. A., Slamovits, C. H., Dacks, J. B. & Wideman, J. G. The evolution of MICOS: Ancestral and derived functions and interactions. *Commun. Integr. Biol.* **8**, e1094593 (2015).
- Allen, R. D. Membrane tubulation and proton pumps. *Protoplasma* **189**, 1–8 (1995).
- Giraud, M. F. et al. Is there a relationship between the supramolecular organization of the mitochondrial ATP synthase and the formation of cristae? *Biochim. Biophys. Acta* **1555**, 174–180 (2002).
- Paumard, P. et al. The ATP synthase is involved in generating mitochondrial cristae morphology. *EMBO J.* **21**, 221–230 (2002).
- Dudkina, N. V., Sunderhaus, S., Braun, H. P. & Boekema, E. J. Characterization of dimeric ATP synthase and cristae membrane ultrastructure from *Saccharomyces* and *Polytomella* mitochondria. *FEBS Lett.* **580**, 3427–3432 (2006).
- Bornhvd, C., Vogel, F., Neupert, W. & Reichert, A. S. Mitochondrial membrane potential is dependent on the oligomeric state of F1F0-ATP synthase supercomplexes. *J. Biol. Chem.* **281**, 13990–13998 (2006).
- Rampelt, H., Zerbes, R. M., van der Laan, M., & Pfanner, N. Role of the mitochondrial contact site and cristae organizing system in membrane architecture and dynamics. *Biochim. Biophys. Acta* **1864**, 737–746 (2016).
- Strauss, M., Hofhaus, G., Schroder, R. R. & Kuhlbrandt, W. Dimer ribbons of ATP synthase shape the inner mitochondrial membrane. *EMBO J.* **27**, 1154–1160 (2008).
- Rabl, R. et al. Formation of cristae and crista junctions in mitochondria depends on antagonism between Fc1 and Su c/g. *J. Cell. Biol.* **185**, 1047–1063 (2009).
- Baker, I. A., Watt, I. N., Runswick, M. J., Walker, J. E. & Rubinstein, J. I. Arrangement of subunits in intact mammalian mitochondrial ATP synthase determined by cryo-EM. *Proc. Natl Acad. Sci. U. S. A.* **109**, 11675–11680 (2012).
- Glytsou, C. et al. Optic Atrophy 1 Is epistatic to the core MICOS Component MIC60 in mitochondrial cristae shape control. *Cell Rep.* **17**, 3024–3034 (2016).
- Banerjee, S. & Chinthapalli, B. A proteomic screen with *Drosophila* Opa1-like identifies Hsc70-5/Mortalin as a regulator of mitochondrial morphology and cellular homeostasis. *Int. J. Biochem. Cell. Biol.* **54**, 36–48 (2014).
- Patten, D. A. et al. OPA1-dependent cristae modulation is essential for cellular adaptation to metabolic demand. *EMBO J.* **33**, 2676–2691 (2014).
- Gilkerson, R. W., Selker, J. M. & Capaldi, R. A. The cristal membrane of mitochondria is the principal site of oxidative phosphorylation. *FEBS Lett.* **546**, 355–358 (2003).
- Vogel, F., Bornhvd, C., Neupert, W. & Reichert, A. S. Dynamic subcompartmentalization of the mitochondrial inner membrane. *J. Cell. Biol.* **175**, 237–247 (2006).
- Reid, R. A., Moyle, J. & Mitchell, P. Synthesis of adenosine triphosphate by a protonmotive force in rat liver mitochondria. *Nature* **212**, 257–258 (1966).
- Walker, J. E. The ATP synthase: the understood, the uncertain and the unknown. *Biochem. Soc. Trans.* **41**, 1–16 (2013).
- Giorgio, V. et al. Dimers of mitochondrial ATP synthase form the permeability transition pore. *Proc. Natl Acad. Sci. U. S. A.* **110**, 5887–5892 (2013).
- Santo-Domingo, J., Giacometti, M., Poburko, D., Scorrano, L. & Demareux, N. OPA1 promotes pH flashes that spread between contiguous mitochondria without matrix protein exchange. *EMBO J.* **32**, 1927–1940 (2013).
- Porcelli, A. M. et al. Respiratory complex I dysfunction due to mitochondrial DNA mutations shifts the voltage threshold for opening of the permeability transition pore toward resting levels. *J. Biol. Chem.* **284**, 2045–2052 (2009).
- Chen, H. et al. Mitochondrial fusion is required for mtDNA stability in skeletal muscle and tolerance of mtDNA mutations. *Cell* **141**, 280–289 (2010).
- Chinopoulos, C., Tretter, L. & Adam-Vizi, V. Depolarization of in situ mitochondria due to hydrogen peroxide-induced oxidative stress in nerve terminals: inhibition of alpha-ketoglutarate dehydrogenase. *J. Neurochem.* **73**, 220–228 (1999).
- Imamura, H. et al. Visualization of ATP levels inside single living cells with fluorescence resonance energy transfer-based genetically encoded indicators. *Proc. Natl Acad. Sci. USA* **106**, 15651–15656 (2009).
- Wei, M. C. et al. Proapoptotic BAX and BAK: a requisite gateway to mitochondrial dysfunction and death. *Science* **292**, 727–730 (2001).
- Arnold, I., Pfeiffer, K., Neupert, W., Stuart, R. A. & Schagger, H. Yeast mitochondrial F1F0-ATP synthase exists as a dimer: identification of three dimer-specific subunits. *EMBO J.* **17**, 7170–7178 (1998).
- Habersetzer, J. et al. Human F1F0 ATP synthase, mitochondrial ultrastructure and OXPHOS impairment: a (super-)complex matter? *PLoS One* **8**, e75429 (2013).
- Arselin, G. et al. The modulation in subunits e and g amounts of yeast ATP synthase modifies mitochondrial cristae morphology. *J. Biol. Chem.* **279**, 40392–40399 (2004).
- Arselin, G. et al. The GxxxG motif of the transmembrane domain of subunit e is involved in the dimerization/oligomerization of the yeast ATP synthase complex in the mitochondrial membrane. *Eur. J. Biochem.* **270**, 1875–1884 (2003).
- Cabezón, E., Butler, P. J., Runswick, M. J. & Walker, J. E. Modulation of the oligomerization state of the bovine F1-ATPase inhibitor protein, IF1, by pH. *J. Biol. Chem.* **275**, 25460–25464 (2000).
- Minauro-Sanmiguel, F., Wilkens, S. & Garcia, J. J. Structure of dimeric mitochondrial ATP synthase: novel F0 bridging features and the structural basis of mitochondrial cristae biogenesis. *Proc. Natl Acad. Sci. USA* **102**, 12356–12358 (2005).
- Hahn, A. et al. Structure of a complete ATP synthase dimer reveals the molecular basis of inner mitochondrial membrane morphology. *Mol. Cell* **63**, 445–456 (2016).
- Seelert, H. & Dencher, N. A. ATP synthase superassemblies in animals and plants: two or more are better. *Biochim. Biophys. Acta* **1807**, 1185–1197 (2011).
- Davies, K. M., Anselmi, C., Wittig, I., Faraldo-Gomez, J. D. & Kuhlbrandt, W. Structure of the yeast F1F0-ATP synthase dimer and its role in shaping the mitochondrial cristae. *Proc. Natl Acad. Sci. USA* **109**, 13602–13607 (2012).
- Ramonet, D. et al. Optic atrophy 1 mediates mitochondria remodeling and dopaminergic neurodegeneration linked to complex I deficiency. *Cell Death Differ.* **20**, 77–85 (2013).

50. Davies, K. M. et al. Macromolecular organization of ATP synthase and complex I in whole mitochondria. *Proc. Natl Acad. Sci. USA* **108**, 14121–14126 (2011).
51. Rieger, B., Junge, W. & Busch, K. B. Lateral pH gradient between OXPHOS complex IV and F<sub>0</sub>F<sub>1</sub> ATP-synthase in folded mitochondrial membranes. *Nat. Commun.* **5**, 3103 (2014).
52. Campanella, M. et al. Regulation of mitochondrial structure and function by the F<sub>1</sub>F<sub>0</sub>-ATPase inhibitor protein, IF1. *Cell. Metab.* **8**, 13–25 (2008).
53. Boyle, G. M., Roucou, X., Nagley, P., Devenish, R. J. & Prescott, M. Identification of subunit g of yeast mitochondrial F<sub>1</sub>F<sub>0</sub>-ATP synthase, a protein required for maximal activity of cytochrome c oxidase. *Eur. J. Biochem.* **262**, 315–323 (1999).
54. Gohil, V. M. et al. Nutrient-sensitized screening for drugs that shift energy metabolism from mitochondrial respiration to glycolysis. *Nat. Biotechnol.* **28**, 249–255 (2010).
55. Rossignol, R. et al. Energy substrate modulates mitochondrial structure and oxidative capacity in cancer cells. *Cancer Res.* **64**, 985–993 (2004).
56. Facenda, D., Tan, C. H., Seraphim, A., Duchon, M. R. & Campanella, M. IF1 limits the apoptotic-signalling cascade by preventing mitochondrial remodelling. *Cell Death Differ.* **20**, 686–697 (2013).
57. Lodi, R. et al. Deficit of in vivo mitochondrial ATP production in OPA1-related dominant optic atrophy. *Ann. Neurol.* **56**, 719–723 (2004).
58. Zanna, C. et al. OPA1 mutations associated with dominant optic atrophy impair oxidative phosphorylation and mitochondrial fusion. *Brain* **131**, 352–367 (2008).
59. Kucharczyk, R. et al. Mitochondrial ATP synthase disorders: molecular mechanisms and the quest for curative therapeutic approaches. *Biochim. Biophys. Acta* **1793**, 186–199 (2009).
60. Ghezzi, D. et al. Mutations in TTC19 cause mitochondrial complex III deficiency and neurological impairment in humans and flies. *Nat. Genet.* **43**, 259–263 (2011).
61. Benit, P., Lebon, S. & Rustin, P. Respiratory-chain diseases related to complex III deficiency. *Biochim. Biophys. Acta* **1793**, 181–185 (2009).
62. Teixeira, F. K. et al. ATP synthase promotes germ cell differentiation independent of oxidative phosphorylation. *Nat. Cell Biol.* **17**, 689–696 (2015).
63. Burie, F., Carelli, V., Chinnery, P. F. & Yu-Wai-Man, P. Disturbed mitochondrial dynamics and neurodegenerative disorders. *Nat. Rev. Neurol.* **11**, 11–24 (2015).
64. Garcia-Bermudez, J. et al. PKA Phosphorylates the ATPase Inhibitory Factor 1 and Inactivates Its Capacity to Bind and Inhibit the Mitochondrial H<sup>+</sup>-ATP Synthase. *Cell Rep.* **12**, 2143–2155 (2015).
65. Caro, P. et al. Metabolic signatures uncover distinct targets in molecular subsets of diffuse large B cell lymphoma. *Cancer Cell* **22**, 547–560 (2012).
66. Buck, M. D. et al. Mitochondrial dynamics controls T cell fate through metabolic programming. *Cell* **166**, 63–76 (2016).
67. Frezza, C., Cipolat, S. & Scorrano, L. Organelle isolation: functional mitochondria from mouse liver, muscle and cultured fibroblasts. *Nat. Protoc.* **2**, 287–295 (2007).
68. Jiko, C. et al. Bovine F<sub>1</sub>F<sub>0</sub> ATP synthase monomers bend the lipid bilayer in 2D membrane crystals. *eLife* **4**, e06119 (2015).
69. Gomes, L. C., Di, B. G. & Scorrano, L. During autophagy mitochondria elongate, are spared from degradation and sustain cell viability. *Nat. Cell Biol.* **13**, 589–598 (2011).
70. Alirol, E. et al. The mitochondrial fission protein hFis1 requires the endoplasmic reticulum gateway to induce apoptosis. *Mol. Biol. Cell* **17**, 4593–4605 (2006).

## Acknowledgements

The authors thank Drs. F. Caicci and E. Boldrin (Department of Biology, University of Padova) for EM sample preparation; Drs. N. Demareux (University of Geneva, Switzerland), H. Imamura and H. Koji (University of Kyoto, Japan) for reagents, J.P. Bolaños and A. Almeida (University of Salamanca, Spain) for facilities and discussion. R.Q.-C. was supported by an AIRC Postdoctoral Fellowship, a Fondazione Umberto Veronesi Postdoctoral Fellowship and is currently a recipient of a Juan de la Cierva-Incorporación fellowship from the Spanish Ministry of Economy, Industry and Competitiveness (IJCI-2015-26225). This work was supported by Telethon-Italy GPP10005, GGP14187, GGP15091; AIRC Italy IG-15748, ERC FP7-282280, FP7 CIG PCIG13-GA-2013-618697; Italian Ministry of Research FIRB RBAP11Z3YA\_005 to L.S. C.Ge. is supported by JST, CREST Grant JPMJCR13M4 (to Genji Kurisu and C.Ge.), the Platform for Drug Design, Discovery and Development from MEXT, Japan and the Grants-in-Aid for Scientific Research (Kiban B: 17H03647) from MEXT, Japan. JAE is supported by Spanish Ministry of Economy, Industry and Competitiveness (SAF2015-65633-R; SAF2015-71521-REDC). The CNIC is supported by MINECO and Pro-CNIC Foundation and is a SO-MINECO (award SEV-2015-0505).

## Author contributions

R.Q.-C. and L.S. conceived the project, acquired funds and wrote the manuscript. R.Q.-C., C.GI., M.C., C.Q., A.P., A.U., and M.E.S. performed and analyzed experiments. E.C. and M.E.S. wrote software and analyzed data; J.V., J.A.E., C.Ge., P.B., M.E.S. provided reagents, conceptualized experiments and edited the manuscript; L.S. supervised the project.

## Additional information

**Supplementary Information** accompanies this paper at <https://doi.org/10.1038/s41467-018-05655-x>.

**Competing interests:** The authors declare no competing interests.

**Reprints and permission** information is available online at <http://npg.nature.com/reprintsandpermissions/>

**Publisher's note:** Springer Nature remains neutral with regard to jurisdictional claims in published maps and institutional affiliations.



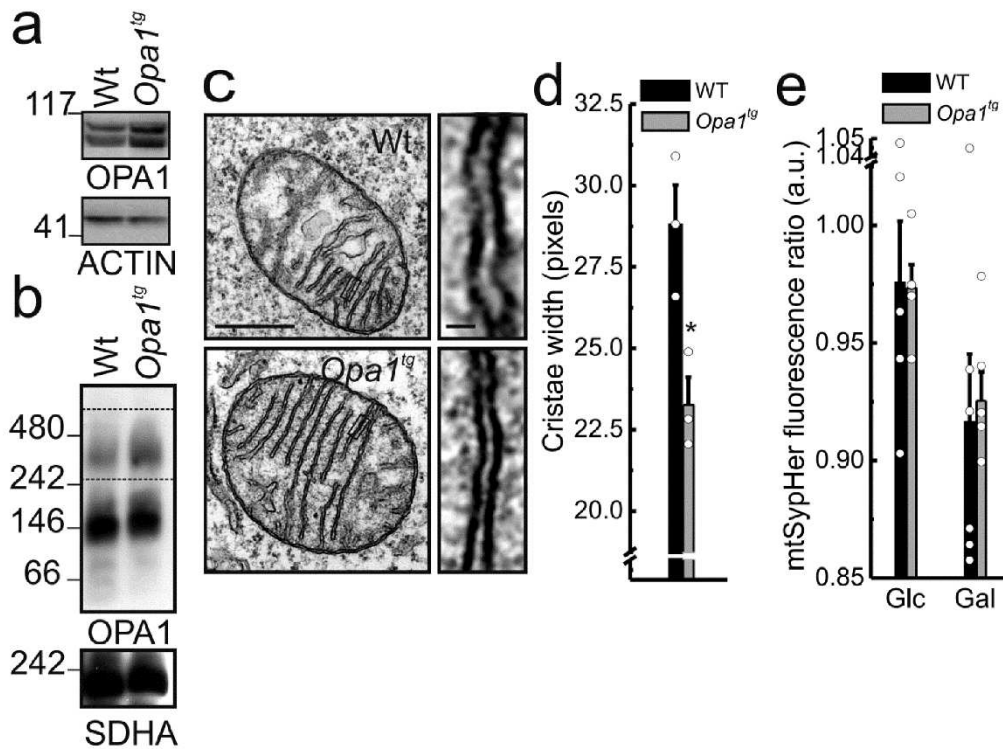
**Open Access** This article is licensed under a Creative Commons Attribution 4.0 International License, which permits use, sharing, adaptation, distribution and reproduction in any medium or format, as long as you give appropriate credit to the original author(s) and the source, provide a link to the Creative Commons license, and indicate if changes were made. The images or other third party material in this article are included in the article's Creative Commons license, unless indicated otherwise in a credit line to the material. If material is not included in the article's Creative Commons license and your intended use is not permitted by statutory regulation or exceeds the permitted use, you will need to obtain permission directly from the copyright holder. To view a copy of this license, visit <http://creativecommons.org/licenses/by/4.0/>.

© The Author(s) 2018

### **Supplementary Information**

Quintana-Cabrera et al., "The cristae modulator Optic atrophy 1 requires mitochondrial ATP synthase oligomers to safeguard mitochondrial function"

## Supplementary Figures



**Supplementary Figure 1. OPA1 overexpression decreases cristae width without affecting basal matrix pH. Related to Fig. 1**

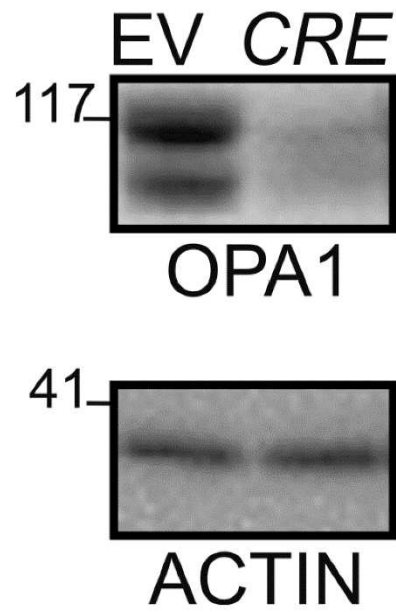
(a) Protein extracts (30  $\mu$ g) from cells of the indicated genotype were separated by SDS-PAGE and immunoblotted with the indicated antibodies.

(b) BNGE analysis of OPA1 HMW complexes. Protein extracts (30  $\mu$ g) from cells of the indicated genotype were separated by BNGE and immunodecorated with the indicated antibodies. The dashed box indicate OPA1 HMW complexes.

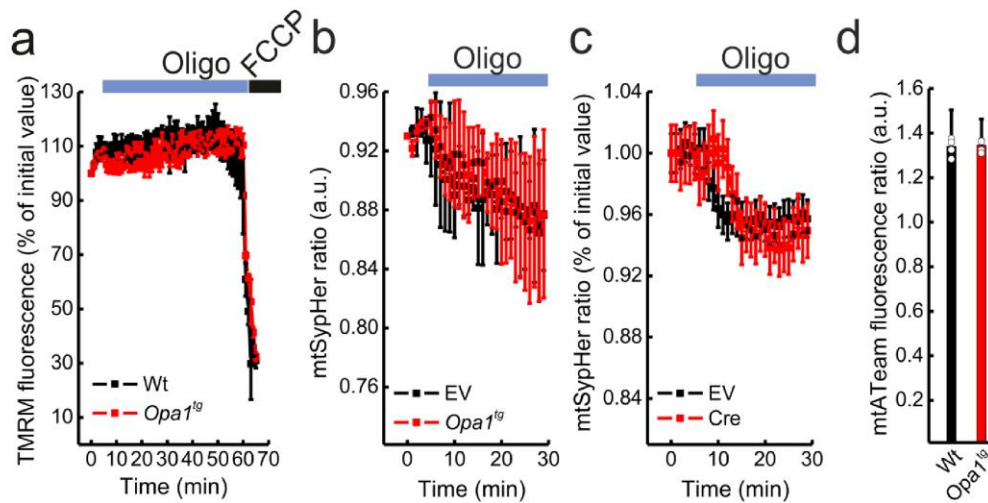
(c) Representative EM micrographs of mitochondria in cells of the indicated genotype. Boxed areas are magnified in the right panels. Scale bars, 500 pixels in left and 20 pixels in right panels.

(d) Mean $\pm$ SEM values of morphometric analysis of cristae width in 3 independent experiments as in (c). \* $p$ <0.05 in an unpaired two-sample Student's  $t$  test

(e) Matrix mySypHer fluorescence in cells of the indicated genotype cultured in media supplemented with the indicated hexose. Data represent mean $\pm$ SEM of 5 independent experiments.



**Supplementary Figure 2. Cre delivery deletes OPA1 in *Opa1<sup>flx/flx</sup>* MAFs. Related to Fig. 1**  
Protein extracts (30  $\mu$ g) from *Opa1<sup>flx/flx</sup>* MAFs transfected with the indicated plasmids for 48 h were separated by SDS-PAGE and immunoblotted with the indicated antibodies.



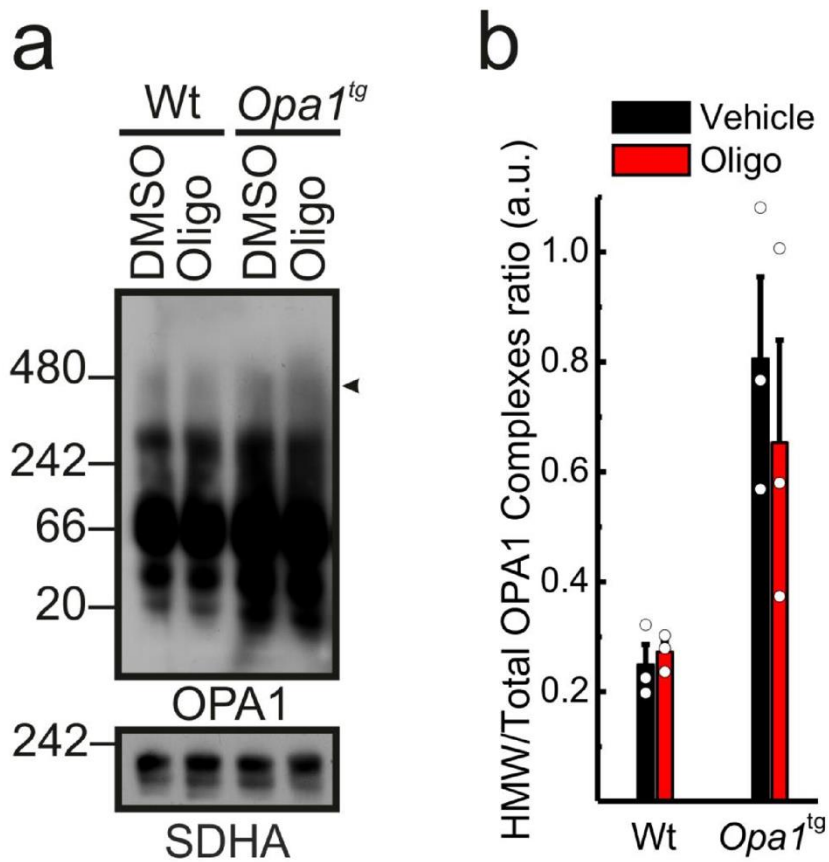
**Supplementary Figure 3. OPA1 requires ATPase activity to sustain the mitochondrial electrochemical gradient, Related to Fig. 2**

(a) Mean $\pm$ SEM from at least 3 independent experiments of TMRM fluorescence real time imaging in cells of the indicated genotype. Where indicated, cells were treated with 1  $\mu$ M oligomycin (Oligo) and 2  $\mu$ M FCCP.

(b) Mean $\pm$ SEM SypHer fluorescence ratios from cells of the indicated genotypes treated where indicated with 1  $\mu$ M Oligo.

(c) Mean $\pm$ SEM of at least 4 independent experiments of mtSypHer fluorescence ratios imaging in *Opa1<sup>flx/flx</sup>* cells, cotransfected with SypHer and the indicated plasmid (EV, Empty vector; Cre: Cre recombinase). Where indicated cells were treated with 1  $\mu$ M Oligo.

(d) Basal mean $\pm$ SEM mtATeam ratios from at least 4 independent experiments performed in cells of the indicated genotype incubated for 24 h in galactose medium.

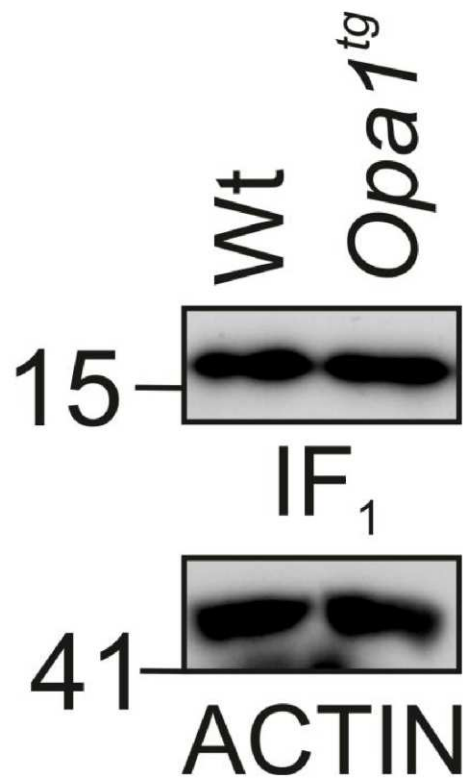


**Supplementary Figure 4. Oligomycin does not destabilize OPA1 HMW complexes. Related to Fig. 2**

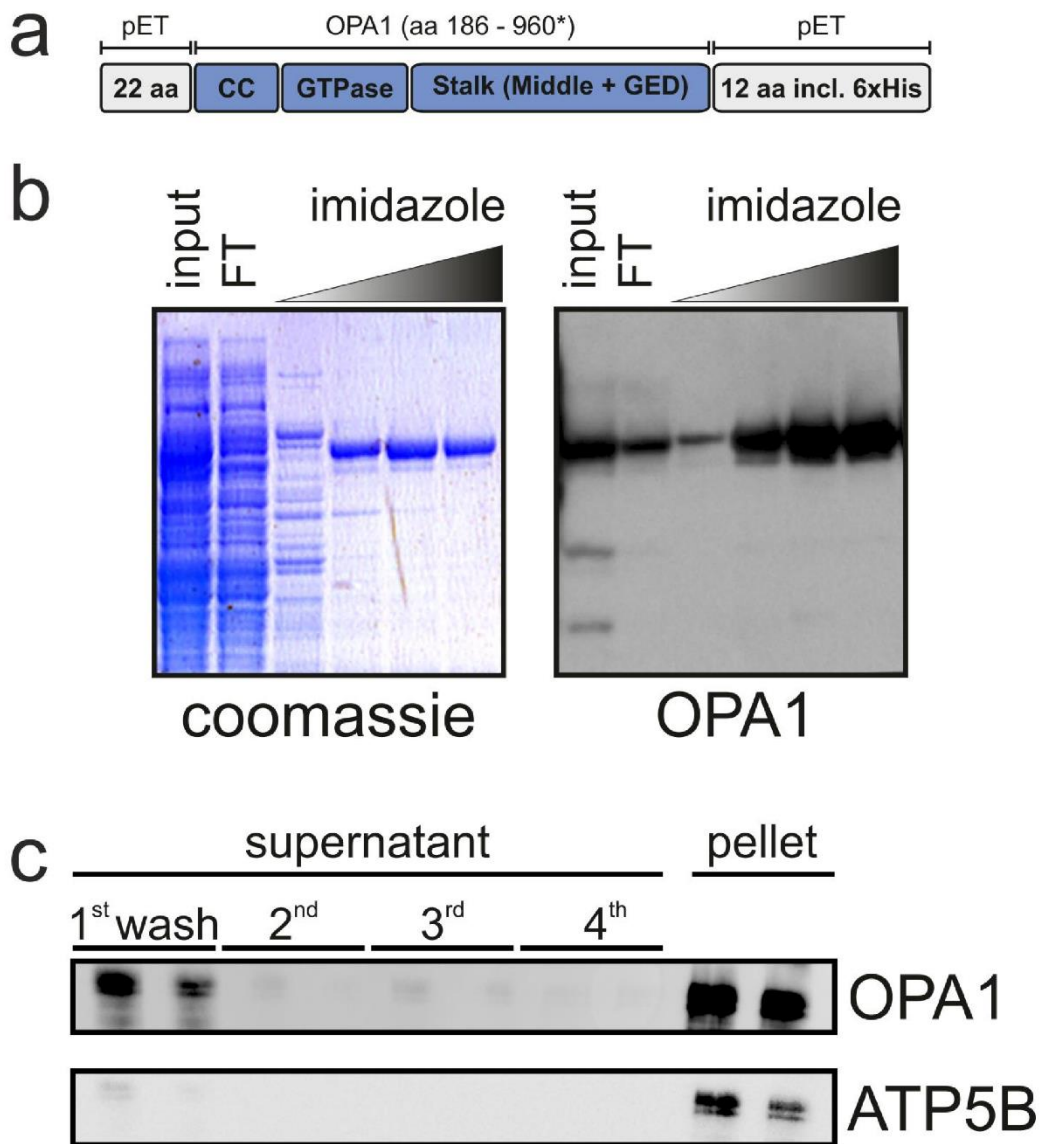
(a) BNGE analysis of OPA1 HMW complexes. Protein extracts (40  $\mu$ g) from cells of the indicated genotype treated where indicated with 1  $\mu$ M oligomycin for 30 min were separated by BNGE and immunodecorated with the indicated antibodies. Arrowhead indicates OPA1 HMW complex. SDHA: succinate dehydrogenase A.

(b) Mean  $\pm$  SEM of densitometric analysis of OPA1 high molecular weight (HMW, arrowheads) complexes versus total OPA1 conformations in 3 independent experiments as in (a).





**Supplementary Figure 5. IF<sub>1</sub> levels are comparable in WT and *Opa1<sup>tg</sup>* MAFs, Related to Fig. 3**  
Protein extracts (30 µg) from WT and *Opa1<sup>tg</sup>* MAFs were separated by SDS-PAGE and immunoblotted with the indicated antibodies.

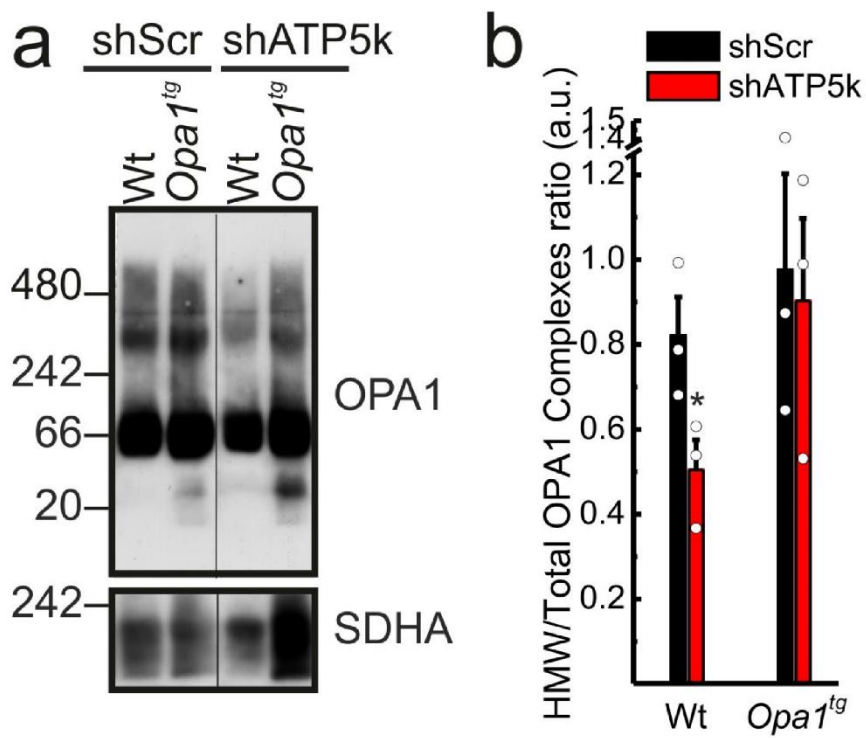


**Supplementary Figure 6. Production, purification and incorporation of rOPA1 in proteoliposomes. Related to Fig. 5**

(a) Cartoon of the produced recombinant OPA1 (rOPA1).

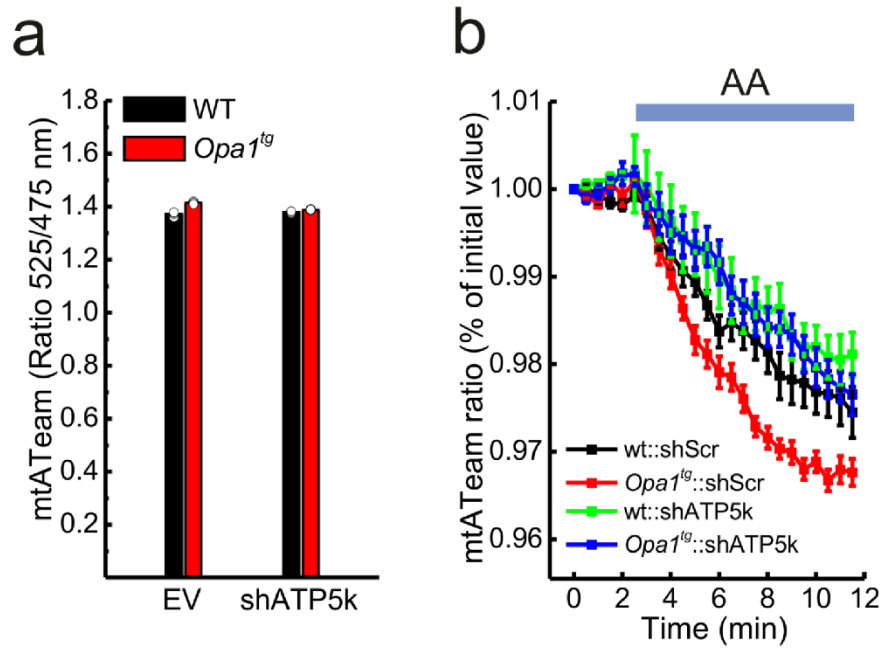
(b) Representative purification of rOPA1 analyzed by sampling at the indicated steps of the purification process and subsequent separation by SDS-PAGE. Proteins were visualized by immunoblotting with an anti-OPA1 antibody or Coomassie staining.

(c) Incorporation of rOPA1 in ATP synthase containing liposomes. Proteoliposomes incorporating purified ATP synthase (20  $\mu$ g) were prepared in the presence of 20  $\mu$ g rOPA1. Proteoliposomes were washed by centrifugation at 100,000xg. Proteins from the final pellet and the prior supernatants were separated by SDS-PAGE and immunoblotted using the indicated antibodies.



**Supplementary Figure 7. ATP5k silencing destabilizes OPA1 oligomers in Wt MAFs. Related to Fig. 6**

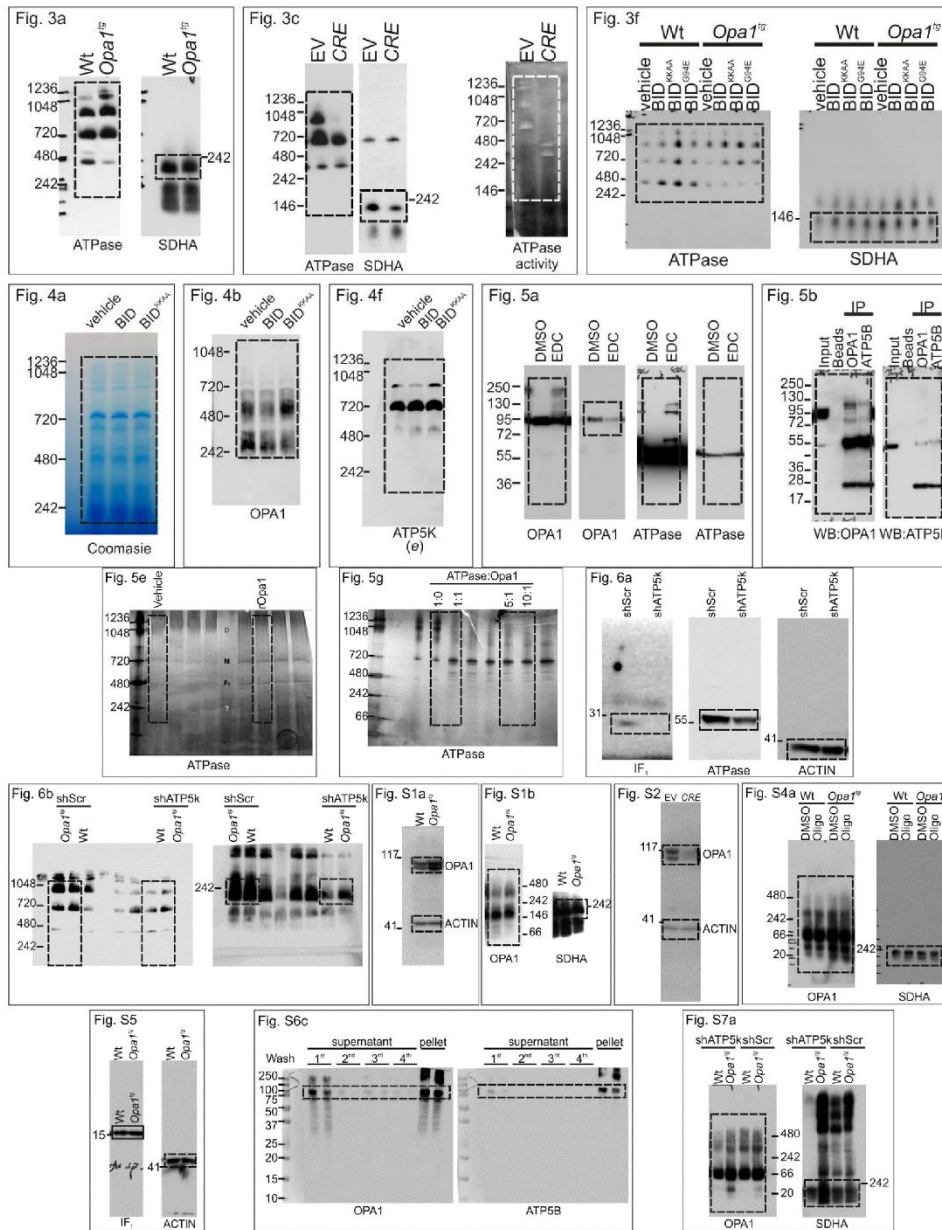
(a) BNGE analysis of OPA1 HMW complexes in protein extracts (30  $\mu$ g) from cells of the indicated genotype transfected for 48 h with the indicated shRNA. SDHA: succinate dehydrogenase A.  
 (b) Mean  $\pm$  SEM of densitometric analysis of OPA1 HMW/CII ratio, calculated from 3 independent experiments as in (a).



**Supplemental Figure 8. OPA1 requires ATP5k to promote ATPase activity, Related to Fig. 7.**

(a) Basal mtATeam mean±SEM FRET fluorescence emission ratios (525/475 nm) from at least 3 independent experiments performed in MAFs of the indicated genotype transfected with the indicated shRNA for 72 h.

(b) Mean±SEM normalized real time mtATeam FRET fluorescence analysis from 3 independent experiments as in (a). When indicated, cells were treated with 2 μM AA.



**Supplemental Figure 9. Uncropped blots**

Uncropped blots of the areas indicated in the shown figures. If not added here, full blots are shown in the figures. Dashed boxes indicate the cropped area





**3. A high throughput screening identifies a small molecule inhibitor of the GTPase activity of OPA1 that enhances apoptotic release of cytochrome c.**

Anna Pellattiero<sup>1,2\*</sup>, Charlotte Quirin<sup>1,2\*</sup>, Stéphanie Herkenne<sup>1,2</sup>, Nikolaos Biris<sup>3</sup>, Laura Cendron<sup>1</sup>, Eviropidis Gavathiotis<sup>3</sup>, and Luca Scorrano<sup>1,2\*</sup>



**A high throughput screening identifies a small molecule inhibitor of the GTPase activity of OPA1 that enhances apoptotic release of cytochrome c.**

Anna Pellattiero<sup>1,2\*</sup>, Charlotte Quirin<sup>1,2\*</sup>, Stéphanie Herkenne<sup>1,2</sup>, Nikolaos Biris<sup>3</sup>, Laura Cendron<sup>1</sup>, Eviropidis Gavathiotis<sup>3</sup>, and Luca Scorrano<sup>1,2\*</sup>

<sup>1</sup>Department of Biology, University of Padova, Via U. Bassi 58B, 35121 Padova, Italy

<sup>2</sup>Venetian Institute of Molecular Medicine, Via Orus 2, 35129 Padova, Italy

<sup>3</sup>Departments of Biochemistry and Medicine, Albert Einstein College of Medicine, Bronx, NY, United States

\* these authors contributed equally to this study.

\* Corresponding author.

Address correspondence to Luca Scorrano: [luca.scorrano@unipd.it](mailto:luca.scorrano@unipd.it)



## **SUMMARY**

The GTPase activity of OPA1, a dynamin-related mitochondrial protein upregulated in several tumors, controls cristae remodeling, cytochrome c release and apoptosis. To pharmacologically target OPA1 in cancer, we setup and iterated a high-throughput screening of a diversity based chemical library of 10,000 drug-like small molecules for recombinant purified OPA1 GTPase activity inhibition, identifying 8 candidates that were confirmed in a secondary screen. The most promising hit (MYLS22) was highly specific, as it could bind to recombinant OPA1 GTPase and did not inhibit recombinant Dynamin 1 GTPase activity. MYLS22 was not mitochondriotoxic, but it increased OPA1 oligomers disassembly and cytochrome c release in response to the proapoptotic stimulus BID in purified mitochondria and to hydrogen peroxide in cells, where MYLS22 caused the expected mitochondrial fragmentation. MYLS22 also phenocopied the inhibition of breast cancer cells migration caused by OPA1 silencing. Thus, we identified a first-in-kind OPA1 inhibitor with potential anti-cancer properties.



## INTRODUCTION

Mitochondria are multifunctional organelles that regulate several fundamental physiological and pathological cellular processes. They play crucial roles in metabolism, bioenergetics (Danial et al., 2003),  $Ca^{2+}$  signaling (Rizzuto et al., 2000), oxidative stress response (Orrenius et al., 2007), and integration and amplification of apoptotic signals (Green and Kroemer, 2004). Mitochondrial morphology is the result of a fine balance between fission and fusion processes, mediated by the “mitochondrial-shaping” proteins. The dynamin related protein (Drp) 1, along with its receptor proteins mitochondrial fission factor (Mff) and fission (Fis) 1, mediate mitochondrial fission, while fusion is controlled by mitofusins (Mfn) 1 and 2 at the outer membrane, and by optic atrophy (OPA) 1 at the inner membrane.

Mitochondrial dynamics ensures organelle plasticity, but it is also associated with several human disorders and tumors (Wallace, 2005). Mitochondrial-shaping proteins were first linked to cancer because of their role in apoptosis, whose inhibition is a hallmark of cancer cells (Hanahan and Weinberg, 2011). Subsequent studies revealed that changes in mitochondrial fission-fusion balance confer cancer cells the capacity to adapt their metabolism to environmental modifications, such as hypoxia, starvation, stress signals and even drug treatments (Patten et al., 2014; Rossignol et al., 2004).

Apoptosis is a natural barrier to uncontrolled cell proliferation and, thus, a crucial cancer defense. Indeed, dysregulation of apoptotic pathway is an hallmark of cancer (Hanahan and Weinberg, 2011). Tumor cells evolved different strategies to limit or overcome apoptosis, for example loss of tumor suppressors (as p53), activation of proto-oncogenes, upregulation of antiapoptotic protein (like Bcl-2 or IAPs) or

downregulation of proapoptotic factors (as Bax and Bak) (Hanahan and Weinberg, 2011).

The recent advances in high-throughput technologies allowed the genetic characterization of several tumor types and expanded the number of molecular targets. These advances rapidly increased the rush to the personalized cancer therapies. However, many challenges need to be overcome, as tumor heterogeneity and evolution, potential morbidity of biopsies, but especially the lack of effective drugs against most genomic aberrations and the absence of a specific genetic profile for each tumor type (Meric-Bernstam and Mills, 2012). On the other hand, conventional cancer drugs, as etoposide, cisplatin or doxorubicin, still widely employed in the clinics, exert their function by indirectly inducing apoptosis by engaging signaling pathways that lie upstream of mitochondria (Fulda et al., 2010). Unfortunately, cancer cells often become resistant to these treatments through modifications of the apoptotic mechanisms. For these reasons, drugs that directly target mitochondria are becoming of great interest because they reactivate cell death by bypassing the resistance mechanisms and sensitizing chemoresistant cells. Examples of mitochondria targeted drugs include the mitochondrial division inhibitor-1 (mdivi-1) that inhibits mitochondrial fission by reducing DRP1 self-assembly (Cassidy-Stone et al., 2008). Aurilide, which targets prohibitin 1 (PHB1), activating the proteolytic processing of OPA1 (Sato et al., 2011), or SMAC-mimetics that enhance caspase activity (Li et al., 2004) result in mitochondria-induced apoptosis. Manipulation of mitochondrial shaping proteins can also correct mitochondrial pathology caused by defective or imbalanced mitochondrial dynamics, as Charcot Marie Tooth disease type 2A (CMT2A). Recently, Rocha et al. identified the specific residues of MFN2 that contribute to the disease and restored

mitochondrial fusion and activity in the sciatic nerves of mice using a class of MFN2-agonist drugs (Rocha et al., 2018). TAT-367-384Gly, is a cell-permeable minipeptide that can reverse mitochondrial dysmorphologies in neurons harboring CMT2A gene defects by destabilizing the fusion-constrained conformation of MFN2 and promoting the fusion-permissive conformation (Franco et al., 2016).

Among all mitochondria-shaping proteins, OPA1 plays a central antiapoptotic role. Upon apoptosis induction, Bcl-2 family proteins permeabilize OMM and mitochondria undergo an ultrastructural remodeling (Scorrano, 2009; Scorrano et al., 2002; Scorrano and Korsmeyer, 2003). OPA1 controls this process, independently from its role in mitochondrial fusion. Indeed, OPA1 oligomers, containing both the membrane bound and the soluble forms of the protein, participate in the formation and in the maintenance of tight cristae, sequestering cytochrome c in the intra-cristae compartment (Frezza et al., 2006b). During apoptosis, OPA1 oligomers are early targets of BID, BIM-1, BNIP3 (Frezza et al., 2006b; Landes et al., 2010; Yamaguchi et al., 2008), and they are rapidly dissociated leading to cristae widening, cytochrome c mobilization from cristae for its subsequent release into the cytosol. (Frezza et al., 2006b; Scorrano et al., 2002). Downregulation of OPA1 leads to mitochondrial network fragmentation and increases cell sensitivity towards apoptosis, while mutations that abolish OPA1 catalytic activity impair its antiapoptotic function (Frezza et al., 2006b).

Interestingly, OPA1 is overexpressed in different type of cancers where it correlates with an increased chemotherapy resistance and a lower survival rate. For example, OPA1 is overexpressed in lung adenocarcinoma (LADC) patients where it increases cisplatin resistance via inactivation of caspase-dependent apoptosis; knockdown of

OPA1 sensitizes hepatocellular carcinoma cells to cytotoxic treatment and Akt-dependent downregulation of OPA1 facilitates cytochrome c release and apoptosis in lung cancer cells (Fang et al., 2012; Kong et al., 2014; Zhao et al., 2013). Two very recent reports consolidate the promising role of OPA1 inhibition in anti cancer therapy: first, OPA1 was identified as a member of a group of eight prognosis-related genes (including EBAG9, MTDH, ATP6V1C1, ATCL6A, BCL6, SENP5 and KRAS) likely to be important cross-cancer target genes for therapies and perhaps also associated with overall patient's survival rate, due to their recurrent copy number amplification across pan-cancer (Wee et al., 2018). Second, not only genes controlling mitochondrial dynamics were found to be recurrently amplified in multiple tumor types, but deletion of OPA1 (and DRP1) in a proof of principle experiment increased sensitivity of multiple cancer cells (lung, ovarian) toward specific SMAC-mimetic anticancer drugs (Anderson et al., 2018).

Because OPA1 function in apoptosis depends on its GTPase activity and is diminished by mutations in crucial GTPase domain amino acids, we explored the possibility that chemical inhibition of OPA1 GTPase activity could mimic these mutants. To this end we setup and implemented an *in vitro* high-throughput screening assay to test a library of chemical compounds for their effect on the GTPase activity of recombinant, purified OPA1 (Quintana-Cabrera et al., 2018). Screening a library of 10,000 diversity based, drug-like small molecules identified 8 compounds that block OPA1 GTP hydrolysis. We characterized the best hit, called MYLS22, that can bind to recombinant OPA1, inhibits OPA1 but not Dynamin 1, lacks mitochondriotoxic effects, but especially increases apoptotic release of cytochrome c from mitochondria *in vitro* and *in situ*.



## RESULTS

### **A high throughput screening for GTPase activity of recombinant OPA1.**

Since the three-dimensional crystal structure of OPA1 is unavailable and there are no published inhibitors of OPA1, we could not perform a virtual screening or create a lead pharmacophore model for molecular docking. Therefore, we first built a structural model based on the homology of OPA1 with twenty protein templates selected to maximize confidence, percentage identity and alignment coverage of OPA1 (Figure 3B). Inspection of this model revealed an overall structural organization resembling that of crystallized proteins of the family, including dynamin (Ford et al., 2011a) and DRP1 (Daumke and Praefcke, 2016). It revealed the organization of the GTPase domain, with the position of residues unique to OPA1 (e.g., 402-VINTVT-407) that can in principle confer OPA1 specificity over other members of the superfamily. However, in order to identify lead molecules that could inhibit OPA1, we turned to a wet biology approach, capitalizing on our experience with *E. coli* expression and affinity chromatography purification of a recombinant OPA1 (rOPA1) protein, corresponding to *Mus musculus* isoform 1 (Uniprot: P58281) lacking the mitochondria targeting sequence and the transmembrane domain (aa 1-167), fused to a C-terminal 6X His-tag (Quintana-Cabrera et al., 2018) (Figure 3A). We therefore scaled up Ni-NTA beads affinity chromatography protein purification, yielding approximately 1 mg of rOPA1 per liter of BL(DE3) *E. coli*.  $K_m$  and  $V_{max}$  of the dialyzed rOPA1 measured by reverse phase chromatography (RPC) were  $274.1 \pm 20.5 \mu\text{M}$  and  $0.75 \pm 0.18 \mu\text{M}$ , respectively, in the range of other dynamin like proteins (Cassidy-Stone et al., 2008) and with very limited batch variability. Because reverse phase chromatography is unsuitable for high throughput analysis, we turned to the malachite green (MG) colorimetric assay that

quantifies the free phosphate released during the hydrolysis of GTP into GDP (Leonard et al., 2005). Kinetic properties of rOPA1 measured with the MG assay were superimposable to those obtained by RPC, further supporting the use of this approach to screen for OPA1 inhibitors (Supplementary Figure S1A).

We therefore adapted our assay to a high-throughput mode. We first optimized the enzyme to substrate ratio (rOPA1/GTP) to increase the sensitivity of the miniaturized assay without affecting the specificity of the detection and we fixed rOPA1 at 0.2  $\mu$ M and GTP at 500  $\mu$ M. Next, we confirmed that rOPA1 activity could be inhibited by increasing concentrations of the non-hydrolysable GTP analogues GTP $\gamma$ S and GMPPNP (Supplementary Figure S2B). We also evaluated the potential interference of dimethyl sulfoxide (DMSO), the solvent used to solubilize the compounds from the chosen library, on measured rOPA1 activity, and we excluded that a final 2.5% (V/V) DMSO concentration affected the measured rOPA1 activity or interfered with MG absorbance (Supplementary Figure S2C). We then looked for a strong positive control for rOPA1 inhibition. We compared inhibition by GTP $\gamma$ S and ethylenediaminetetraacetic acid (EDTA) which chelates the Mg<sup>2+</sup> ions required for GTP hydrolysis. While we retrieved a residual rOPA1 activity upon GTP $\gamma$ S treatment, EDTA stably and fully inhibited GTP hydrolysis. Moreover, GTP $\gamma$ S strongly altered the absorbance readout, further complicating its use in a high-throughput setting (Supplementary Figure S2C). To understand whether rOPA1 inhibition was affected by the duration of incubation time with the inhibitor before GTP addition, we assessed the influence of different GTP $\gamma$ S incubation times on rOPA1 activity. Although no significant difference was observed, incubation for 10 minutes appeared to be sufficient to fully inhibit the enzyme ((Supplementary Figure S2E), in line with the

general suggestion that equilibration between enzyme and the potential inhibitor prior to addition of the substrate shall be allowed (Copeland, 2003). Finally, we optimized buffer conditions for rOPA1 GTPase activity measurements (Quintana-Cabrera et al., 2018). Like the other dynamin superfamily GTPases, rOPA1 required  $Mg^{2+}$  as cofactor for GTP hydrolysis (Supplementary Figure S1A), which was irreplaceable by  $Mn^{2+}$  (Supplementary Figure S2G-H) and a low ionic strength buffer to prevent the protein oligomerization and precipitation. Furthermore, rOPA1 GTPase activity was not influenced by 500  $\mu M$  GDP, excluding inhibition by GDP throughout the incubation time of the assay (Supplementary Figure S2F). These parameters were used to design a pipeline for a semi-automated 384-well plates HTS (Table 1).

### **HTS for rOPA1 small molecule inhibitors: data-processing and hit identification**

We next proceeded to perform the MG based, rOPA1 GTPase activity HTS on a library of 10,000 selected, pure drug-like small molecules (MyriaScreen, Aldrich) enriched with privileged motifs computed to fulfil the “Lipinski’s rule of 5”, which defines the essential chemical and physical properties of drugs to ensure their permeability and bioavailability (Lipinski et al., 2001). The 10,000 small compounds of the MyriaScreen library were tested at a single concentration ranging from 50 to 200  $\mu M$ . Because high-throughput assays may show large variability with respect to intra-plate and inter-plate results, day-to-day and batch-to-batch comparisons (Goktug et al., 2013), we employed graphical and statistical quality control metrics to validate the quality of our developed assay and to meet minimum standards ensuring that positive hits can be distinguished from the noise of the assay.

We used strictly standardized mean difference [SSMD, i.e. the ratio of the mean to the standard deviation (SD) of the difference between the two populations (Zhang, 2007)] that measures the strength of the difference between two compared groups, to assess the difference between positive and te negative control samples. The larger the value of the SSMD between the two controls, the greater the difference between the two populations. In assays resembling ours, where positive controls (maximal inhibition of rOPA1) have a value smaller than negative controls (minimal inhibition of OPA1), plates with SSMD values  $\leq -3$  pass the quality control (Zhang, 2007). In our case the assay remained sufficiently robust throughout the screening and, as demonstrated by the plate-specific SSMD values, only 4 plates did not pass quality control (Figure 1B). The graphical raw data visualization also contributes to the quality control review process. We plotted raw data of each sample of the 32 assayed 384-well plates against its well number. The resulting scatter plot indicated that the assay was well behaved: with few exceptions, we identified an average robust assay signal window between positive and negative controls, even if negative controls spanned a larger range of values than the positive controls. Also, the scatter plot revealed that the 10,000 small-molecules could be divided in two clearly distinct populations: most of the compounds were inactive, i.e. their effect on rOPA1 activity resembled that of the negative controls. A second population comprised active compounds, whose rOPA1 inhibition levels falling in between negative and positive controls (Figure 1B). Comforted that our HTS passed these two quality controls, we decided to normalize MG raw data as normalized percent of inhibition (NPI), i.e. as percentage activity relative to negative controls. We then binned the NPI values in a corresponding trellis heat map of the 32 screened 384-well plates, where wells were colored according to

the binning, encoded by continuous color changes from dark red (high inhibition) to dark blue (low inhibition). The heat map did not reveal any noticeable systematic pattern that may represent error of reagent pipetting (Figure 1D). In both the heat map and the scatter plot representations, control and sample areas matched with respect to the raw measurement values (Figure 1C-D). A more careful inspection allowed us to identify the 4 excluded plates with lower variability in the positive and negative controls, already readily apparent in the SSMD plot (Figure 1B). Nonetheless, these 4 plates did not exhibit significantly different patterns in the distribution of the NPI values of the compounds.

Due to the low activity of rOPA1 and the assay detection limits, the primary screen was performed with relatively high GTP concentrations, as 500  $\mu$ M GTP is above the  $K_m$  of OPA1 (Quintana-Cabrera et al., 2018). Generally, this enriches the identification of uncompetitive compounds and non-competitive inhibitors instead of competitive inhibitors (Copeland, 2003). Running the assay at higher substrate concentrations was however inevitable to obtain a sufficiently robust assay. Yet, the conditions were merely met, and we compensated for the assay's limitations by setting a conservative threshold that included only the most potent inhibitors of the screen. The calculated NPI values from the raw data allowed ranking the samples based on their inhibitory potential (Figure 1E). Most of the tested compounds showed no effect on OPA1 GTPase activity, as shown before, and hence had a value around 1, similar to the negative controls. Compounds that affected OPA1 activity displayed values smaller than 1 with a minimum of 0, as the positive control containing EDTA. Considering the compounds with a NPI value between 1 and 0 (Figure 1F), we selected as inhibitors the compounds that decreased the activity of OPA1 by at least 30%, corresponding to

NPI < 0.7 (dashed line in Figure 1E-F). After two rounds of library screening, only compounds identified in both individual and replicate analysis were retained (Table 2). Of these, the compounds that *per se* reduced the absorbance at the measured wavelength were considered as false positives and were excluded from the list. Eventually, we identified 8 potential inhibitor molecules that decreased OPA1 GTPase activity by at least 30% and that were christened MYLS2, MYLS3, MYLS5, MYLS9, MYLS10, MYLS14, MYLS16 and MYLS22 (Figure 1G and 2A-H).

### **Hit validation by concentration response curve**

The screened library contains small compounds selected based on their drug-likeness and for their chemical diversity. Hence, all identified compounds fulfilled the Lipinski's rule of 5 (Lipinski et al., 2001). Only MYLS21, also known as Suramin, is an exception to these rules, yet it is the only compound already in the clinics (Kaur et al., 2002).

To evaluate the 8 compounds selected from the primary HTS for their ability to inhibit rOPA1 GTPase activity, we tested them in a dose-response experiment at concentrations ranging from 1 nM to 750  $\mu$ M. All 8 inhibitors showed an inhibitory activity increasing with the rising of their concentrations (Figure 2A-H), confirming that they truly inhibit rOPA1 GTPase activity. We fitted data with a four-parameter curve to evaluate the potency as half-maximal inhibitory concentration ( $IC_{50}$ ) and maximal inhibition ( $I_{max}$ ), as well as the nature of the inhibition, based on the calculation of Hill coefficient (Figure 2). We grouped the compounds into moderate (Figure 2D, E, G, H) and potent inhibitors (Figure 2A, B, C, F), according to the maximal rOPA1 inhibition they exerted. Compounds that bind a single site on an enzyme yield Hill slopes of 1 and deviations may indicate that the inhibitor blocks activity nonspecifically. Most of

the identified inhibitors showed a Hill slope bigger than 1 except for MYLS5, MYLS22 and MYLS16, which may suggest unspecific inhibition through aggregation. In conclusion, we identified the first in class *in vitro* inhibitors of OPA1 GTPase activity. Among them MYLS22 was recognized as the most potent inhibitor of OPA1 activity ( $IC_{50}=96.5 \mu\text{M}$ ,  $I_{\text{max}}=0.78$ ) (Figure 2A).

### **MYLS22 is a specific OPA1 GTPase activity inhibitor.**

To identify possible MYLS22-binding sites within OPA1 structure and to confirm the results of the *in vitro* screening, we set up a molecular docking analysis. Interestingly, the best scoring pose of MYLS22 was identified within the hydrophobic GTP-binding pocket of OPA1 (Figure 3F-G). A close analysis of the MYLS22 binding pose suggested hydrogen bonding interactions with the residues Gln-297, Gly-319 and Asn-404 in the active site of OPA1 (Figure 3E). Gln-297 and Gly-319 are two well conserved residues in the P-loop and in the Switch I regions of dynamins, that participate in the GTP hydrolysis process of OPA1 and show a high degree of similarity with the other dynamin superfamily proteins. Notably, beyond the GTP-binding motif, MYLS22 also potentially contacts an OPA1-specific region that include Asn-404 and does not present similarity with other dynamins (Supplementary Figure S2A). This interaction appears to be important for defining potential specificity of the inhibitor.

Indeed, to verify the interaction between MYLS22 and the G domain of OPA1, we purified a recombinant mouse OPA1 fusion protein consisting of the G domain connected by a linker with the BSE domain of GED (Figure 3C-D). To investigate the OPA1 G domain-MYLS22 interactions in solution, we took advantage of the saturation

transfer difference (STD) Nuclear Magnetic Resonance (NMR) spectroscopy technique. This is a powerful tool for detecting also weakly binding ligands by recording one-dimensional NMR spectra, using relatively small amount of protein. The protons that are in close contact with the OPA1 protein receive a higher degree of saturation, resulting in stronger STD NMR signals. Protons that are either less or not involved in the binding process reveal no STD NMR signals. The difference between a STD spectrum and a reference NMR spectrum can identify the binding between the protein and the compound. Thus, we performed the STD NMR experiment to explore the propensity of MYLS22 to interact with the G domain of OPA1. The reference spectrum exhibited narrow and well resolved lines (Figure 3H). Although modest, the STD spectrum exhibited specific signals that confirm the interaction of the inhibitor with OPA1.

Even though the *in silico* docking results suggested some potential specificity of OPA1 inhibition by MYLS22, we were faced with the fact that the GTPase domain is the most conserved region among the dynamin superfamily proteins. We therefore decided to test the specificity of MYLS22 toward OPA1, by comparing the effects of the identified OPA1 inhibitors on the GTPase activity of Dynamin-1 (Dyn1), one of the closest homologues of OPA1 (Ford et al., 2011b). We successfully expressed and purified in *E. coli* a recombinant Dynamin-1 protein lacking the proline rich domain (PRD) (Dyn1 $\Delta$ PRD) (Figure 4D). Using the MG assay, we measured the GTPase activity of the Dyn1 $\Delta$ PRD in the presence of MYLS22. While the other identified inhibitors displayed different degrees of Dyn1 $\Delta$ PRD inhibition, MYLS22 did not, even at concentrations four times above the calculated IC<sub>50</sub> for OPA1 (Figure 4E). In



conclusion, MYLS22 binds to OPA1 GTPase domain and selectively inhibits OPA1 GTPase activity.

### **MYLS22 is a cell-permeable lipophilic small molecule.**

The determination of the cellular bioavailability of small-molecule inhibitors is a critical step for interpreting cell-based data and directing inhibitor optimization (Teuscher et al., 2017). The discrepancies between the results obtained in biochemical and cell-based assays have been a recurring problem when novel inhibitors identified from biochemical studies are assessed in cells (Bunnage et al., 2013; Hann and Simpson, 2014; Morgan et al., 2012). This difference has traditionally been ascribed to the low permeability of the compound through the cell membrane. Thus, we first assessed MYLS22 physicochemical properties, which included its aqueous solubility and stability in cell culture medium. MYLS22 is a drug-like molecule that meets all the physicochemical requirements indicated in the Lipinski's rule of five (Lipinski et al., 2001). Nevertheless, the inhibitor is characterized by a low aqueous solubility and a low hydrophilicity (Log P = 3.67, Log D = 3.51) (Supplementary Table S1). MYLS22 is soluble in DMSO up to 1 mM and in cell culture medium up to 150  $\mu$ M.

Fluorescence provides a sensitive mean to assess whether a drug can be taken up by cells, but its use is limited by the occurrence of a chromophore that can absorb UV or visible light providing fluorescence at a longer wavelength. MYLS22 is characterized by absorption and emission bands in the UV region of the electromagnetic spectrum and, unfortunately, it does not have any chemical structure that produces a fluorescence signal. Therefore, we could not take advantage of the fluorescence

properties of the molecule for its direct visualization in complex media. Nevertheless, we succeeded in measuring the cell permeability of MYLS22 with two independent and complementary methods by exploiting its absorbance at 280 nm. We incubated mouse embryonic fibroblasts (MEFs) with MYLS22 in HBSS, to avoid the strong 280nm absorption by proteins of DMEM and we measured the remaining MYLS22 (by using its 280nm absorption as a proxy) over time (Supplementary Figure S3A). The concentration of MYLS22 in the extracellular medium decreased with incubation time (Figure 4A). However, this did not exclude its non-specific binding to the culture dish. To verify the effective presence of MYLS22 inside the cells we turned to a reversed-phase high-performance liquid chromatography (HPLC)-UV method on lysates preprocessed with solid-phase extraction (SPE), which significantly enhanced the sensitivity of the HPLC-UV method. The SPE led to the double advantage of separating small hydrophobic molecules from cell lysate proteins and of simultaneously changing the solvent, thus improving MYLS22 solubility. After SPE, samples were injected into an analytical reversed-phase C18 column with a gradient of trifluoroacetic acid (TFA) (0.1% v/v)/acetonitrile as mobile phase. The HPLC method was optimized so that the retention time of the inhibitor did not overlap with any other components present in the cell lysates. We succeed in isolating the elution peak of MYLS22 detected by the absorbance at 280 nm, in a total run time of 15 min (Figure 4B). The cells were incubated with the inhibitor and, after 24 h, were lysed and the inhibitor was subjected to the SPE. MYLS22 intracellular concentrations were calculated using a calibration curves of the amount of the inhibitor extracted over the initial amount of the inhibitor directly added to the cell lysate prior to SPE. The amount of inhibitor uptake from cells was determined by comparing the area under the curves

(AUCs) in the HPLC chromatograms. The cellular uptake for MYLS22 resulted to be 20% when the input concentration was 100  $\mu$ M. Overall, these results demonstrated that MYLS22 is a membrane-permeable molecule that can enter mammalian cells.

**MYLS22 *per se* does not cause cell death and is not mitochondriotoxic.**

We next verified if MYLS22 induced direct cytotoxic effects. We found that concentrations of MYLS22 up to 100  $\mu$ M did not cause MEFs death (Figure 4C). Because cultured cells can survive extensive mitochondrial dysfunction by operating the reversal mode of the ATP synthase (Quintana-Cabrera et al., 2018), we decided to measure if MYLS22 stimulated mitochondrial depolarization in response to the  $F_1F_0$  ATPase inhibitor oligomycin, a sensitive test of latent mitochondrial dysfunction in intact cells (Irwin et al., 2003). Real-time imaging of the mitochondrial potentiometric dye tetramethyl rhodamine methyl ester (TMRM) fluorescence in response to oligomycin showed that membrane potential was stable in MEFs treated with MYLS22 over a range of concentrations well above rOPA1  $IC_{50}$  (Figure 4F). We further confirmed the lack of mitochondrial toxicity *in vitro*, using mitochondria purified from mouse liver. Irrespective of whether mitochondria were energized using complex I (glutamate/malate, Figure 4G) or complex II (succinate, Figure 4H) substrates, MYLS22 pretreatment did not reduce uptake of the potentiometric dye Rhodamine 123, over a range of concentrations well above rOPA1  $IC_{50}$ . Thus, MYLS22 does not induce *per se* primary mitochondrial dysfunction and we defined a safe range of MYLS22 concentrations that could be used to assess inhibitor-specific cellular function devoid of unrelated cytotoxic side effects.

### **MYLS22 induces mitochondrial fragmentation.**

OPA1 is a mitochondrial-shaping protein involved in inner mitochondrial membrane fusion (Chen et al., 2005; Cipolat et al., 2004; Song et al., 2007) and as expected, OPA1<sup>-/-</sup> cells display fragmented mitochondrial network with defects in cristae shape (Cogliati et al., 2013a). Notably, OPA1 requires an intact GTPase domain to fuse mitochondria and GTPase mutants expressed in cells harbouring WT OPA1 cause mitochondrial fragmentation (Frezza et al., 2006a). Because of these aspects of OPA1 biology, any chemical OPA1 inhibitor is expected to cause mitochondrial fragmentation. We therefore tested whether a panel of MYLS22 concentrations led to fragmentation of WT MEFs mitochondria. Visual inspection of confocal images of MEFs expressing mitochondrially targeted YFP (mtYFP) revealed that MYLS22 caused a dose dependent mitochondrial fragmentation and decrease in mitochondrial length, leading to the appearance of completely fragmented organelles similar to the ones imaged in OPA1<sup>-/-</sup> MEFs (Figure 5A-B). In conclusion, MYLS22 causes extensive mitochondrial fission in situ.

### **MYLS22 enhances cytochrome c release from mitochondria during apoptosis.**

In addition to, and independently from its role in mitochondrial fusion, OPA1 plays a key function in the regulation of apoptotic cell death, (Frezza et al., 2006b). Its downregulation increases cell sensitivity to induced apoptosis (Frezza et al., 2006b; Lee et al., 2004; Olichon et al., 2003b; Olichon et al., 2007b), while its overexpression

protects from apoptosis by preventing cytochrome c release (Frezza et al., 2006b). Because OPA1 requires integrity of the GTPase domain also to prevent cytochrome c release (Frezza et al., 2006b), we expected that OPA1 inhibition by MYLS22 would lead to enhanced cytochrome c release. Indeed, MYLS22 enhanced in a concentration-dependent manner the amount of cytochrome c released from purified mouse liver mitochondria in response to the active form of the proapoptotic Bcl2 molecule BID (cBID) (Frezza et al., 2006a), irrespective of whether we measured it by immunoblotting or by an established quantitative cytochrome c ELISA. Already at a low concentration of 25 $\mu$ M, MYLS22 increased by 1.7-fold the amount of cytochrome c release, that was more than doubled when mitochondria were treated with 125  $\mu$ M MYLS22. (Figure 6A-B). Interestingly, these two MYLS22 concentrations enhanced the cBID-mediated disruption of the chemically crosslinkable OPA1 oligomers, whose destabilization correlates with cristae remodeling and complete cytochrome c release (Frezza et al., 2006a; Varanita et al., 2015) (Figure 6C).

We next verified whether MYLS22 similarly influenced the release of cytochrome c in a cell-based assay. Following treatment with the intrinsic apoptotic, mitochondria dependent stimulus H<sub>2</sub>O<sub>2</sub> (Scorrano et al., 2003a), MEFs incubated with 50 $\mu$ M MYLS22 released cytochrome c significantly more rapidly than cells incubated with 25  $\mu$ M MYLS22 or with DMSO, reaching maximal release already 30 min after apoptosis induction (Figure 6D-E). Taken together, these data show that MYLS22 treatment enhances in a dose-dependent manner the release of cytochrome c in response to an apoptotic stimulus.

## **Breast cancer cells migration is sensitive to genetic and pharmacological inhibition of OPA1.**

While our data confirm that processes controlled by OPA1 (mitochondrial fusion and cytochrome c release) can be targeted by OPA1 inhibitors in vivo, they have been obtained on normal mouse organelles and tissues and we lacked evidence that MYLS22 could target human cancer cells. Very recently, OPA1 was identified as one of the eight prognosis-related genes that exhibit high alteration frequency and amplification across pan-cancer including breast cancer where OPA1 was significantly overexpressed (Wee et al., 2018). We therefore turned our attention to MDA-MB-231 cells, a human metastatic breast adenocarcinoma cell line, and measured if MYLS22 could block MDA-MB-231 migration, an essential feature of cancer metastatization that in these cells is controlled by mitochondrial morphology (Zhao et al., 2012). When we blocked OPA1 genetically, by efficient siRNA-mediated silencing of *OPA1* (Figure 7A), migration was reduced by ~50% in a classic scratch assay. A very similar inhibition was achieved by treatment with MYLS22 (Figure 7B). Most importantly, the effect of MYLS22 on cell migration was not additive to that of OPA1 silencing (Figure 7C), indicating that MYLS22 acts specifically by blocking OPA1. Overall, these results demonstrate that safe concentrations of MYLS22 decrease cancer cell migration and suggest that MYLS22 act on the same OPA1-dependent pathway that controls cell migration.

## DISCUSSION

The alteration of apoptotic mechanisms allows cancer cells to escape from drug-induced death, proliferate in unfavorable conditions, acquire further genetic mutations, induce angiogenesis and perhaps metastatisation (Hanahan and Weinberg, 2011; Lopez and Tait, 2015). Since survival of tumor cells hinges on dysregulation of their apoptotic pathway, novel drugs that selectively target mitochondrial protein are becoming of great interest.

Numerous studies demonstrated that OPA1 is an antiapoptotic protein that plays a fundamental role in the control of the apoptotic cristae remodeling to achieve a complete release of cytochrome c from the mitochondria (Del Dotto et al., 2017; Frezza et al., 2006b; Griparic et al., 2004; Olichon et al., 2003b). Higher levels of OPA1 protein were reported in different tumor types, as lung adenocarcinoma, breast and endometrial cancers (Anderson et al., 2018; Fang et al., 2012; Wee et al., 2018). Overexpression of OPA1 correlates with an increased resistance to conventional chemotherapeutics, such as cisplatin and sorafenib, and with a lower survival rate (Fang et al., 2012; Kong et al., 2014; Zhao et al., 2012). Indeed, knockdown of OPA1 in hepatocellular carcinoma cells sensitized them to cytotoxic treatment (Zhao et al., 2012) and indirect Akt-dependent downregulation of OPA1 facilitated cytochrome c release and apoptosis in lung cancer cells (Cho, 2011). Recently, Anderson and colleagues discovered that the recurrent amplification of OPA1 gene in multiple tumors is responsible of different cell sensitivities toward specific category of anticancer drugs (Anderson et al., 2018). Furthermore, OPA1 has been ascribed as a potential cancer biomarker along with other seven genes that showed recurrent copy number

amplification across pan-cancer (Wee et al., 2018). Of note, the OPA1 antiapoptotic activity depends on its ability of hydrolyze GTP, since mutations that abolish OPA1 GTPase activity also impair its antiapoptotic function (Frezza et al., 2006b). Given these observations, we decided to develop an HTS to discover small molecule inhibitors of OPA1 GTPase activity, with the aim of using them in combination therapy to increase apoptosis sensitivity and overcome drug resistance of tumor cells.

Through a specifically designed HTS of a library of 10,000 drug-like molecules, we successfully identify a potent and selective *in vitro* inhibitor of OPA1 GTPase activity, named MYLS22. The use of an *in vitro* HTS instead of a cell-based assay, allowed us to directly measure, in a quantitative manner, the potency of potential OPA1 inhibitors, without the risk of off-targets or indirect effects. Docking experiments using a molecular homology model of rOPA1, revealed that the best scoring pose of MYLS22 was within the hydrophobic GTP-binding pocket of OPA1, lending further support to the *in vitro* assay. Nevertheless, the *in vitro* conditions do not reproduce the physiological environment of the targets, thus they cannot predict the activity of the compounds *in vivo*. For this reason, once identified the most potent compound, we tested its inhibitory capacity in a MEF cells culture model. Given the low water solubility of the compound, the determination of its cellular bioavailability represents a critical step for interpreting cell-based results (Teuscher et al., 2017) and compared them with the *in vitro* data of the screening. Solid-phase extraction followed by reverse-phase HPLC, allowed us to detect MYLS22 in the cell lysates, confirming its cellular uptake. Although the cellular uptake of MYLS22 is low, the conjugation with a positively charged lipophilic cation, as the triphenyl-phosphonium group (TPP<sup>+</sup>) could represent an efficient method to increase the potency of the drug.



The major struggles in the development of an effective dynamin inhibitor is the specificity of the compound. Some examples of published dynamin inhibitors have failed to selectively block a specific isoform of dynamin. For example, the DRP1 inhibitor mdivi-1 can stimulate cell death also in DRP1 knockout cells and has off-target effects, like complex I inhibition (Bordt, 2017). The lack of specificity of dynamin inhibitors could be explained considering the high homology and conservation of the GTPase catalytic domain of the dynamin superfamily proteins. In this regard, MYLS22, even if it targets the GTP-binding pocket of OPA1, appeared to retain a high grade of specificity, since it does not inhibit Dynamin-1 activity, even at concentration four times higher than its IC<sub>50</sub>. This is likely due to the ability of the drug to bind to specific residues that lie out of the GTPase domain and are OPA1 specific.

By capitalizing on a variety of in vitro and in vivo assay for mitochondrial function, we defined a safe range of MYLS22 concentrations, that do not induce cell death *per se* or lead to mitochondrial toxicity. These allowed us to assess the inhibitor-specific cellular functions without unrelated cytotoxic side effects. MYLS22 induces mitochondrial network fragmentation and decreases mitochondrial length in a concentration-dependent manner, recapitulating the mitochondrial morphology of OPA1<sup>-/-</sup> cells. Furthermore, MYLS22 stimulates in a concentration-dependent manner the release of cytochrome c in response to apoptotic stimuli. Notably, in cells treated with MYLS22 without any apoptotic stimuli, mitochondria were fragmented, but still retained cytochrome c, further confirming that MYLS22 *per se* is not cytotoxic. Finally, MYLS22 was efficacious against metastatic MDA breast cancer cells migration, where MYLS22 did not produce any additive effects over OPA1 silencing on cell migration, confirming its specificity for OPA1.

Overall, MYLS22 represents the first reported OPA1 inhibitor that specifically target OPA1 GTPase activity and enhances apoptotic cytochrome c release. This small molecule could be employed as a tool for further investigation of the OPA1-controlled pathways or to shed light on still undefined OPA1-related processes, as the mechanism of OPA1 oligomers disruption by BID during apoptosis induction. The significance of this work also resides in the identification of a candidate and a chemical signature that can be used for further evaluations as anticancer drug leads to design more effective therapeutic treatments. Improvements could be obtained via the optimization of the dose and by improving the delivery strategy, for example by prompting mitochondrial accumulation of MYLS22 through its functionalization with a polycationic chemical group, as the TPP<sup>+</sup>. Further work is also required to investigate possible combinations and synergistic effects of MYLS22 with classic chemotherapeutic drugs, as doxorubicin, etoposide or cisplatin.

## **EXPERIMENTAL PROCEDURES**

### **Cell culture**

WT OPA1 SV40 transformed mouse adult fibroblast (MAFs) were generated from WT mice as previously described (Cogliati et al., 2013). Cell lines were cultured in Dulbecco's Modified Eagle Medium (DMEM, Invitrogen) supplemented with 10% FBS (Invitrogen), 2 mM Glutamine, 50 U/ml Penicillin, 50 µg/ml Streptomycin, 50 µg/ml Uridine, and 0.1 mM non-essential aminoacids (Invitrogen).

### **OPA1 silencing**

MDA-MB-231 cells were transfected for 72 h with the OPA1 siRNA using Lipofectamine 2000 following manufacturer's instruction. MDA-MB-231 cells transfected with scrambled siRNA were used as control. The siRNAs were transfected at a final concentration of 100 nM. Silencing efficiency was evaluated by OPA1 immunoblotting.

### **Production and purification of recombinant proteins**

OPA1 mouse transcript variant 2 (NM\_133752) was amplified from position 502 to the stop codon to produce recombinant OPA1 (rOPA1) lacking the N-terminal mitochondrial targeting sequence and the transmembrane domain. For the rOPA1 Chimera, were amplified only the sequences corresponding to the G domain and the GED of OPA1, connected with a linker and all cysteines were mutated into alanines.

The PCR products were cloned into pET21+ (Novagen) which adds a His-tag to the C-terminus of the encoded proteins and expressed in *E. coli*. Proteins expression was induced with 0.5  $\mu$ M IPTG for 20 hours at 18 °C. Cells were collected by centrifugation and the pellet was resuspended in lysis buffer (40 mM Hepes/KOH, 500 mM NaCl, 10% glycerol, 5 mM MgCl<sub>2</sub>, 5 mM  $\beta$ -mercaptoethanol, 0.5% Triton-X-100, 2% Tween-20, 1 mM PMSF, 20 mM Imidazole, Roche protease inhibitor cocktail, pH 8.0), were lysed by sonication and cell debris was removed by centrifugation at 14000g for 45 minutes, 4 °C. rOPA1 was purified by Ni-NTA batch chromatography. Prior to elution, beads were washed with 1 mM ATP and 10 mM MgCl<sub>2</sub> in lysis buffer for 30 minutes at room temperature followed by a washing step in wash buffer (40 mM Hepes/KOH, 300 mM NaCl, 0.05% Triton-X-100, 5 mM MgCl<sub>2</sub>, 5 mM  $\beta$ -mercaptoethanol, 10% glycerol, 20 mM Imidazole, pH 8.0). rOPA1 and rOPA1 Chimera were eluted with increasing concentrations of imidazole in elution buffer (40 mM Hepes/KOH, 0.05% Triton-X-100, 5 mM  $\beta$ -mercaptoethanol, 10% glycerol, pH 7.4). Imidazole was removed by dialysis and the proteins were concentrated in storage buffer (40 mM Hepes/KOH, 0.05% Triton-X-100, 0.3 mM TCEP, 10% glycerol) and stored at -80 °C until use. The activities of the proteins were verified and measured with the malachite green assay.

p7/p15 recombinant cBID was expressed, purified and cleaved with caspase-8 as previously described (Frezza et al., 2006).

### **Analysis of protein expression**

Protein concentration from total cell extracts or mitochondria lysates was assessed with Bradford reagent (Bio-Rad) and equal amounts of proteins were separated by 3-8% Tris-Acetate SDS-PAGE (NuPage, Invitrogen). Fractions of the affinity purification of rOPA1 were resolved by 4-12% Bis-Tris SDS-PAGE (NuPage, Invitrogen). Western blotting was performed by transferring proteins onto PVDF membranes (Merck) and probed using anti-OPA1 monoclonal (1:1000, BD Pharmingen™), anti-cytochrome c monoclonal (1:1000, BD Pharmingen™) anti-GRP75 (1:1000, Santa Cruz Biotechnology) antibodies. Isotype matched secondary antibodies were conjugated to horseradish peroxidase and chemiluminescence (Amersham) was detected using Image Quant LAS 4000 (GE Healthcare Life Sciences).

### **MyriaScreen II library**

The MyriaScreen II library was used for the high-throughput screening. It comprised 10,000 small molecules Sigma that fulfill the “Lipinski’s rule of 5”, indicating their high druglikeness potential (Lipinski et al., 2001). The compounds were dissolved in DMSO 10 mg/ml. For each round of screening The compounds were diluted 10 times into 40 mM Hepes/KOH pH 7.4 into one sets of 32 384-well plates and stored at -20°C until use. To reach their final concentration they were further diluted 4 times into the assay plate resulting in final concentrations ranging from 50 to 200 µM.

### **Malachite Green GTPase activity assay**

GTPase activity was measured using a modified version of the previously described Malachite Green assay (Leonard et al., 2005), based on the change of absorbance of malachite green in the presence of free  $\text{PO}_4$  ions that results from the hydrolysis of GTP into GDP. A mixture containing containing 8 mM ammonium molybdate and 1.5 mM malachite green was freshly prepared the day of use. The change in absorbance molybdate and the free phosphate form a phosphomolybdate complex (Cogan et al., 1999) that then binds the malachite green dye resulting in a change of absorbance depending on the contained phosphate concentration that was measured at 595 nm after a 15 minutes incubation period at room temperature.

The assay was performed in 96 well-plates in a final volume of 190  $\mu\text{l}$ /well. To start the hydrolysis reaction, 10  $\mu\text{l}$  of 0.5  $\mu\text{M}$  of rOPA1 in 40 mM HEPES/KOH pH 7.4 was mixed with 10  $\mu\text{l}$  of 500  $\mu\text{M}$  GTP and 10 mM  $\text{MgCl}_2$  and incubated for 2 hours at 37  $^\circ\text{C}$ . The reaction was then halted by adding to each well 5  $\mu\text{l}$  of 500  $\mu\text{M}$  EDTA, which chelates the  $\text{Mg}^{2+}$  required for GTP hydrolysis. To measure the phosphate content, 150  $\mu\text{L}$  of the Malachite Green-ammonium molybdate solution (1 mM Malachite Green, 10 mM ammonium molybdate in 1N HCl) was added at each well. After 15 minutes incubation at 25  $^\circ\text{C}$ , was measured the absorbance at 595 nm using a microplate reader. Phosphate concentration of each sample was calculated from a standard curve ranging from 1 to 100  $\mu\text{M}$  Pi generated for each experiment.

To test the inhibition of rOPA1 GTPase activity by the compounds, 5  $\mu\text{l}$  of the inhibitor dissolved in DMSO, or DMSO alone as solvent control, were incubated with rOPA1 for 20 minutes at 37  $^\circ\text{C}$  before to initiating the hydrolysis reaction. As positive control of OPA1 activity inhibition, 5  $\mu\text{l}$  of 500  $\mu\text{M}$  EDTA were added before incubation with

GTP to prevent the hydrolysis reaction. Samples with only buffer and 500  $\mu$ M GTP were used as blank controls.

### **High-throughput GTPase Assay**

GTPase activity of the rOPA1 was measured using the aforementioned malachite green assay. The screen was started by plating 0.5  $\mu$ M of OPA1 and 5  $\mu$ L of the library compound in 10% DMSO in a total volume of 12  $\mu$ L per well of a 384-well plate, using an automated microplate pipetting system Precision XS, Biotek. Four columns were used for negative controls: 10 % DMSO dissolved in 40 mM Hepes/KOH pH 7.4. Alternating control wells received 5  $\mu$ L of 0.5 mM EDTA to prevent  $Mg^{2+}$ -dependent hydrolysis of GTP as positive controls for the inhibition of OPA1 activity. The hydrolysis reaction was initiated after 10 min incubation at room temperature by the addition of the 500  $\mu$ M GTP, 10 mM  $MgCl_2$  solution. The final reaction volume per well was 20  $\mu$ L. Plates were sealed and incubated for 2 h at 37°C. Subsequently, to stop the hydrolysis reaction 5  $\mu$ L of 0.5 M EDTA was added to each well excluding the ones serving as positive controls. To measure the phosphate content, 60  $\mu$ L of the malachite green-ammonium molybdate mixture was added per well. After 15 min incubation at room temperature, absorbance was read at 595 nm.

### **IC50 determination**

GTPase activity was measured using the malachite green assay, as described above. Values were expressed as normalized percent inhibition (NPI) considering wells

containing EDTA at timepoint zero as positive controls and wells containing the DMSO (the vehicle) as negative control. The half maximal inhibitory concentration (IC<sub>50</sub>) was calculated based on the dose-response curves fitted with a four-parameter logistic curve using OriginPro software.

### **Molecular modelling and docking analysis**

Recombinant OPA1 structure model was built with Phyre2 using an intensive model generation approach, that created a complete full-length model of the protein through a combination of multiple template modeling and simplified *ab initio* folding simulation, as described in (Kelley et al., 2015). The top four protein templates selected to model rOPA1 structure based on heuristics were: (i) gtpase hflx (PDB: c5ady6), (ii) dynamin-1 (PDB: c3zvrA), (iii) dynamin 3 (PDB: c5a3fD), dynamin-1 (PDB: c3snhA). The 93% of the final rOPA1 model was modelled at >90% confidence, 7% (residues: 1-42, 86-91) was modelled *ab initio*. GTP-binding site was used to dock MYLS22 using the Induced Fit Docking of GLIDE (Glide, version 7.1, Schrödinger, LLC). Pymol (The PyMOL Molecular Graphics System, version 2.2.2; Schrödinger, LLC: New York, 2018) was used for preparing images.

### **Analysis of cell death**

$1 \times 10^5$  MEFs were grown in 12-well plates. After 24 h cells were treated with MYLS22 or DMSO, as solvent control. After different timepoints, indicated in the figure legends, cells were stained with Annexin-V-FICT and propidium iodide (PI), according to



manufacturer's protocol (eBioscience™). Cell death was measured by flow cytometry (FACSCalibur) as the percentage of Annexin-V and PI positive events.

### **Mitochondrial isolation and in vitro assays.**

Mitochondria from mouse liver were isolated as described elsewhere (Frezza et al., 2007b).

To measure cytochrome c release, mitochondria (1 mg/ml final concentration) were treated with 50 pmol/mg cBID in Experimental Buffer (EB; 150 mM KCl, 10 mM Tris MOPS, 10 μM EGTA-Tris, 1 mM Pi and 5 mM glutamate/2.5 mM malate as respiration substrate, pH 7.4) at 25 °C. After 15 min, mitochondria were pelleted by centrifugation at 12000 × g at 4 °C for 10 min and resuspended in the same volume of EB. Quantitative determination of cytochrome c in the pellet and the supernatant fractions was determined using the rat/mouse specific ELISA Cytochrome c Immunoassay (R&D Systems).

Respiratory chain dysfunctions and membrane potential were assayed by monitoring the release of rhodamine123 from pre-stained mitochondria. 0.5 mg/ml mitochondria were incubated with 0.3 μM rhodamine 123 (Molecular Probes) in EB and the indicated substrates. Rhodamine 123 fluorescence, before and after the addition of the uncoupler agent FCCP, were measured with a fluorescence spectrometer (Infinite 200 Pro, TECAN) at 25 °C, setting at 485 nm and 538 nm the excitation and the emission wavelengths, respectively.

### **Live imaging of mitochondrial network**

To visualize mitochondrial network,  $5 \times 10^4$  MEF cells expressing mtYFP were seeded onto 25 mm coverslips and treated with the indicated concentrations of the inhibitor MYLS22. After 24 h, the coverslips were incubated in Hank's Balanced Salt Solution (HBSS) supplemented with 10 mM Hepes and placed on the stage of the microscope. Fluorescence signals were analyzed using IMIC Andromeda system (Fondis Electronic) equipped with ORCA-03G Camera (Hamamatsu), a 60x oil objective (UPLAN  $\times$  60 oil, 1.35NA, Olympus). A laser was used to excite at 488 nm and FF01-446/523/600/677 (Semrock) as emission filter. Stacks of 25 images separated by 0.3  $\mu$ m along the z axis were acquired. Convolution and z-stack project were performed using a plug-in of the ImageJ software (National Institutes of Health). Mitochondrial length was quantified with Image J by measuring the average mitochondrial major axis length of 10 mitochondria per cell in 20 cells per sample.

### **Mitochondrial membrane potential**

For imaging of mitochondrial membrane potential, MEFs grown on coverslips and treated with the MYLS22 inhibitor were loaded with 10 nM TMRM (Molecular Probes) in the presence of 2  $\mu$ g/ml cyclosporine H, a P-glycoprotein inhibitor, and incubated at 37 °C 30 min. Sequential images of TMRM fluorescence were acquired using a High Content Imaging System Operetta confocal microscope (Perkin Elmer) equipped with Harmony software for images analysis.

## **Cytochrome c immunolocalization**

For cytochrome c immunolocalization, MEFs were grown on coverslips and treated with the indicated concentration of MYLS22 or DMSO. After 24 h cells were treated with 1 mM H<sub>2</sub>O<sub>2</sub> to induce apoptosis. After the indicated times, MEFs were fixed and immunostained, as described in (Scorrano and Korsmeyer, 2003), with Alexa Fluor 488-conjugated anti-cytochrome c antibody and Alexa Fluor 568-conjugated anti-TOM20 antibody. For cytochrome c and TOM20 detection, green and red channel images respectively were acquired simultaneously using two separate color channels on the detector assembly of a Zeiss LSM 700 confocal microscope. The localization index was calculated as described in (Frezza et al., 2007a; Petronilli et al., 2001).

## **Scratch wound migration assay**

HUVEC and MDA cells were cultured in 48-well plates in 800 µl of EGM2 for 48 hours and were wounded with the head of 200 µl tips. Migration of the cells into the wound was recorded 8 hours later, unless otherwise specified.

## **HTS Data Analysis**

The absorbance data obtained from two replicates of the HTS were analyzed using the Bioconductor/R package, *cellHTS* (Michael Boutros, 2006), modified according to our purposes. The data was normalized in a plate-to-plate fashion using the normalization per inhibition method. The normalized data of each replicate experiment

was subsequently standardized to obtain a z-score using equation 1, in which  $y_{ki}$  is the normalized value for the specific well and M and S are the median and the median absolute deviation of the distribution of sample values across all plates and sample wells of one replicate experiment. Computing their mean summarized the obtained single values per well of the standardized values per replicate.

$$k_{ki} = \pm (y_{ki} - M)/S \quad \text{Equation 1}$$

To identify positive modulators of OPA1 GTPase activity a threshold was set considering compounds that reduce the OPA1 activity by at least 30%. After two rounds of library screening, only compounds identified in both individual and replicate analysis were retained. Of these, the compounds that *per se* reduced the absorbance at the measured wavelength were considered as false positives and were excluded from the list. Outliers with values lower than the average of the positive control wells were excluded from the analysis. The strictly standardized mean difference SSMD per plate was determined according to (Zhang, 2007).

### **Statistical analysis**

Results are expressed as mean  $\pm$  SEM values of the indicated number of independent experiments (n). Origin software was used for statistical data analysis. Statistical significance was determined by Student's t-test for paired comparison. P values are indicated in the figure legends and P < 0.05 was considered significant.

## REFERENCES

- Anderson, G.R., Wardell, S.E., Cakir, M., Yip, C., Ahn, Y.R., Ali, M., Yllanes, A.P., Chao, C.A., McDonnell, D.P., and Wood, K.C. (2018). Dysregulation of mitochondrial dynamics proteins are a targetable feature of human tumors. *Nat Commun* *9*, 1677.
- Bordt, E.A.e.a. (2017). The Putative Drp1 Inhibitor mdivi-1 Is a Reversible Mitochondrial Complex I Inhibitor that Modulates Reactive Oxygen Species: Developmental Cell. *Dev Cell*.
- Bunnage, M.E., Chekler, E.L., and Jones, L.H. (2013). Target validation using chemical probes. *Nat Chem Biol* *9*, 195-199.
- Cassidy-Stone, A., Chipuk, J.E., Ingerman, E., Song, C., Yoo, C., Kuwana, T., Kurth, M.J., Shaw, J.T., Hinshaw, J.E., Green, D.R., *et al.* (2008). Chemical inhibition of the mitochondrial division dynamin reveals its role in Bax/Bak-dependent mitochondrial outer membrane permeabilization. *Dev Cell* *14*, 193-204.
- Chen, H., Chomyn, A., and Chan, D.C. (2005). Disruption of fusion results in mitochondrial heterogeneity and dysfunction. *J Biol Chem* *280*, 26185-26192.
- Cipolat, S., Martins de Brito, O., Dal Zilio, B., and Scorrano, L. (2004). OPA1 requires mitofusin 1 to promote mitochondrial fusion. *Proc Natl Acad Sci U S A* *101*, 15927-15932.
- Cogliati, S., Frezza, C., Soriano, M.E., Varanita, T., Quintana-Cabrera, R., Corrado, M., Cipolat, S., Costa, V., Casarin, A., Gomes, L.C., *et al.* (2013). Mitochondrial cristae shape determines respiratory chain supercomplexes assembly and respiratory efficiency. *Cell* *155*, 160-171.
- Copeland, R.A. (2003). Mechanistic considerations in high-throughput screening. *Analytical Biochemistry* *320*, 1-12.
- Danial, N.N., Gramm, C.F., Scorrano, L., Zhang, C.Y., Krauss, S., Ranger, A.M., Datta, S.R., Greenberg, M.E., Licklider, L.J., Lowell, B.B., *et al.* (2003). BAD and glucokinase reside in a mitochondrial complex that integrates glycolysis and apoptosis. *Nature* *424*, 952-956.
- Daumke, O., and Praefcke, G.J. (2016). Invited review: Mechanisms of GTP hydrolysis and conformational transitions in the dynamin superfamily. *Biopolymers* *105*, 580-593.
- Del Dotto, V., Mishra, P., Vidoni, S., Fogazza, M., Maresca, A., Caporali, L., McCaffery, J.M., Cappelletti, M., Baruffini, E., Lenaers, G., *et al.* (2017). OPA1 Isoforms in the Hierarchical Organization of Mitochondrial Functions. *Cell Rep* *19*, 2557-2571.
- Fang, H.Y., Chen, C.Y., Chiou, S.H., Wang, Y.T., Lin, T.Y., Chang, H.W., Chiang, I.P., Lan, K.J., and Chow, K.C. (2012). Overexpression of optic atrophy 1 protein increases cisplatin resistance via inactivation of caspase-dependent apoptosis in lung adenocarcinoma cells. *Hum Pathol* *43*, 105-114.

- Ford, M.G., Jenni, S., and Nunnari, J. (2011). The crystal structure of dynamin. *Nature* 477, 561-566.
- Franco, A., Kitsis, R.N., Fleischer, J.A., Gavathiotis, E., Kornfeld, O.S., Gong, G., Biris, N., Benz, A., Qvit, N., Donnelly, S.K., *et al.* (2016). Correcting mitochondrial fusion by manipulating mitofusin conformations. *Nature* 540, 74-79.
- Frezza, C., Cipolat, S., Martins, d.B., Micaroni, M., Beznoussenko, G.V., Rudka, T., Bartoli, D., Polishuck, R.S., Danial, N.N., De Strooper, B., *et al.* (2006). OPA1 Controls Apoptotic Cristae Remodeling Independently from Mitochondrial Fusion. *Cell* 126, 177-189.
- Frezza, C., Cipolat, S., and Scorrano, L. (2007). Measuring mitochondrial shape changes and their consequences on mitochondrial involvement during apoptosis. *Methods Mol Biol* 372, 405-420.
- Fulda, S., Galluzzi, L., and Kroemer, G. (2010). Targeting mitochondria for cancer therapy. *Nature Reviews Drug Discovery* 9, 447-464.
- Goktug, A.N., Chai, S.C., and Chen, T. (2013). Data Analysis Approaches in High Throughput Screening.
- Green, D.R., and Kroemer, G. (2004). The pathophysiology of mitochondrial cell death. *Science* 305, 626-629.
- Griparic, L., van der Wel, N.N., Orozco, I.J., Peters, P.J., and van der Blik, A.M. (2004). Loss of the intermembrane space protein Mgm1/OPA1 induces swelling and localized constrictions along the lengths of mitochondria. *J Biol Chem* 279, 18792-18798.
- Hanahan, D., and Weinberg, R.A. (2011). Hallmarks of cancer: the next generation. *Cell* 144, 646-674.
- Hann, M.M., and Simpson, G.L. (2014). Intracellular drug concentration and disposition--the missing link? *Methods* 68, 283-285.
- Irwin, W.A., Bergamin, N., Sabatelli, P., Reggiani, C., Megighian, A., Merlini, L., Braghetta, P., Columbaro, M., Volpin, D., Bressan, G.M., *et al.* (2003). Mitochondrial dysfunction and apoptosis in myopathic mice with collagen VI deficiency. *Nat Genet* 35, 367-371.
- Kaur, M., Reed, E., Sartor, O., Dahut, W., and Figg, W.D. (2002). Suramin's development: what did we learn? *Invest New Drugs* 20, 209-219.
- Kelley, L.A., Mezulis, S., Yates, C.M., Wass, M.N., and Sternberg, M.J. (2015). The Phyre2 web portal for protein modeling, prediction and analysis. *Nat Protoc* 10, 845-858.
- Kong, B., Wang, Q., Fung, E., Xue, K., and Tsang, B.K. (2014). p53 is required for cisplatin-induced processing of the mitochondrial fusion protein L-Opa1 that is

mediated by the mitochondrial metallopeptidase Oma1 in gynecologic cancers. *J Biol Chem* 289, 27134-27145.

Landes, T., Emorine, L.J., Courilleau, D., Rojo, M., Belenguer, P., and Arnaune-Pelloquin, L. (2010). The BH3-only Bnip3 binds to the dynamin Opa1 to promote mitochondrial fragmentation and apoptosis by distinct mechanisms. *EMBO Rep* 11, 459-465.

Lee, Y.J., Jeong, S.Y., Karbowski, M., Smith, C.L., and Youle, R.J. (2004). Roles of the mammalian mitochondrial fission and fusion mediators Fis1, Drp1, and Opa1 in apoptosis. *Mol Biol Cell* 15, 5001-5011.

Leonard, M., Doo Song, B., Ramachandran, R., and Schmid, S.L. (2005). Robust Colorimetric Assays for Dynamin's Basal and Stimulated GTPase Activities. In *Methods in Enzymology* (Academic Press), pp. 490-503.

Li, L., Thomas, R.M., Suzuki, H., De Brabander, J.K., Wang, X., and Harran, P.G. (2004). A small molecule Smac mimic potentiates TRAIL- and TNFalpha-mediated cell death. *Science* 305, 1471-1474.

Lipinski, C.A., Lombardo, F., Dominy, B.W., and Feeney, P.J. (2001). Experimental and computational approaches to estimate solubility and permeability in drug discovery and development settings. *Adv Drug Deliv Rev* 46, 3-26.

Lopez, J., and Tait, S.W. (2015). Mitochondrial apoptosis: killing cancer using the enemy within. *Br J Cancer* 112, 957-962.

Meric-Bernstam, F., and Mills, B.G. (2012). Overcoming implementation challenges of personalized cancer therapy. *Nature Reviews Clinical Oncology* 9, 542.

Morgan, P., Van Der Graaf, P.H., Arrowsmith, J., Feltner, D.E., Drummond, K.S., Wegner, C.D., and Street, S.D. (2012). Can the flow of medicines be improved? Fundamental pharmacokinetic and pharmacological principles toward improving Phase II survival. *Drug Discov Today* 17, 419-424.

Olichon, A., Baricault, L., Gas, N., Guillou, E., Valette, A., Belenguer, P., and Lenaers, G. (2003). Loss of OPA1 perturbs the mitochondrial inner membrane structure and integrity, leading to cytochrome c release and apoptosis. *J Biol Chem* 278, 7743-7746.

Olichon, A., Landes, T., Arnaune-Pelloquin, L., Emorine, L.J., Mils, V., Guichet, A., Delettre, C., Hamel, C., Amati-Bonneau, P., Bonneau, D., *et al.* (2007). Effects of OPA1 mutations on mitochondrial morphology and apoptosis: relevance to ADOA pathogenesis. *J Cell Physiol* 211, 423-430.

Orrenius, S., Gogvadze, V., and Zhivotovsky, B. (2007). Mitochondrial oxidative stress: implications for cell death. *Annu Rev Pharmacol Toxicol* 47, 143-183.

Patten, D.A., Wong, J., Khacho, M., Soubannier, V., Mailloux, R.J., Pilon-Larose, K., MacLaurin, J.G., Park, D.S., McBride, H.M., Trinkle-Mulcahy, L., *et al.* (2014). OPA1-dependent cristae modulation is essential for cellular adaptation to metabolic demand. *EMBO J* 33, 2676-2691.

- Petronilli, V., Penzo, D., Scorrano, L., Bernardi, P., and Di Lisa, F. (2001). The mitochondrial permeability transition, release of cytochrome c and cell death. Correlation with the duration of pore openings in situ. *J Biol Chem* *276*, 12030-12034.
- Quintana-Cabrera, R., Quirin, C., Glytsou, C., Corrado, M., Urbani, A., Pellattiero, A., Calvo, E., Vazquez, J., Enriquez, J.A., Gerle, C., *et al.* (2018). The cristae modulator Optic atrophy 1 requires mitochondrial ATP synthase oligomers to safeguard mitochondrial function. *Nature communications* *9*, 3399.
- Rizzuto, R., Bernardi, P., and Pozzan, T. (2000). Mitochondria as all-round players of the calcium game. *J Physiol* *529 Pt 1*, 37-47.
- Rocha, A.G., Franco, A., Krezel, A.M., Rumsey, J.M., Alberti, J.M., Knight, W.C., Biris, N., Zacharioudakis, E., Janetka, J.W., Baloh, R.H., *et al.* (2018). MFN2 agonists reverse mitochondrial defects in preclinical models of Charcot-Marie-Tooth disease type 2A. *Science* *360*, 336-341.
- Rosignol, R., Gilkerson, R., Aggeler, R., Yamagata, K., Remington, S.J., and Capaldi, R.A. (2004). Energy substrate modulates mitochondrial structure and oxidative capacity in cancer cells. *Cancer Res* *64*, 985-993.
- Sato, S.-i., Murata, A., Orihara, T., Shirakawa, T., Suenaga, K., Kigoshi, H., and Uesugi, M. (2011). Marine Natural Product Aurilide Activates the OPA1-Mediated Apoptosis by Binding to Prohibitin. *Chemistry & Biology* *18*, 131-139.
- Scorrano, L. (2009). Opening the doors to cytochrome c: changes in mitochondrial shape and apoptosis. *Int J Biochem Cell Biol* *41*, 1875-1883.
- Scorrano, L., Ashiya, M., Buttle, K., Weiler, S., Oakes, S.A., Mannella, C.A., and Korsmeyer, S.J. (2002). A distinct pathway remodels mitochondrial cristae and mobilizes cytochrome c during apoptosis. *Dev Cell* *2*, 55-67.
- Scorrano, L., and Korsmeyer, S.J. (2003). Mechanisms of cytochrome c release by proapoptotic BCL-2 family members. *Biochem Biophys Res Commun* *304*, 437-444.
- Scorrano, L., Oakes, S.A., Opferman, J.T., Cheng, E.H., Sorcinelli, M.D., Pozzan, T., and Korsmeyer, S.J. (2003). BAX and BAK regulation of endoplasmic reticulum Ca<sup>2+</sup>: a control point for apoptosis. *Science* *300*, 135-139.
- Song, Z., Chen, H., Fiket, M., Alexander, C., and Chan, D.C. (2007). OPA1 processing controls mitochondrial fusion and is regulated by mRNA splicing, membrane potential, and Yme1L. *J Cell Biol* *178*, 749-755.
- Teuscher, K.B., Zhang, M., and Ji, H. (2017). A Versatile Method to Determine the Cellular Bioavailability of Small-Molecule Inhibitors.
- Varanita, T., Soriano, M.E., Romanello, V., Zaglia, T., Quintana-Cabrera, R., Semenzato, M., Menabo, R., Costa, V., Civiletto, G., Pesce, P., *et al.* (2015). The OPA1-dependent mitochondrial cristae remodeling pathway controls atrophic, apoptotic, and ischemic tissue damage. *Cell Metab* *21*, 834-844.



Wallace, D.C. (2005). A mitochondrial paradigm of metabolic and degenerative diseases, aging, and cancer: a dawn for evolutionary medicine. *Annu Rev Genet* 39, 359-407.

Wee, Y., Liu, Y., Lu, J., Li, X., and Zhao, M. (2018). Identification of novel prognosis-related genes associated with cancer using integrative network analysis. *Sci Rep* 8, 3233.

Yamaguchi, R., Lartigue, L., Perkins, G., Scott, R.T., Dixit, A., Kushnareva, Y., Kuwana, T., Ellisman, M.H., and Newmeyer, D.D. (2008). Opa1-mediated cristae opening is Bax/Bak and BH3 dependent, required for apoptosis, and independent of Bak oligomerization. *Mol Cell* 31, 557-569.

Zhang, X.D. (2007). A pair of new statistical parameters for quality control in RNA interference high-throughput screening assays. *Genomics* 89, 552-561.

Zhao, J., Zhang, J., Yu, M., Xie, Y., Huang, Y., Wolff, D.W., Abel, P.W., and Tu, Y. (2012). Mitochondrial dynamics regulates migration and invasion of breast cancer cells. *Oncogene* 32, 4814.

Zhao, X., Tian, C., Puszyk, W.M., Ogunwobi, O.O., Cao, M., Wang, T., Cabrera, R., Nelson, D.R., and Liu, C. (2013). OPA1 downregulation is involved in sorafenib-induced apoptosis in hepatocellular carcinoma. *Lab Invest* 93, 8-19.

## FIGURE LEGENDS

### Figure 1. HTS data processing, quality control and hits identification.

- (A) Schematic representation of the major steps followed for the identification of a small-molecule inhibitor of OPA1 GTPase activity.
- (B) Strictly standardized mean difference (SSMD) values of each plate plotted against the plate number (32 total tested plates). The dashed line at a  $y = -3$  specifies the threshold for a robust assay. Plates with SSMD values  $> -3$  (red) failed the quality control. The plate-specific SSMD values demonstrate that the assay remained sufficiently robust throughout the screening. Values represent the average of two HTS replicates.
- (C) Trellis scatter plot of all the samples tested in the HTS. The inhibitory activity of the compounds was measured using the malachite green assay. Median raw absorbance values at 595 nm were plotted against their well number. The large separation between the positive (green circles) and the negative (red circles) control populations confirming the robustness of the assay. The compounds (blue circles) form two populations: inactive compounds in the upper part and potential inhibitors in the lower part.
- (D) Trellis heat map of the 32 384-well plates screened during the HTS. The screen was run including in each plate positive control samples containing vehicle (DMSO) and negative control samples containing EDTA. NPI values are expressed as percentage of the positive controls. The NPI values of each sample are indicated using the reported pseudocolor scale, where dark red (NPI  $< 0$ ) indicates the maximal inhibition, while dark blue (NPI  $> 1.8$ ) represents the

minimal inhibition of GTPase activity of rOPA1. The inhibitory activity of the compounds was measured using the malachite green assay. NPI values of 1 represent 0% inhibition, while values of 0 represent 100% inhibition.

- (E) Normalized percent inhibition (NPI) values of each compound (blue circles) and control samples (red circles) were plotted against their z-score. The dashed line indicates the threshold set at 0.7 corresponding to 30% inhibition of the measured GTPase activity of OPA1. Data represent the average of two HTS replicates.
- (F) Magnification of plot (D) reporting compounds with NPI between 0 and 1. Compounds with  $NPI < 0.69$  were selected for the subsequent analysis.
- (G) Graphical representation of the flowchart followed during the selection of the OPA1 inhibitors. 8 of the 10,000 initial compounds were identified as potential OPA1 inhibitors and were subjected to further analysis.
- (H) The red spectrum represents the  $^1H$  NMR of aromatic protons of MYLS22 in the presence of rOPA1, while the blue spectrum represents the STD NMR difference spectrum of MYLS22 after selective saturation of rOPA1  $^1H$  methyl resonances.

**Table 1: Malachite green assay pipeline adapted for the HTS.**

**Table 2. Physicochemical properties and potency of potential inhibitors of OPA1 activity identified with the HTS.**

Chemical structures, physicochemical properties required for the fulfillment of the Lipinski's "rule of five" and potencies calculated with dose-response experiments of 11 potential OPA1 inhibitors selected after the primary HTS.

**Figure 2. Dose response curves of the 8 compounds selected from the primary screen.**

**(A-H)** Dose-response curves for inhibition of rOPA1 GTPase activity by the eight potential OPA1 inhibitors selected after two rounds of the screening. Normalized percent of inhibition (NPI) values are plotted against the logarithmic concentration of the inhibitor. Data are normalized using EDTA-containing samples as positive controls and vehicle (DMSO) containing samples as negative controls. A four parametric curve was fit to the data to obtain the stated half-maximal inhibition value ( $IC_{50}$ ), maximum inhibition ( $I_{50}$ ) and Hill slope values using OriginPro software. Data represent the mean of 3 independent experiments  $\pm$  SEM.

**Figure 3. *In silico* docking analysis of the interaction of MYLS22with rOPA1.**

- (A)** Domain architecture of recombinant OPA1 (rOPA1) correspondent to *Mus musculus* isoform 1 (Uniprot: P58281), lacking the mitochondrial targeting sequence (MTS) and the transmembrane domain (TM), with a C-terminal 6 x His tag. The correspondent structural-based domain assignment is indicated below the figure.
- (B)** Ribbon-type representation of predicted rOPA1 protein. Regions modelled *ab initio* are indicated in gray. Structural domains are labelled and represented with the same color-code as in **(A)**.
- (C)** Domain architecture of recombinant OPA1 fusion protein, consisting of the G domain connected with a linker to BSE domain of GED. The correspondent structural-based domain assignment is indicated below the figure.

- (D) Ribbon-type representation of predicted OPA1 fusion protein. Structural domains are labelled and represented with the same color-code as in (A).
- (E) Schematic representation of the interactions of MYLS22 in the best scoring pose with the GTPase domain of OPA1. Purple arrows indicate backbone hydrogen bond interactions. Purple dashed arrows indicate side-chain hydrogen bond interactions. Amino acids are depicted as colored cycles: blue for positively charged, red for negatively charged, cyan for polar, and green for hydrophobic residues.
- (F) Ribbon and surface-type representation of GTPase pocket of rOPA1 (red) in complex with GTP. The residues that form hydrogen bonds with GTP are indicated.
- (G) Surface representations of the predicted GTPase domain of rOPA1 in complex with GTP (left) or MYLS22 (right). The rOPA1-ligand interacting surfaces are coloured in red.
- (H) rOPA1-MYLS22 interaction measured by NMR. The red spectrum represents the <sup>1</sup>H NMR of aromatic protons of MYLS22 in the presence of rOPA1, while the black spectrum represents the STD NMR difference spectrum of MYLS22 after selective saturation of rOPA1 <sup>1</sup>H methyl resonances.

**Figure 4: Analysis of membrane-permeability, cellular and mitochondrial toxicity of MYLS22.**

- (A) Measurement of concentration of MYLS22 in the extracellular medium. MEF cells were incubated with MYLS22 in HBSS medium and after the reported timepoints, cells were washed and remaining concentration of MYLS22 in the medium was assessed by measuring its absorbance at 280 nm.

- (B)** Elution peak of MYLS22 inhibitor detected by its absorbance at 280 nm using the reverse phase HPLC (experimental procedures). MYLS22 was detected in the lysates of MEFs incubated 24h with 50  $\mu$ M of the compound (red line). The peak was not detected in the lysates of cells incubated with DMSO (negative control, black line). The peak of the inhibitor was identified with a solution of the compound in the HPLC buffer (green line).
- (C)** MYLS22 does not induce cell death. WT MEFs were incubated with the indicated concentrations of MYLS22. After 24h, viability was measured cytofluorimetrically as the percentage of Annexin V and propidium iodide negative cells. Data represents average  $\pm$  SEM of six independent experiments.
- (D)** Representative SDS-PAGE of the lysate of *E. coli* expressing the recombinant Dynamin-1 (band at  $\sim$ 70 kDa).
- (E)** Specificity of MYLS22 inhibition of OPA1 GTPase activity. Dose response curves of recombinant Dynamin-1 activity after incubation with OPA1 inhibitors. Data were fitted with a four-parametric curve, values represent mean  $\pm$  SEM of two independent experiments.
- (F)** MYLS22 does not induce mitochondrial membrane potential depolarization in WT MEFs. Cells were treated with MYLS22 and TMRM fluorescence was recorded in response to oligomycin and the uncoupler FCCP. Cells treated with MYLS22 do not present a reduction of the membrane potential.
- (G-H)** MYLS22 does not induce mitochondrial potential depolarization in isolated mitochondria. Effect of MYLS22 on isolated mitochondrial membrane potential represented by the ratio of rhodamine 123 (Rh123) fluorescence before and after treatment with the uncoupler FCCP. Mitochondria were treated with MYLS22 in

the presence of glutamate/malate (Glu/Mal) as complex I substrate or succinate as complex II substrate. Data represents mean  $\pm$  SEM of three independent experiments.

**Figure 5. MYLS22 induces mitochondrial network fragmentation.**

- (A) Representative confocal images of changes in mitochondrial morphology induced by MYLS22. WT MEFs expressing mitochondrially targeted YFP (mtYFP) were treated with 50  $\mu$ M (upper right) or 100  $\mu$ M (bottom left) MYLS22 or DMSO (upper left) for 24h. Bottom right: representative image of knockdown of mitochondrial network fragmentation induced by OPA1 knockdown. Bar = 10  $\mu$ m.
- (B) Average of mitochondrial major axis lengths of WT MEFs treated as in (A) or OPA1 KO MEFs. Data represent the average  $\pm$  SEM of five independent experiments. 50 cells and at least 10 mitochondria/cell were measured for each experiment. The asterisk denotes  $p < 0.01$  in a pair-sample Student's t-test versus solvent control (0  $\mu$ M MYLS22).

**Figure 6. MYLS22 enhances apoptotic cytochrome c release from mitochondrial cristae.**

- (A) Immunoblot of *In vitro* cytochrome c release by recombinant cBID protein. Mitochondria purified by mouse liver were incubated with cBID and the indicated concentrations of MYLS22. Mitochondria were subsequently centrifuged and pellet (p) and supernatant (s) were assayed for cytochrome c release.

- (B) Isolated mitochondria from mouse liver were treated as in (A) and cytochrome c release was measured by ELISA. Data represent mean  $\pm$  SEM of three independent experiments.
- (C) Isolated mitochondria from mouse liver were treated with cBID as in (A) and then crosslinked with EDC. Proteins were separated by SDS-PAGE and immunoblotted using the OPA1 antibody. Proteins > 100 kDa represents OPA1 oligomers.
- (D) Representative confocal images of intracellular cytochrome c distribution. WT MEFs were treated with 50  $\mu$ M MYLS22 (bottom) or left untreated (upper). Then cells were treated with 1 mM H<sub>2</sub>O<sub>2</sub> for 30 min or 60 min, fixed and immunostained for cytochrome c (green) and TOM20 (red). Bar corresponds to 10  $\mu$ m.
- (E) Localization index for cytochrome c. Experiments were performed as in (D). Localization index was calculated from 30 images randomly selected. Data represent mean  $\pm$  SEM of three independent experiments.

**Figure 7. MYLS22 reduces breast cancer cell migration.**

- (A) Western blot analysis of OPA1 protein levels in wt MDA-MB-231 72 h post-transfection with scramble (scr) or OPA1 siRNA oligos. GRP75 was used as protein loading control. Changes in protein expression were quantified by densitometry analysis. Changes in protein expression were quantified by densitometry analysis by normalizing to GRP75 protein levels.
- (B) MDA-MB-231 cells were incubated with 20  $\mu$ M of MYLS22 or DMSO as negative control. After 24 h the cells were then subjected to *in vitro* scratch assay. The images were captured at 0 and 6 h.



**(C)** MDA-MB-231 cells were transfected with scr or OPA1 siRNA oligos and after 72 h, were incubated with 20  $\mu$ M of MYLS22 or DMSO as negative control. Cells migration was measured by scratch assay. The migration of the cells into the wound was measured after 6 hours. Data represent the mean  $\pm$  SEM of three independent experiments.

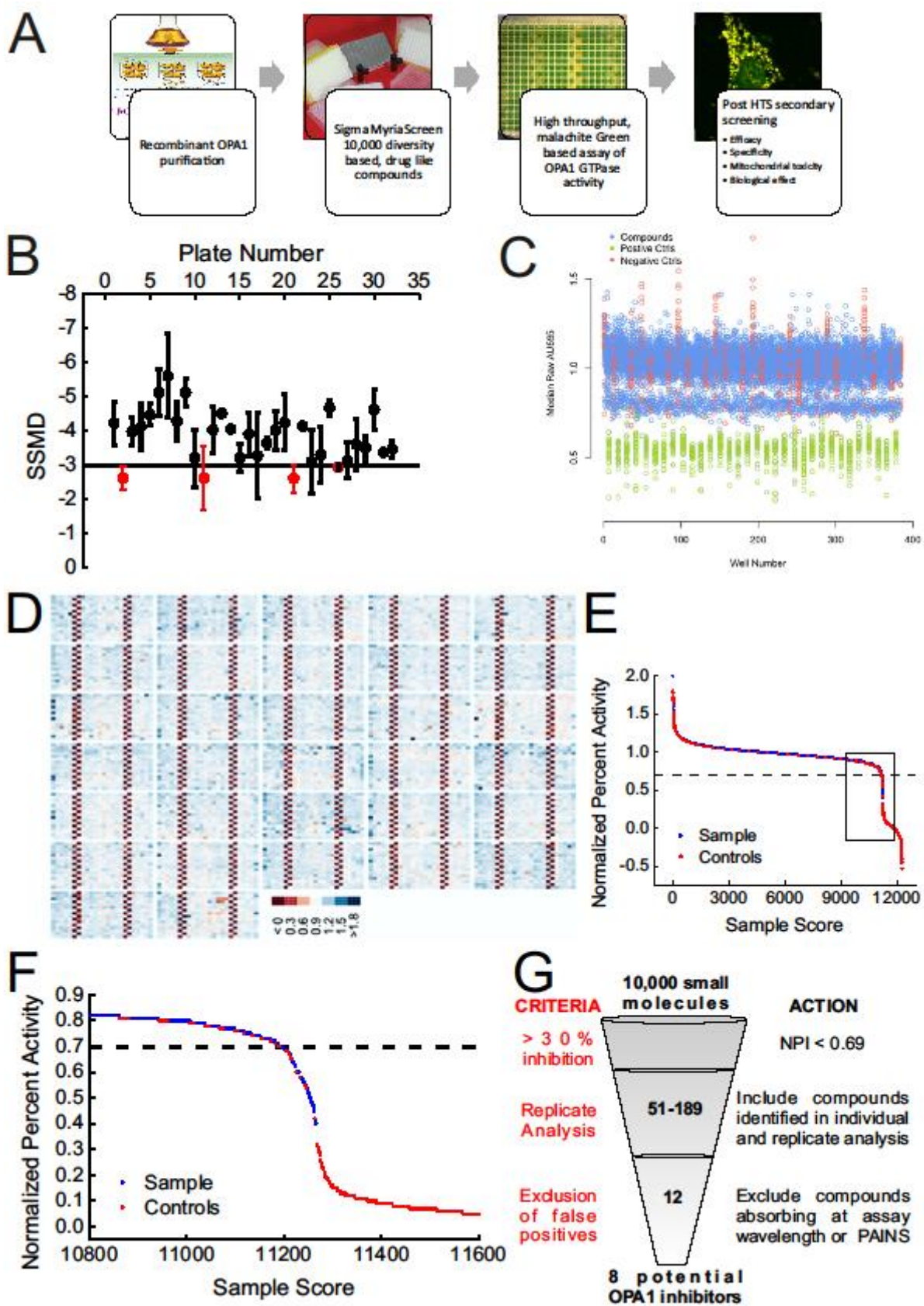


Figure 1

Step	Parameter	Value	Description
1	<i>Library compounds</i>	5 $\mu$ l	From 200 $\mu$ M to 830 $\mu$ M stock compounds
2	<i>rOPA1</i>	8 $\mu$ l	1.2 $\mu$ M stock
3	<i>Incubation time</i>	10 min	Room temperature
4	<i>Positive controls</i>	5 $\mu$ l	0.5 M EDTA stock, pH 8.0
5	<i>Start reaction</i>	7 $\mu$ l	1.43 mM GTP stock, 28.6 mM MgCl <sub>2</sub> stock
6	<i>Incubation time</i>	2 h	37°C
7	<i>Stop reaction</i>	5 $\mu$ l	0.5 M EDTA stock, pH 8.0
8	<i>Reporter reagent</i>	60 $\mu$ l	1.5 mM malachite green stock, 8 mM ammonium molybdate stock
9	<i>Incubation time</i>	15 min	Room temperature
10	<i>Assay readout</i>	595 nm	Microplate reader, absorbance mode

Step	Notes
1	Library "MyriaScreen" (Aldrich) of 10,000 drug-like small molecule dissolved in 10% DMSO.
2	rOPA1 correspondent to Mus Musculus isoform 1 (Uniprot: P58281) expressed and purified from E. coli.
3	Plates lidded to allow compound-rOPA1 interaction.
4	EDTA chelates Mg <sup>2+</sup> that cannot be used for rOPA1 GTP hydrolysis reaction.
5	Fresh solutions mixed just before use.
6	Plates are sealed to avoid evaporation and leaved in an incubator.
7	Add to all the wells excluding positive control wells. EDTA chelates Mg <sup>2+</sup> stopping the GTP hydrolysis reaction.
8	Malachite green and ammonium sulphate are stored at 4°C in the dark and mixed just before use. Mix gently by tapping the plate.
9	Plates lidded until color development.

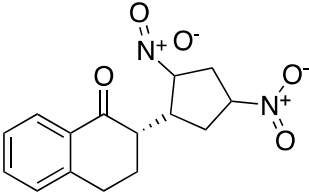
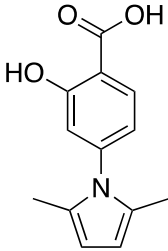
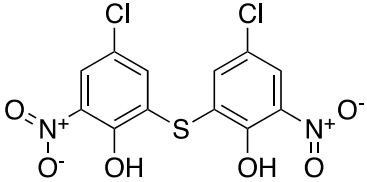
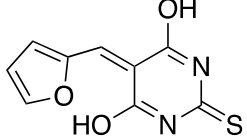
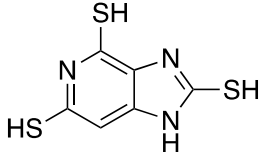
*Assay format: 384-well plates.*

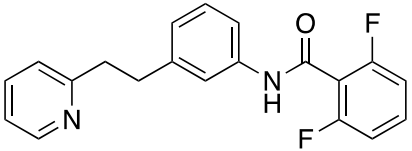
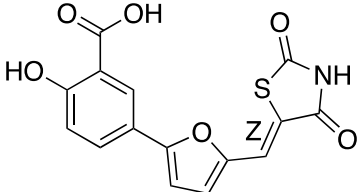
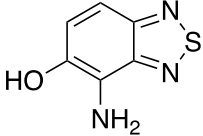
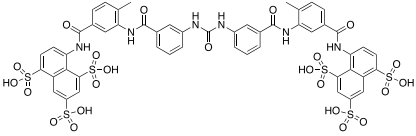
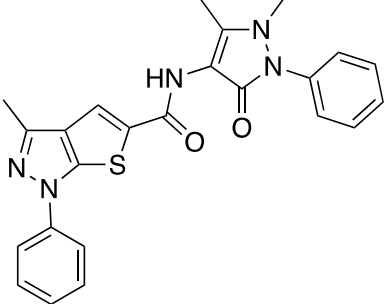
*Assay volume/well = 20  $\mu$ l.*

*Final concentrations/well: 0.5  $\mu$ M rOPA1, 500  $\mu$ M GTP, 10 mM MgCl<sub>2</sub>, 2.5% DMSO.*

**Table 1**



Name	Structure	Chemical formula	MW (Da)	LogP	H-donor	H-acceptor	Calculated solubility	OPA1 IC <sub>50</sub> (μM)	OPA1 I <sub>max</sub> (NPI)	ΔΨ <sub>m</sub> (μM)	Dyn-1 IC <sub>50</sub> (μM)
MYLS2		C <sub>14</sub> H <sub>10</sub> N <sub>2</sub> O <sub>5</sub> S	318.3	3.49	5	0	-4.29	370.7	0.35	> 10	91.21
MYLS3		C <sub>13</sub> H <sub>13</sub> NO <sub>3</sub>	231.3	3.98	3	2	-3.97	481.3	0.25	< 100	104.8
MYLS5		C <sub>12</sub> H <sub>6</sub> Cl <sub>2</sub> N <sub>2</sub> O <sub>6</sub> S	377.2	4.13	6	2	-4.27	65.8	0.71	> 10	22.8
MYLS9		C <sub>9</sub> H <sub>6</sub> N <sub>2</sub> O <sub>3</sub> S	222.2	1.8	3	2	-3.20	254.7	0.74	> 500	256.5
MYLS10		C <sub>5</sub> H <sub>4</sub> N <sub>4</sub> S <sub>3</sub>	216.3	-0.82	0	1	-2.48	139.8	0.57	> 100	16.7

MYLS15		$C_{20}H_{16}F_2N_2O$	338.4	4.68	1	1	-4.85	5.58	0.44	No effect	-
MYLS16		$C_{15}H_9NO_6S$	331.3	1.87	6	3	-3.56	71.2	0.56	> 100	87.4
MYLS17		$C_6H_5N_3OS$	167.2	0.77	1	3	-2.65	16.04	0.43	> 500	381.3
MYLS21		$C_{51}H_{40}N_6O_{23}S_6$	1297.2 6	5.58	12	23	-0.12	0.64	0.60	> 100	8.4
MYLS22		$C_{24}H_{21}N_5O_2S$	443.53	5.15	2	1	-5.62	96.5	0.78	No effect	No effect

**Table 2**

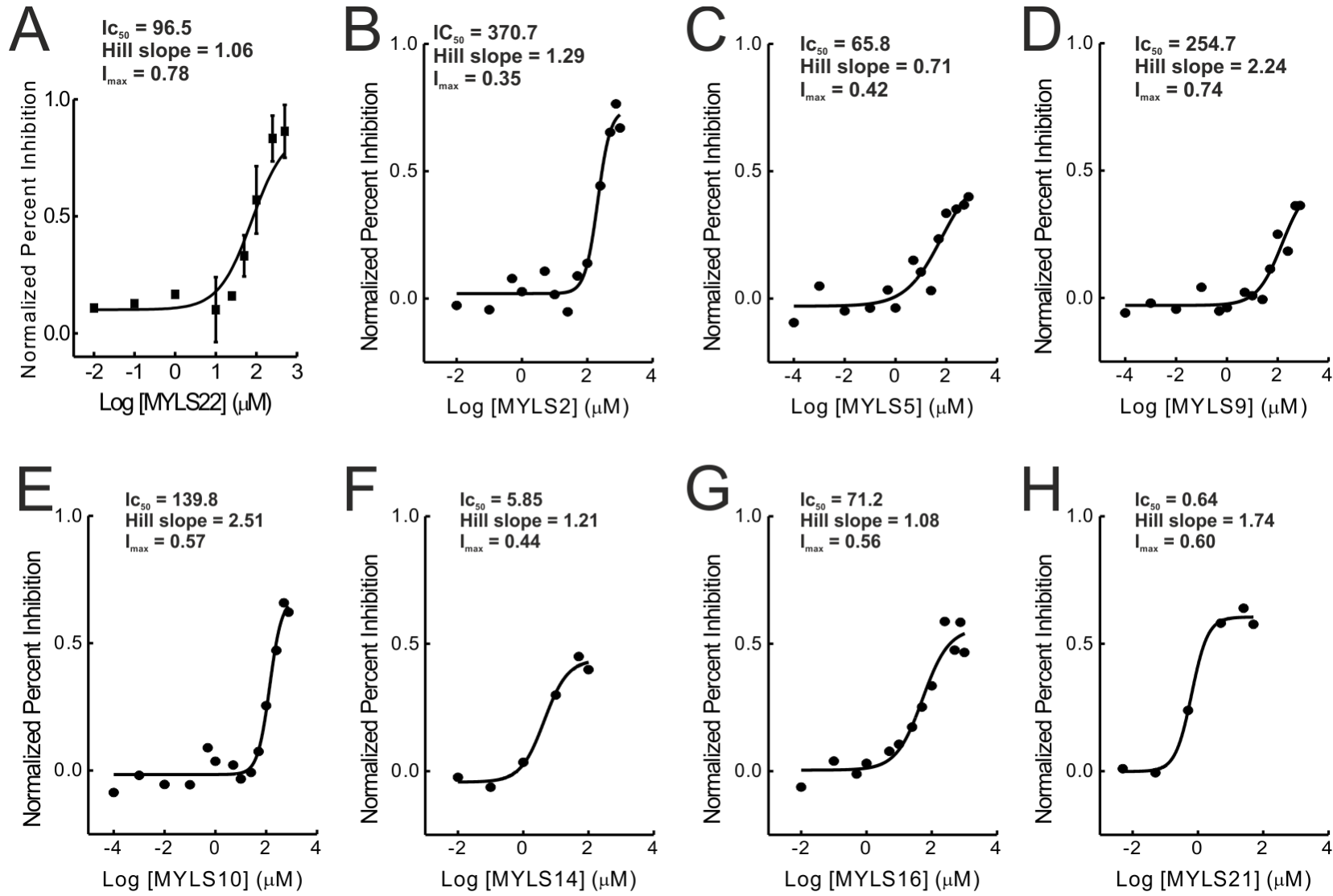


**Figure 2**





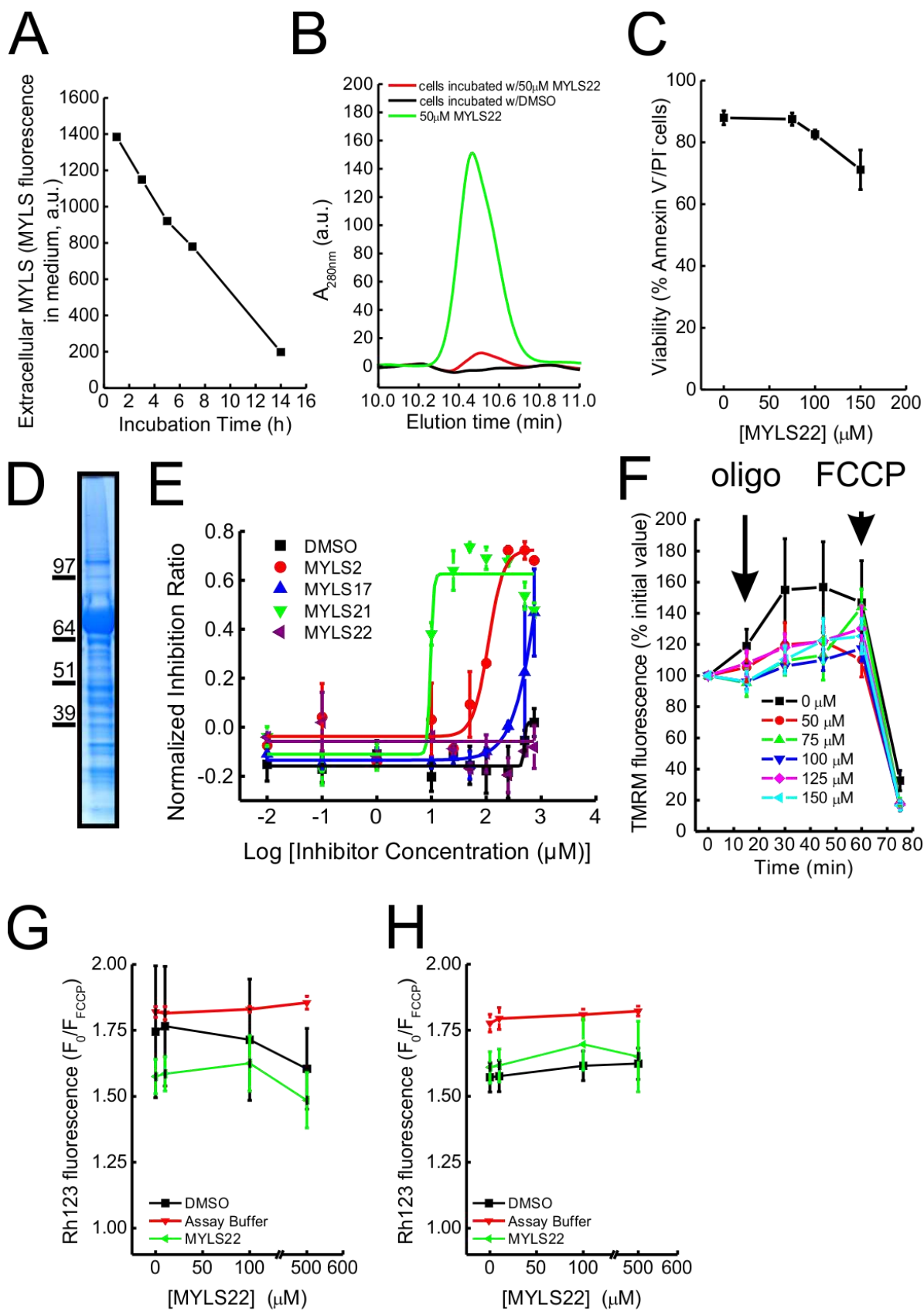


**Figure 4**

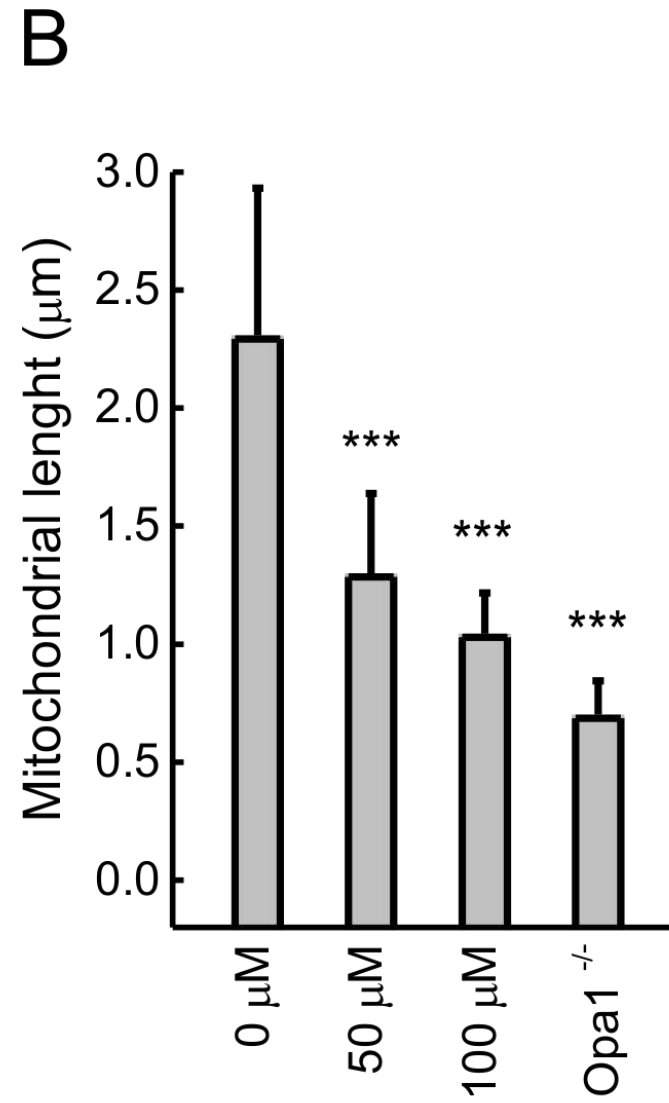
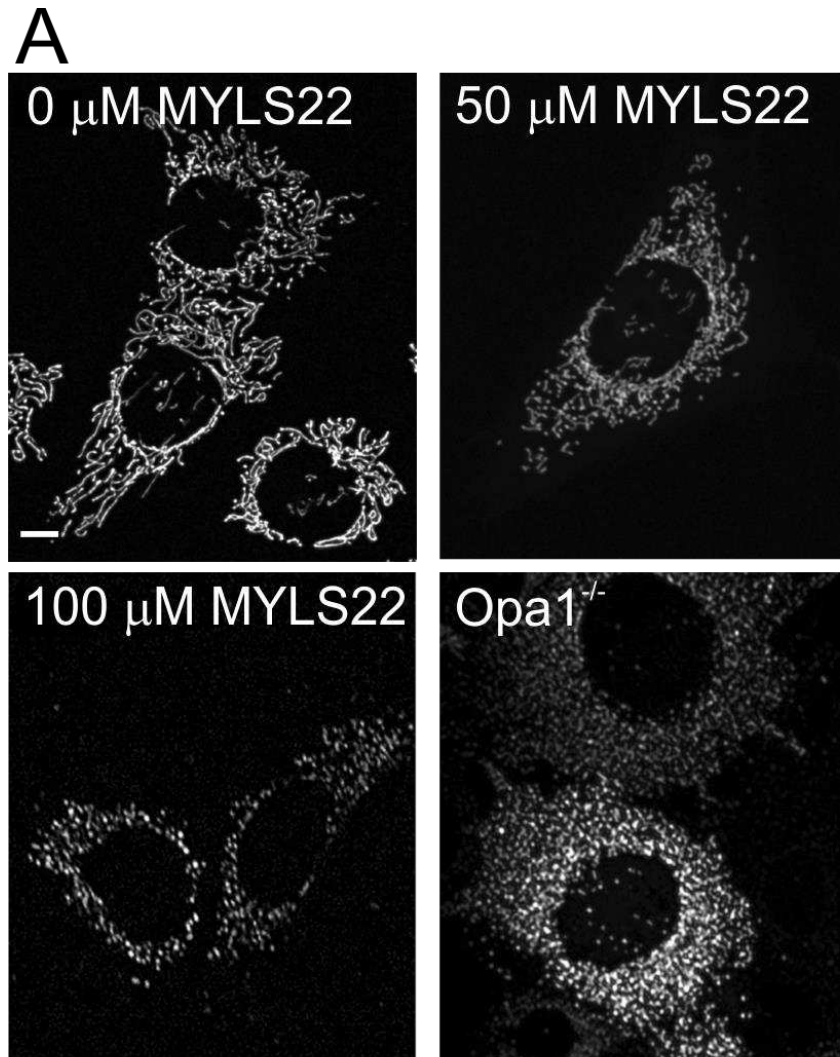
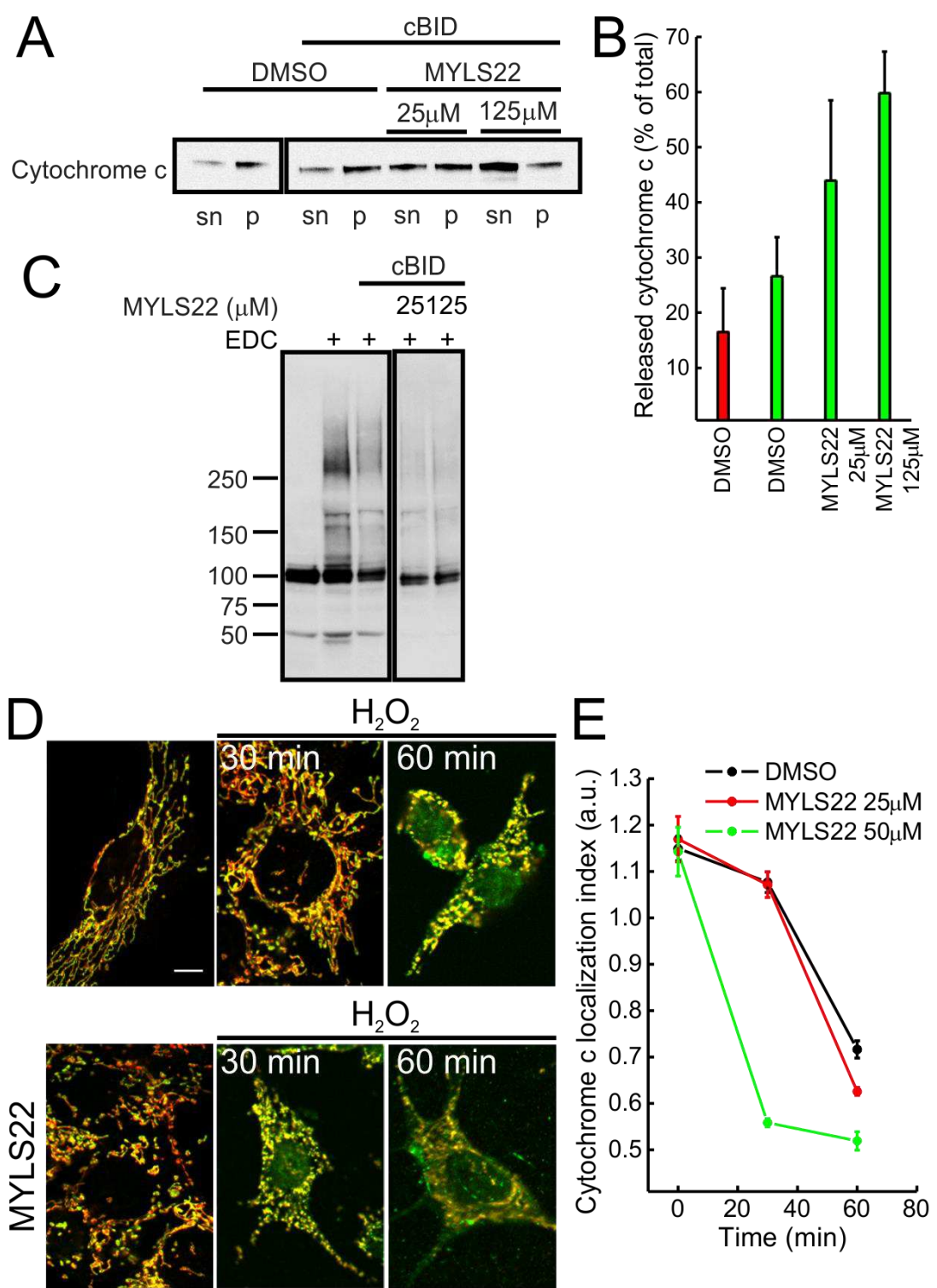


Figure 5



**Figure 6**

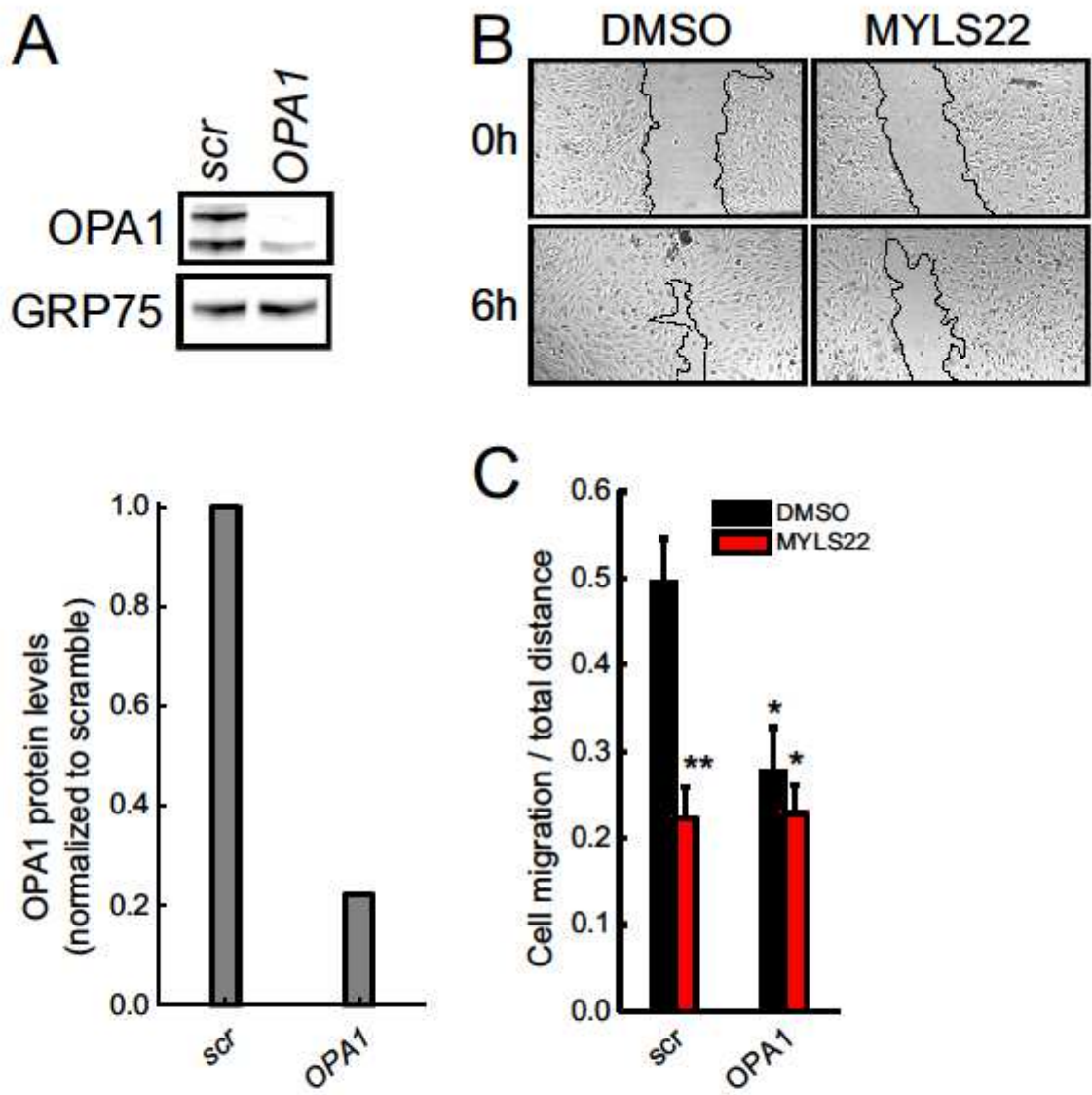


Figure 7

## SUPPLEMENTARY

### Supplementary Figure S1. Optimization of the malachite green assay for the HTS.

- (A) Kinetics of GTP hydrolysis by 0.2  $\mu\text{g}$  rOPA1 measured with the malachite green assay or the reverse phase chromatography (RPC). Data represents the mean of 3 independent experiments.
- (B) Hydrolysis kinetics of 750  $\mu\text{M}$  GTP by 0.2  $\mu\text{g}$  rOPA1 in the presence of different concentrations of GTP $\gamma$ S or GMPPNP. Reactions were stopped after 90 minutes by addition of EDTA and phosphate content was measured using the malachite green assay. Data are expressed as percentage of the positive control that lacked GTP analogues.
- (C) Kinetics of GTP hydrolysis by rOPA1 incubated at 37°C in the absence (black) or in the presence of 2.5% DMSO (red). Reactions started with the addition of 500  $\mu\text{M}$  GTP and were stopped at the indicated timepoints by additions of EDTA and phosphate content was determined using the malachite green assay.
- (D) Kinetics of GTP hydrolysis by rOPA1 incubated with 750  $\mu\text{M}$  GTP (black) or with the addition of 1000  $\mu\text{M}$  GTP $\gamma$ S (green) or EDTA (red). Reactions were stopped at the indicated timepoints by additions of EDTA and phosphate content was determined using the malachite green assay.
- (E) Hydrolysis of 750  $\mu\text{M}$  GTP by recombinant OPA1 in the presence of 1000  $\mu\text{M}$  GTP $\gamma$ S. OPA1 was incubated with GTP $\gamma$ S for the indicated minutes prior to adding GTP. Reactions were stopped after 60 minutes by additions of EDTA. Data is expressed as percentage of positive control without GTP $\gamma$ S.

- (F) Kinetics of GTP hydrolysis by rOPA1 incubated at 37°C in the absence (black) or in the presence of 500 μM GDP (red). Reactions started with the addition of 500 μM GTP and were stopped at the indicated timepoints by additions of EDTA and phosphate content was determined using the malachite green assay.
- (G) Effect of different MgCl<sub>2</sub> concentrations on the GTPase activity of rOPA1. Free phosphate content was measured using the malachite green assay. The OPA1 was incubated with 750 μM GTP and the reaction was stopped after 2h and 30 min.
- (H) Different effect of Mg<sup>2+</sup> and Mn<sup>2+</sup> on the GTPase activity of rOPA1. The reactions conditions are the same as in (G).

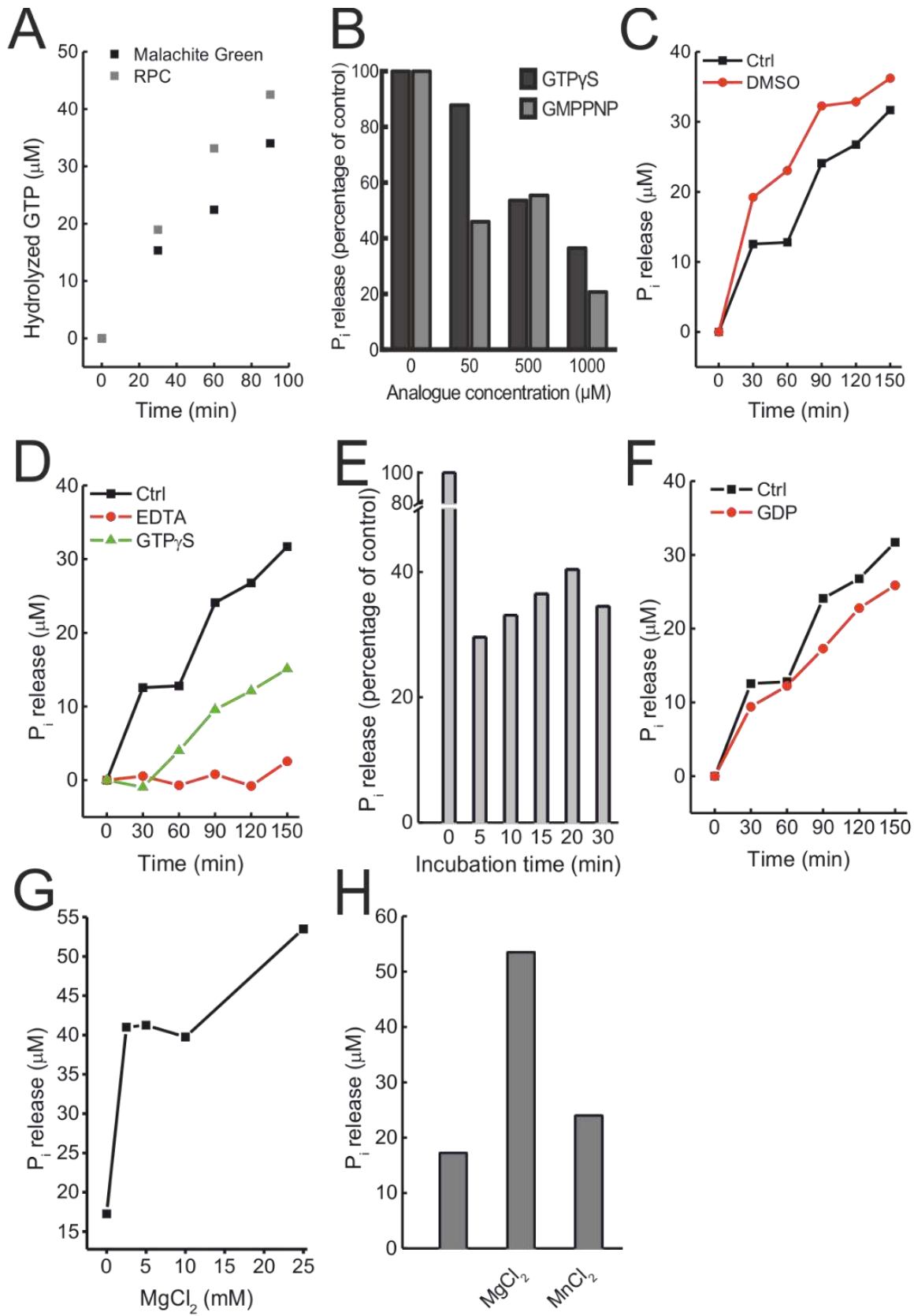
**Supplementary Table S1. Summary of the physiochemical properties of MYLS22.**

**Supplementary Figure S2.**

Clustal O aminoacid sequence alignment of the G domains of representative dynamin superfamily proteins and OPA1. The four conserved regions that characterize the dynamin G domains are reported along with their consensus motifs. Residues that are identical among the sequences have a black background, while the similar residues are colored with various shades of grey, depending on their degree of similarity. The aminoacids that are predicted to bind MYLS22 are colored in red.

**Supplementary Figure S3. Absorbance spectra of MYLS22 in extracellular media.**

Absorbance spectra of 50  $\mu$ M MYLS22 in the extracellular HBSS medium of MEF cells. The absorbance values for each timepoint were used to calculate the amount of MYLS22 uptaken by the cells in Figure 4A.



Supplementary Figure S1



	Calculated values for Inh#22	Desirable values
Molecular Weight	443.53 Da	< 500 Da
pI	6.12	-
Log P	3.67	-
Log D (pH 7.4)	3.51	< 5
H-donors	1	< 5
H-acceptors (pH 7.4)	6 (< 10)	< 10
Rotatable bounds	1	< 10
Molar Refractivity	125.25	from 40 to 130
Hydrophilic-lipophilic balance number (HLB)	8.05 (Davies) 11.11 (Griffin) 9.27 (combined method)	-
Intrinsic solubility (Log S) (pH 7.4)	-5.72	from 30 to 130
Polar surface area (pH 7.4)	70.47 Å	< 140 Å
Number of atoms	50	from 20 to 70

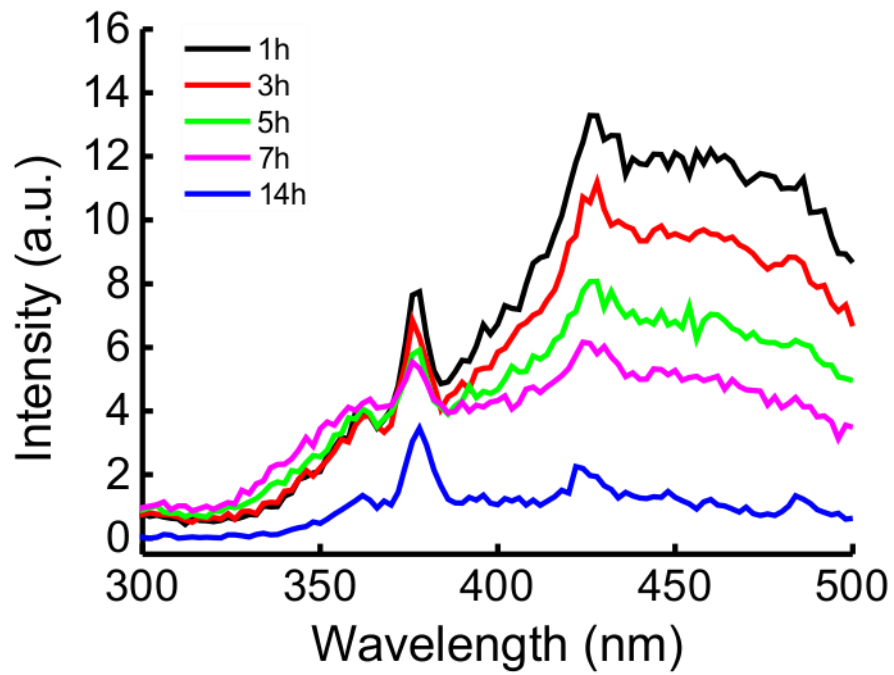
### Supplementary Table S1

# A

Region Consensus	G1 / P-loop GxxxxGKS/T	G2 / Switch I T	G3 / Switch 2 DxxG
OPA1_HUMAN/285-561	QDHLPRVVVGGQAAKSVLEMLIAQAR..IFPRGSEmTRSPVKVTLSEGPH.....	HVALFKDSSREFdlTKEDLAALRHEIELMRKNVKEGCTVSP-.ETISLNVKPGQLQRMVLDLPCVINTVTSGMAd	
DNM1L_HUMAN/22-302	IIQLPQIVVVGTSSGKSSVLESVGRD..LLPRGTIV.TRRPLILQLVHVSQEdkrk(8)eaeEWGKFLHTKNK-..	LYTDFDEIRQEIENETERISGNKGVSP-.EPIHLKIFSPNVNLTFLVDLPCMTKVPVGDQPKd	
DYN1_HUMAN/28-294	DLDLFQIIVVGGQSAKSSVLENFVGRD..FLPRGSCIV.TRRPLVLQLVNATT-.....	EYAEFLHCKGK-..-KFTDFEEVRLIEAETDRVVTGNTKGISP-.VPINLRVYSPHVLNLTFLVDLPCMTKVPVGDQPPd	
DYN2_HUMAN/28-294	HLDLPQIIVVGGQSAKSSVLENFVGRD..FLPRGSCIV.TRRPLILQLIFSKT-.....	EHAFLHCKSK-..-KFTDFEVRQIEAETDRVVTGNTKGISP-.VPINLRVYSPHVLNLTFLVDLPCITKVPVGDQPPd	
EHD2_HUMAN/55-286	FDGKPMVLVACQYSAGKTSFIQYLLEQE..VPGSRVPE-.....	PTTD.....CFVAVMHGDE-..-GTVPGNALVVDPPKPFRLNPFNTFLN-.RFMCAQLPNQVLESISIDTTPCI--LSGAKQrvs	
MFN1_HUMAN/72-321	SRRHMKVAFRCRTSSCKSSVINAMLWDK..VLPSGICHI-....	TNCFLSVEGTDg.....dKAYLMTGSEDEK..KSVKTVNQLAHALHMDKDLKAGCLVRFVWPkKACAL----LRDDLVLVDSPTCDVTTTELDS-..	
MFN2_HUMAN/93-342	ARRHMKVAFRCRTSNCKSTVINAMLWDK..VLPSGICHT-....	TNCFLRVEGTDg.....heAFLLEGESEK..RSAKTVNQLAHALHMDKDLKAGCLVRFVWPkKACAL----LKDDLVLVDSPTCDVTTTELDS-..	
MX1_HUMAN/67-340	DLALPAIIVVGGQSSGKSSVLEALSGV-..ALPRGSCIV.TRCPLVLKLLKLVned.....	KWRGKVSVDYE..IEISDASEVEKEINKAQNAIAGEGMGISH-.ELITLIESSRDVDDLTLFLVDLPCITRVAVGNQPad	
MX2_HUMAN/115-387	DLALPAIIVVGGQSSGKSSVLEALSGV-..ALPRGSCIV.TRCPLVLKLLKQPCe.....	AWAGRISYRNTE..LELQDPGQVEKEIHKAQNVNMGNGRGISH-.ELISLEITSPVDPDLTLFLVDLPCITRVAVGNQPrd	
SRCA_HUMAN/549-790	ITSKPMVLFVLPVSVKSTMINYLLGLEnTRYQLYTAe-.....	PTTS.....EFTVLMHGPKL-..-KTIEGIVMAADSARSFSPLEKFGQNFLE-.KLIGIEVPHKLLERVTFVDTPCIIENRKOQER..	

Region Consensus	G4 N/TKxD
OPA1_HUMAN/285-561	tKETIFSISKAMQNPNAIICIQDGSVAERSIVTDLVSQMDPHGRRTIFVLTIVLAEKNVA.SPSRIQQIIEGKLFPMKALGYFAVVTGK-.GNSSESIEAIREYEEFQNS..KLLKTSMLKAHQVTRRNISLAVSDCFWKMVRE..SVE
DNM1L_HUMAN/22-302	IELQIRELILRISNPNIIAVTAANTMATSEALKISREVPDGRRTLAVITKLLMDAGTD.-AMDV---LMGRVIPVKLGIIGVVNRSQldINNKKSVDTSIRDEYAFLOKky.PSLANRN----GTKYARTLNRLMHIRD..CIE
DYN1_HUMAN/28-294	IEFQIRDMLQVTKENCLIAVSPANSIANSDALKVAKEVDPQGRITIGVITKLLMDDEGTD.-ARDV---LENKLLPLRRGYIGVVNRSQkdIDGKDDITAALAAERKFLSH..PSYRHLADR--MGTPYQKVLNQQLTNHIRD..TIE
DYN2_HUMAN/28-294	IEYQIKDMILQISRESSLIHAVTPANMANSDALKVAKEVDPQGLRTIGVITKLLMDDEGTD.-ARDV---LENKLLPLRRGYIGVVNRSQkdIEGKDDIRAALAAERKFLSH..PAYRHMADR--MGTPYQKVLNQQLTNHIRE..SLF
EHD2_HUMAN/55-286	rGYDFPAVLRWAERVDLIILFDHAKLEISD-EFSEAIGALRGHEDKIRVVLNADMVVE--TQQLMRV---YGALMWALGK-----VVGTPPEVLRVYIGSWSQ..PLLVDPNR----RUFEELEQDLFRDIQ-.GLF
MFN1_HUMAN/72-321	.....WIDKCLDADVFVIVANSESTLMQTEKHFHFKVNERLSKPNIFILNRRWASASEPE.YMEDVRRQHMERCLHFLV-----EELKVVNALEAQNRIIFVSakeVLSARKQKAQ.-GMPESGVALAEGFHARLQEFqNFE
MFN2_HUMAN/93-342	.....WIDKCLDADVFVIVANSESTLMQTEKHFHFKVNERLSKPNIFILNRRWASASEPE.YMEEVRRQHMERCTSFVLD-----ELGVVDRSQAGDRIIFVSakeVNLARIQKAQ.-GMPEGGGALAEQVVMFEfqnFE
MX2_HUMAN/115-387	iGYKIKTLIKKIQRQETISVVVPSNVIIATTEALSMAQEVDPEDRTIGILTIPDLVDKGTGdKVVVDV---VRNLVFLKKGGMIVKCRGQqeIQDQLSLEALQREKIFENH..PYFRDLLEEG.ATVPCIAEKLTELITHICK..SLF
MX1_HUMAN/67-340	iGLQIKALIKKIQRQQTINVVVPCNVIIATTEALSMAHEVDPEDRTIGILTIPDLMDRGTEKSVMNV---VRNLTYPLKKGGMIVKCRGQqeITNRLSLAEATKKEITFQTH..PYFRVLEEGS.ATVPRIAERLTTELIMHIQK..SLF
SRCA_HUMAN/549-790	.GYPFNDVCQWIDRADLIFVVFDPTKLVGL-ELEMLFRQLKGRESQIRIILNADNLA--TQ.MLMRV---YGALFWSLA-----PLINVTEPPRVVYSSWPQ..EYKPDTHQELFQEEISLEDINQVIENRLEN..KIA

**A**







## Discussion

The work of this thesis describes the identification of MYLS22 as a potent and selective *in vitro* inhibitor of OPA1 GTPase activity that enhances the apoptotic release of cytochrome c.

The HTS of a chemical library of 10,000 drug-like small molecules described in the last manuscript allowed the identification of a specific inhibitor of rOPA1 GTPase activity. The inhibitor MYLS22 is not mitochondriotoxic and induces mitochondrial fragmentation. In response to the apoptotic stimulus BID in purified mitochondria and to hydrogen peroxide in cells, MYLS22 stimulates OPA1 oligomers disassembly and the release of cytochrome c, in a concentration-dependent manner. Interestingly, MYLS22 also phenocopied the inhibition of breast cancer cells migration caused by OPA1 silencing, thus indicating a potential anti-cancer property.

Recent studies revealed that changes in mitochondrial fission-fusion balance confer cancer cells the ability to adapt their metabolism to environmental modifications, as hypoxia, starvation, stress signals and drug treatments. The modification of apoptotic mechanisms allows cancer cells to escape from drug-induced cellular death, proliferate in unfavourable conditions, acquire further genetic mutations, and induce angiogenesis and perhaps metastatisation (Hanahan and Weinberg, 2011; Lopez and Tait, 2015). Among all shaping-proteins, OPA1 activity exerts a central role in apoptosis resistance. In fact, downregulation of OPA1 increases cell sensitivity towards apoptosis, while mutations that abolish OPA1 catalytic activity impair its antiapoptotic function (Frezza et al., 2006b). Moreover, it was discovered that OPA1 is overexpressed in different type of cancers and it correlates with a poor prognosis, an increased chemotherapy resistance and a lower survival rate (Fang et al., 2012; Kong et al., 2014; Zhao et al., 2012). Knockdown of OPA1 in hepatocellular carcinoma cells sensitized them to cytotoxic treatment (Zhao et al., 2013) and downregulation of OPA1 facilitated cytochrome c release and apoptosis in lung cancer cells (Hwang et al., 2012).

Noteworthy, the OPA1 antiapoptotic activity strictly depends on its ability of hydrolyse GTP, since mutations that abolish OPA1 GTPase activity also impair its antiapoptotic function (Frezza et al., 2006b). Given these observations, we are investigating the use OPA1 GTPase activity inhibitors, in combination with other

chemotherapeutic drugs, as sensitizing agents to target OPA1 antiapoptotic functions to induce cancer cell death and, possibly, overcome drug resistance of tumor cells. This approach would be particularly helpful in cancer cells characterized by high levels of OPA1 expression, like non-small cell lung cancer, or specific breast, melanoma, and ovary cancer subtypes.

In addition to the aforementioned role of OPA1 in the apoptotic process, OPA1 oligomers also regulate mitochondrial metabolism by controlling the cristae morphology and stabilizing the respiratory chain supercomplexes (Cogliati et al., 2013a).

In this context, the work of Quintana Cabrera et al., 2018 analyzes the relationship between the cristae shaping protein OPA1 and the ATP synthase. It demonstrates that OPA1 favors ATP synthase oligomerization and reversal activity. This discovery unravels a fundamental bioenergetic function of OPA1 in maintaining the mitochondrial electrochemical gradient during respiratory chain inhibition. By promoting the ATP synthase oligomerization and the stabilization of mitochondrial cristae, OPA1 exerts a protective role against mitochondrial dysfunctions. Thus, OPA1 overexpression might be beneficial to sustain bioenergetics in mitochondriopathies (Benit et al., 2009; Kucharczyk et al., 2009; Lodi et al., 2004; Zanna et al., 2008), it can be exploited as a target to correct oxidative phosphorylation changes in cancer (Buck et al., 2016; Caro et al., 2012; Garcia-Bermudez et al., 2015).

During the last years, numerous data emerged indicating mitochondrial metabolism as a target for cancer therapy. In respect to the activated oncogenes, the tumor microenvironment and the tumor stage, the bioenergetic profile of a specific cancer cell can widely vary from glycolytic to oxidative. The “glycolytic” cancer cells have a low efficient OXPHOS system and mainly rely on their glycolytic machinery and maintain; while the “OXPHOS” cancer cells mainly utilize mitochondrial respiration to produce ATP from glucose and glutamine oxidation. Mitochondrial energy production is required for many cancer types, and there is strong evidence to suggest that its inhibition may provide a valuable clinical target.

Given the above, what is bioenergetic profile of tumors with elevated expression of OPA1 protein? Could the levels of OPA1 in part contribute to the decision of cancer cells between the “glycolytic” and the “OXPHOS” metabolic profile? Since MYLS22 does not induce any changes in mitochondrial potential of MEF cells, we wanted to investigate the effect of the OPA1 inhibition on OXPHOS and mitochondrial potential of different cancer cell types.

OPA1 overexpression protects cells from mitochondrial dysfunctions. Quintana-Cabrera et al., 2018 demonstrated that the loss of electrochemical potential caused by the respiratory chain complex III inhibition is reduced by the overexpression



of OPA1 protein. Could the inhibition of the GTPase activity of OPA1 revert this condition? In the subset of tumors that depend on OXPHOS for survival, the OXPHOS disruption produces an energy and macromolecule depletion that leads to cell cycle arrest and death. As OPA1 promotes ATP synthase oligomerization and reversal activity by modulating cristae shape, the dissociation of OPA1 oligomers and the cristae remodeling by MYLS22 could indirectly affect OXPHOS and ATP synthase functionality of cancer cells.

Finally, high cellular levels of OPA1 correlate with increased chemotherapy resistance (Fang et al., 2012). In this context, we aim to investigate if the inhibition of OPA1 could sensitize resistant cancer cell to death. Specifically, by placing OPA1 at the crossroad of anti-apoptotic process and bioenergetic metabolism sustainment, we wanted to study if inhibiting OPA1 GTPase activity would synergize with tumor type-specific therapies, as drugs that promote apoptosis or impair ATP synthesis.

In conclusion, some issues need to be addressed before translating effective drugs that target mitochondrial functions to the clinical trials in patients. First, the drug co-treatment toxicity to normal cells compared to cancer cells has to be established. Second, the drug has to cross not only the cell membrane, but also the mitochondrial membrane. For this purpose, the conjunction of a lipophilic cation, as the PTT<sup>+</sup>, to the small molecule can increase the accumulation of the drug in the mitochondrial matrix.



## References

Accola, M.A., Huang, B., Al Masri, A., and McNiven, M.A. (2002). The antiviral dynamin family member, MxA, tubulates lipids and localizes to the smooth endoplasmic reticulum. *J Biol Chem* 277, 21829-21835.

Acin-Perez, R., Fernandez-Silva, P., Peleato, M.L., Perez-Martos, A., and Enriquez, J.A. (2008). Respiratory active mitochondrial supercomplexes. *Mol Cell* 32, 529-539.

Adachi, Y., Itoh, K., Yamada, T., Cervený, K.L., Suzuki, T.L., Macdonald, P., Frohman, M.A., Ramachandran, R., Iijima, M., and Sesaki, H. (2016). Coincident Phosphatidic Acid Interaction Restrains Drp1 in Mitochondrial Division. *Mol Cell* 63, 1034-1043.

Agier, V., Oliviero, P., Laine, J., L'Hermitte-Stead, C., Girard, S., Fillaut, S., Jardel, C., Bouillaud, F., Bulteau, A.L., and Lombes, A. (2012). Defective mitochondrial fusion, altered respiratory function, and distorted cristae structure in skin fibroblasts with heterozygous OPA1 mutations. *Biochim Biophys Acta* 1822, 1570-1580.

Alavi, M.V., Bette, S., Schimpf, S., Schuettauf, F., Schraermeyer, U., Wehrl, H.F., Ruttiger, L., Beck, S.C., Tonagel, F., Pichler, B.J., *et al.* (2007). A splice site mutation in the murine Opa1 gene features pathology of autosomal dominant optic atrophy. *Brain* 130, 1029-1042.

Alexander, C., Votruba, M., Pesch, U.E., Thiselton, D.L., Mayer, S., Moore, A., Rodriguez, M., Kellner, U., Leo-Kottler, B., Auburger, G., *et al.* (2000). OPA1, encoding a dynamin-related GTPase, is mutated in autosomal dominant optic atrophy linked to chromosome 3q28. *Nat Genet* 26, 211-215.

Amati-Bonneau, P., Guichet, A., Olichon, A., Chevrollier, A., Viala, F., Miot, S., Ayuso, C., Odent, S., Arrouet, C., Verny, C., *et al.* (2005). OPA1 R445H mutation in optic atrophy associated with sensorineural deafness. *Ann Neurol* 58, 958-963.

Amati-Bonneau, P., Milea, D., Bonneau, D., Chevrollier, A., Ferre, M., Guillet, V., Gueguen, N., Loiseau, D., de Crescenzo, M.A., Verny, C., *et al.* (2009). OPA1-associated disorders: phenotypes and pathophysiology. *Int J Biochem Cell Biol* 41, 1855-1865.

Amati-Bonneau, P., Odent, S., Derrien, C., Pasquier, L., Malthiery, Y., Reynier, P., and Bonneau, D. (2003). The association of autosomal dominant optic atrophy and moderate deafness may be due to the R445H mutation in the OPA1 gene. *Am J Ophthalmol* 136, 1170-1171.

Amati-Bonneau, P., Valentino, M.L., Reynier, P., Gallardo, M.E., Bornstein, B., Boissiere, A., Campos, Y., Rivera, H., de la Aleja, J.G., Carroccia, R., *et al.* (2008). OPA1 mutations induce mitochondrial DNA instability and optic atrophy 'plus' phenotypes. *Brain* *131*, 338-351.

Amchenkova, A.A., Bakeeva, L.E., Chentsov, Y.S., Skulachev, V.P., and Zorov, D.B. (1988). Coupling membranes as energy-transmitting cables. I. Filamentous mitochondria in fibroblasts and mitochondrial clusters in cardiomyocytes. *J Cell Biol* *107*, 481-495.

Anand, R., Wai, T., Baker, M.J., Kladt, N., Schauss, A.C., Rugarli, E., and Langer, T. (2014). The i-AAA protease YME1L and OMA1 cleave OPA1 to balance mitochondrial fusion and fission. *J Cell Biol* *204*, 919-929.

Anderson, G.R., Wardell, S.E., Cakir, M., Yip, C., Ahn, Y.R., Ali, M., Yllanes, A.P., Chao, C.A., McDonnell, D.P., and Wood, K.C. (2018). Dysregulation of mitochondrial dynamics proteins are a targetable feature of human tumors. *Nat Commun* *9*, 1677.

Anderson, S.L., Carton, J.M., Lou, J., Xing, L., and Rubin, B.Y. (1999). Interferon-induced guanylate binding protein-1 (GBP-1) mediates an antiviral effect against vesicular stomatitis virus and encephalomyocarditis virus. *Virology* *256*, 8-14.

Andrews, R.M., Griffiths, P.G., Johnson, M.A., and Turnbull, D.M. (1999). Histochemical localisation of mitochondrial enzyme activity in human optic nerve and retina. *Br J Ophthalmol* *83*, 231-235.

Ardail, D., Privat, J.P., Egret-Charlier, M., Levrat, C., Lerme, F., and Louisot, P. (1990). Mitochondrial contact sites. Lipid composition and dynamics. *J Biol Chem* *265*, 18797-18802.

Arnoult, D., Grodet, A., Lee, Y.J., Estaquier, J., and Blackstone, C. (2005a). Release of OPA1 during apoptosis participates in the rapid and complete release of cytochrome c and subsequent mitochondrial fragmentation. *J Biol Chem* *280*, 35742-35750.

Arnoult, D., Rismanchi, N., Grodet, A., Roberts, R.G., Seeburg, D.P., Estaquier, J., Sheng, M., and Blackstone, C. (2005b). Bax/Bak-dependent release of DDP/TIMM8a promotes Drp1-mediated mitochondrial fission and mitoptosis during programmed cell death. *Curr Biol* *15*, 2112-2118.

Ashkenazi, A., and Dixit, V.M. (1998). Death receptors: signaling and modulation. *Science* *281*, 1305-1308.

Ban, T., Heymann, J.A., Song, Z., Hinshaw, J.E., and Chan, D.C. (2010). OPA1 disease alleles causing dominant optic atrophy have defects in cardiolipin-stimulated GTP hydrolysis and membrane tubulation. In *Hum Mol Genet*, pp. 2113-2122.

Ban, T., Ishihara, T., Kohno, H., Saita, S., Ichimura, A., Maenaka, K., Oka, T., Mihara, K., and Ishihara, N. (2017). Molecular basis of selective mitochondrial fusion by heterotypic action between OPA1 and cardiolipin. *Nat Cell Biol* *19*, 856-863.

- Ban, T., Kohno, H., Ishihara, T., and Ishihara, N. (2018). Relationship between OPA1 and cardiolipin in mitochondrial inner-membrane fusion. *Biochim Biophys Acta* 1859, 951-957.
- Belenguer, P., and Pellegrini, L. (2013). The dynamin GTPase OPA1: More than mitochondria? *Biochimica et Biophysica Acta (BBA) - Molecular Cell Research* 1833, 176-183.
- Benit, P., Lebon, S., and Rustin, P. (2009). Respiratory-chain diseases related to complex III deficiency. *Biochim Biophys Acta* 1793, 181-185.
- Bernardi, P., and Azzone, G.F. (1981). Cytochrome c as an electron shuttle between the outer and inner mitochondrial membranes. *J Biol Chem* 256, 7187-7192.
- Bleazard, W., McCaffery, J.M., King, E.J., Bale, S., Mozdy, A., Tieu, Q., Nunnari, J., and Shaw, J.M. (1999). The dynamin-related GTPase Dnm1 regulates mitochondrial fission in yeast. *Nat Cell Biol* 1, 298-304.
- Bordt, E.A.e.a. (2017). The Putative Drp1 Inhibitor mdivi-1 Is a Reversible Mitochondrial Complex I Inhibitor that Modulates Reactive Oxygen Species: Developmental Cell. *Dev Cell*.
- Braschi, E., Zunino, R., and McBride, H.M. (2009). MAPL is a new mitochondrial SUMO E3 ligase that regulates mitochondrial fission. *EMBO Rep* 10, 748-754.
- Brdiczka, D.G., Zorov, D.B., and Sheu, S.S. (2006). Mitochondrial contact sites: their role in energy metabolism and apoptosis. *Biochim Biophys Acta* 1762, 148-163.
- Brill, A., Torchinsky, A., Carp, H., and Toder, V. (1999). The role of apoptosis in normal and abnormal embryonic development. *J Assist Reprod Genet* 16, 512-519.
- Bristow, E.A., Griffiths, P.G., Andrews, R.M., Johnson, M.A., and Turnbull, D.M. (2002). The distribution of mitochondrial activity in relation to optic nerve structure. *Arch Ophthalmol* 120, 791-796.
- Brooks, C., Wei, Q., Feng, L., Dong, G., Tao, Y., Mei, L., Xie, Z.J., and Dong, Z. (2007). Bak regulates mitochondrial morphology and pathology during apoptosis by interacting with mitofusins. *Proc Natl Acad Sci U S A* 104, 11649-11654.
- Buck, M.D., O'Sullivan, D., Klein Geltink, R.I., Curtis, J.D., Chang, C.H., Sanin, D.E., Qiu, J., Kretz, O., Braas, D., van der Windt, G.J., *et al.* (2016). Mitochondrial Dynamics Controls T Cell Fate through Metabolic Programming. *Cell* 166, 63-76.
- Bunnage, M.E., Chekler, E.L., and Jones, L.H. (2013). Target validation using chemical probes. *Nat Chem Biol* 9, 195-199.
- Cao, H., Garcia, F., and McNiven, M.A. (1998). Differential Distribution of Dynamin Isoforms in Mammalian Cells. In *Mol Biol Cell*, pp. 2595-2609.

Cao, Y.L., Meng, S., Chen, Y., Feng, J.X., Gu, D.D., Yu, B., Li, Y.J., Yang, J.Y., Liao, S., Chan, D.C., *et al.* (2017). MFN1 structures reveal nucleotide-triggered dimerization critical for mitochondrial fusion. *Nature* *542*, 372-376.

Caro, P., Kishan, A.U., Norberg, E., Stanley, I.A., Chapuy, B., Ficarro, S.B., Polak, K., Tondera, D., Gounarides, J., Yin, H., *et al.* (2012). Metabolic signatures uncover distinct targets in molecular subsets of diffuse large B cell lymphoma. *Cancer Cell* *22*, 547-560.

Cassidy-Stone, A., Chipuk, J.E., Ingerman, E., Song, C., Yoo, C., Kuwana, T., Kurth, M.J., Shaw, J.T., Hinshaw, J.E., Green, D.R., *et al.* (2008). Chemical inhibition of the mitochondrial division dynamin reveals its role in Bax/Bak-dependent mitochondrial outer membrane permeabilization. *Dev Cell* *14*, 193-204.

Cereghetti, G.M., Stangherlin, A., Martins de Brito, O., Chang, C.R., Blackstone, C., Bernardi, P., and Scorrano, L. (2008). Dephosphorylation by calcineurin regulates translocation of Drp1 to mitochondria. *Proc Natl Acad Sci U S A* *105*, 15803-15808.

Chakrabarti, R., Ji, W.K., Stan, R.V., de Juan Sanz, J., Ryan, T.A., and Higgs, H.N. (2018). INF2-mediated actin polymerization at the ER stimulates mitochondrial calcium uptake, inner membrane constriction, and division. *J Cell Biol* *217*, 251-268.

Chan, D.C. (2012). Fusion and fission: interlinked processes critical for mitochondrial health. *Annu Rev Genet* *46*, 265-287.

Chan, N.C., Salazar, A.M., Pham, A.H., Sweredoski, M.J., Kolawa, N.J., Graham, R.L., Hess, S., and Chan, D.C. (2011). Broad activation of the ubiquitin-proteasome system by Parkin is critical for mitophagy. *Hum Mol Genet* *20*, 1726-1737.

Chang, C.R., and Blackstone, C. (2007). Cyclic AMP-dependent protein kinase phosphorylation of Drp1 regulates its GTPase activity and mitochondrial morphology. *J Biol Chem* *282*, 21583-21587.

Chang, C.R., and Blackstone, C. (2010). Dynamic regulation of mitochondrial fission through modification of the dynamin-related protein Drp1. *Ann N Y Acad Sci* *1201*, 34-39.

Chappie, J.S., Acharya, S., Leonard, M., Schmid, S.L., and Dyda, F. (2010). G domain dimerization controls dynamin's assembly-stimulated GTPase activity. *Nature* *465*, 435-440.

Chen, H., Chomyn, A., and Chan, D.C. (2005). Disruption of fusion results in mitochondrial heterogeneity and dysfunction. *J Biol Chem* *280*, 26185-26192.

Chen, H., Detmer, S.A., Ewald, A.J., Griffin, E.E., Fraser, S.E., and Chan, D.C. (2003). Mitofusins Mfn1 and Mfn2 coordinately regulate mitochondrial fusion and are essential for embryonic development. *J Cell Biol* *160*, 189-200.

- Chen, H., McCaffery, J.M., and Chan, D.C. (2007). Mitochondrial fusion protects against neurodegeneration in the cerebellum. *Cell* *130*, 548-562.
- Chen, H., Vermulst, M., Wang, Y.E., Chomyn, A., Prolla, T.A., McCaffery, J.M., and Chan, D.C. (2010). Mitochondrial fusion is required for mtDNA stability in skeletal muscle and tolerance of mtDNA mutations. *Cell* *141*, 280-289.
- Chen, M., Chen, Z., Wang, Y., Tan, Z., Zhu, C., Li, Y., Han, Z., Chen, L., Gao, R., Liu, L., *et al.* (2016). Mitophagy receptor FUNDC1 regulates mitochondrial dynamics and mitophagy. *Autophagy* *12*, 689-702.
- Chen, Y., and Dorn, G.W., 2nd (2013). PINK1-phosphorylated mitofusin 2 is a Parkin receptor for culling damaged mitochondria. *Science* *340*, 471-475.
- Cheng, E.H., Sheiko, T.V., Fisher, J.K., Craigen, W.J., and Korsmeyer, S.J. (2003). VDAC2 inhibits BAK activation and mitochondrial apoptosis. *Science* *301*, 513-517.
- Cho, B., Cho, H.M., Jo, Y., Kim, H.D., Song, M., Moon, C., Kim, H., Kim, K., Sesaki, H., Rhyu, I.J., *et al.* (2017). Constriction of the mitochondrial inner compartment is a priming event for mitochondrial division. *Nat Commun* *8*, 15754.
- Cho, D.H., Nakamura, T., and Lipton, S.A. (2010). Mitochondrial dynamics in cell death and neurodegeneration. *Cell Mol Life Sci* *67*, 3435-3447.
- Cipolat, S., Martins de Brito, O., Dal Zilio, B., and Scorrano, L. (2004). OPA1 requires mitofusin 1 to promote mitochondrial fusion. *Proc Natl Acad Sci U S A* *101*, 15927-15932.
- Cipolat, S., Rudka, T., Hartmann, D., Costa, V., Serneels, L., Craessaerts, K., Metzger, K., Frezza, C., Annaert, W., D'Adamio, L., *et al.* (2006). Mitochondrial rhomboid PARL regulates cytochrome c release during apoptosis via OPA1-dependent cristae remodeling. *Cell* *126*, 163-175.
- Civiletto, G., Varanita, T., Cerutti, R., Gorletta, T., Barbaro, S., Marchet, S., Lamperti, C., Viscomi, C., Scorrano, L., and Zeviani, M. (2015). Opa1 overexpression ameliorates the phenotype of two mitochondrial disease mouse models. *Cell Metab* *21*, 845-854.
- Cocucci, E., Gaudin, R., and Kirchhausen, T. (2014). Dynamin recruitment and membrane scission at the neck of a clathrin-coated pit. *Mol Biol Cell* *25*, 3595-3609.
- Cogliati, S., Frezza, C., Soriano, M.E., Varanita, T., Quintana-Cabrera, R., Corrado, M., Cipolat, S., Costa, V., Casarin, A., Gomes, L.C., *et al.* (2013a). Mitochondrial cristae shape determines respiratory chain supercomplexes assembly and respiratory efficiency. *Cell* *155*, 160-171.
- Cogliati, S., Frezza, C., Soriano, M.E., Varanita, T., Quintana-Cabrera, R., Corrado, M., Cipolat, S., Costa, V., Casarin, A., Gomes, L.C., *et al.* (2013b). Mitochondrial

cristae shape determines respiratory chain supercomplexes assembly and respiratory efficiency. *Cell* 155, 160-171.

Cohen, J.J., Duke, R.C., Fadok, V.A., and Sellins, K.S. (1992). Apoptosis and programmed cell death in immunity. *Annu Rev Immunol* 10, 267-293.

Cohn, A.C., Toomes, C., Potter, C., Towns, K.V., Hewitt, A.W., Inglehearn, C.F., Craig, J.E., and Mackey, D.A. (2007). Autosomal dominant optic atrophy: penetrance and expressivity in patients with OPA1 mutations. *Am J Ophthalmol* 143, 656-662.

Copeland, R.A. (2003). Mechanistic considerations in high-throughput screening. *Analytical Biochemistry* 320, 1-12.

Costa, V., Giacomello, M., Hudec, R., Lopreiato, R., Ermak, G., Lim, D., Malorni, W., Davies, K.J.A., Carafoli, E., and Scorrano, L. (2010). Mitochondrial fission and cristae disruption increase the response of cell models of Huntington's disease to apoptotic stimuli.

Cribbs, J.T., and Strack, S. (2007). Reversible phosphorylation of Drp1 by cyclic AMP-dependent protein kinase and calcineurin regulates mitochondrial fission and cell death. *EMBO Rep* 8, 939-944.

Danial, N.N., Gramm, C.F., Scorrano, L., Zhang, C.Y., Krauss, S., Ranger, A.M., Datta, S.R., Greenberg, M.E., Licklider, L.J., Lowell, B.B., *et al.* (2003). BAD and glucokinase reside in a mitochondrial complex that integrates glycolysis and apoptosis. *Nature* 424, 952-956.

Danial, N.N., and Korsmeyer, S.J. (2004). Cell death: critical control points. *Cell* 116, 205-219.

Daumke, O., and Praefcke, G.J. (2016). Invited review: Mechanisms of GTP hydrolysis and conformational transitions in the dynamin superfamily. *Biopolymers* 105, 580-593.

Davies, K.M., Anselmi, C., Wittig, I., Faraldo-Gómez, J.D., and Kühlbrandt, W. (2012). Structure of the yeast F1Fo-ATP synthase dimer and its role in shaping the mitochondrial cristae.

Davies, V.J., Hollins, A.J., Piechota, M.J., Yip, W., Davies, J.R., White, K.E., Nicols, P.P., Boulton, M.E., and Votruba, M. (2007). Opa1 deficiency in a mouse model of autosomal dominant optic atrophy impairs mitochondrial morphology, optic nerve structure and visual function. *Hum Mol Genet* 16, 1307-1318.

de Brito, O.M., and Scorrano, L. (2008). Mitofusin 2 tethers endoplasmic reticulum to mitochondria. *Nature* 456, 605-610.

de Kroon, A.I., Dolis, D., Mayer, A., Lill, R., and de Kruijff, B. (1997). Phospholipid composition of highly purified mitochondrial outer membranes of rat liver and *Neurospora crassa*. Is cardiolipin present in the mitochondrial outer membrane? *Biochim Biophys Acta* 1325, 108-116.



Del Dotto, V., Mishra, P., Vidoni, S., Fogazza, M., Maresca, A., Caporali, L., McCaffery, J.M., Cappelletti, M., Baruffini, E., Lenaers, G., *et al.* (2017). OPA1 Isoforms in the Hierarchical Organization of Mitochondrial Functions. *Cell Rep* *19*, 2557-2571.

Delettre, C., Griffoin, J.M., Kaplan, J., Dollfus, H., Lorenz, B., Faivre, L., Lenaers, G., Belenguer, P., and Hamel, C.P. (2001). Mutation spectrum and splicing variants in the OPA1 gene. *Hum Genet* *109*, 584-591.

Delettre, C., Lenaers, G., Griffoin, J.M., Gigarel, N., Lorenzo, C., Belenguer, P., Pelloquin, L., Grosgeorge, J., Turc-Carel, C., Perret, E., *et al.* (2000). Nuclear gene OPA1, encoding a mitochondrial dynamin-related protein, is mutated in dominant optic atrophy. *Nat Genet* *26*, 207-210.

Delivani, P., and Martin, S.J. (2006). Mitochondrial membrane remodeling in apoptosis: an inside story. *Cell Death Differ* *13*, 2007-2010.

Desagher, S., Osen-Sand, A., Nichols, A., Eskes, R., Montessuit, S., Lauper, S., Maundrell, K., Antonsson, B., and Martinou, J.C. (1999). Bid-induced conformational change of Bax is responsible for mitochondrial cytochrome c release during apoptosis. *J Cell Biol* *144*, 891-901.

DeVay, R.M., Dominguez-Ramirez, L., Lackner, L.L., Hoppins, S., Stahlberg, H., and Nunnari, J. (2009). Coassembly of Mgm1 isoforms requires cardiolipin and mediates mitochondrial inner membrane fusion. *J Cell Biol* *186*, 793-803.

DiMauro, S., and Schon, E.A. (2003). Mitochondrial respiratory-chain diseases. *N Engl J Med* *348*, 2656-2668.

Ding, C., Wu, Z., Huang, L., Wang, Y., Xue, J., Chen, S., Deng, Z., Wang, L., and Song, Z. (2015). Mitofilin and CHCHD6 physically interact with Sam50 to sustain cristae structure. *Sci Rep* *5*, 16064.

Dorn, G.W., 2nd, and Maack, C. (2013). SR and mitochondria: calcium cross-talk between kissing cousins. *J Mol Cell Cardiol* *55*, 42-49.

Duvezin-Caubet, S., Koppen, M., Wagener, J., Zick, M., Israel, L., Bernacchia, A., Jagasia, R., Rugarli, E.I., Imhof, A., Neupert, W., *et al.* (2007). OPA1 processing reconstituted in yeast depends on the subunit composition of the m-AAA protease in mitochondria. *Mol Biol Cell* *18*, 3582-3590.

Ehse, S., Raschke, I., Mancuso, G., Bernacchia, A., Geimer, S., Tondera, D., Martinou, J.C., Westermann, B., Rugarli, E.I., and Langer, T. (2009). Regulation of OPA1 processing and mitochondrial fusion by m-AAA protease isoenzymes and OMA1. In *J Cell Biol*, pp. 1023-1036.

Elachouri, G., Vidoni, S., Zanna, C., Pattyn, A., Boukhaddaoui, H., Gaget, K., Yu-Wai-Man, P., Gasparre, G., Sarzi, E., Delettre, C., *et al.* (2011). OPA1 links human

mitochondrial genome maintenance to mtDNA replication and distribution. *Genome Res* 21, 12-20.

Eskes, R., Desagher, S., Antonsson, B., and Martinou, J.C. (2000). Bid induces the oligomerization and insertion of Bax into the outer mitochondrial membrane. *Mol Cell Biol* 20, 929-935.

Eura, Y., Ishihara, N., Yokota, S., and Mihara, K. (2003). Two mitofusin proteins, mammalian homologues of FZO, with distinct functions are both required for mitochondrial fusion. *J Biochem* 134, 333-344.

Faelber, K., Posor, Y., Gao, S., Held, M., Roske, Y., Schulze, D., Haucke, V., Noe, F., and Daumke, O. (2011). Crystal structure of nucleotide-free dynamin. *Nature* 477, 556-560.

Fang, H.Y., Chen, C.Y., Chiou, S.H., Wang, Y.T., Lin, T.Y., Chang, H.W., Chiang, I.P., Lan, K.J., and Chow, K.C. (2012). Overexpression of optic atrophy 1 protein increases cisplatin resistance via inactivation of caspase-dependent apoptosis in lung adenocarcinoma cells. *Hum Pathol* 43, 105-114.

Faust, J.E., Desai, T., Verma, A., Ulengin, I., Sun, T.L., Moss, T.J., Betancourt-Solis, M.A., Huang, H.W., Lee, T., and McNew, J.A. (2015). The Atlastin C-terminal tail is an amphipathic helix that perturbs the bilayer structure during endoplasmic reticulum homotypic fusion. *J Biol Chem* 290, 4772-4783.

Fernandez-Silva, P., Enriquez, J.A., and Montoya, J. (2003). Replication and transcription of mammalian mitochondrial DNA. *Exp Physiol* 88, 41-56.

Ferre, M., Caignard, A., Milea, D., Leruez, S., Cassereau, J., Chevrollier, A., Amati-Bonneau, P., Verny, C., Bonneau, D., Procaccio, V., *et al.* (2015). Improved locus-specific database for OPA1 mutations allows inclusion of advanced clinical data. *Hum Mutat* 36, 20-25.

Filadi, R., Greotti, E., Turacchio, G., Luini, A., Pozzan, T., and Pizzo, P. (2015). Mitofusin 2 ablation increases endoplasmic reticulum-mitochondria coupling. *Proc Natl Acad Sci U S A* 112, E2174-2181.

Fong, W.G., Liston, P., Rajcan-Separovic, E., St Jean, M., Craig, C., and Korneluk, R.G. (2000). Expression and genetic analysis of XIAP-associated factor 1 (XAF1) in cancer cell lines. *Genomics* 70, 113-122.

Ford, M.G., Jenni, S., and Nunnari, J. (2011a). The crystal structure of dynamin. *Nature* 477, 561-566.

Ford, M.G., Jenni, S., and Nunnari, J. (2011b). The crystal structure of dynamin. *Nature* 477, 561-566.

- Franco, A., Kitsis, R.N., Fleischer, J.A., Gavathiotis, E., Kornfeld, O.S., Gong, G., Biris, N., Benz, A., Qvit, N., Donnelly, S.K., *et al.* (2016). Correcting mitochondrial fusion by manipulating mitofusin conformations. *Nature* 540, 74-79.
- Frank, S., Gaume, B., Bergmann-Leitner, E.S., Leitner, W.W., Robert, E.G., Catez, F., Smith, C.L., and Youle, R.J. (2001). The role of dynamin-related protein 1, a mediator of mitochondrial fission, in apoptosis. *Dev Cell* 1, 515-525.
- Frey, T.G., Renken, C.W., and Perkins, G.A. (2002). Insight into mitochondrial structure and function from electron tomography. *Biochim Biophys Acta* 1555, 196-203.
- Frezza, C., Cipolat, S., Martins, d.B., Micaroni, M., Beznoussenko, G.V., Rudka, T., Bartoli, D., Polishuck, R.S., Danial, N.N., De Strooper, B., *et al.* (2006a). OPA1 Controls Apoptotic Cristae Remodeling Independently from Mitochondrial Fusion. *Cell* 126, 177-189.
- Frezza, C., Cipolat, S., Martins de Brito, O., Micaroni, M., Beznoussenko, G.V., Rudka, T., Bartoli, D., Polishuck, R.S., Danial, N.N., De Strooper, B., *et al.* (2006b). OPA1 Controls Apoptotic Cristae Remodeling Independently from Mitochondrial Fusion. *Cell* 126, 177-189.
- Frezza, C., Cipolat, S., and Scorrano, L. (2007a). Measuring mitochondrial shape changes and their consequences on mitochondrial involvement during apoptosis. *Methods Mol Biol* 372, 405-420.
- Frezza, C., Cipolat, S., and Scorrano, L. (2007b). Organelle isolation: functional mitochondria from mouse liver, muscle and cultured fibroblasts. *Nat Protoc* 2, 287-295.
- Friedman, J.R., Lackner, L.L., West, M., DiBenedetto, J.R., Nunnari, J., and Voeltz, G.K. (2011). ER tubules mark sites of mitochondrial division. *Science* 334, 358-362.
- Fulda, S., Galluzzi, L., and Kroemer, G. (2010). Targeting mitochondria for cancer therapy. *Nature Reviews Drug Discovery* 9, 447-464.
- Fulop, L., Rajki, A., Maka, E., Molnar, M.J., and Spat, A. (2015). Mitochondrial Ca<sup>2+</sup> uptake correlates with the severity of the symptoms in autosomal dominant optic atrophy. *Cell Calcium* 57, 49-55.
- Gammie, A.E., Kurihara, L.J., Vallee, R.B., and Rose, M.D. (1995). DNM1, a dynamin-related gene, participates in endosomal trafficking in yeast. *J Cell Biol* 130, 553-566.
- Gandre-Babbe, S., and van der Bliek, A.M. (2008). The novel tail-anchored membrane protein Mff controls mitochondrial and peroxisomal fission in mammalian cells. *Mol Biol Cell* 19, 2402-2412.
- Garcia-Bermudez, J., Sanchez-Arago, M., Soldevilla, B., Del Arco, A., Nuevo-Tapióles, C., and Cuezva, J.M. (2015). PKA Phosphorylates the ATPase Inhibitory

Factor 1 and Inactivates Its Capacity to Bind and Inhibit the Mitochondrial H(+)-ATP Synthase. *Cell Rep* 12, 2143-2155.

Gavathiotis, E., Reyna, D.E., Davis, M.L., Bird, G.H., and Walensky, L.D. (2010). BH3-triggered structural reorganization drives the activation of proapoptotic BAX. *Mol Cell* 40, 481-492.

Gawłowski, T., Suarez, J., Scott, B., Torres-Gonzalez, M., Wang, H., Schwappacher, R., Han, X., Yates, J.R., 3rd, Hoshijima, M., and Dillmann, W. (2012). Modulation of dynamin-related protein 1 (DRP1) function by increased O-linked-beta-N-acetylglucosamine modification (O-GlcNAc) in cardiac myocytes. *J Biol Chem* 287, 30024-30034.

Gegg, M.E., Cooper, J.M., Chau, K.Y., Rojo, M., Schapira, A.H., and Taanman, J.W. (2010). Mitofusin 1 and mitofusin 2 are ubiquitinated in a PINK1/parkin-dependent manner upon induction of mitophagy. *Hum Mol Genet* 19, 4861-4870.

Germain, M., Mathai, J.P., McBride, H.M., and Shore, G.C. (2005). Endoplasmic reticulum BIK initiates DRP1-regulated remodelling of mitochondrial cristae during apoptosis. *Embo j* 24, 1546-1556.

Ghosh, A., Praefcke, G.J., Renault, L., Wittinghofer, A., and Herrmann, C. (2006). How guanylate-binding proteins achieve assembly-stimulated processive cleavage of GTP to GMP. *Nature* 440, 101-104.

Glytsou, C., Calvo, E., Cogliati, S., Mehrotra, A., Anastasia, I., Rigoni, G., Raimondi, A., Shintani, N., Loureiro, M., Vazquez, J., *et al.* (2016). Optic Atrophy 1 Is Epistatic to the Core MICOS Component MIC60 in Mitochondrial Cristae Shape Control. *Cell Rep* 17, 3024-3034.

Goktug, A.N., Chai, S.C., and Chen, T. (2013). Data Analysis Approaches in High Throughput Screening.

Goldstein, J.C., Munoz-Pinedo, C., Ricci, J.E., Adams, S.R., Kelekar, A., Schuler, M., Tsiens, R.Y., and Green, D.R. (2005). Cytochrome c is released in a single step during apoptosis. *Cell Death Differ* 12, 453-462.

Goldstein, J.C., Waterhouse, N.J., Juin, P., Evan, G.I., and Green, D.R. (2000). The coordinate release of cytochrome c during apoptosis is rapid, complete and kinetically invariant. *Nat Cell Biol* 2, 156-162.

Gomes, L.C., Di Benedetto, G., and Scorrano, L. (2011). During autophagy mitochondria elongate, are spared from degradation and sustain cell viability. *Nat Cell Biol* 13, 589-598.

Gonzalez, F., Pariselli, F., Jalmar, O., Dupaigne, P., Sureau, F., Dellinger, M., Hendrickson, E.A., Bernard, S., and Petit, P.X. (2010). Mechanistic issues of the interaction of the hairpin-forming domain of tBid with mitochondrial cardiolipin. *PLoS One* 5, e9342.

- Grandemange, S., Herzig, S., and Martinou, J.C. (2009). Mitochondrial dynamics and cancer. *Semin Cancer Biol* 19, 50-56.
- Grassart, A., Cheng, A.T., Hong, S.H., Zhang, F., Zenzer, N., Feng, Y., Briner, D.M., Davis, G.D., Malkov, D., and Drubin, D.G. (2014). Actin and dynamin2 dynamics and interplay during clathrin-mediated endocytosis. *J Cell Biol* 205, 721-735.
- Green, D.R., and Kroemer, G. (2004). The pathophysiology of mitochondrial cell death. *Science* 305, 626-629.
- Griffin, E.E., Graumann, J., and Chan, D.C. (2005). The WD40 protein Caf4p is a component of the mitochondrial fission machinery and recruits Dnm1p to mitochondria. *J Cell Biol* 170, 237-248.
- Griparic, L., Kanazawa, T., and van der Bliek, A.M. (2007). Regulation of the mitochondrial dynamin-like protein Opa1 by proteolytic cleavage. In *J Cell Biol*, pp. 757-764.
- Griparic, L., van der Wel, N.N., Orozco, I.J., Peters, P.J., and van der Bliek, A.M. (2004). Loss of the intermembrane space protein Mgm1/OPA1 induces swelling and localized constrictions along the lengths of mitochondria. *J Biol Chem* 279, 18792-18798.
- Grosse, L., Wurm, C.A., Bruser, C., Neumann, D., Jans, D.C., and Jakobs, S. (2016). Bax assembles into large ring-like structures remodeling the mitochondrial outer membrane in apoptosis. *Embo j* 35, 402-413.
- Gruver-Yates, A.L., and Cidlowski, J.A. (2013). Tissue-Specific Actions of Glucocorticoids on Apoptosis: A Double-Edged Sword. In *Cells*, pp. 202-223.
- Guillery, O., Malka, F., Landes, T., Guillou, E., Blackstone, C., Lombes, A., Belenguer, P., Arnoult, D., and Rojo, M. (2008). Metalloprotease-mediated OPA1 processing is modulated by the mitochondrial membrane potential. *Biol Cell* 100, 315-325.
- Guillou, E., Bousquet, C., Daloyau, M., Emorine, L.J., and Belenguer, P. (2005). Msp1p is an intermembrane space dynamin-related protein that mediates mitochondrial fusion in a Dnm1p-dependent manner in *S. pombe*. *FEBS Lett* 579, 1109-1116.
- Hackenbrock, C.R. (1966). Ultrastructural bases for metabolically linked mechanical activity in mitochondria. I. Reversible ultrastructural changes with change in metabolic steady state in isolated liver mitochondria. *J Cell Biol* 30, 269-297.
- Hajek, P., Villani, G., and Attardi, G. (2001). Rate-limiting step preceding cytochrome c release in cells primed for Fas-mediated apoptosis revealed by analysis of cellular mosaicism of respiratory changes. *J Biol Chem* 276, 606-615.
- Hales, K.G., and Fuller, M.T. (1997). Developmentally regulated mitochondrial fusion mediated by a conserved, novel, predicted GTPase. *Cell* 90, 121-129.

Hanahan, D., and Weinberg, R.A. (2011). Hallmarks of cancer: the next generation. *Cell* 144, 646-674.

Hann, M.M., and Simpson, G.L. (2014). Intracellular drug concentration and disposition--the missing link? *Methods* 68, 283-285.

Haun, F., Nakamura, T., Shiu, A.D., Cho, D.H., Tsunemi, T., Holland, E.A., La Spada, A.R., and Lipton, S.A. (2013). S-nitrosylation of dynamin-related protein 1 mediates mutant huntingtin-induced mitochondrial fragmentation and neuronal injury in Huntington's disease. *Antioxid Redox Signal* 19, 1173-1184.

Head, B., Griparic, L., Amiri, M., Gandre-Babbe, S., and van der Bliek, A.M. (2009). Inducible proteolytic inactivation of OPA1 mediated by the OMA1 protease in mammalian cells. *J Cell Biol* 187, 959-966.

Heiduschka, P., Schnichels, S., Fuhrmann, N., Hofmeister, S., Schraermeyer, U., Wissinger, B., and Alavi, M.V. (2010). Electrophysiological and histologic assessment of retinal ganglion cell fate in a mouse model for OPA1-associated autosomal dominant optic atrophy. *Invest Ophthalmol Vis Sci* 51, 1424-1431.

Hengartner, M.O. (2000). The biochemistry of apoptosis. *Nature* 407, 770-776.

Henson, P.M., and Hume, D.A. (2006). Apoptotic cell removal in development and tissue homeostasis. *Trends Immunol* 27, 244-250.

Heymann, J.A., and Hinshaw, J.E. (2009). Dynamins at a glance. *J Cell Sci* 122, 3427-3431.

Hinshaw, J.E. (2000). Dynamin and its role in membrane fission. *Annu Rev Cell Dev Biol* 16, 483-519.

Holzerova, E., and Prokisch, H. (2015). Mitochondria: Much ado about nothing? How dangerous is reactive oxygen species production? *Int J Biochem Cell Biol* 63, 16-20.

Hom, J.R., Gewandter, J.S., Michael, L., Sheu, S.S., and Yoon, Y. (2007). Thapsigargin induces biphasic fragmentation of mitochondria through calcium-mediated mitochondrial fission and apoptosis. *J Cell Physiol* 212, 498-508.

Hoppins, S., Collins, S.R., Cassidy-Stone, A., Hummel, E., Devay, R.M., Lackner, L.L., Westermann, B., Schuldiner, M., Weissman, J.S., and Nunnari, J. (2011). A mitochondrial-focused genetic interaction map reveals a scaffold-like complex required for inner membrane organization in mitochondria. *J Cell Biol* 195, 323-340.

Hwang, S.K., Minai-Tehrani, A., Yu, K.N., Chang, S.H., Kim, J.E., Lee, K.H., Park, J., Beck, G.R., Jr., and Cho, M.H. (2012). Carboxyl-terminal modulator protein induces apoptosis by regulating mitochondrial function in lung cancer cells. *Int J Oncol* 40, 1515-1524.

Irwin, W.A., Bergamin, N., Sabatelli, P., Reggiani, C., Megighian, A., Merlini, L., Braghetta, P., Columbaro, M., Volpin, D., Bressan, G.M., *et al.* (2003). Mitochondrial dysfunction and apoptosis in myopathic mice with collagen VI deficiency. *Nat Genet* *35*, 367-371.

Ishihara, N., Eura, Y., and Mihara, K. (2004). Mitofusin 1 and 2 play distinct roles in mitochondrial fusion reactions via GTPase activity. *J Cell Sci* *117*, 6535-6546.

Ishihara, N., Fujita, Y., Oka, T., and Mihara, K. (2006). Regulation of mitochondrial morphology through proteolytic cleavage of OPA1. *Embo j* *25*, 2966-2977.

Ishihara, N., Nomura, M., Jofuku, A., Kato, H., Suzuki, S.O., Masuda, K., Otera, H., Nakanishi, Y., Nonaka, I., Goto, Y., *et al.* (2009). Mitochondrial fission factor Drp1 is essential for embryonic development and synapse formation in mice. *Nat Cell Biol* *11*, 958-966.

Iyer, S., Bell, F., Westphal, D., Anwari, K., Gulbis, J., Smith, B.J., Dewson, G., and Kluck, R.M. (2015). Bak apoptotic pores involve a flexible C-terminal region and juxtaposition of the C-terminal transmembrane domains. *Cell Death Differ* *22*, 1665-1675.

Jiang, X., Jiang, H., Shen, Z., and Wang, X. (2014). Activation of mitochondrial protease OMA1 by Bax and Bak promotes cytochrome c release during apoptosis. *Proc Natl Acad Sci U S A* *111*, 14782-14787.

Jones, B.A., and Fangman, W.L. (1992). Mitochondrial DNA maintenance in yeast requires a protein containing a region related to the GTP-binding domain of dynamin. *Genes Dev* *6*, 380-389.

Jouaville, L.S., Ichas, F., Holmuhamedov, E.L., Camacho, P., and Lechleiter, J.D. (1995). Synchronization of calcium waves by mitochondrial substrates in *Xenopus laevis* oocytes. *Nature* *377*, 438-441.

Kalia, R., Wang, R.Y., Yusuf, A., Thomas, P.V., Agard, D.A., Shaw, J.M., and Frost, A. (2018). Structural basis of mitochondrial receptor binding and constriction by DRP1. *Nature* *558*, 401-405.

Kane, M.S., Alban, J., Desquiret-Dumas, V., Gueguen, N., Ishak, L., Ferre, M., Amati-Bonneau, P., Procaccio, V., Bonneau, D., Lenaers, G., *et al.* (2017). Autophagy controls the pathogenicity of OPA1 mutations in dominant optic atrophy. In *J Cell Mol Med*, pp. 2284-2297.

Karbowski, M., Lee, Y.J., Gaume, B., Jeong, S.Y., Frank, S., Nechushtan, A., Santel, A., Fuller, M., Smith, C.L., and Youle, R.J. (2002). Spatial and temporal association of Bax with mitochondrial fission sites, Drp1, and Mfn2 during apoptosis. *J Cell Biol* *159*, 931-938.

- Kashatus, D.F., Lim, K.H., Brady, D.C., Pershing, N.L., Cox, A.D., and Counter, C.M. (2011). RALA and RALBP1 regulate mitochondrial fission at mitosis. *Nat Cell Biol* *13*, 1108-1115.
- Kashatus, J.A., Nascimento, A., Myers, L.J., Sher, A., Byrne, F.L., Hoehn, K.L., Counter, C.M., and Kashatus, D.F. (2015). Erk2 phosphorylation of Drp1 promotes mitochondrial fission and MAPK-driven tumor growth. *Mol Cell* *57*, 537-551.
- Kaur, M., Reed, E., Sartor, O., Dahut, W., and Figg, W.D. (2002). Suramin's development: what did we learn? *Invest New Drugs* *20*, 209-219.
- Kelley, L.A., Mezulis, S., Yates, C.M., Wass, M.N., and Sternberg, M.J. (2015). The Phyre2 web portal for protein modeling, prediction and analysis. *Nat Protoc* *10*, 845-858.
- Kerr, J.F., Wyllie, A.H., and Currie, A.R. (1972). Apoptosis: a basic biological phenomenon with wide-ranging implications in tissue kinetics. *Br J Cancer* *26*, 239-257.
- Khodjakov, A., Rieder, C., Mannella, C.A., and Kinnally, K.W. (2004). Laser micro-irradiation of mitochondria: is there an amplified mitochondrial death signal in neural cells? *Mitochondrion* *3*, 217-227.
- Kim, D.I., Lee, K.H., Gabr, A.A., Choi, G.E., Kim, J.S., Ko, S.H., and Han, H.J. (2016). Abeta-Induced Drp1 phosphorylation through Akt activation promotes excessive mitochondrial fission leading to neuronal apoptosis. *Biochim Biophys Acta* *1863*, 2820-2834.
- Kim, S.J., Syed, G.H., Khan, M., Chiu, W.W., Sohail, M.A., Gish, R.G., and Siddiqui, A. (2014). Hepatitis C virus triggers mitochondrial fission and attenuates apoptosis to promote viral persistence. *Proc Natl Acad Sci U S A* *111*, 6413-6418.
- Knott, A.B., Perkins, G., Schwarzenbacher, R., and Bossy-Wetzler, E. (2008). Mitochondrial fragmentation in neurodegeneration. *Nat Rev Neurosci* *9*, 505-518.
- Koch, A., Thiemann, M., Grabenbauer, M., Yoon, Y., McNiven, M.A., and Schrader, M. (2003). Dynamin-like protein 1 is involved in peroxisomal fission. *J Biol Chem* *278*, 8597-8605.
- Kong, B., Wang, Q., Fung, E., Xue, K., and Tsang, B.K. (2014). p53 is required for cisplatin-induced processing of the mitochondrial fusion protein L-Opa1 that is mediated by the mitochondrial metallopeptidase Oma1 in gynecologic cancers. *J Biol Chem* *289*, 27134-27145.
- Krishnan, K.S., Rikhy, R., Rao, S., Shivalkar, M., Mosko, M., Narayanan, R., Etter, P., Estes, P.S., and Ramaswami, M. (2001). Nucleoside diphosphate kinase, a source of GTP, is required for dynamin-dependent synaptic vesicle recycling. *Neuron* *30*, 197-210.



Kucharczyk, R., Zick, M., Bietenhader, M., Rak, M., Couplan, E., Blondel, M., Caubet, S.D., and di Rago, J.P. (2009). Mitochondrial ATP synthase disorders: molecular mechanisms and the quest for curative therapeutic approaches. *Biochim Biophys Acta* *1793*, 186-199.

Kukat, C., Davies, K.M., Wurm, C.A., Spahr, H., Bonekamp, N.A., Kuhl, I., Joos, F., Polosa, P.L., Park, C.B., Posse, V., *et al.* (2015). Cross-strand binding of TFAM to a single mtDNA molecule forms the mitochondrial nucleoid. *Proc Natl Acad Sci U S A* *112*, 11288-11293.

Kushnareva, Y., Seong, Y., Andreyev, A.Y., Kuwana, T., Kiosses, W.B., Votruba, M., and Newmeyer, D.D. (2016). Mitochondrial dysfunction in an Opa1(Q285STOP) mouse model of dominant optic atrophy results from Opa1 haploinsufficiency. *Cell Death Dis* *7*, e2309.

Kushnareva, Y.E., Gerencser, A.A., Bossy, B., Ju, W.K., White, A.D., Waggoner, J., Ellisman, M.H., Perkins, G., and Bossy-Wetzell, E. (2013). Loss of OPA1 disturbs cellular calcium homeostasis and sensitizes for excitotoxicity. *Cell Death Differ* *20*, 353-365.

Kvansakul, M., Yang, H., Fairlie, W.D., Czabotar, P.E., Fischer, S.F., Perugini, M.A., Huang, D.C., and Colman, P.M. (2008). Vaccinia virus anti-apoptotic F1L is a novel Bcl-2-like domain-swapped dimer that binds a highly selective subset of BH3-containing death ligands. *Cell Death Differ* *15*, 1564-1571.

Labrousse, A.M., Zappaterra, M.D., Rube, D.A., and van der Bliek, A.M. (1999). *C. elegans* dynamin-related protein DRP-1 controls severing of the mitochondrial outer membrane. *Mol Cell* *4*, 815-826.

Landes, T., Emorine, L.J., Courilleau, D., Rojo, M., Belenguer, P., and Arnaune-Pelloquin, L. (2010). The BH3-only Bnip3 binds to the dynamin Opa1 to promote mitochondrial fragmentation and apoptosis by distinct mechanisms. *EMBO Rep* *11*, 459-465.

Lang, A., Anand, R., Altinoluk-Hambuchen, S., Ezzahoini, H., Stefanski, A., Iram, A., Bergmann, L., Urbach, J., Bohler, P., Hansel, J., *et al.* (2017). SIRT4 interacts with OPA1 and regulates mitochondrial quality control and mitophagy. *Aging (Albany NY)* *9*, 2163-2189.

Lapiente-Brun, E., Moreno-Loshuertos, R., Acin-Perez, R., Latorre-Pellicer, A., Colas, C., Balsa, E., Perales-Clemente, E., Quiros, P.M., Calvo, E., Rodriguez-Hernandez, M.A., *et al.* (2013). Supercomplex assembly determines electron flux in the mitochondrial electron transport chain. *Science* *340*, 1567-1570.

Leboucher, G.P., Tsai, Y.C., Yang, M., Shaw, K.C., Zhou, M., Veenstra, T.D., Glickman, M.H., and Weissman, A.M. (2012). Stress-induced phosphorylation and proteasomal degradation of mitofusin 2 facilitates mitochondrial fragmentation and apoptosis. *Mol Cell* *47*, 547-557.

- Lee, H., Smith, S.B., and Yoon, Y. (2017). The short variant of the mitochondrial dynamin OPA1 maintains mitochondrial energetics and cristae structure. *J Biol Chem* 292, 7115-7130.
- Lee, J.Y., Kapur, M., Li, M., Choi, M.C., Choi, S., Kim, H.J., Kim, I., Lee, E., Taylor, J.P., and Yao, T.P. (2014). MFN1 deacetylation activates adaptive mitochondrial fusion and protects metabolically challenged mitochondria. *J Cell Sci* 127, 4954-4963.
- Lee, Y.J., Jeong, S.Y., Karbowski, M., Smith, C.L., and Youle, R.J. (2004). Roles of the mammalian mitochondrial fission and fusion mediators Fis1, Drp1, and Opa1 in apoptosis. *Mol Biol Cell* 15, 5001-5011.
- Lenaers, G., Hamel, C., Delettre, C., Amati-Bonneau, P., Procaccio, V., Bonneau, D., Reynier, P., and Milea, D. (2012). Dominant optic atrophy. *Orphanet J Rare Dis* 7, 46.
- Leonard, M., Doo Song, B., Ramachandran, R., and Schmid, S.L. (2005). Robust Colorimetric Assays for Dynamin's Basal and Stimulated GTPase Activities. In *Methods in Enzymology* (Academic Press), pp. 490-503.
- Li, C., Kosmorsky, G., Zhang, K., Katz, B.J., Ge, J., and Traboulsi, E.I. (2005). Optic atrophy and sensorineural hearing loss in a family caused by an R445H OPA1 mutation. *Am J Med Genet A* 138a, 208-211.
- Li, H., Zhu, H., Xu, C.J., and Yuan, J. (1998). Cleavage of BID by caspase 8 mediates the mitochondrial damage in the Fas pathway of apoptosis. *Cell* 94, 491-501.
- Li, J., Zhou, J., Li, Y., Qin, D., and Li, P. (2010). Mitochondrial fission controls DNA fragmentation by regulating endonuclease G. *Free Radic Biol Med* 49, 622-631.
- Li, L., Thomas, R.M., Suzuki, H., De Brabander, J.K., Wang, X., and Harran, P.G. (2004). A small molecule Smac mimic potentiates TRAIL- and TNFalpha-mediated cell death. *Science* 305, 1471-1474.
- Lipinski, C.A., Lombardo, F., Dominy, B.W., and Feeney, P.J. (2001). Experimental and computational approaches to estimate solubility and permeability in drug discovery and development settings. *Adv Drug Deliv Rev* 46, 3-26.
- Liu, T.Y., Bian, X., Sun, S., Hu, X., Klemm, R.W., Prinz, W.A., Rapoport, T.A., and Hu, J. (2012). Lipid interaction of the C terminus and association of the transmembrane segments facilitate atlastin-mediated homotypic endoplasmic reticulum fusion. *Proc Natl Acad Sci U S A* 109, E2146-2154.
- Liu, X., Weaver, D., Shirihai, O., and Hajnóczky, G. (2009). Mitochondrial 'kiss-and-run': interplay between mitochondrial motility and fusion-fission dynamics. In *EMBO J*, pp. 3074-3089.
- Lodi, R., Tonon, C., Valentino, M.L., Iotti, S., Clementi, V., Malucelli, E., Barboni, P., Longanesi, L., Schimpf, S., Wissinger, B., *et al.* (2004). Deficit of in vivo mitochondrial ATP production in OPA1-related dominant optic atrophy. *Ann Neurol* 56, 719-723.

Lodi, R., Tonon, C., Valentino, M.L., Manners, D., Testa, C., Malucelli, E., La Morgia, C., Barboni, P., Carbonelli, M., Schimpf, S., *et al.* (2011). Defective mitochondrial adenosine triphosphate production in skeletal muscle from patients with dominant optic atrophy due to OPA1 mutations. *Arch Neurol* 68, 67-73.

Lopez, J., and Tait, S.W. (2015). Mitochondrial apoptosis: killing cancer using the enemy within. *Br J Cancer* 112, 957-962.

Loson, O.C., Liu, R., Rome, M.E., Meng, S., Kaiser, J.T., Shan, S.O., and Chan, D.C. (2014). The mitochondrial fission receptor MiD51 requires ADP as a cofactor. *Structure* 22, 367-377.

Low, H.H., Sachse, C., Amos, L.A., and Lowe, J. (2009). Structure of a bacterial dynamin-like protein lipid tube provides a mechanism for assembly and membrane curving. *Cell* 139, 1342-1352.

Lu, B., Kennedy, B., Clinton, R.W., Wang, E.J., McHugh, D., Stepanyants, N., Macdonald, P.J., Mears, J.A., Qi, X., and Ramachandran, R. (2018). Steric interference from intrinsically disordered regions controls dynamin-related protein 1 self-assembly during mitochondrial fission. *Sci Rep* 8, 10879.

Luo, X., Budihardjo, I., Zou, H., Slaughter, C., and Wang, X. (1998). Bid, a Bcl2 interacting protein, mediates cytochrome c release from mitochondria in response to activation of cell surface death receptors. *Cell* 94, 481-490.

Lutter, M., Fang, M., Luo, X., Nishijima, M., Xie, X., and Wang, X. (2000). Cardiolipin provides specificity for targeting of tBid to mitochondria. *Nat Cell Biol* 2, 754-761.

Mannella, C.A., Marko, M., Penczek, P., Barnard, D., and Frank, J. (1994). The internal compartmentation of rat-liver mitochondria: tomographic study using the high-voltage transmission electron microscope. *Microsc Res Tech* 27, 278-283.

Margulis, L. (1971). Symbiosis and evolution. *Sci Am* 225, 48-57.

Meeusen, S., DeVay, R., Block, J., Cassidy-Stone, A., Wayson, S., McCaffery, J.M., and Nunnari, J. (2006). Mitochondrial inner-membrane fusion and crista maintenance requires the dynamin-related GTPase Mgm1. *Cell* 127, 383-395.

Meglei, G., and McQuibban, G.A. (2009). The dynamin-related protein Mgm1p assembles into oligomers and hydrolyzes GTP to function in mitochondrial membrane fusion. *Biochemistry* 48, 1774-1784.

Meric-Bernstam, F., and Mills, B.G. (2012). Overcoming implementation challenges of personalized cancer therapy. *Nature Reviews Clinical Oncology* 9, 542.

Merkwirth, C., Dargazanli, S., Tatsuta, T., Geimer, S., Lower, B., Wunderlich, F.T., von Kleist-Retzow, J.C., Waisman, A., Westermann, B., and Langer, T. (2008). Prohibitins control cell proliferation and apoptosis by regulating OPA1-dependent cristae morphogenesis in mitochondria. *Genes Dev* 22, 476-488.

- Millet, A.M., Bertholet, A.M., Daloyau, M., Reynier, P., Galinier, A., Devin, A., Wissinguer, B., Belenguer, P., and Davezac, N. (2016). Loss of functional OPA1 unbalances redox state: implications in dominant optic atrophy pathogenesis. *Ann Clin Transl Neurol* 3, 408-421.
- Misaka, T., Miyashita, T., and Kubo, Y. (2002). Primary structure of a dynamin-related mouse mitochondrial GTPase and its distribution in brain, subcellular localization, and effect on mitochondrial morphology. *J Biol Chem* 277, 15834-15842.
- Mishra, P., and Chan, D.C. (2014). Mitochondrial dynamics and inheritance during cell division, development and disease. *Nat Rev Mol Cell Biol* 15, 634-646.
- Mitra, K., Wunder, C., Roysam, B., Lin, G., and Lippincott-Schwartz, J. (2009). A hyperfused mitochondrial state achieved at G1-S regulates cyclin E buildup and entry into S phase. *Proc Natl Acad Sci U S A* 106, 11960-11965.
- Montessuit, S., Somasekharan, S.P., Terrones, O., Lucken-Ardjomande, S., Herzig, S., Schwarzenbacher, R., Manstein, D.J., Bossy-Wetzler, E., Basanez, G., Meda, P., *et al.* (2010). Membrane remodeling induced by the dynamin-related protein Drp1 stimulates Bax oligomerization. *Cell* 142, 889-901.
- Mootha, V.K., Wei, M.C., Buttle, K.F., Scorrano, L., Panoutsakopoulou, V., Mannella, C.A., and Korsmeyer, S.J. (2001). A reversible component of mitochondrial respiratory dysfunction in apoptosis can be rescued by exogenous cytochrome c. *Embo j* 20, 661-671.
- Morgan, P., Van Der Graaf, P.H., Arrowsmith, J., Feltner, D.E., Drummond, K.S., Wegner, C.D., and Street, S.D. (2012). Can the flow of medicines be improved? Fundamental pharmacokinetic and pharmacological principles toward improving Phase II survival. *Drug Discov Today* 17, 419-424.
- Mozdy, A.D., McCaffery, J.M., and Shaw, J.M. (2000). Dnm1p GTPase-mediated mitochondrial fission is a multi-step process requiring the novel integral membrane component Fis1p. *J Cell Biol* 151, 367-380.
- Nagashima, S., Tokuyama, T., Yonashiro, R., Inatome, R., and Yanagi, S. (2014). Roles of mitochondrial ubiquitin ligase MITOL/MARCH5 in mitochondrial dynamics and diseases. *J Biochem* 155, 273-279.
- Nakada, K., Inoue, K., and Hayashi, J. (2001). Interaction theory of mammalian mitochondria. *Biochem Biophys Res Commun* 288, 743-746.
- Niemann, H.H., Knetsch, M.L., Scherer, A., Manstein, D.J., and Kull, F. (2001). Crystal structure of a dynamin GTPase domain in both nucleotide-free and GDP-bound forms. In *EMBO J*, pp. 5813-5821.
- Norbury, C.J., and Hickson, I.D. (2001). Cellular responses to DNA damage. *Annu Rev Pharmacol Toxicol* 41, 367-401.

Nouraini, S., Six, E., Matsuyama, S., Krajewski, S., and Reed, J.C. (2000). The putative pore-forming domain of Bax regulates mitochondrial localization and interaction with Bcl-X(L). *Mol Cell Biol* *20*, 1604-1615.

Oakes, S.A., Scorrano, L., Opferman, J.T., Bassik, M.C., Nishino, M., Pozzan, T., and Korsmeyer, S.J. (2005). Proapoptotic BAX and BAK regulate the type 1 inositol trisphosphate receptor and calcium leak from the endoplasmic reticulum. *Proc Natl Acad Sci U S A* *102*, 105-110.

Oh, K.J., Singh, P., Lee, K., Foss, K., Lee, S., Park, M., Aluvila, S., Kim, R.S., Symersky, J., and Walters, D.E. (2010). Conformational changes in BAK, a pore-forming proapoptotic Bcl-2 family member, upon membrane insertion and direct evidence for the existence of BH3-BH3 contact interface in BAK homo-oligomers. *J Biol Chem* *285*, 28924-28937.

Olichon, A., Baricault, L., Gas, N., Guillou, E., Valette, A., Belenguer, P., and Lenaers, G. (2003a). Loss of OPA1 Perturbates the Mitochondrial Inner Membrane Structure and Integrity, Leading to Cytochrome c Release and Apoptosis.

Olichon, A., Baricault, L., Gas, N., Guillou, E., Valette, A., Belenguer, P., and Lenaers, G. (2003b). Loss of OPA1 perturbates the mitochondrial inner membrane structure and integrity, leading to cytochrome c release and apoptosis. *J Biol Chem* *278*, 7743-7746.

Olichon, A., Elachouri, G., Baricault, L., Delettre, C., Belenguer, P., and Lenaers, G. (2007a). OPA1 alternate splicing uncouples an evolutionary conserved function in mitochondrial fusion from a vertebrate restricted function in apoptosis. *Cell Death Differ* *14*, 682-692.

Olichon, A., Emorine, L.J., Descoins, E., Pelloquin, L., Brichese, L., Gas, N., Guillou, E., Delettre, C., Valette, A., Hamel, C.P., *et al.* (2002). The human dynamin-related protein OPA1 is anchored to the mitochondrial inner membrane facing the intermembrane space. *FEBS Lett* *523*, 171-176.

Olichon, A., Landes, T., Arnaune-Pelloquin, L., Emorine, L.J., Mils, V., Guichet, A., Delettre, C., Hamel, C., Amati-Bonneau, P., Bonneau, D., *et al.* (2007b). Effects of OPA1 mutations on mitochondrial morphology and apoptosis: relevance to ADOA pathogenesis. *J Cell Physiol* *211*, 423-430.

Orrenius, S., Gogvadze, V., and Zhivotovsky, B. (2007). Mitochondrial oxidative stress: implications for cell death. *Annu Rev Pharmacol Toxicol* *47*, 143-183.

Osellame, L.D., Singh, A.P., Stroud, D.A., Palmer, C.S., Stojanovski, D., Ramachandran, R., and Ryan, M.T. (2016). Cooperative and independent roles of the Drp1 adaptors Mff, MiD49 and MiD51 in mitochondrial fission. *J Cell Sci* *129*, 2170-2181.

Otera, H., Miyata, N., Kuge, O., and Mihara, K. (2016). Drp1-dependent mitochondrial fission via MiD49/51 is essential for apoptotic cristae remodeling.

Otera, H., Wang, C., Cleland, M.M., Setoguchi, K., Yokota, S., Youle, R.J., and Mihara, K. (2010). Mff is an essential factor for mitochondrial recruitment of Drp1 during mitochondrial fission in mammalian cells. *J Cell Biol* 191, 1141-1158.

Ott, M., Robertson, J.D., Gogvadze, V., Zhivotovsky, B., and Orrenius, S. (2002). Cytochrome c release from mitochondria proceeds by a two-step process. *Proc Natl Acad Sci U S A* 99, 1259-1263.

Palmer, C.S., Elgass, K.D., Parton, R.G., Osellame, L.D., Stojanovski, D., and Ryan, M.T. (2013). Adaptor proteins MiD49 and MiD51 can act independently of Mff and Fis1 in Drp1 recruitment and are specific for mitochondrial fission. *J Biol Chem* 288, 27584-27593.

Park, Y.Y., Nguyen, O.T., Kang, H., and Cho, H. (2014). MARCH5-mediated quality control on acetylated Mfn1 facilitates mitochondrial homeostasis and cell survival. *Cell Death Dis* 5, e1172.

Patten, D.A., Wong, J., Khacho, M., Soubannier, V., Mailloux, R.J., Pilon-Larose, K., MacLaurin, J.G., Park, D.S., McBride, H.M., Trinkle-Mulcahy, L., *et al.* (2014). OPA1-dependent cristae modulation is essential for cellular adaptation to metabolic demand. *Embo j* 33, 2676-2691.

Payne, M., Yang, Z., Katz, B.J., Warner, J.E., Weight, C.J., Zhao, Y., Pearson, E.D., Treft, R.L., Hillman, T., Kennedy, R.J., *et al.* (2004). Dominant optic atrophy, sensorineural hearing loss, ptosis, and ophthalmoplegia: a syndrome caused by a missense mutation in OPA1. *Am J Ophthalmol* 138, 749-755.

Pelloquin, L., Belenguer, P., Menon, Y., and Ducommun, B. (1998). Identification of a fission yeast dynamin-related protein involved in mitochondrial DNA maintenance. *Biochem Biophys Res Commun* 251, 720-726.

Petronilli, V., Penzo, D., Scorrano, L., Bernardi, P., and Di Lisa, F. (2001). The mitochondrial permeability transition, release of cytochrome c and cell death. Correlation with the duration of pore openings in situ. *J Biol Chem* 276, 12030-12034.

Pfeiffer, D.R., Gudz, T.I., Novgorodov, S.A., and Erdahl, W.L. (1995). The peptide mastoparan is a potent facilitator of the mitochondrial permeability transition. *J Biol Chem* 270, 4923-4932.

Pinkoski, M.J., Waterhouse, N.J., and Green, D.R. (2006). Mitochondria, apoptosis and autoimmunity. *Curr Dir Autoimmun* 9, 55-73.

Polletta, L., Vernucci, E., Carnevale, I., Arcangeli, T., Rotili, D., Palmerio, S., Steegborn, C., Nowak, T., Schutkowski, M., Pellegrini, L., *et al.* (2015). SIRT5 regulation of ammonia-induced autophagy and mitophagy. *Autophagy* 11, 253-270.

Poole, A.C., Thomas, R.E., Yu, S., Vincow, E.S., and Pallanck, L. (2010). The mitochondrial fusion-promoting factor mitofusin is a substrate of the PINK1/parkin pathway. *PLoS One* 5, e10054.

Praefcke, G.J., Kloep, S., Benschaid, U., Lilie, H., Prakash, B., and Herrmann, C. (2004). Identification of residues in the human guanylate-binding protein 1 critical for nucleotide binding and cooperative GTP hydrolysis. *J Mol Biol* *344*, 257-269.

Praefcke, G.J., and McMahon, H.T. (2004). The dynamin superfamily: universal membrane tubulation and fission molecules? *Nat Rev Mol Cell Biol* *5*, 133-147.

Prieto, J., Leon, M., Ponsoda, X., Sendra, R., Bort, R., Ferrer-Lorente, R., Raya, A., Lopez-Garcia, C., and Torres, J. (2016). Early ERK1/2 activation promotes DRP1-dependent mitochondrial fission necessary for cell reprogramming. *Nat Commun* *7*, 11124.

Prudent, J., Zunino, R., Sugiura, A., Mattie, S., Shore, G.C., and McBride, H.M. (2015). MAPL SUMOylation of Drp1 Stabilizes an ER/Mitochondrial Platform Required for Cell Death. *Mol Cell* *59*, 941-955.

Pyakurel, A., Savoia, C., Hess, D., and Scorrano, L. (2015). Extracellular regulated kinase phosphorylates mitofusin 1 to control mitochondrial morphology and apoptosis. *Mol Cell* *58*, 244-254.

Qi, X., Disatnik, M.H., Shen, N., Sobel, R.A., and Mochly-Rosen, D. (2011). Aberrant mitochondrial fission in neurons induced by protein kinase C $\{\delta\}$  under oxidative stress conditions in vivo. *Mol Biol Cell* *22*, 256-265.

Quintana-Cabrera, R., Quirin, C., Glytsou, C., Corrado, M., Urbani, A., Pellattiero, A., Calvo, E., Vazquez, J., Enriquez, J.A., Gerle, C., *et al.* (2018). The cristae modulator Optic atrophy 1 requires mitochondrial ATP synthase oligomers to safeguard mitochondrial function. *Nature communications* *9*, 3399.

Ramachandran, R., Surka, M., Chappie, J.S., Fowler, D.M., Foss, T.R., Song, B.D., and Schmid, S.L. (2007). The dynamin middle domain is critical for tetramerization and higher-order self-assembly. In *EMBO J*, pp. 559-566.

Rambold, A.S., Kostecky, B., Elia, N., and Lippincott-Schwartz, J. (2011). Tubular network formation protects mitochondria from autophagosomal degradation during nutrient starvation. *Proc Natl Acad Sci U S A* *108*, 10190-10195.

Rapaport, D., Brunner, M., Neupert, W., and Westermann, B. (1998). Fzo1p is a mitochondrial outer membrane protein essential for the biogenesis of functional mitochondria in *Saccharomyces cerevisiae*. *J Biol Chem* *273*, 20150-20155.

Reichert, A.S., and Neupert, W. (2002). Contact sites between the outer and inner membrane of mitochondria-role in protein transport. *Biochim Biophys Acta* *1592*, 41-49.

Renault, T.T., Floros, K.V., Elkhali, R., Corrigan, K.A., Kushnareva, Y., Wieder, S.Y., Lindtner, C., Serasinghe, M.N., Ascioia, J.J., Buettner, C., *et al.* (2015). Mitochondrial shape governs BAX-induced membrane permeabilization and apoptosis. *Mol Cell* *57*, 69-82.

- Reubold, T.F., Faelber, K., Plattner, N., Posor, Y., Ketel, K., Curth, U., Schlegel, J., Anand, R., Manstein, D.J., Noe, F., *et al.* (2015a). Crystal structure of the dynamin tetramer. *Nature* *525*, 404-408.
- Reubold, T.F., Faelber, K., Plattner, N., Posor, Y., Ketel, K., Curth, U., Schlegel, J., Anand, R., Manstein, D.J., Noé, F., *et al.* (2015b). Crystal structure of the dynamin tetramer. *Nature* *525*, 404.
- Richter, V., Palmer, C.S., Osellame, L.D., Singh, A.P., Elgass, K., Stroud, D.A., Sesaki, H., Kvensakul, M., and Ryan, M.T. (2014). Structural and functional analysis of MiD51, a dynamin receptor required for mitochondrial fission. *J Cell Biol* *204*, 477-486.
- Rizzuto, R., Bernardi, P., and Pozzan, T. (2000). Mitochondria as all-round players of the calcium game. *J Physiol* *529 Pt 1*, 37-47.
- Rocha, A.G., Franco, A., Krezel, A.M., Rumsey, J.M., Alberti, J.M., Knight, W.C., Biris, N., Zacharioudakis, E., Janetka, J.W., Baloh, R.H., *et al.* (2018). MFN2 agonists reverse mitochondrial defects in preclinical models of Charcot-Marie-Tooth disease type 2A. *Science* *360*, 336-341.
- Rojo, M., Legros, F., Chateau, D., and Lombes, A. (2002). Membrane topology and mitochondrial targeting of mitofusins, ubiquitous mammalian homologs of the transmembrane GTPase Fzo. *J Cell Sci* *115*, 1663-1674.
- Rosselin, M., Santo-Domingo, J., Bermont, F., Giacomello, M., and Demarex, N. (2017). L-OPA1 regulates mitoflash biogenesis independently from membrane fusion. *EMBO Rep* *18*, 451-463.
- Rossignol, R., Gilkerson, R., Aggeler, R., Yamagata, K., Remington, S.J., and Capaldi, R.A. (2004). Energy substrate modulates mitochondrial structure and oxidative capacity in cancer cells. *Cancer Res* *64*, 985-993.
- Salvador-Gallego, R., Mund, M., Cosentino, K., Schneider, J., Unsay, J., Schraermeyer, U., Engelhardt, J., Ries, J., and Garcia-Saez, A.J. (2016). Bax assembly into rings and arcs in apoptotic mitochondria is linked to membrane pores. *Embo j* *35*, 389-401.
- Samant, S.A., Zhang, H.J., Hong, Z., Pillai, V.B., Sundaresan, N.R., Wolfgeher, D., Archer, S.L., Chan, D.C., and Gupta, M.P. (2014). SIRT3 deacetylates and activates OPA1 to regulate mitochondrial dynamics during stress. *Mol Cell Biol* *34*, 807-819.
- Santel, A., and Fuller, M.T. (2001). Control of mitochondrial morphology by a human mitofusin. *J Cell Sci* *114*, 867-874.
- Santo-Domingo, J., Giacomello, M., Poburko, D., Scorrano, L., and Demarex, N. (2013). OPA1 promotes pH flashes that spread between contiguous mitochondria without matrix protein exchange. *Embo j* *32*, 1927-1940.



- Saraste, M., Sibbald, P.R., and Wittinghofer, A. (1990). The P-loop--a common motif in ATP- and GTP-binding proteins. *Trends Biochem Sci* *15*, 430-434.
- Sato, S.-i., Murata, A., Orihara, T., Shirakawa, T., Suenaga, K., Kigoshi, H., and Uesugi, M. (2011). Marine Natural Product Aurilide Activates the OPA1-Mediated Apoptosis by Binding to Prohibitin. *Chemistry & Biology* *18*, 131-139.
- Satoh, M., Hamamoto, T., Seo, N., Kagawa, Y., and Endo, H. (2003). Differential sublocalization of the dynamin-related protein OPA1 isoforms in mitochondria. *Biochem Biophys Res Commun* *300*, 482-493.
- Schapira, A.H. (2000). Mitochondrial disorders. *Curr Opin Neurol* *13*, 527-532.
- Schellenberg, B., Wang, P., Keeble, J.A., Rodriguez-Enriquez, R., Walker, S., Owens, T.W., Foster, F., Tanianis-Hughes, J., Brennan, K., Streuli, C.H., *et al.* (2013). Bax exists in a dynamic equilibrium between the cytosol and mitochondria to control apoptotic priming. *Mol Cell* *49*, 959-971.
- Schimpf, S., Fuhrmann, N., Schaich, S., and Wissinger, B. (2008). Comprehensive cDNA study and quantitative transcript analysis of mutant OPA1 transcripts containing premature termination codons. *Hum Mutat* *29*, 106-112.
- Schleich, K., and Lavrik, I.N. (2013). Mathematical modeling of apoptosis. *Cell Commun Signal* *11*, 44.
- Schwaiger, M., Herzog, V., and Neupert, W. (1987). Characterization of translocation contact sites involved in the import of mitochondrial proteins. *J Cell Biol* *105*, 235-246.
- Schwemmler, M., and Staeheli, P. (1994). The interferon-induced 67-kDa guanylate-binding protein (hGBP1) is a GTPase that converts GTP to GMP. *J Biol Chem* *269*, 11299-11305.
- Scorrano, L. (2009). Opening the doors to cytochrome c: changes in mitochondrial shape and apoptosis. *Int J Biochem Cell Biol* *41*, 1875-1883.
- Scorrano, L., Ashiya, M., Buttler, K., Weiler, S., Oakes, S.A., Mannella, C.A., and Korsmeyer, S.J. (2002). A distinct pathway remodels mitochondrial cristae and mobilizes cytochrome c during apoptosis. *Dev Cell* *2*, 55-67.
- Scorrano, L., and Korsmeyer, S.J. (2003). Mechanisms of cytochrome c release by proapoptotic BCL-2 family members. *Biochem Biophys Res Commun* *304*, 437-444.
- Scorrano, L., Oakes, S.A., Opferman, J.T., Cheng, E.H., Sorcinelli, M.D., Pozzan, T., and Korsmeyer, S.J. (2003a). BAX and BAK regulation of endoplasmic reticulum Ca<sup>2+</sup>: a control point for apoptosis. *Science* *300*, 135-139.
- Scorrano, L., Oakes, S.A., Opferman, J.T., Cheng, E.H., Sorcinelli, M.D., Pozzan, T., and Korsmeyer, S.J. (2003b). BAX and BAK regulation of endoplasmic reticulum Ca<sup>2+</sup>: a control point for apoptosis. *Science* *300*, 135-139.

- Serasinghe, M.N., Wieder, S.Y., Renault, T.T., Elkholi, R., Ascioffa, J.J., Yao, J.L., Jabado, O., Hoehn, K., Kageyama, Y., Sesaki, H., *et al.* (2015). Mitochondrial division is requisite to RAS-induced transformation and targeted by oncogenic MAPK pathway inhibitors. *Mol Cell* *57*, 521-536.
- Sesaki, H., and Jensen, R.E. (1999). Division versus fusion: Dnm1p and Fzo1p antagonistically regulate mitochondrial shape. *J Cell Biol* *147*, 699-706.
- Sesaki, H., Southard, S.M., Yaffe, M.P., and Jensen, R.E. (2003). Mgm1p, a dynamin-related GTPase, is essential for fusion of the mitochondrial outer membrane. *Mol Biol Cell* *14*, 2342-2356.
- Shin, H.W., Shinotsuka, C., Torii, S., Murakami, K., and Nakayama, K. (1997). Identification and subcellular localization of a novel mammalian dynamin-related protein homologous to yeast Vps1p and Dnm1p. *J Biochem* *122*, 525-530.
- Shpetner, H.S., and Vallee, R.B. (1989). Identification of dynamin, a novel mechanochemical enzyme that mediates interactions between microtubules. *Cell* *59*, 421-432.
- Siegel, R.L., Miller, K.D., and Jemal, A. (2018). Cancer statistics, 2018. *CA Cancer J Clin* *68*, 7-30.
- Skulachev, V.P. (2001). Mitochondrial filaments and clusters as intracellular power-transmitting cables. *Trends Biochem Sci* *26*, 23-29.
- Slupe, A.M., Merrill, R.A., Flippo, K.H., Lobas, M.A., Houtman, J.C., and Strack, S. (2013). A calcineurin docking motif (LXVP) in dynamin-related protein 1 contributes to mitochondrial fragmentation and ischemic neuronal injury. *J Biol Chem* *288*, 12353-12365.
- Smirnova, E., Griparic, L., Shurland, D.L., and van der Bliek, A.M. (2001). Dynamin-related protein Drp1 is required for mitochondrial division in mammalian cells. *Mol Biol Cell* *12*, 2245-2256.
- Son, J.M., Sarsour, E.H., Kakkerla Balaraju, A., Fussell, J., Kalen, A.L., Wagner, B.A., Buettner, G.R., and Goswami, P.C. (2017). Mitofusin 1 and optic atrophy 1 shift metabolism to mitochondrial respiration during aging. *Aging Cell* *16*, 1136-1145.
- Song, Z., Chen, H., Fiket, M., Alexander, C., and Chan, D.C. (2007). OPA1 processing controls mitochondrial fusion and is regulated by mRNA splicing, membrane potential, and Yme1L. *J Cell Biol* *178*, 749-755.
- Song, Z., Ghochani, M., McCaffery, J.M., Frey, T.G., and Chan, D.C. (2009). Mitofusins and OPA1 mediate sequential steps in mitochondrial membrane fusion. *Mol Biol Cell* *20*, 3525-3532.

- Staeheli, P., Haller, O., Boll, W., Lindenmann, J., and Weissmann, C. (1986). Mx protein: constitutive expression in 3T3 cells transformed with cloned Mx cDNA confers selective resistance to influenza virus. *Cell* *44*, 147-158.
- Stojanovski, D., Koutsopoulos, O.S., Okamoto, K., and Ryan, M.T. (2004). Levels of human Fis1 at the mitochondrial outer membrane regulate mitochondrial morphology. *J Cell Sci* *117*, 1201-1210.
- Sugiura, A., Nagashima, S., Tokuyama, T., Amo, T., Matsuki, Y., Ishido, S., Kudo, Y., McBride, H.M., Fukuda, T., Matsushita, N., *et al.* (2013). MITOL regulates endoplasmic reticulum-mitochondria contacts via Mitofusin2. *Mol Cell* *51*, 20-34.
- Taguchi, N., Ishihara, N., Jofuku, A., Oka, T., and Mihara, K. (2007). Mitotic phosphorylation of dynamin-related GTPase Drp1 participates in mitochondrial fission. *J Biol Chem* *282*, 11521-11529.
- Takahashi, K., Ohsawa, I., Shirasawa, T., and Takahashi, M. (2017). Optic atrophy 1 mediates coenzyme Q-responsive regulation of respiratory complex IV activity in brain mitochondria. *Exp Gerontol* *98*, 217-223.
- Tanaka, A., Cleland, M.M., Xu, S., Narendra, D.P., Suen, D.F., Karbowski, M., and Youle, R.J. (2010). Proteasome and p97 mediate mitophagy and degradation of mitofusins induced by Parkin. *J Cell Biol* *191*, 1367-1380.
- Tatsuta, T., Scharwey, M., and Langer, T. (2014). Mitochondrial lipid trafficking. *Trends Cell Biol* *24*, 44-52.
- Teuscher, K.B., Zhang, M., and Ji, H. (2017). A Versatile Method to Determine the Cellular Bioavailability of Small-Molecule Inhibitors.
- Tezze, C., Romanello, V., Desbats, M.A., Fadini, G.P., Albiero, M., Favaro, G., Ciciliot, S., Soriano, M.E., Morbidoni, V., Cerqua, C., *et al.* (2017). Age-Associated Loss of OPA1 in Muscle Impacts Muscle Mass, Metabolic Homeostasis, Systemic Inflammation, and Epithelial Senescence. *Cell Metab* *25*, 1374-1389.e1376.
- Tieu, Q., and Nunnari, J. (2000). Mdv1p is a WD repeat protein that interacts with the dynamin-related GTPase, Dnm1p, to trigger mitochondrial division. *J Cell Biol* *151*, 353-366.
- Tilokani, L., Nagashima, S., Paupe, V., and Prudent, J. (2018). Mitochondrial dynamics: overview of molecular mechanisms. *Essays Biochem* *62*, 341-360.
- Todt, F., Cakir, Z., Reichenbach, F., Emschermann, F., Lauterwasser, J., Kaiser, A., Ichim, G., Tait, S.W., Frank, S., Langer, H.F., *et al.* (2015). Differential retrotranslocation of mitochondrial Bax and Bak. *Embo j* *34*, 67-80.
- Todt, F., Cakir, Z., Reichenbach, F., Youle, R.J., and Edlich, F. (2013). The C-terminal helix of Bcl-x(L) mediates Bax retrotranslocation from the mitochondria. *Cell Death Differ* *20*, 333-342.

Tondera, D., Grandemange, S., Jourdain, A., Karbowski, M., Mattenberger, Y., Herzig, S., Da Cruz, S., Clerc, P., Raschke, I., Merkwirth, C., *et al.* (2009). SLP-2 is required for stress-induced mitochondrial hyperfusion. *Embo j* 28, 1589-1600.

Toyama, E.Q., Herzig, S., Courchet, J., Lewis, T.L., Jr., Loson, O.C., Hellberg, K., Young, N.P., Chen, H., Polleux, F., Chan, D.C., *et al.* (2016). Metabolism. AMP-activated protein kinase mediates mitochondrial fission in response to energy stress. *Science* 351, 275-281.

Tsushima, K., Bugger, H., Wende, A.R., Soto, J., Jenson, G.A., Tor, A.R., McGlaufflin, R., Kenny, H.C., Zhang, Y., Souvenir, R., *et al.* (2018). Mitochondrial Reactive Oxygen Species in Lipotoxic Hearts Induce Post-Translational Modifications of AKAP121, DRP1, and OPA1 That Promote Mitochondrial Fission. *Circ Res* 122, 58-73.

Twig, G., Elorza, A., Molina, A.J., Mohamed, H., Wikstrom, J.D., Walzer, G., Stiles, L., Haigh, S.E., Katz, S., Las, G., *et al.* (2008). Fission and selective fusion govern mitochondrial segregation and elimination by autophagy. *Embo j* 27, 433-446.

Varanita, T., Soriano, M.E., Romanello, V., Zaglia, T., Quintana-Cabrera, R., Semenzato, M., Menabo, R., Costa, V., Civiletto, G., Pesce, P., *et al.* (2015). The OPA1-dependent mitochondrial cristae remodeling pathway controls atrophic, apoptotic, and ischemic tissue damage. *Cell Metab* 21, 834-844.

Vetter, I.R., and Wittinghofer, A. (2001). The guanine nucleotide-binding switch in three dimensions. *Science* 294, 1299-1304.

Vogel, F., Bornhovd, C., Neupert, W., and Reichert, A.S. (2006). Dynamic subcompartmentalization of the mitochondrial inner membrane. *J Cell Biol* 175, 237-247.

Wakabayashi, J., Zhang, Z., Wakabayashi, N., Tamura, Y., Fukaya, M., Kensler, T.W., Iijima, M., and Sesaki, H. (2009). The dynamin-related GTPase Drp1 is required for embryonic and brain development in mice. *J Cell Biol* 186, 805-816.

Walczak, H., and Krammer, P.H. (2000). The CD95 (APO-1/Fas) and the TRAIL (APO-2L) apoptosis systems. *Exp Cell Res* 256, 58-66.

Wallace, D.C. (2005). A mitochondrial paradigm of metabolic and degenerative diseases, aging, and cancer: a dawn for evolutionary medicine. *Annu Rev Genet* 39, 359-407.

Wang, H., Song, P., Du, L., Tian, W., Yue, W., Liu, M., Li, D., Wang, B., Zhu, Y., Cao, C., *et al.* (2011). Parkin ubiquitinates Drp1 for proteasome-dependent degradation: implication of dysregulated mitochondrial dynamics in Parkinson disease. *J Biol Chem* 286, 11649-11658.

Wang, L., Dong, J., Cull, G., Fortune, B., and Cioffi, G.A. (2003). Varicosities of intraretinal ganglion cell axons in human and nonhuman primates. *Invest Ophthalmol Vis Sci* 44, 2-9.

- Wang, W., Wang, Y., Long, J., Wang, J., Haudek, S.B., Overbeek, P., Chang, B.H., Schumacker, P.T., and Danesh, F.R. (2012a). Mitochondrial fission triggered by hyperglycemia is mediated by ROCK1 activation in podocytes and endothelial cells. *Cell Metab* *15*, 186-200.
- Wang, X. (2001). The expanding role of mitochondria in apoptosis. *Genes Dev* *15*, 2922-2933.
- Wang, Z., Jiang, H., Chen, S., Du, F., and Wang, X. (2012b). The mitochondrial phosphatase PGAM5 functions at the convergence point of multiple necrotic death pathways. *Cell* *148*, 228-243.
- Wasiak, S., Zunino, R., and McBride, H.M. (2007). Bax/Bak promote sumoylation of DRP1 and its stable association with mitochondria during apoptotic cell death. *J Cell Biol* *177*, 439-450.
- Weaver, D., Eisner, V., Liu, X., Varnai, P., Hunyady, L., Gross, A., and Hajnoczky, G. (2014). Distribution and apoptotic function of outer membrane proteins depend on mitochondrial fusion. *Mol Cell* *54*, 870-878.
- Wee, Y., Liu, Y., Lu, J., Li, X., and Zhao, M. (2018). Identification of novel prognosis-related genes associated with cancer using integrative network analysis. *Sci Rep* *8*, 3233.
- Wei, M.C., Lindsten, T., Mootha, V.K., Weiler, S., Gross, A., Ashiya, M., Thompson, C.B., and Korsmeyer, S.J. (2000). tBID, a membrane-targeted death ligand, oligomerizes BAK to release cytochrome c. *Genes Dev* *14*, 2060-2071.
- Wei, M.C., Zong, W.X., Cheng, E.-Y., Lindsten, T., Panoutsakopoulou, V., Ross, A.J., Roth, K.A., MacGregor, G.R., Thompson, C.B., and Korsmeyer, S.J. (2001). Proapoptotic BAX and BAK: A Requisite Gateway to Mitochondrial Dysfunction and Death. *Science* *292*, 727-730.
- Westermann, B. (2010). Mitochondrial fusion and fission in cell life and death. *Nat Rev Mol Cell Biol* *11*, 872-884.
- White, K.E., Davies, V.J., Hogan, V.E., Piechota, M.J., Nichols, P.P., Turnbull, D.M., and Votruba, M. (2009). OPA1 deficiency associated with increased autophagy in retinal ganglion cells in a murine model of dominant optic atrophy. *Invest Ophthalmol Vis Sci* *50*, 2567-2571.
- Williams, P.A., Piechota, M., von Ruhland, C., Taylor, E., Morgan, J.E., and Votruba, M. (2012). Opa1 is essential for retinal ganglion cell synaptic architecture and connectivity. *Brain* *135*, 493-505.
- Wong, E.D., Wagner, J.A., Gorsich, S.W., McCaffery, J.M., Shaw, J.M., and Nunnari, J. (2000). The dynamin-related GTPase, Mgm1p, is an intermembrane space protein required for maintenance of fusion competent mitochondria. *J Cell Biol* *151*, 341-352.

- Xu, S., Cherok, E., Das, S., Li, S., Roelofs, B.A., Ge, S.X., Polster, B.M., Boyman, L., Lederer, W.J., Wang, C., *et al.* (2016a). Mitochondrial E3 ubiquitin ligase MARCH5 controls mitochondrial fission and cell sensitivity to stress-induced apoptosis through regulation of MiD49 protein. *Mol Biol Cell* *27*, 349-359.
- Xu, S., Wang, P., Zhang, H., Gong, G., Gutierrez Cortes, N., Zhu, W., Yoon, Y., Tian, R., and Wang, W. (2016b). CaMKII induces permeability transition through Drp1 phosphorylation during chronic beta-AR stimulation. *Nat Commun* *7*, 13189.
- Yamaguchi, R., Lartigue, L., Perkins, G., Scott, R.T., Dixit, A., Kushnareva, Y., Kuwana, T., Ellisman, M.H., and Newmeyer, D.D. (2008). Opa1-mediated cristae opening is Bax/Bak and BH3 dependent, required for apoptosis, and independent of Bak oligomerization. *Mol Cell* *31*, 557-569.
- Yan, J., Liu, X.H., Han, M.Z., Wang, Y.M., Sun, X.L., Yu, N., Li, T., Su, B., and Chen, Z.Y. (2015). Blockage of GSK3beta-mediated Drp1 phosphorylation provides neuroprotection in neuronal and mouse models of Alzheimer's disease. *Neurobiol Aging* *36*, 211-227.
- Yoon, Y., Krueger, E.W., Oswald, B.J., and McNiven, M.A. (2003). The mitochondrial protein hFis1 regulates mitochondrial fission in mammalian cells through an interaction with the dynamin-like protein DLP1. *Mol Cell Biol* *23*, 5409-5420.
- Yu, T., Fox, R.J., Burwell, L.S., and Yoon, Y. (2005). Regulation of mitochondrial fission and apoptosis by the mitochondrial outer membrane protein hFis1. *J Cell Sci* *118*, 4141-4151.
- Yu-Wai-Man, P., Griffiths, P.G., Gorman, G.S., Lourenco, C.M., Wright, A.F., Auer-Grumbach, M., Toscano, A., Musumeci, O., Valentino, M.L., Caporali, L., *et al.* (2010a). Multi-system neurological disease is common in patients with OPA1 mutations. *Brain* *133*, 771-786.
- Yu-Wai-Man, P., Sitarz, K.S., Samuels, D.C., Griffiths, P.G., Reeve, A.K., Bindoff, L.A., Horvath, R., and Chinnery, P.F. (2010b). OPA1 mutations cause cytochrome c oxidase deficiency due to loss of wild-type mtDNA molecules. *Hum Mol Genet* *19*, 3043-3052.
- Zanna, C., Ghelli, A., Porcelli, A.M., Karbowski, M., Youle, R.J., Schimpf, S., Wissinger, B., Pinti, M., Cossarizza, A., Vidoni, S., *et al.* (2008). OPA1 mutations associated with dominant optic atrophy impair oxidative phosphorylation and mitochondrial fusion. *Brain* *131*, 352-367.
- Zhang, J., Liu, X., Liang, X., Lu, Y., Zhu, L., Fu, R., Ji, Y., Fan, W., Chen, J., Lin, B., *et al.* (2017). A novel ADOA-associated OPA1 mutation alters the mitochondrial function, membrane potential, ROS production and apoptosis. *Sci Rep* *7*, 5704.
- Zhang, P., and Hinshaw, J.E. (2001). Three-dimensional reconstruction of dynamin in the constricted state. *Nat Cell Biol* *3*, 922-926.

- Zhang, X.D. (2007). A pair of new statistical parameters for quality control in RNA interference high-throughput screening assays. *Genomics* 89, 552-561.
- Zhao, J., Zhang, J., Yu, M., Xie, Y., Huang, Y., Wolff, D.W., Abel, P.W., and Tu, Y. (2012). Mitochondrial dynamics regulates migration and invasion of breast cancer cells. *Oncogene* 32, 4814.
- Zhao, X., Tian, C., Puszyk, W.M., Ogunwobi, O.O., Cao, M., Wang, T., Cabrera, R., Nelson, D.R., and Liu, C. (2013). OPA1 downregulation is involved in sorafenib-induced apoptosis in hepatocellular carcinoma. *Lab Invest* 93, 8-19.
- Zhivotovsky, B., Orrenius, S., Brustugun, O.T., and Doskeland, S.O. (1998). Injected cytochrome c induces apoptosis. *Nature* 391, 449-450.
- Zhu, P.P., Patterson, A., Lavoie, B., Stadler, J., Shoeb, M., Patel, R., and Blackstone, C. (2003). Cellular localization, oligomerization, and membrane association of the hereditary spastic paraplegia 3A (SPG3A) protein atlastin. *J Biol Chem* 278, 49063-49071.
- Zick, M., Duvezin-Caubet, S., Schafer, A., Vogel, F., Neupert, W., and Reichert, A.S. (2009a). Distinct roles of the two isoforms of the dynamin-like GTPase Mgm1 in mitochondrial fusion. *FEBS Lett* 583, 2237-2243.
- Zick, M., Rabl, R., and Reichert, A.S. (2009b). Cristae formation—linking ultrastructure and function of mitochondria. *Biochimica et Biophysica Acta (BBA) - Molecular Cell Research* 1793, 5-19.

